Chemical Probes for the Study of Mitochondrial Oxidative Stress

Linsey Robertson

A thesis submitted in part fulfilment of the requirements of the degree of Doctor of Philosophy.

Department of Chemistry

University of Glasgow

September 2009

Abstract

The implication of oxidative stress in ageing, and various disease states, has resulted in great interest in understanding the processes associated with it. Mitochondria are the major source of reactive oxygen species (ROS) via the electron transport chain. ROS may be free radicals, or molecules that rapidly form free radicals. These free radicals can undergo various rapid reactions with cellular components resulting in cell damage, and eventually cell death. Therefore, there is much interest in studying ROS production particularly from mitochondria.

In this thesis three novel classes of chemical probes for the study of oxidative stress are presented.

Firstly, progress was made towards a novel mitochondria-targeted hydroxylamine **iii** based on the 1,1,3,3-tetraethylisoindoline (TEIO) scaffold. This hydroxylamine **iii** should undergo reaction with radicals to form a stable nitroxide which gives a simple, persistent, quantifiable EPR (electron paramagnetic resonance) signal. Phosphonium salt **i** was prepared and EPR spectroscopy studies in a trial oxidation reaction indicated the formation of the late stage nitroxide precursor **ii**.

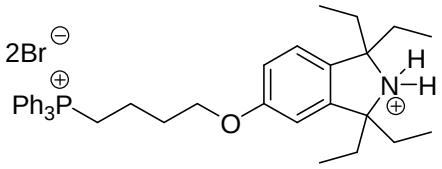

i

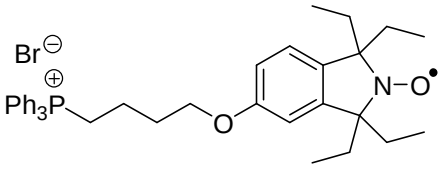

ii

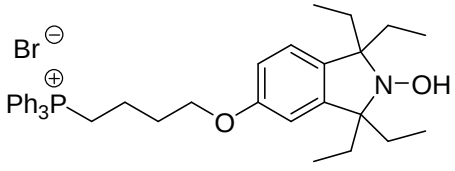

iii

Three new pyridinium salt nitrone spin traps **iv**-**vi**, designed to accumulate in mitochondria, were synthesised using the Zincke reaction as the key pyridinium salt forming reaction. The compatibility of nitrones with the Zincke reaction was demonstrated for the first time. The capability of spin traps **iv**-**vi** to trap methyl radicals was demonstrated using EPR spectroscopy.

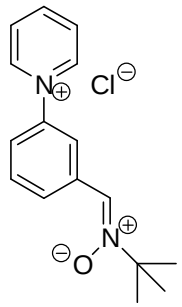

iv

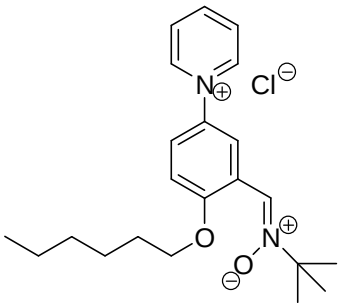

v

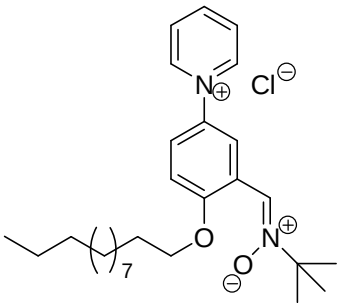

vi

Two novel selective uncoupling molecules (SUMs), DNP-SUM **vii** and FCCP-SUM **viii**, were designed to react with H_2O_2 and release a mitochondrial uncoupler. These were synthesised and their reaction with H_2O_2 was examined using UV spectrophotometry. DNP-SUM **vii** reacted slowly with a second order rate constant of 0.20 $M^{-1}s^{-1}$ and was deemed unsuitable for further investigation. However, the reaction of H_2O_2 and FCCP-SUM **viii** displayed good *pseudo*-first order kinetics when FCCP-SUM **viii** was used in excess and a second order rate constant of 64 $M^{-1}s^{-1}$ for the release of the mitochondrial uncoupler FCCP (carbonyl cyanide 4-(trifluoromethoxy)phenylhydrazone) in its ionised form. New analogues of FCCP-SUM **viii** are now in development to enable targeting to mitochondria.

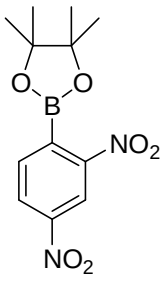

vii

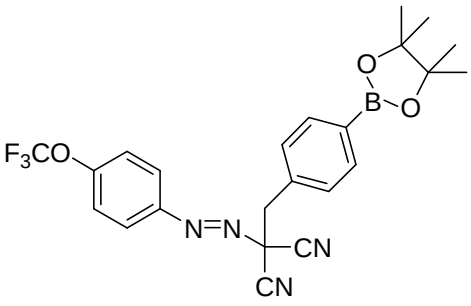

viii

Table of Contents

Acknowledgements 7

Abbreviations 9

Chapter 1: Oxidative stress 12

1.1 Oxygen chemistry 12

1.2 ROS production by metal ions 15

1.3 ROS production by mitochondria 16

1.4 Cellular damage caused by oxidative stress 19

1.4.1 Lipid peroxidation 19

1.4.2 Nucleic acid damage 23

1.4.3 Protein damage 24

1.5 Antioxidant defences 24

1.6 Small molecule antioxidants 26

1.7 Implications of oxidative stress 31

1.8 Conclusion 32

Chapter 2: The study of oxidative stress 34

2.1 Background 34

2.2 Introduction to EPR 35

2.3 Nitroxides 38

2.4 Hydroxylamine hydrogen-atom transfer agents 40

2.4 Nitrones and spin trapping 42

2.5 Nitroso spin traps 51

2.6 Conclusion 52

Chapter 3: Targeting mitochondria 54

3.1 Delocalised, lipophilic cations as a mitochondria targeting strategy 54

3.2 Antioxidants targeted with triphenylphosphonium cations 56

3.3 Nitroxides targeted with TPP cations 59

3.4 Nitrones targeted with TPP cations 61

3.5 Fluorescent sensors targeted with TPP cations 63

3.6 Synthesis of TPP salts 64

3.7. Other lipophilic cations for studying oxidative stress 68

3.8. Alternative mitochondria-targeting groups 70

3.9 Conclusion 71

Chapter 4: Synthesis of a mitochondria-targeted *N*-hydroxyisoindoline 72
4.1 Isoindoline nitroxides 72
4.2 Synthesis of isolindoline nitroxides 75
4.3 Novel probe design 78
4.4 Proposed synthesis of target hydroxylamine 174 79
4.5 Second route to target hydroxylamine 210 – Methoxy precursor 88
4.6 Conclusion 94
Chapter 5: Synthesis of Pyridinium Salt Nitrone Spin Traps 95
5.1 Pyridinium salts 95
5.2 Pyridinium salts by the Menschutkin reaction and S_NAr 96
5.3 Furaldehyde reaction 97
5.4 Zincke reaction 98
5.5 Design of new spin traps 102
5.6 First target N-arylpyridinium salt 269 104
5.6.1 Route via a benzylic alcohol 104
5.6.2 Route employing acetal protecting groups 107
5.6.3 Chemoselective route using a pre-formed nitrone 113
5.7 Synthesis of lipophilic nitrone spin traps 115
5.7.1 Route using a lipophilic Zincke salt 115
5.7.2 Route using a lipophilic aniline 116
5.8 Attempts to trap hydroxyl radicals 118
5.9 Trapping of methyl radicals 119
5.10 Conclusion 125
Chapter 6: Synthesis of selective uncoupling molecules 126
6.1 Mitochondrial uncoupling 126
6.2 Aim of the project 128
6.3 Reaction of Boronates with H_2O_2 129
6.4 Literature examples 130
6.5 Synthesis of selective uncoupling molecules (SUMs) 136
6.5.1 Synthesis of DNP-SUM 360 136
6.5.2 Synthesis of FCCP-SUMs 138
6.6 Kinetic Experiments with DNP-SUM 360 143
6.7 Kinetic experiments with FCCP-SUM 380 146
6.8 Conclusions from kinetic experiments 149

6.9 Synthesis of a mitochondrial targeted FCCP-SUM 150
6.10 Future direction of the project 151
6.11 Conclusion 151
Chapter 7: Experimental 152
7.1 General experimental 152
7.2 Synthesis 152
7.3 EPR experiments 189
7.4 Kinetic experiments 190
References 192

Acknowledgements

Firstly, I would like to say a huge thank you to my supervisor, Dr Richard Hartley, for being a constant source of help, support and encouragement throughout my PhD. I don't know how he put up with me sometimes! I would also like to thank Professor Nick Price for all his help with kinetic experiments. Additional thanks to my second supervisor Dr Graeme Cooke and to Dr Lucien Marx for kindly providing me information from his thesis.

I would also like to thank Prof. Bill Cushley, Prof. Darren Monckton and Dr Olwyn Byron, the Wellcome programme directors in Glasgow, not only for giving me the opportunity to come and study here, but also for their never-ending enthusiasm and belief in us. Financial support from the Wellcome Trust is gratefully acknowledged.

Many thanks to the technical support staff at the University of Glasgow: David Adam, Jim Tweedie, Kim Wilson, Arlene Douglas, Stuart Mackay, Alec James and Ted Easdon.

The Loudon lab was a great place to work thanks to all the past and present members of the Hartley group; Stuart, Carolyn, Calver, Louis, Guilaine, and Adam, and the Sutherland group; Caroline, Kate, Jenny, Mike, Louise, Lorna and Lindsay. They were always on hand for helpful discussions or laughs when it all got too much!

Huge thanks go to five ladies who lunch; Caroline, Ching, Claire, Louise and Nicola for random chats, great nights out, and all the help and understanding that you only get from fellow PhD students. Thanks to all my friends; Sarah, Susan, Laura, Laurie and Carolyn for making my return trips to Arbroath lots of fun and a welcome distraction; MM and Murray for fun-filled days and nights, tea, cakes, and understanding what chemistry's like, and Kristina for trying her best!

I would also like to thank all my family for their love and support, even when they didn't really understand what I've been doing for the past three years.

Lastly I would like to thank Ross for being so patient, putting up with my stressing and becoming my personal chef – promise I'm making all the lunches now!

Author's Declaration

This thesis represents the original work of Linsey Robertson unless explicitly stated otherwise in the text. The research was carried out at the University of Glasgow in the Henderson Laboratory and the Loudon Laboratory under the supervision of Dr Richard Hartley during the period October 2005 to October 2008. Portions of the work described herein have been published elsewhere as listed below.

Robertson, L.; Hartley, R.C. *Tetrahedron* **2009**, *65*, 5284-5292.

Abbreviations

Ac	acetate
ADP	adenosine diphosphate
amu	atomic mass unit
app	apparent
aq.	aqueous
ATP	adenosine triphosphate
ATR	attenuated total reflectance
br	broad
BuOH	butanol
cat.	catalytic
$CDCl_3$	deuterated chloroform
CI	chemical ionisation
CP	carboxy proxyl
d	doublet
DCM	dichloromethane
dd	doublet of doublets
ddd	doublet of doublet of doublets
DEPMPO	5-diethoxyphosphoryl-5-methyl-1-pyrroline-*N*-oxide
DLC	delocalised lipophilic cation
DMF	*N*,*N*'-dimethylformamide
DMPO	5,5-dimethyl-1-pyrroline-*N*-oxide
DMSO	dimethylsulfoxide
DNA	deoxyribonucleic acid
DNP	2,4-dinitrophenol
dppf	1,1'-bis(diphenylphosphino)ferrocene
dt	doublet of triplets
EI	electron impact
EPR	electron paramagnetic resonance
eq.	equivalents
Et	ethyl
ETC	electron transport chain
Et_2O	diethyl ether
EtOAc	ethyl acetate

EtOH	ethanol
FAB	fast atom bombardment
FCCP	carbonylcyanide *p*-(trifluoromethoxy)phenylhydrazone
FMN	flavin mononucleotide
g	gram(s)
GPX	glutathione peroxidase
GSH	reduced glutathione
GSSG	oxidised glutathione
h	hour(s)
4-HNE	4-hydroxy-2-*E*-nonenal
HPLC	high performance liquid chromatography
HRMS	high-resolution mass spectrometry
IBX	2-iodoxybenzoic acid
IR	infrared
J	NMR coupling constant
k_{Cat}	turnover number
K_M	Michaelis constant
L	litre or ligand
LDA	lithium diisopropylamine
lit.	literature
LRMS	low-resolution mass spectrometry
M	molar
m	multiplet
m-CPBA	3-chloroperbenzoic acid
Me	methyl
MeOD	d_4-deuterated methanol
MeOH	methanol
mg	milligram(s)
mL	millilitre(s)
mM	millimolar
mol	mole(s)
mp	melting point
NAD^+	nicotinamide adenine dinucleotide
NBS	*N*-bromosuccinamide
NMR	nuclear magnetic resonance
PBN	*N-tert*-butyl-α-phenylnitrone

Pd/C	palladium on carbon
Ph	phenyl
ppm	parts per million
PUFA	polyunsaturated fatty acid
q	quartet
RNA	ribonucleic acid
ROS	reactive oxygen species
rt	room temperature
s	singlet
SET	single electron transfer
sIBX	stabilised 2-iodoxybenzoic acid
SOD	superoxide dismutase
SUM	selective uncoupling molecule
t	triplet
tt	triplet of triplets
TEIO	1,1,3,3-tetraethylisoindoline
TEMPO	2,2,6,6-tetramethylpiperidine-*N*-oxyl
TEMPONE	4-oxo-2,2,6,6-tetramethylpiperidine-*N*-oxyl
THF	tetrahydrofuran
TMIO	1,1,3,3-tetramethylisoindoline
TLC	thin layer chromatography
TPP	triphenylphosphonium
UC	uncoupler
UCP	uncoupling protein
µL	microlitre
µM	micromolar
℃	degrees Celsius

Chapter 1: Oxidative stress

Oxidative stress has been defined as “An imbalance between oxidants and antioxidants in favour of the oxidants, potentially leading to damage”.[1]

This imbalance usually occurs through increased production of reactive oxygen species (ROS), highly reactive species i.e. radicals or molecules that can rapidly undergo conversion to radicals. If left unchecked, these molecules can react with cellular components such as lipids or DNA, causing cell damage and eventually triggering apoptosis. Under normal conditions, our body’s natural antioxidant defence mechanisms ensure that these ROS do not cause damage. However, if there is a sudden increase in oxidising species or decrease of defences, oxidative stress occurs.

Oxidative stress has been linked to a number of diseases as well as the ageing process. The biology of oxidative stress and ROS has been comprehensively reviewed.[1, 2] A full review is not possible in this thesis but an overview is provided. Unless otherwise referenced the cited reviews are the source of the information in the following discussion. To understand how ROS can cause so much damage we must first consider how they are formed.

1.1 Oxygen chemistry

Oxygen, although essential for aerobic life, is also toxic to most living organisms. The harmful effects of oxygen have been documented since its discovery in the 18th century. However, it was not until 1954 that Rebecca Gerschman first proposed that these effects were mediated by free radicals.[3] Shortly after this Denman Harman proposed his “Free Radical Theory of Ageing”.[4] Oxygen toxicity is primarily through oxidation of cellular components by molecular oxygen, O_2, and its related ROS.

When examining the electronic arrangement of molecular oxygen we can see it is a diradical (Figure 1). Each oxygen atom has six outer shell electrons. When looking at the molecular orbital energy diagram for the ground (triplet) state diatomic oxygen molecule we see there are two electrons in the degenerate $2\pi^*$ antibonding orbitals. Each electron has the same spin and occupies one orbital in accordance with Hund’s rule of maximum multiplicity.

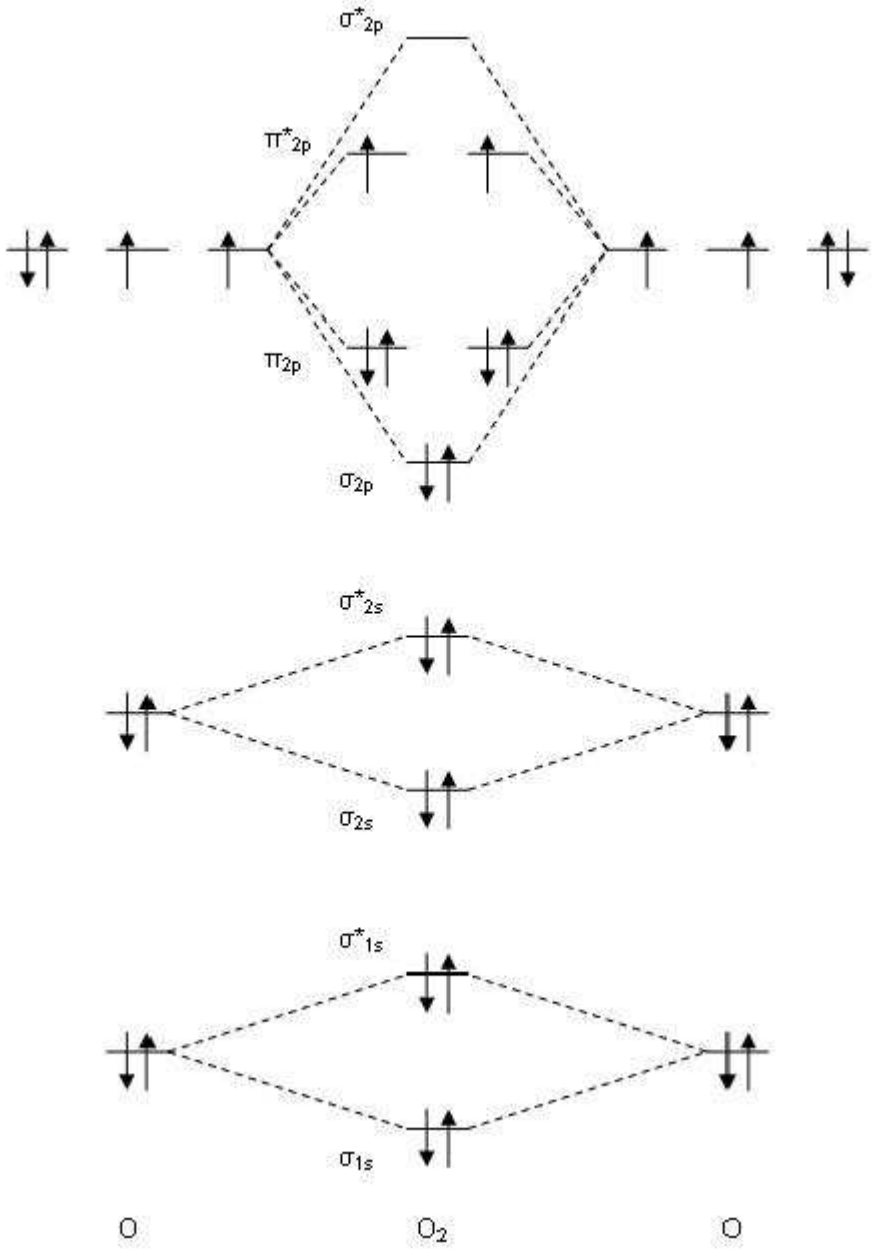

Figure 1: Molecular orbital diagram of triplet oxygen

Two higher energy states (Figure 2, A and B) also exist. The first A is very short lived and occurs when the spin of one electron is flipped but the orbital filling remains the same. The second B (usually referred to as singlet oxygen) is longer lived and results from the flipping of one spin and a pairing up of the electrons. If triplet oxygen gains a single electron it becomes the superoxide radical anion, $O_2^{\bullet-}$ (Figure 2, C). This electron must enter one of the π* antibonding orbitals, reducing the number of unpaired electrons and therefore the overall radical character of the molecule. The peroxide anion is formed when another electron is added to superoxide, pairing up with the final unpaired electron and reducing the O-O bond order to one (Figure 2, D). This dianion can gain two protons to form hydrogen

peroxide. Addition of a further electron gives the hydroxyl radical, $HO^{\bullet}$, and a hydroxide ion. Finally, addition of a fourth electron gives another hydroxide ion.

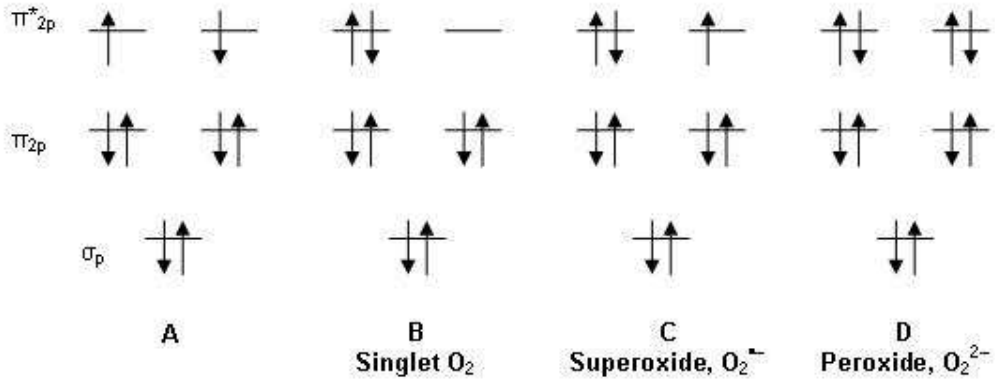

Figure 2

A 'pecking order' was established placing these oxidising species, along with others, in order of oxidising capability based on their one electron reduction potentials (Figure 3).[5] The hydroxyl radical is the most oxidising species in the pecking order and superoxide is much lower down the list. However, superoxide can readily disproportionate (or in biological terminology, dismutate) to hydrogen peroxide, a more oxidising species, and water. Further reactions can occur to convert less oxidising species into more reactive ones and these will be discussed further in later sections.

Couple (Oxidant/Antioxidant)	**E^0/mV**	
$^{\bullet}OH, H^+/H_2O$	2310	Highly oxidising
$RO^{\bullet}, H^+/ROH$	1600	
$HOO^{\bullet}, H^+/H_2O_2$	1150	
$ROO^{\bullet}$ (lipid peroxyl radical), $H^+/ROOH$	1060	
$O_2^{\bullet-}, 2H^+/H_2O_2$	940	
$PUFA^{\bullet}$ (polyunsaturated fatty acid radical), $H^+/PUFA$	600	
α-tocopheroxyl$^{\bullet}$, H^+/ α-tocopherol	500	
acorbate$^{\bullet}$, H^+/ ascorbate monoanion	282	
Fe(III)/Fe(II)	110	Highly reducing

Figure 3: 'Pecking order' of some species[5]

Radicals can interact with other molecules in a number of ways (Figure 4). Firstly, a radical can abstract a hydrogen atom from another molecule, giving a neutral molecule and a new radical species (Figure 4, reaction A). Two mechanisms of single electron transfer (SET) may occur. A radical can donate its unpaired electron to a molecule (Figure 4, reaction B). Conversely, it can also accept a single electron from another molecule (Figure 4, reaction C). Radicals can also form addition products. This generates a new radical if the reaction partner is not a radical (Figure 4, reaction D). If the reacting partner is another radical their electrons can pair up and generate a non-radical adduct (Figure 4, reaction E).

A $R^{\bullet} + XH \longrightarrow RH + X^{\bullet}$

B $R^{\bullet} + X \longrightarrow R^{+} + X^{-\bullet}$

C $R^{\bullet} + X \longrightarrow R^{-} + X^{+\bullet}$

D $R^{\bullet} + X \longrightarrow R\text{-}X^{\bullet}$

E $R^{\bullet} + X^{\bullet} \longrightarrow R\text{-}X$

Figure 4: Radical reactions

Radicals do not always play a harmful role. For example, superoxide can function as a signalling molecule.[6] However, there are a number of harmful radicals centred on oxygen, carbon, nitrogen or sulphur atoms within molecules, with the most damaging being the oxygen-centred radicals. Therefore, from now on the discussion will focus on ROS. Radicals can be produced from external sources. Many of the harmful effects of smoking and UV exposure can be attributed to the formation and subsequent reactions of radicals. However, the majority of ROS production occurs internally, and it is this route of production that I will now focus on.[7]

1.2 ROS production by metal ions

Metal ions play a hugely important biological role, particularly as enzyme cofactors. However, many of the first row transition metals are also capable of catalysing ROS production.

Fenton first reported the oxidation of an organic compound using iron(II) salts and H_2O_2[8], and the redox chemistry of iron which leads to hydroxyl radical formation now bears his name. Paradoxically, the most important biological role of iron is in

oxygen transport, as part of the haem complex. Iron has two common oxidation states, iron(II) and iron(III). The one electron difference between these stable oxidation states allows it to take part in radical reactions.

$$Fe^{2+} + H_2O_2 \longrightarrow Fe^{3+} + HO^{\bullet} + HO^{-}$$

Scheme 1: The Fenton reaction

Fe(II) ions reduce H_2O_2 (produced by enzymatic disproportionation of superoxide, reduction of molecular oxygen or via other redox reactions) to give Fe(III), a hydroxide ion and a hydroxyl radical (Scheme 1). Other metals, such as vanadium, can undergo similar reactions but are much less abundant within the body.

Copper ions can also exert a pro-oxidant effect in biological systems. Like iron, copper has two common oxidation states that differ by a single electron, copper(I) and copper(II). Copper can undergo an analogous reaction to the Fenton reaction.

$$Cu^{+} + H_2O_2 \longrightarrow Cu^{2+} + HO^{\bullet} + HO^{-}$$

Scheme 2: Reaction of copper(I) with H_2O_2

Toxic metals including cadmium, chromium, mercury and lead can also induce oxidative stress through a variety of mechanisms. This is thought to be one of the factors contributing to their toxicity.[9]

1.3 ROS production by mitochondria

Mitochondria are known as the ‘powerhouse’ of the cell. They are organelles that produce energy by reducing oxygen to water and synthesising adenosine triphosphate (ATP). This process is known as oxidative phosphorylation, and accounts for the consumption of 85-90% of all oxygen taken up by mammals.[2] Mitochondria possess two lipid membranes, an outer and an inner membrane with an intermembrane space between the two. The inner membrane has a large surface area due to the formation of folds, or cristae. The space within the inner membrane is known as the mitochondrial matrix (Figure 5).

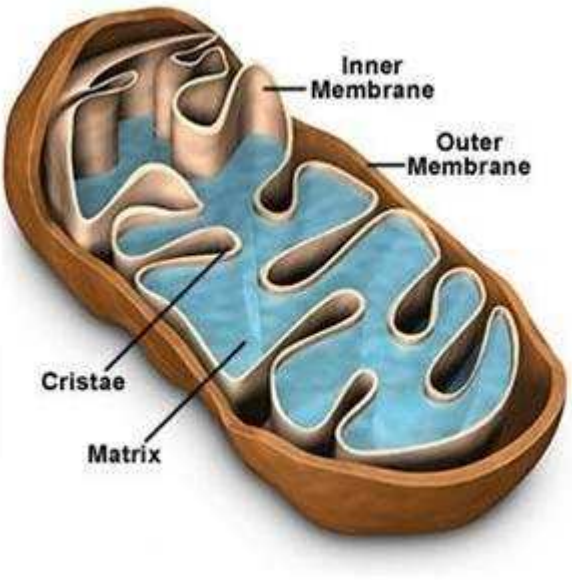

Figure 5: Structure of a mitochondrion[10]

Oxidative phosphorylation occurs within the electron transport chain, a series of enzymes embedded within the inner mitochondrial membrane (Figure 6).

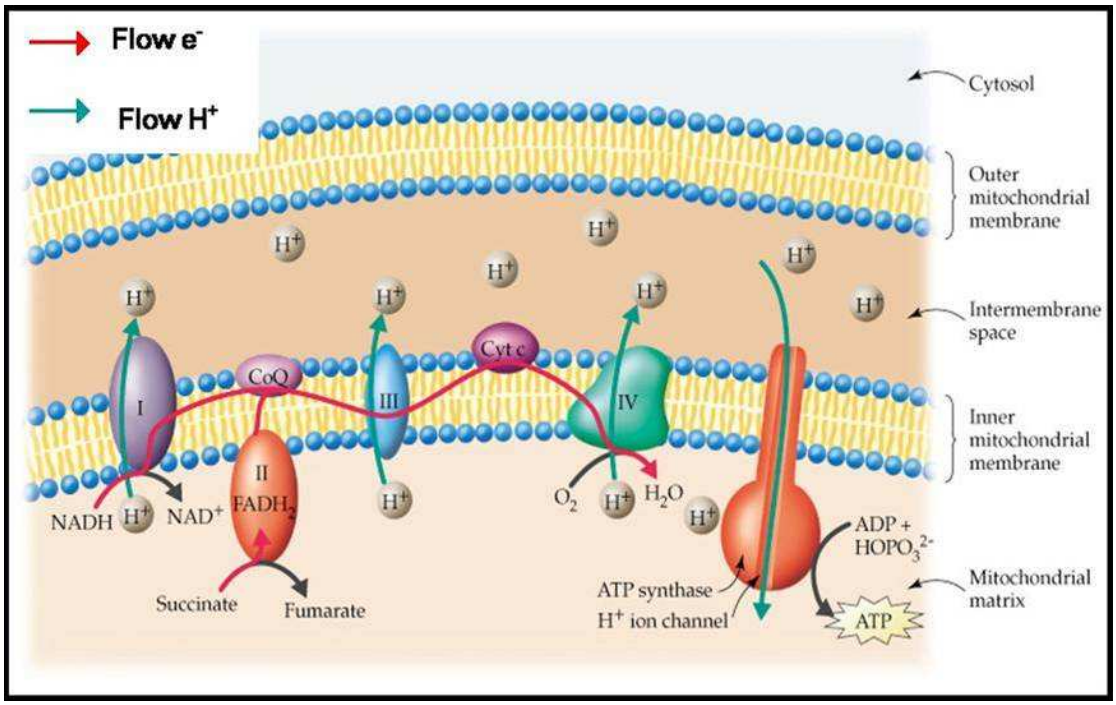

Figure 6: The mitochondrial electron transport chain[11]

Essentially, food molecules are oxidised and lose electrons. These electrons are taken up by electron carriers such as NAD^+ or flavins. The reduced forms of these molecules can subsequently undergo oxidation by O_2 through the action of the electron transport chain. These oxidations are mediated in a stepwise fashion by

some of the complexes. During the transfer of electrons down the carriers in the electron transport chain protons are pumped into the intermembrane space, creating a potential gradient across the inner membrane and generating a proton-motive force. In the final stage of the electron transport chain, O_2 (termed the terminal electron acceptor) undergoes four one-electron reductions to form water, catalysed by cyctochrome *c* oxidase (Complex IV). The protons pass back into the matrix from the intermembrane space through the membrane-spanning enzyme complex ATP synthase, which uses the proton-motive force to synthesise ATP from ADP.[12]

Although the electron transport chain is efficient, a percentage (estimated at up to ~2% *in vitro*[13]) of the oxygen undergoes a one-electron reduction to superoxide, $O_2^{\bullet -}$. In isolated mitochondria it has been shown that this mainly occurs at complex I (NADH-Coenzyme Q Reductase).[13] Complex I is a complex, multi sub-unit protein of ~1 MDa. It has a characteristic L-shape and Figure 7 shows a schematic of its location and catalytic reaction.

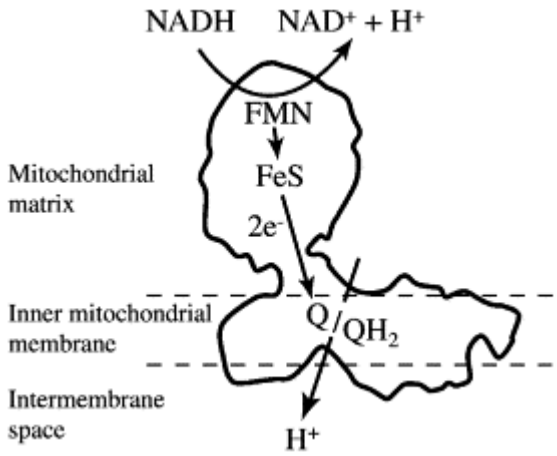

Figure 7: Complex I of the electron transport chain[14]

The flavin mononucleide (FMN) co-factor accepts electrons from NADH and passes them down a series of seven FeS (iron-sulfur) clusters to ubiquinone **1** (Coenzyme Q). Ubiquinone **1** is converted to ubiquinol **3** via a ubisemiquinone intermediate **2**. Ubiquinol **3** is then reoxidised back by the cytochrome bc_1 complex (Scheme 3).

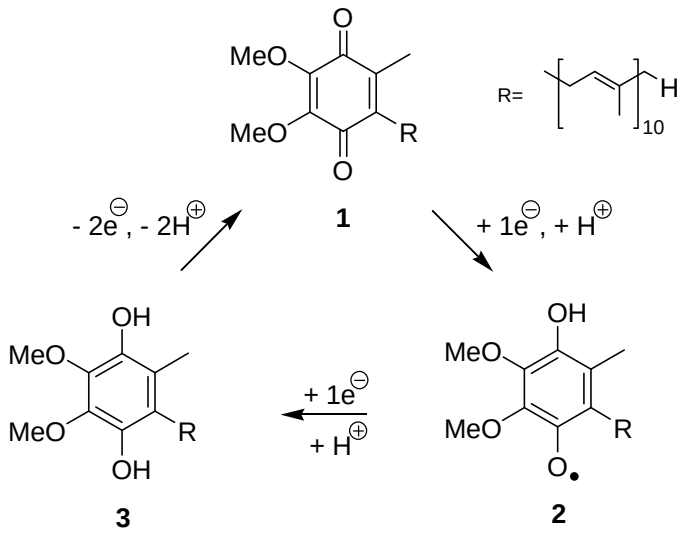

Scheme 3: The Q Cycle

O_2 can react with electrons on the FMN or ubiquinone sites. Most of the FeS clusters appear to be shielded from O_2, but may also be capable of reducing it to $O_2^{\bullet-}$. Superoxide can then undergo conversion into other ROS.

1.4 Cellular damage caused by oxidative stress

Cells have a number of different responses to oxidative stress. In fact, some types of cell undergo proliferation under mild oxidative stress conditions. Cells can adapt to mild oxidative stress, for example by upregulating their antioxidant defences. Higher oxidative stress causes damage to cellular components such as DNA, lipids and proteins. This can lead to cellular senescence (cells stop dividing) or cell death by one of two mechanisms, apotosis or necrosis. The products of cellular damage can be detected, and are often used as markers of oxidative stress. The targets of oxidative stress depend on the type of cell, the type of oxidising species and the severity of the stress. However, the three major targets are lipids, DNA and proteins.

1.4.1 Lipid peroxidation

Cell membranes are mostly made up of lipids and proteins. The most prevalent lipids in animal cell membranes are the phospholipids **4** as they contain hydrophilic and hydrophobic regions (Figure 8). The long chain fatty acid groups R_1 and R_2 present in these molecules can differ in length and degree of unsaturation, two examples are shown in Figure 8.

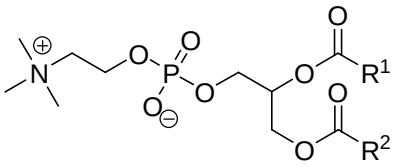

Phosphatidylcholine **4**

Examples of possible fatty acid side chains R_1 and R_2:

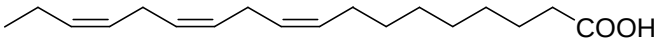

Linolenic acid **5**

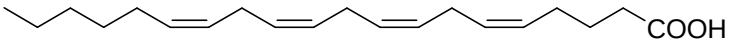

Arachidonic acid **6**

Figure 8: General structure of phosphatidyl cholines and some example fatty acid side chains

These phospholipids arrange themselves into a bilayer structure with the polar headgroups at the surface and the hydrophobic lipid tails pointing into the centre. Proteins can be embedded in the membrane, span the membrane (transmembrane proteins), or be associated with the surface of the membrane (Figure 9).

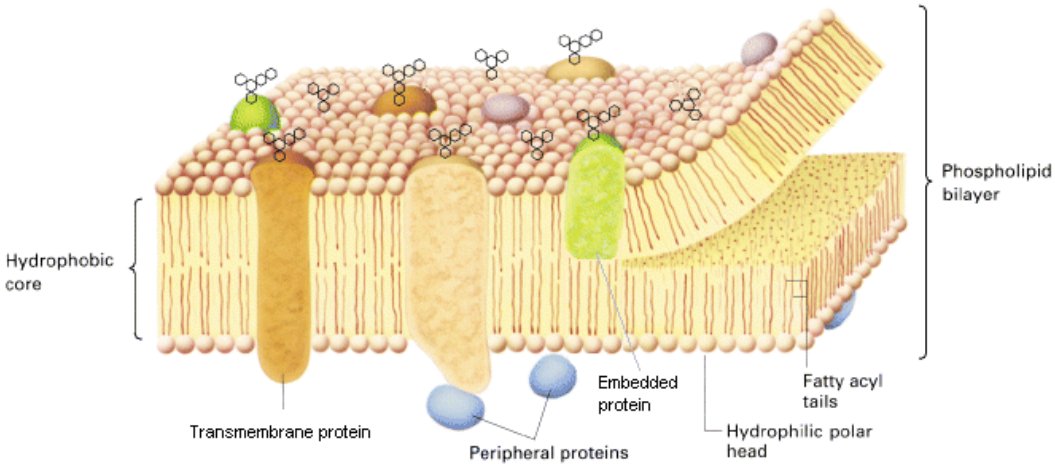

Figure 9: Plasma membrane structure (adapted from Lodish *et al.*[15])

The structure of the membrane is not rigid and is usually regarded as a 2-dimensional fluid or a ‘fluid mosiac’. This fluidity is largely determined by the degree of unsaturation of the fatty acid tail of the lipid, as the more carbon-carbon

double bonds present, the lower the melting point. However, polyunsaturated fatty acids (PUFAs), such as arachidonic acid **6**, are also more susceptible to oxidative damage. This damage occurs mainly via a free radical chain reaction pathway that results in lipid peroxide formation (Scheme 4). Allylic or bis-allylic hydrogen atoms are preferentially abstracted by radicals as the resulting allylic radical is stabilised by resonance. The reduction potential of a bis-allylic PUFA$^{\bullet}$/PUFA couple has been estimated at +0.6 V compared to ~ +1.9 V for an alkyl H/alkyl radical couple.[5] Therefore, most ROS are thermodynamically capable of oxidising PUFAs. In practise only uncharged species such as $HO^{\bullet}$ and $HO_2^{\bullet}$ can enter the membrane.

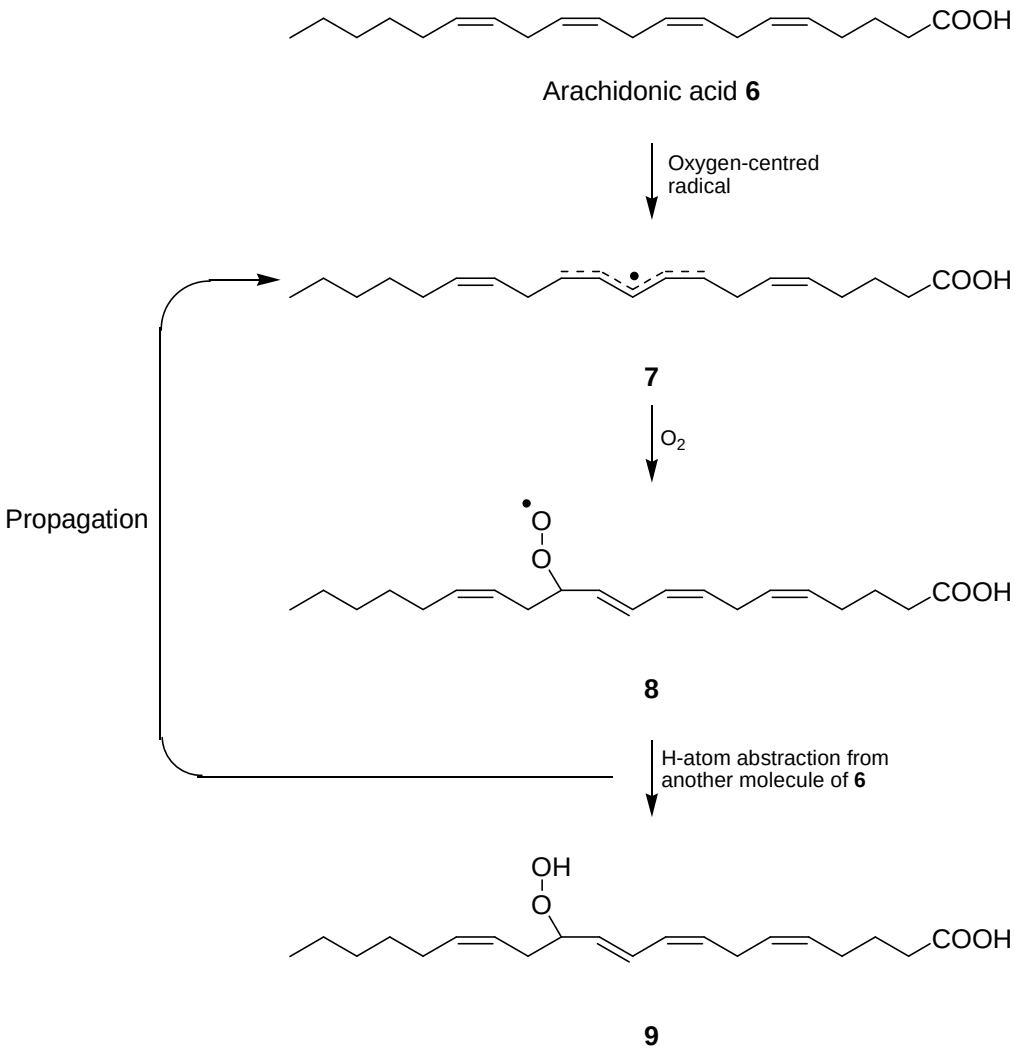

Scheme 4: Initiation and propagation of lipid peroxidation

The formation of allylic radical **7** is the initiation step of lipid peroxidation (Scheme 4). This radical can then undergo reaction with O_2 to form a peroxyl radical, $ROO^{\bullet}$ **8**. The peroxyl radical **8** can abstract a hydrogen atom from an adjacent fatty acid chain, forming a lipid hydroperoxide **9** and another allylic radical, e.g. bis-allylic

radical **7,** which can then carry out another similar reaction, and so on. This constitutes the propagation phase of lipid peroxidation and can continue hundreds of times. The chain is terminated when a peroxyl radical **8** reacts with another radical, such as a bis-allylic radical, or by addition of $H^{\bullet}$ from another source that does not form a reactive species e.g. vitamin E. Lipid peroxidation increases the rigidity of membranes and limits the movement of membrane proteins. It also compromises the integrity of the membrane, allowing it to be more easily permeated. Lipid peroxides themselves appear to have low toxicity, but can undergo further reaction to form cytotoxic products such as 4-hydroxy-2-*E*-nonenal (4-HNE) **10** as well as other aldehydes (Figure 10).

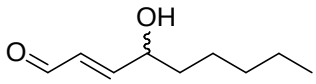

10

Figure 10: Structure of 4-HNE

Additionally, if peroxyl radicals react intramolecularly they form cyclic peroxides (e.g. cyclic peroxide **11** derived from arachidonic acid), which can break down via several different pathways and can result in formation of isoprostanes such as **12** and related compounds, or malondialdehyde (MDA) **13** (Scheme 5). Isoprostanes and MDA are commonly used as indicators of lipid peroxidation.

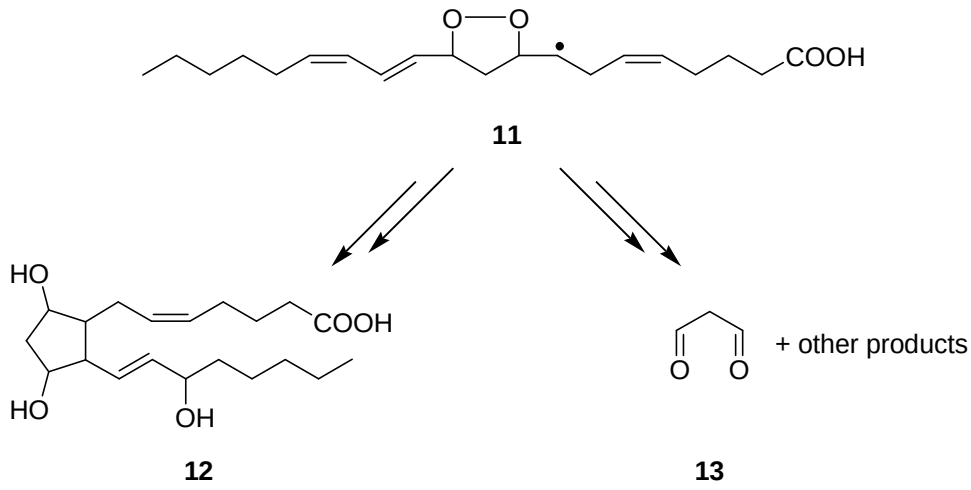

11 **12** **13**

Scheme 5: Possible products from breakdown of cyclic peroxide **11**

1.4.2 Nucleic acid damage

DNA and RNA are susceptible to damage by ROS, most commonly by attack of $HO^{\bullet}$. $HO^{\bullet}$ can add to a number of sites on the purine or pyrimidine ring and can fragment the sugar moiety. This may be followed by further reactions that give rise to a large number of possible products. 8-Hydroxyguanine **17** (8-OHdG) is one of the most studied of these products and is often measured as a biomarker of oxidative DNA damage.

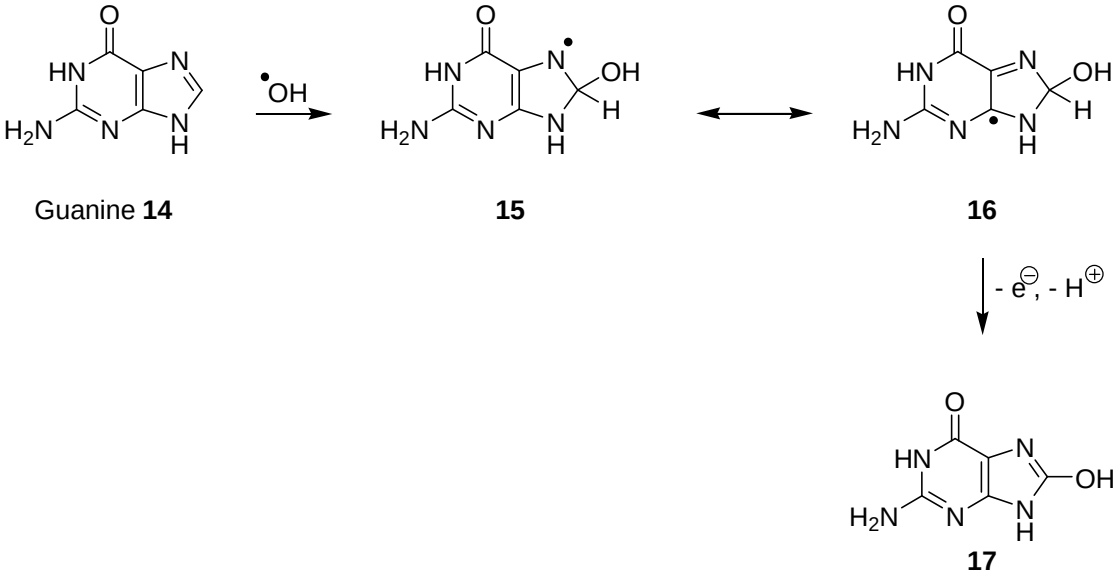

Guanine **14** **15** **16**

17

Scheme 6: Formation of 8-OHdG **17**

Aldehydes derived from lipid peroxidation e.g MDA **13** or 4-HNE **10**, can also form DNA adducts. This modification of DNA can lead to mutations and DNA strand breaks. Several of the modified bases are capable of mismatches e.g. hypoxanthine **19**, the deamination product of adenine **18**, can pair with cytosine instead of thymine, resulting in an AT→GC transmutation. If too much DNA damage accumulates the cell can enter apoptosis. Although DNA damage can be extremely harmful and potentially fatal, mutations generally occur at a level that allows repair mechanisms to cope, including a set of mismatch repair proteins.

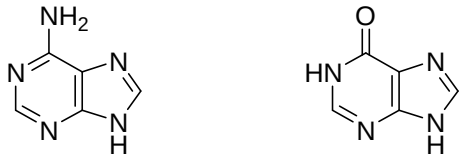

Adenine **18** Hypoxanthine **19**

Figure 11: Structures of adenine **18** and hypoxanthine **19**

1.4.3 Protein damage

Oxidative protein damage is important due to the vast array of functions that proteins carry out within our cells. Oxidative damage may alter or completely abolish the function of particular enzymes. This could have consequences as a result of incorrect function, for example, if a DNA polymerase did not replicate accurately mutations would arise. Alternatively, the body may recognise an oxidised protein as foreign and illicit an immune response against it, as in rheumatoid arthritis. Proteins can be attacked or oxidised at a number of different sites and residues. For example, thiol groups on cysteine residues can be oxidised by ROS to give disulfides. Membrane proteins can also react with lipid peroxyl radicals, forming lipid-protein crosslinks which restrict their motion. Damaged proteins can be degraded or exported from the cell.

1.5 Antioxidant defences

As we have seen, oxidative damage to cellular components can have serious effects. The body has evolved a number of antioxidant defences to counteract the production and effects of ROS. These can be categorised as either enzymatic defences or small molecule defences.

A number of enzymatic systems catalyse the conversion of ROS into more innocuous molecules. The two main classes of antioxidant enzyme are superoxide dismutases (SOD) and catalases. A third class, peroxidases, will also be discussed.

SODs are metalloproteins that catalyse the reaction (disproportionation/ dismutation) of two superoxide radicals to form hydrogen peroxide and molecular oxygen (Scheme 7).

$$O_2^{\bullet-} + O_2^{\bullet-} + 2H^+ \longrightarrow H_2O_2 + O_2$$

Scheme 7: Reaction catalysed by SOD

They are found in a range of organisms, from bacteria to humans, and contain either Cu/Zn, Mn or Fe. When first discovered, no catalytic ability was detected for SODs and they were thought to be metal storage proteins. However, in 1969 it was discovered that one of these proteins could catalytically remove superoxide radicals. SODs appear to be completely specific for this function.

SODs are highly efficient enzymes with a k_{cat}/K_M value of 7×10^9 $s^{-1}M^{-1}$. k_{cat}/K_M is an indicator of catalytic efficiency and it has an upper limit of between 10^8 and 10^9

$s^{-1}M^{-1}$, controlled by the rate of diffusion.[12] As SODs have a value within this range, they can be considered 'catalytically perfect'.

The most common SOD used in eukaryotes is the CuZnSOD. It is present in virtually all cells and is predominantly found in the cytosol but is also present in smaller quantities in lysosomes, nuclei and the mitochondrial intermembrane space. The amino-acid sequence of CuZnSOD enzymes is highly conserved across organisms and the crystal structures of several of these have been solved. CuZnSOD is a 32 kDa homodimer with one subunit binding Cu^{2+} and one binding Zn^{2+}. Copper is directly involved in the catalytic cycle whereas the zinc ions are not and appear instead to play a role in the stability. Manganese SODs are larger enzymes (~40 kDa) that can have 2 or 4 subunits. In humans it is located in the mitochondria and is also present in many other organisms including bacteria. Despite the differences between CuZnSOD and MnSOD they essentially carry out the same reaction (Scheme 7). Mouse MnSOD null mutants die at a very young age, indicating the importance of this enzyme.[16] Some bacteria also contain an FeSOD, however this is not found in humans.

Although hydrogen peroxide is less damaging than superoxide, it is still a ROS and is capable of generating hydroxyl radicals, as shown earlier. Therefore another set of metallo-enzymes, known as catalases, are used to catalyse the removal of hydrogen peroxide, forming water and molecular oxygen (Scheme 8).

$$2H_2O_2 \longrightarrow 2H_2O + O_2$$

Scheme 8: Reaction catalysed by catalase

Catalase is found in nearly all aerobic organisms and is also a highly efficient enzyme ($k_{cat}/K_M = 4 \times 10^7\ s^{-1}M^{-1}$).[12] In animals it is located in all major organs, particularly the liver, and is contained within subcellular organelles known as peroxisomes. Catalase consists of four identical protein subunits which each bind a haem group, containing an Fe^{3+} ion. A manganese-containing catalase is also used by some species of bacteria.

Peroxidases are a class of enzymes that catalyse the removal of hydrogen peroxide by coupling its reduction with the oxidation of another substrate. Catalases can also possess peroxidase activity and catalase/peroxidase enzymes exist, such as KatG found in bacteria.[17] The glutathione peroxidases (GPX) are the most common of these enzymes and use reduced glutathione, GSH **20**, as their substrate (Scheme 9).

$$2GSH + H_2O_2 \rightarrow GSSG + 2H_2O$$

Scheme 9: Reaction catalysed by GPX enzymes

GSH **20** is a tripeptide of glutamic acid-cysteine-glycine with an unusual γ-peptide linkage between cysteine and the glutamic acid side chain. GPX enzymes remove H_2O_2 by using it to oxidise **20** to oxidised glutathione, GSSG **21**, with the thiol side chains of two molecules of **20** forming a disulfide bridge to give one molecule of **21**.

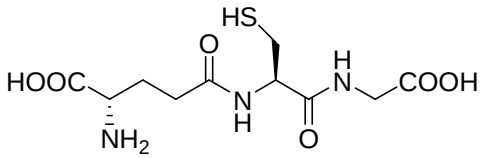

20

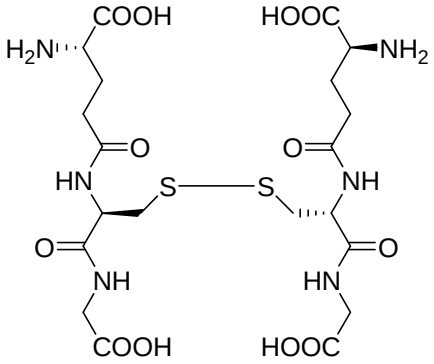

21

Figure 12: Structures of reduced **20** and oxidised **21** glutathione

GPXs can use other peroxides such as fatty acid hydroperoxides as their reduction substrate, but are specific for **20** as their oxidation substrate. There are four known GPX enzymes, all of which contain selenocysteine residues in their active site that are involved in the catalytic process. GSSG **21** is reduced back to GSH **20** by NADPH-dependant glutathione reductase enzymes (GSR). The GSH/GSSG ratio is the primary determinant of intracellular redox status due to its low standard redox potential (E_0 = –240 mV) and its high abundance (0.1-10 mM) compared with other redox couples such as cysteine/cystine (50 μM).[18] As well as acting as the substrate for GPX enzymes, GSH **20** has a number of important cellular roles including the removal of xenobiotics via conjugation catalysed by glutathione transferase enzymes (GST). There are a number of other peroxidases that can remove H_2O_2 as well as other enzymes, such as thioredoxin reductase, that also contribute to regulation of oxidative stress.

1.6 Small molecule antioxidants

Small molecule antioxidants can be further classified into compounds obtained from the diet and those synthesised *in vivo*. There are a number of dietary

compounds that have been proposed to act as antioxidants *in vivo* including vitamin C **22** and vitamin E, the main component of which is d-α-tocopherol **23** (Figure 13).

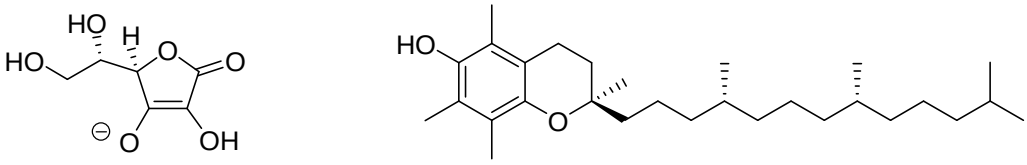

Ascorbic acid monoanion **22** d-α-tocopherol **23**

Figure 13: Structures of vitamin C **22** and vitamin E **23**

L-Ascorbic acid is commonly known as vitamin C and is present in many dietary sources including citrus fruits. The discovery that citrus fruits could prevent scurvy was made in the 16th century but it was not until 1928 that ascorbic acid was first isolated. Ascorbic acid exists as the ascorbate monoanion **22** at physiological pH. Humans are one of only a few mammals that cannot produce their own vitamin C, due to loss of the enzyme gulonolactone oxidase.[19] Vitamin C is an efficient scavenger of many radicals including $HO^{\bullet}$, $O_2^{\bullet-}$, $HO_2^{\bullet}$ and water-soluble $ROO^{\bullet}$ radicals. As shown in Figure 3, it is capable of reducing many other species. It does this by donating an electron to form **24**, the semidehydroascorbate or ascorbyl radical. This radical is relatively inert and may be further oxidised to give dehydroascorbate (DHA) **25** (Scheme 10). Transition metals such as copper and iron can catalyse this reaction. However in doing so, ascorbate **22** can exert a pro-oxidant activity as reduced copper(I) and iron(II) ions can contribute to ROS production as discussed previously. DHA **25** is unstable and either degrades into a mixture of products which can be excreted, or is enzymatically converted back into acorbate **22**. Vitamin C is also capable of regenerating vitamin E, another important dietary antioxidant.

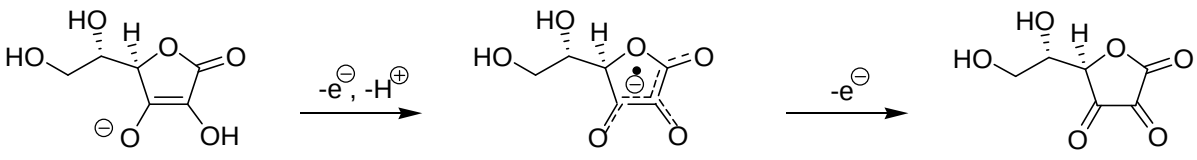

22 **24** DHA **25**

Scheme 10: Oxidation of vitamin C

Strictly speaking, vitamin E is the term used for a mixture of related compounds that exert similar effects. However, d-α-tocopherol **23** is the most effective of these and is often referred to as vitamin E. Vegetable oils, grains and nuts are common dietary sources of vitamin E. In contrast to vitamin C, α-tocopherol is lipid-soluble and concentrates within membranes. Here it carries out its major antioxidant function as a scavenger of lipid peroxyl radicals, thus inhibiting lipid peroxidation. A peroxyl radical such as **8** can abstract the phenolic hydrogen from α-tocopherol **23**, giving the α-tocopheroxyl radical **26** and a lipid peroxide e.g. **9** (Scheme 11). Radical **26** can be recycled back to α-tocopherol **23** or undergo further oxidation to form tocopheryl quinone.

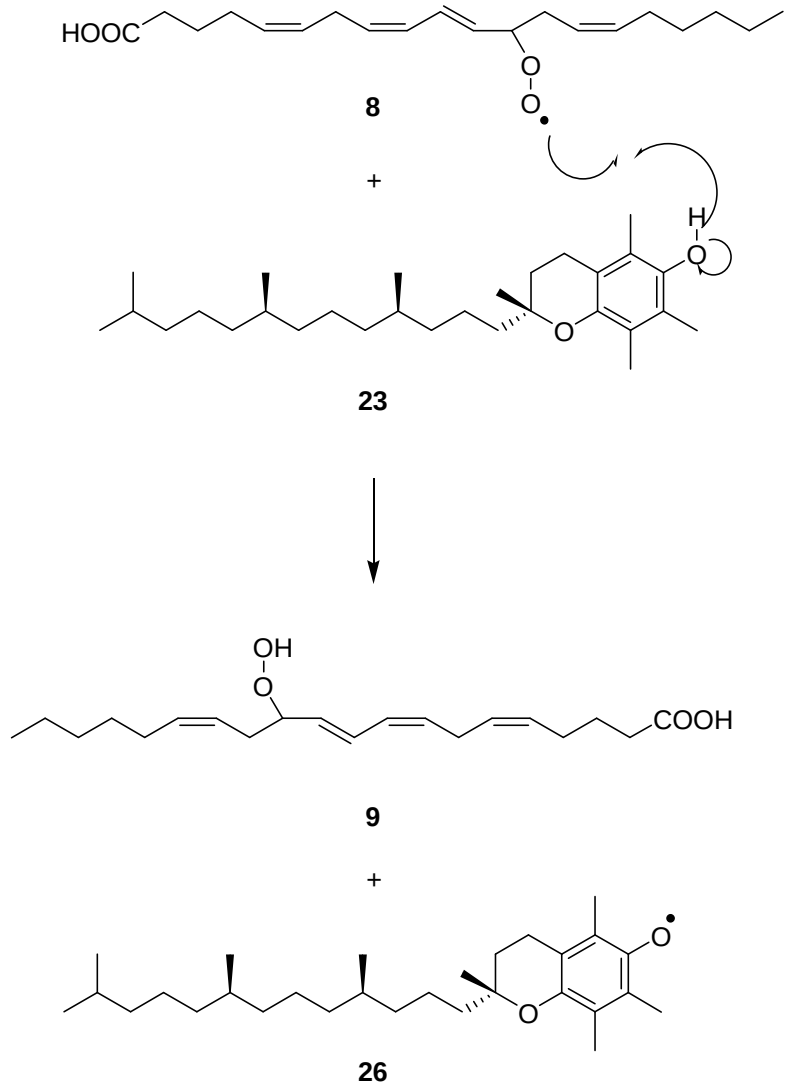

Scheme 11: α-tocopherol radical scavenging

Recycling of α-tocopherol can be achieved by ascorbate **22**. At the membrane/water interface, water-soluble ascorbate **22**, can donate a hydrogen

atom to α-tocopheroxyl radical **26**, yielding α-tocopherol **23** and the ascorbate radical $Asc^{\bullet-}$ **24** (Scheme 12).

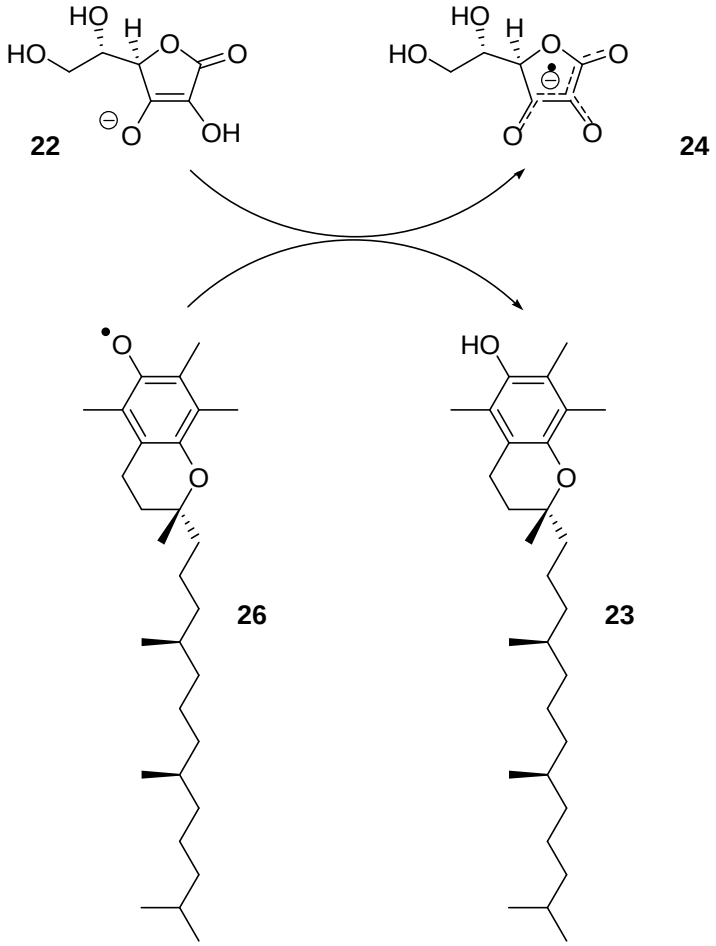

Scheme 12: Recycling of α-tocopherol by ascorbate

This radical can be removed via disproportionation to produce a molecule of **22** and one of DHA **25**. Other reducing agents such as GSH **20** and ubiquinone **1** have also been suggested as playing a role in the recycling of **23**.

Other compounds obtained from the diet have been proposed as *in vivo* antioxidants. Carotenoids are highly coloured, highly conjugated molecules. Different carotenoids have different head groups at the end of the central chain (Figure 14).

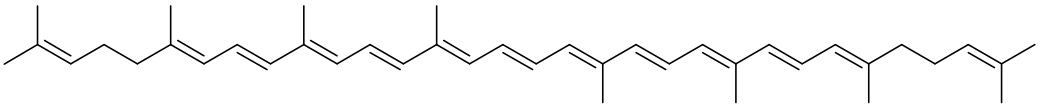

Lycopene **27**

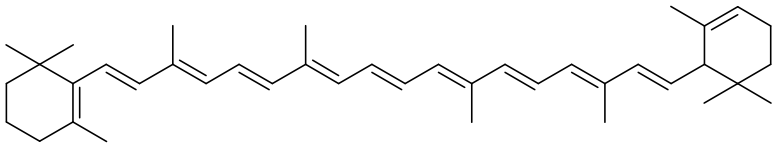

β-Carotene **28**

Figure 14: Two examples of carotenoids

They are found in many plants, for example tomatoes are rich in lycopene **27**. The main role of the carotenoids is as a precursor to retinol, or vitamin A, which is essential for vision. The carotenoids are excellent singlet oxygen quenchers and could potentially scavenge peroxyl radicals by forming carotenoid radicals or carotenoid-peroxyl radical adducts. However, the mechanisms of carotenoid antioxidant activity are complex and not fully understood.[20] Hartley and Kennedy have disputed the role of carotenoids as scavengers of radicals.[21] Indeed, under high oxygen conditions it is also possible for carotenoids to exert a pro-oxidant effect and β-carotene supplementation can lead to increased mortality in smokers.[22] Despite this, the health benefits of ingesting carotenoids have been extolled by many and Cambridge Theranostics have produced a lycopene tablet called Ateronon for the treatment of atherosclerotic conditions.[23]

Plant phenols are another class of molecules that can exert antioxidant effects *in vitro*. There are a huge number of members of this class, all containing one or more phenol groups. They act as radical scavengers via abstraction of their phenolic hydrogen atoms or by deprotonation followed by single electron transfer and some bi- and poly-phenols can also chelate metal ions. The most widely studied of these are the flavonoids and their related compounds, such as (+)-catechin **29** (found in green tea) and quercetin **30** (a flavonol found in onions) (Figure 15). However, these compounds must be absorbed to function as *in vivo* antioxidants and the evidence for this is conflicting. In fact it has been shown in rats that quecertin-4'-glucoside is not absorbed to any great extent, but is highly metabolised.[24]

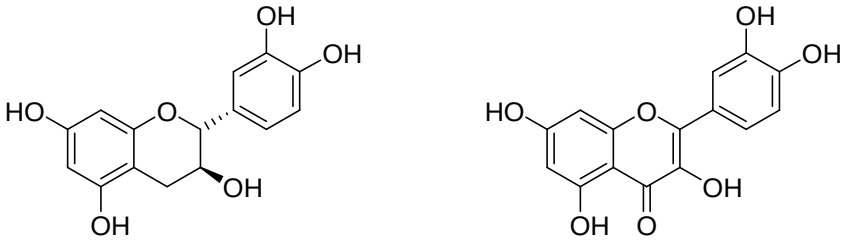

(+)-Catechin 29 **Quercetin 30**

Figure 15: Two examples of plant polyphenols

There are also a number of compounds synthesised *in vivo* that have antioxidant properties. Glutathione **20** has already been discussed. Another example is bilirubin **31** which is formed as an end product of the breakdown of haem. It can scavenge peroxyl and alkoxyl radicals as well as singlet oxygen. However, oxidative degradation of bilirubin can generate potentially dangerous vasoconstrictors.[2] α-Keto acids such as pyruvic acid **32** can also act as antioxidants, scavenging H_2O_2.[25] Ubiquinone **1** is an essential component of mitochondrial electron transport. *In vitro*, the ubisemiquinone radical intermediate **2** in the Q cycle (Scheme 3) can scavenge peroxyl radicals but around ten times slower than α-tocopherol **23**. However, ubiquinone **1** is also implicated in electron leakage during electron transport, one of the major sources of $O_2^{\bullet-}$.

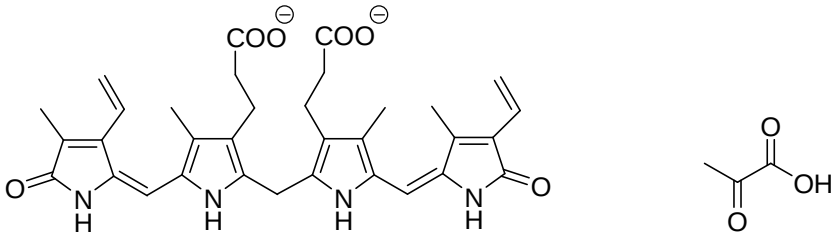

Bilirubin **31** Pyruvic acid **32**

Figure 16: Bilirubin **31** and pyruvic acid **32**

1.7 Implications of oxidative stress

So far the concept of oxidative stress has been introduced. The identity and origin of ROS, the damage they cause, and the defences that are present to limit this damage have all been discussed. Now I will discuss the implications this has for one of the most ubiquitous processes to affect organisms, ageing. In the present day it is expected that people will live into old age and largely due to advances in modern medicine the world's population is ageing at a rapid rate, the so-called 'demographic revolution'.[26]

Harman's free radical theory of ageing proposed that ageing was caused by the cumulative effect of a lifetime of "…deleterious side attacks of free radicals on cell constituents…".[4] In actual fact, the link between oxidative species and ageing was first postulated at the start of the 20th century by Rubner who observed an inverse relationship between metabolic rate and lifespan. The subsequent discovery of antioxidant enzymes such as SOD and the generation of ROS *in vitro* supported Harman's theory. It was later modified to place a central role on mitochondria which has been backed up by evidence that mutations in mitochondrial DNA (mDNA) are induced by oxidative stress and accumulate over time. There is also evidence that oxidative damage to proteins and DNA increases with age.

In recent years genetic manipulation of model organisms has been used to study the effect of over-expressing or "knocking-out" genes involved in oxidative stress. These studies have given conflicting results but many support the theory that free radicals play a role in the ageing process. The most notable of these include over-expression of mitochondrial-targeted catalase increasing maximum lifespan in mice.[27] Also over-expression of MnSOD in *Drosophila melanogaster* increases maximum lifespan[28] but mice over-expressing CuZnSOD show no extension.[29] On the other hand both mouse[30] and *Drosophila* CuZnSOD null mutants have shortened lifespan.[31] These findings support Harman's theory but do not yet give conclusive proof that ROS are the essential driver of ageing.

Oxidative stress has also been implicated in many age-related diseases including cancer, neurodegenerative diseases like Alzheimer's, diabetes and stroke. However in many cases it is unclear whether oxidative stress is a cause or a consequence of the disease. A full discussion of oxidative stress and disease is outside the scope of this introduction but the mechanisms are diverse and also require further research.

1.8 Conclusion

Oxidative stress is a complex biological process that is constantly ongoing within our bodies. ROS production and antioxidant defence are in a delicate balance and any disruption of this balance can cause a multitude of consequences. It is apparent that oxidative stress plays a complex role in ageing and disease and there is a growing body of evidence to support this theory, but there are also conflicting results and the process is still poorly understood. However, it is understandable that isolating and upregulating or "knocking out" single elements of the process may give confusing results as biological systems are very rarely that

simplistic and often organisms can compensate for changes through other components. Clearly further investigation is required before the free radical theory of ageing can be proved or disproved. A more likely conclusion is that ageing involves a multitude of mechanisms with oxidative stress being one. Other factors that play a role in lifespan determination such as caloric restriction and telomere erosion can be linked to oxidative stress, which supports this conclusion.

The study of oxidative stress is interesting due to its complexity and potential involvement in many diseases. Delaying or eliminating the onset of age-related disease could significantly benefit an ageing population both in quality of life and economically.

Chapter 2: The study of oxidative stress

2.1 Background

Oxidative stress is studied in an attempt to elucidate the role it plays in diseases and other biological processes. Due to the reactive nature of ROS, they are generally short-lived, transient molecules that are difficult to study directly. Therefore, methods have been developed to enable investigation of oxidative stress. All of these methods rely on the detection of a secondary species that has undergone reaction with ROS.

Detection of the biological markers of oxidative stress such as lipid peroxides can be used to detect oxidative stress. However, often these tests can give variable results and may in some cases generate the products that they are designed to detect.[2] Fluorescent probes can also be used to study the production of ROS. For example, oxidation of DCFH **33** leads to the production of dichlorofluoroscein **34** which strongly fluoresces at 525 nm (Scheme 13).[32]

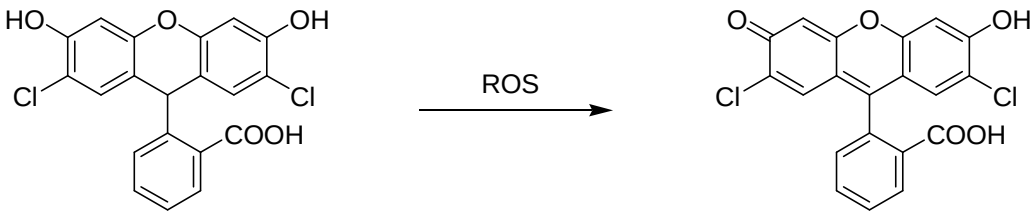

DCFH-Non-fluorescent **33**

Dichlorofluoroscein-fluorescent **34**

Scheme 13: Conversion of DCFH **33** to dichlorofluoroscein **34**

However there are a number of oxidising species that may cause this reaction so this test is not useful in identifying specific ROS. Furthermore, the assay itself appears to produce oxidising species in aerobic environments so the use of this probe may not have much validity.[33] Recently, fluorescent probes have been used successfully for the specific detection of H_2O_2. These rely on the oxidation of a boronate group to a phenol in the presence of H_2O_2 and will be discussed in greater detail in Chapter 6.

2.2 Introduction to EPR

Electron paramagnetic resonance (EPR) spectroscopy is a technique which only detects unpaired electrons.[34] It can be used to study free radicals, defects in materials, and paramagnetic metal complexes. The applications of EPR spectroscopy range from determining the spin state of a complex to monitoring the oxidative degradation of beer. Unlike the methods previously mentioned, EPR signals will only originate from unpaired electrons; therefore it is an unambiguous indicator of the presence of free radicals.

EPR spectroscopy works on a similar principle to that of NMR (nuclear magnetic resonance spectroscopy). An unpaired electron has a spin associated with it, resulting in a magnetic moment, M. When a magnetic field is applied to a sample, the electron can align itself in two orientations; parallel (low energy, $m_s = -1/2$) or antiparallel (high energy, $m_s = +1/2$) to the applied magnetic field, B_0. This is shown in Figure 17.

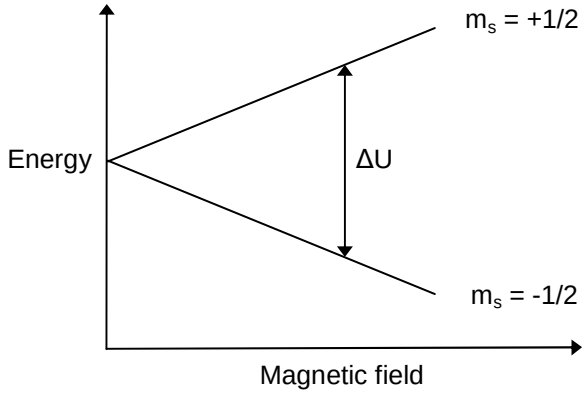

Figure 17: Splitting of energy levels of an unpaired electron

The energy difference (ΔU) between these two states is described in the equation:

$$\Delta U = g_e \mu_B B_0,$$

where g_e is the free electron g-factor and μ_B is the Bohr magneton ($927.400\ 915 \times 10^{-26}$ J T^{-1}). By substituting in two further equations:

$$\Delta U = \varepsilon \text{ and } \varepsilon = h\nu,$$

we arrive at the equation:

$$h\nu = g_e \mu_B B_0$$

By varying the magnetic field, B_0, and fixing the frequency, this equation can be satisfied and an electron can be promoted from the lower energy level to the higher one. This change in energy level is detected and gives a simple single line EPR spectrum as shown in Figure 18.

Figure 18: Single line EPR spectrum[35]

EPR spectra appear as the first derivative of the absorption peak as the signals tend to be broader than those of NMR spectra and this method allows for better interpretation of the data. Each EPR spectrum has individual spectral parameters that are characteristic for different radical species. The first of these is the g-factor which defines the position of the centre of the signal. The electron g-factor, g_e, is only fixed when an electron is free. In molecules, the unpaired electron feels a local magnetic field from the surrounding nuclei and atoms, as well as the applied magnetic field B_0. Therefore the effective magnetic field, B_{eff}, is a combination of these two fields and is dependant on the environment of the electron. It can be described as:

$$B_{eff} = B_0 + B_{local}$$

It is simpler to retain the term B_0 as this can be measured, so the equation is rewritten to include a variable g-factor, g.

$$h\nu = g_e\mu_B B_{eff} = g_e\mu_B B_0(1 - \sigma)$$
$$g_e(1 - \sigma) = g$$

where σ includes the effects of local fields and may be positive or negative.
Giving the final equation:

$$h\nu = g\mu_B B_0$$

The second spectral parameter of an EPR spectrum is the hyperfine splitting. Multiple line spectra are produced when an unpaired electron couples to a spin-

active nucleus. This is due to further splitting of the two energy levels by this nucleus. Each electronic energy level is split into 2N+1 energy levels by a nucleus with spin = N. Figure 19 shows the energy level diagram and resulting EPR spectrum for an electron split by a deuterium atom.

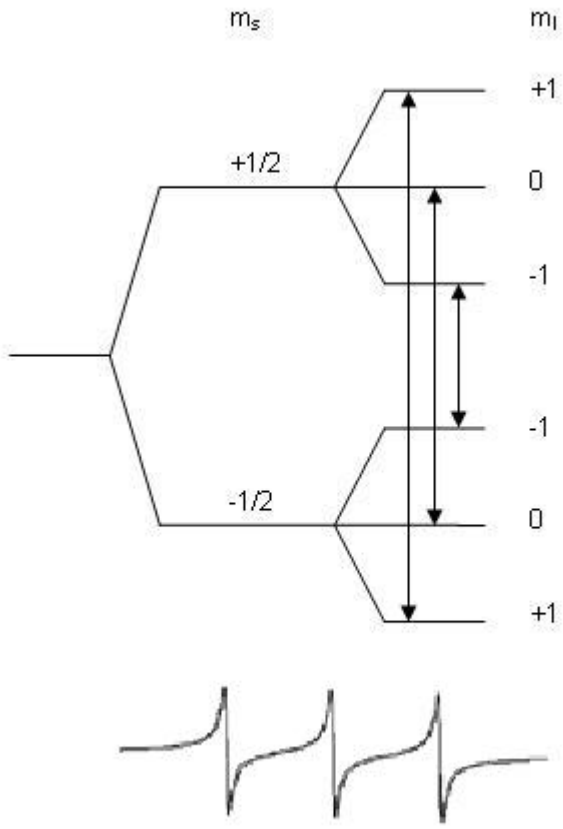

Figure 19: Energy level diagram and resulting EPR spectrum for an electron split by a deuterium nucleus[35]

Deuterium nuclei have spin = 1, therefore splitting each energy level into three new energy levels. EPR transitions follow the selection rules $\Delta M_s = \pm 1$ and $\Delta M_I = 0$, so there are three allowed transitions creating a three line EPR spectrum. The distance between these peaks is known as the hyperfine splitting and is measured in Gauss. Finally, line broadening of an EPR spectrum gives information about the rotational movement of the radical species. Broader lines indicate restricted motion. These spectral parameters provide information about the environment and identity of the radical species being studied.

2.3 Nitroxides

Nitroxides are stable oxygen-centred radicals with the general structure **35**. TEMPO (2,2,6,6-tetramethyl-1-piperidine-1-oxl) **36** is a common example (Figure 20).

35 TEMPO **36**

Figure 20: General structure and example of nitroxides

The stability of nitroxide radicals is achieved by two factors. Firstly, the nitroxide radical is resonance stabilised by interaction with the lone pair on the nitrogen atom (Scheme 14). Also, nitroxides usually contain alkyl substituents on the carbon atoms α to the nitrogen atom, which confer steric hindrance and hence protect the radical from attack. The dimerisation of nitroxide radicals is also unfavourable, both sterically and due to the formation of a weak O-O bond.

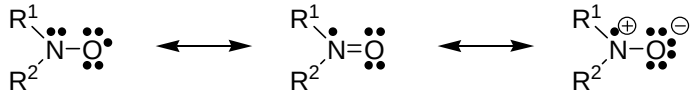

35

Scheme 14: Resonance stabilisation of nitroxides

Due to their stability and unpaired electron, nitroxides are useful tools for EPR spectroscopy. The EPR spectrum of a nitroxide can be used to provide information on the environment of the radical. For example, in site-directed spin labelling, one or more native amino acid residues are mutated to cysteines. Nitroxide spin labels, such as the methane thiosulfonate spin label **37** are covalently attached to these residues (Scheme 15).[36] By constructing a series of these spin-labelled proteins, information can be gleaned about secondary structure and which residues are involved in conformational changes using EPR spectroscopy.[37]

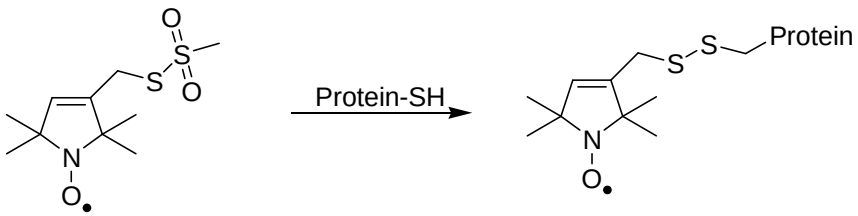

Spin label **37** Spin labelled side chain **38**

Scheme 15: Spin labelling of a cysteine residue

The redox chemistry of nitroxides gives them versatile functionality. In biological systems nitroxides can undergo two redox processes: oxidation to oxoammonium cations **40** and hydrogen atom abstraction from hydroxylamines **39** to give nitroxides (Scheme 16). The oxidation of nitroxides to oxoammonium cations and the back reduction is fully reversible, and the redox couple is tuneable through electronics and ring size selection. Reduction potentials ranging from 0.59 V to over 1 V in acetonitrile have been reported[38] and the stability of both nitroxides and oxoammonium salts has allowed development of this system for organic batteries.[39]

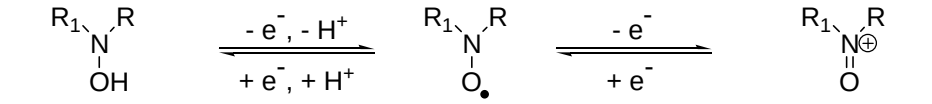

hydroxylamine **39** nitroxide **35** oxoammonium cation **40**

Scheme 16: Nitroxide redox processes

This redox couple is also relevant to oxidative stress and allows nitroxides to act as SOD mimetics, catalysing the disproportionation of $O_2^{\bullet -}$ to O_2 and H_2O_2 through oxidation to the oxoammonium cation **40** and re-reduction (Scheme 17). Consequently the potential for the use of nitroxides as therapeutic antioxidants has been explored.[40] A sub-set of nitroxides, the isoindolines will be further discussed in Chapter 4.

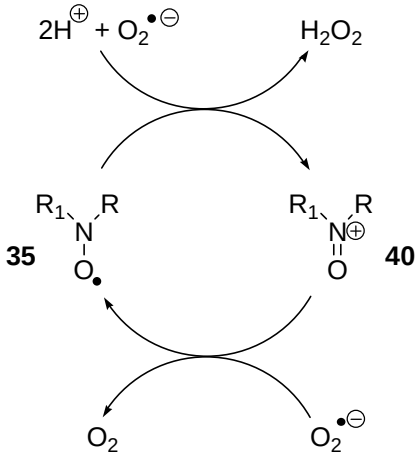

Scheme 17: Nitroxides as SOD mimetics

2.4 Hydroxylamine hydrogen-atom transfer agents

The hydroxylamine-nitroxide couple is not very accessible to electrochemical measurement due to the variety of protonation states possible at the hydroxylamine oxidation state. However, reactions between hydroxylamines and ROS are fast and both the bond dissociation energy, which determines reaction rate, and the pKa of the protonated hydroxylamine are easily tuned together.[41] Hydroxylamines can function as hydrogen-atom transfer agents and have been used in EPR spectroscopy studies. Hydroxylamines react with radical ROS or carbon-centered radicals ($Y^{\bullet}$) to give the same nitroxide radical regardless of the reacting species, e.g. TEMPO-H **41** gives TEMPO **36** upon reaction with either hydroxyl radicals or methyl radicals ($Y^{\bullet}$ = $HO^{\bullet}$ or $Me^{\bullet}$, Scheme 18).

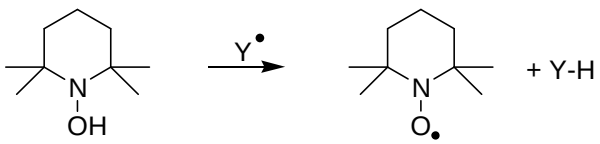

41 **36**

Scheme 18: Reaction of an H-atom transfer agent with radicals

The nitroxide product can be extremely stable (for reasons previously discussed) and a long-lived EPR signal is visualised, with a magnitude proportional to the amount of nitroxide present. The hydroxylamine can be selected to ensure that an uncomplicated, measurable EPR signal grows progressively when a well-chosen hydrogen atom transfer agent is exposed to ROS.

The two most commonly used hydroxylamine hydrogen atom transfer agents are TEMPONE-H **42** (Scheme 19) and CPH **44** (Scheme 20). The EPR spectrum of the nitroxide TEMPONE **43** is shown in Figure 21.

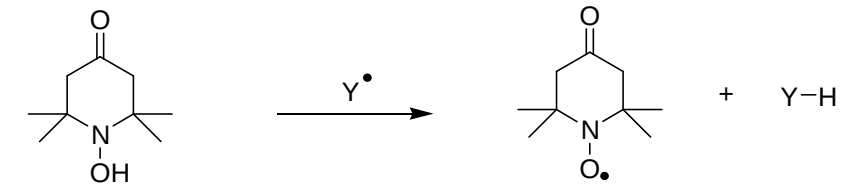

TEMPONE-H **42** TEMPONE **43**

Scheme 19

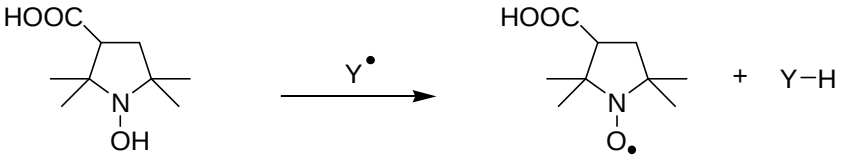

CPH **44** CP **45**

Scheme 20

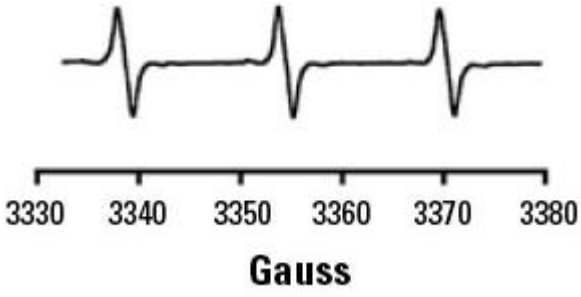

Figure 21: EPR spectrum of TEMPONE **43** (adapted from Miller *et al.* [42])

Dikalov and co-workers first demonstrated the use of TEMPONE-H **42** and CPH **44** for the quantification of superoxide, peroxynitrite ($ONOO^-$) and peroxyl radicals in chemical and biological systems, including vascular cell suspensions and whole blood samples.[43] A more recent example of the application of TEMPONE-H **42** is that of Miller *et al.*[42] They used this agent to assess the superoxide generation from solutions of diesel exhaust particulate (DEP) and found that even in the presence of SOD the nitroxide signal was not completely abolished. This work highlighted the fact that DEP does not require the recruitment of inflammatory cells to induce oxidative stress.

One of the limitations to the use of nitroxides in biological systems is their susceptibility to reduction back to their corresponding EPR silent hydroxylamines, resulting in a decrease in signal magnitude. Dikalov and co-workers subjected TEMPONE **43** and CP **45** to the biological reductants cysteine, glutathione **20** and ascorbate **22**, and to smooth muscle cells.[44] Both were reduced by cysteine at a

similar rate, while reduction of TEMPONE **43** by glutathione and in smooth muscle cells occurred at approximately twice the rate of CP **45**. The largest difference between nitroxide reduction was when ascorbate **22** was used as the reductant. TEMPONE **43** was reduced to TEMPONE-H **42** at an almost 70-fold greater rate than CP **45** reduction proceeded. Although reduction regenerates rather than destroys the hydrogen atom transfer agents, clearly this result indicates that care must be taken when using these agents in biological systems to avoid the generation of artificially low measurements of ROS due to this back reaction. Another limitation of hydrogen atom transfer agents is that they do not allow the reacting species to be identified. Other stable radicals known as spin traps have been developed for this purpose.

2.4 Nitrones and spin trapping

As previously discussed, many ROS are radicals and therefore have one or more unpaired electrons. However, the ROS responsible for oxidative stress are too short lived for direct detection by EPR spectroscopy. Therefore a technique called spin-trapping was developed.[45] Spin trapping involves the addition of a short-lived radical to another molecule (a spin trap) to form a new radical species, a spin adduct e.g. nitroxide **47** is formed by nitrone **46** reacting with a radical $Y^{\bullet}$ (Scheme 21). Spin adducts are characteristically longer-lived radicals that can be detected, and sometimes identified, using EPR spectroscopy. In addition to this, spin traps exert an antioxidant effect by converting highly reactive radical species into relatively stable radicals. The use of spin traps has been well reviewed[46] and the discussion that follows concentrates on the aspects of their design, synthesis and use that are most relevant to my work.

The most common class of spin trapping molecules are nitrones. Their general structure and spin trapping mechanism are shown in Scheme 21.

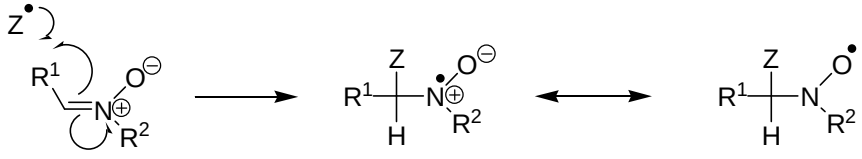

46 **47**

Scheme 21: Spin trapping by a nitrone

There are two common classes of nitrone spin trap; the acyclic aromatic-*tert*-butylnitrones e.g. PBN **48**, and the cyclic pyrroline-*N*-oxides e.g. DMPO **49**. This discussion begins with the acyclic spin traps before moving onto the cyclic spin traps and comparing the features of both.

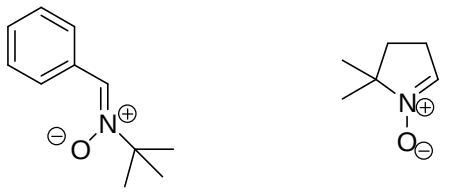

PBN **48** DMPO **49**

Figure 22: Structures of PBN and DMPO

The simplest way to synthesise PBN **48** and its analogues is via condensation of the corresponding aromatic aldehyde **50** with *tert*-butyl hydroxylamine (or another hydroxylamine if required) (Scheme 22).

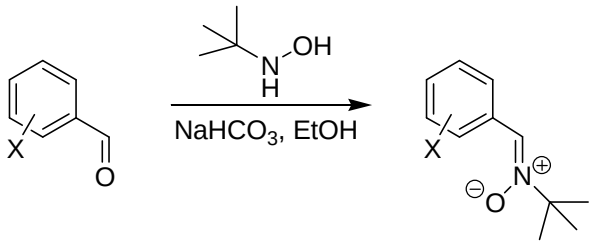

50 **51**

Scheme 22: Synthesis of PBN-type spin traps **51**

PBN-type spin traps form stable adducts with carbon-centred radicals. Figure 23 shows the EPR spectrum of the adduct **53** formed when the spin trap NXY-059 **52** traps the $^{\bullet}CH_2OH$ radical derived from methanol (Scheme 23).[47] The spectrum appears as a triplet of doublets due to hyperfine splittings from the nitrogen atom (triplet) and the β-hydrogen atom (doublet). Spin trapping requires a relatively high concentration of trap (mM) to observe an EPR spectrum, to ensure that the reactive radicals do not dimerise or react with other species present, and because some spin adducts have fairly short lifetimes themselves.

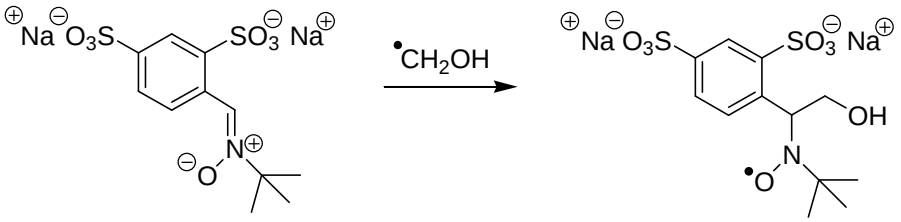

NXY-059 **52** **53**

Scheme 23

Figure 23: Reaction to form spin adduct and resulting EPR spectrum

Due to the availability of a wide variety of aromatic aldehydes, PBN analogues are readily synthetically accessible. PBN itself is relatively lipophilic, but substituted analogues have been synthesised in order to increase or decrease the lipophilicity. 4-POBN **54** is 1000 times more hydrophilic than PBN and has been successfully used as a spin trap. The ionic, water soluble spin traps S-PBN **55** and NXY-059 **52** have also been reported.[48] Gamliel *et al.* reported the synthesis of two families of lipophilic PBN-type spin traps made by attaching a long chain alkyl group on the aromatic ring of either a *tert*-butylnitrone (example **56**, Figure 24) or an admantylnitrone (example **57**, Figure 24).[49]

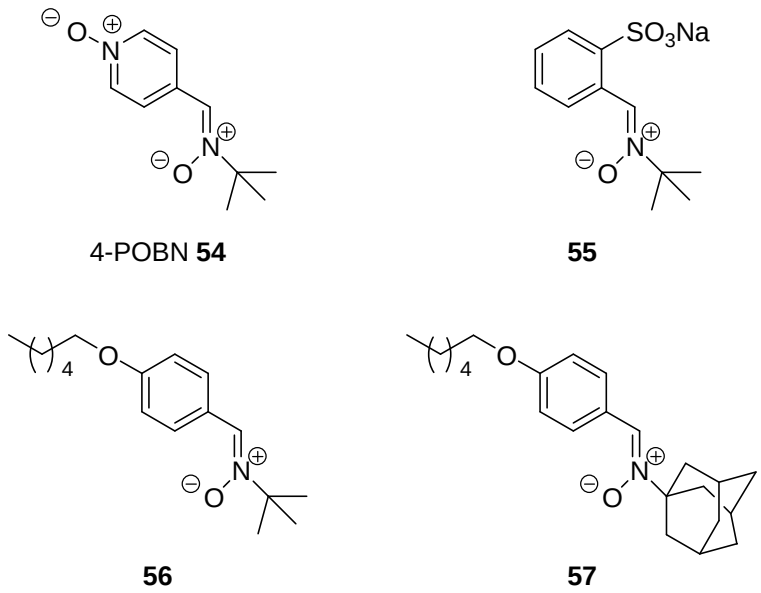

4-POBN **54** **55**

56 **57**

Figure 24: Examples of PBN analogues with varying lipophilicity

Analogues have also been produced in attempts to increase the stability of the adducts of trapping oxygen-centred radicals. Janzen and co-workers synthesised a series of PBN derivatives with different substituents on the aromatic ring and found that the rate of decomposition of their hydroxyl adducts was decreased by electron-withdrawing groups and increased by electron-donating groups.[50,51] Presumably, the hydroxy adducts **58** break down by a unimolecular fragmentation to give a benzylic carbocation stabilised by conjugation with a lone pair on the oxygen atom (Scheme 24). This process will be encouraged by electron-donating groups, particularly in the ortho or para positions, and discouraged by electron-withdrawing groups in the same position.

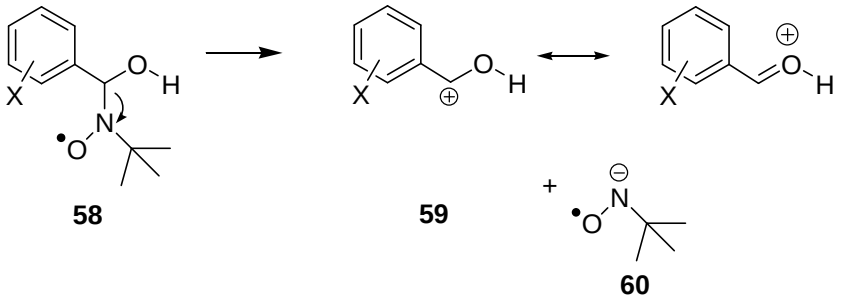

58 **59** **60**

Scheme 24: Breakdown of hydroxy adducts

A series of PBN analogues were designed that replaced one of the methyl groups of the *tert*-butyl group with a diethylphosphonate group with the aim of stabilising the superoxide adducts.[52] Two of these analogues, PPN **61** and 4-PyOPN **62** (Figure 25) had substantially longer-lived superoxide adducts compared with their

non-phosphorylated analogues. The half-lives of the superoxide spin adducts were 425 s, 307 s, 19 s and immeasurably short for the adducts of 4-PyOPN **62**, PPN **61**, 4-POBN **54** and PBN **48** respectively, at pH 5.8.

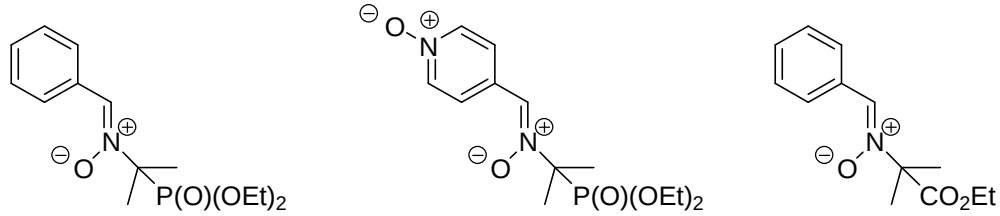

PPN **61** 4-PyOPN **62** EPPN **63**

Figure 25: PBN analogues with modified nitrone groups

The presence of the phosphorous atom also gives rise to an additional hyperfine splitting which enables easier identification of the trapped radical. A series of poly-phosphorylated analogues were also synthesised that showed even greater stability of the superoxide adduct at pH 5.8.[53] The spin trap EPPN **63** features an ethyl ester in place of one of the methyl groups of PBN **48**. This modification did not increase the stability of $HO^{\bullet}$ adducts, but did increase the half-life of the superoxide adduct to 408 s at pH 5.8.[54]

There have been several reported examples of PBN-type spin traps that contain a pyridinium cation (Figure 26). Janzen and co-workers reported the synthesis and spin-trapping properties of three pyridinium salt nitrone spin traps, 2-MePyBN **64**, 3-MePyBN **65** and 4-MePyBN **66**.[55] The spin adducts of these traps were found to be slightly longer lived than those of PBN or 4-POBN adducts.[56] 4-MePyBN **66** has been used to study the effects of sonolysis on H_2O/D_2O mixtures.[57, 58] The lipophilic nitrone 4-laurel PyBN **67** has also been reported.[55] Another lipophilic pyridinium salt nitrone, LinPyBN **68**, was used to study the production of phenyl radicals in erythrocytes treated with phenylhydrazine.[59] Two other pyridinium salt spin traps **69** and **70**, with bulkier nitrone groups, have also been reported.[55, 60] A notable point about these pyridinium salts that will be important in Chapter 5 is that they are all *N*-alkyl rather than *N*-aryl.

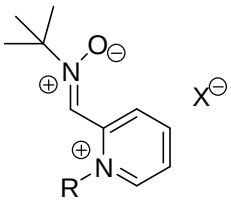

64, R = Me, X = $MeOSO_3$

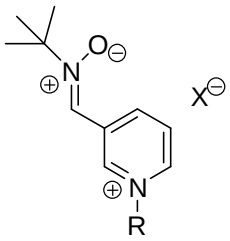

65, R = Me, X = $MeOSO_3$

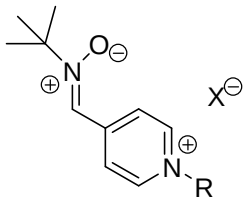

66, R = Me, X = $MeOSO_3$
67, R = $(CH_2)_{11}CH_3$, X = $MeOSO_3$
68, R = $(CH_2)_8CH{=}CH{=}CH_2CH{=}CH(CH_2)_4Me$, X = Cl

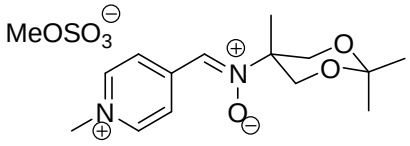

69

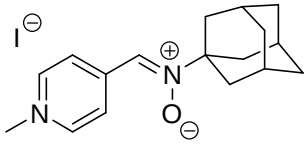

70

Figure 26: Examples of pyridinium salt PBN analogues

Acyclic nitrones have been investigated as therapeutics. Initially most investigations into their effects were carried out using PBN **48** and this nitrone has been shown to exert biological effects in a wide variety of experimental disease models. These include cancer, Alzheimer's disease, and stroke and have been recently reviewed by Floyd *et al*.[61] PBN analogues have also been developed as therapeutics and some examples will be discussed.

The damaging effects of a stroke are due to an interruption in blood flow to the brain and therefore a lack of oxygen (ischemia), followed by reoxygenation when blood flow is restored (reperfusion). Some brain cells die due to oxygen deprivation, but many potentially rescuable cells die when the blood flow is restored as reperfusion results in oxidative damage by ROS. In animal models of stroke PBN **48** was found to exert a neuroprotective activity even when administered after the ischemia/reperfusion insult. The spin trap NXY-059 **52** was developed by Centaur Pharmaceuticals and AstraZeneca and showed extremely promising results. It showed effective neuroprotectant activity at concentrations where PBN was ineffective and this was demonstrated in rodents and primates. Due to these successful findings NXY-059 **52** proceeded through human pre-clinical trials and was the subject of two Phase III clinical trials, known as the Stroke–Acute Ischemic NXY Treatment (SAINT) trials. The SAINT 1 trial involved 1722 acute ischemic stroke patients and used the modified Rankin Scale[62] as an endpoint determinant. In this trial NXY-059 **52** significantly increased scores when compared with placebo. A second, larger SAINT II trial was conducted in the

same manner with 3306 patients. Unfortunately, in this trial NXY-059 **52** had no significant effect compared with placebo and is no longer in development for the treatment of ischemic stroke. It is highly probable that this was because NXY-059 **52** cannot easily cross the blood-brain barrier due to the charged sulphonate groups and therefore cannot act as a neuroprotectant *in vivo*.

Pucci and co-workers have reported a number of glycosylated PBN spin traps, **71**-**78**, that have enhanced membrane-crossing capabilities.[63, 64] Administration of nitrone **74** to cultured fibroblasts with disrupted ETCs decreased caspase-3 mediated apoptosis.[65] LPBNAH **78** shows neuroprotective activity in rat hearts at lower concentrations than PBN **48**.[66]

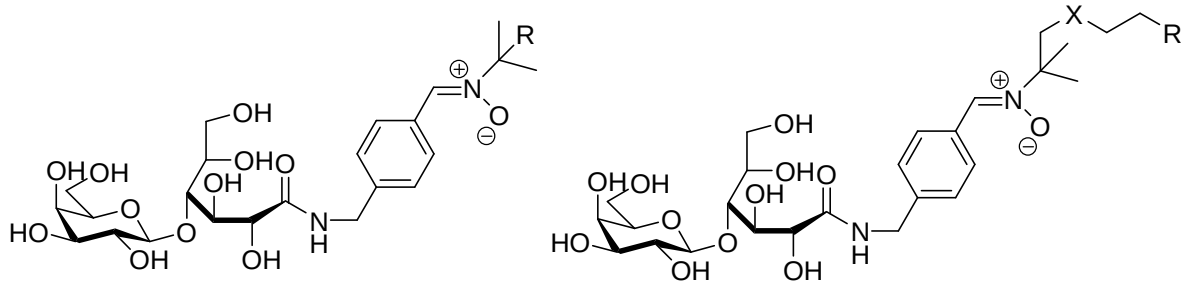

LAMPBN **71**, R = Me
LAMPPN **72**, R = P(O)(OEt)2

73, X = OCONH, R = C_4H_9
74, X = S, R = C_6H_{13}
75, X = S, R = C_6F_{13}
76, X = NHCO, R = C_5H_{11}
77, X = NHCO, R = C_6H_{13}
78, X = NHCO, R = C_7H_{15}

Figure 27: Glycosylated PBN analogues

These derivatives of PBN show interesting biological results, but glycosylation results in rather large molecules that can be synthetically demanding and nitrone **74** exhibited toxicity at 400 μM, close to its critical micelle concentration. This was attributed to a detergent property of these amphiphilic compounds.

Hartley and co-workers reported lipophilic PBN analogue DIDOD **79**, along with the amphiphilic spin traps Bu8C **80**, DOD8C **81** and Bu4C **83**, which had a hydrophilic carboxylate head group (at pH 7 in water), a lipophilic linker chain to a PBN-type spin trap, and a lipophilic anchor.[47] The spin traps differed by the lengths of the lipophilic linker and anchor chains.

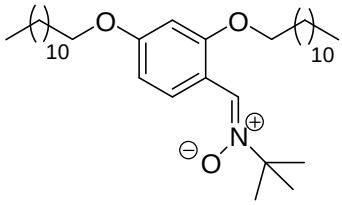

DIDOD **79**

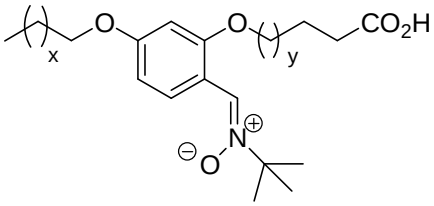

Bu8C **80**, x = 2, y = 5
DOD8C **81**, x = 10, y = 5
Bu6C **82**, x = 2, y = 3
Bu4C **83**, x = 2, y = 1

Figure 28: Long chain alkyl PBN analogues

The amphiphilic molecules were designed to detect radicals at the sites within membranes where they cause most damage. When incorporated into liposomes, all the amphiphilic nitrones **80**, **81** and **83** trapped carbon-centred radicals generated within membranes using a lipophilic copper(I) complex and ^{t}BuOOH. However, only DOD8C **81** gave an anisotropic EPR spectrum consistent with an adduct immobilised in the membrane following trapping of carbon-centred radicals derived from fatty acid side chains. Based on the observed spectra, the authors hypothesised that both DOD8C **81** and Bu8C **80** were incorporated into membranes, but that the adducts from Bu8C could move in a wagging motion. Adducts of DIDOD **79** in liposomes also gave anisotropic spectra, but due to their lack of carboxylate group, were free to bob up and down within the membrane (Figure 29).

The same group tested these nitrones, as well as a range of other amphiphilic nitrones as potential therapeutic antioxidants.[67] Bu6C **82** and Bu4C **83** were found to perform the best as antioxidants, protecting human diploid fibroblasts from oxidative injury from H_2O_2. Nitrones **82** and **83** were tested at their maximum non-toxic doses of 400 μM and 300 μM respectively. The pre-treated fibroblasts showed a substantial reduction in features of senescence following treatment with 150 μM H_2O_2. When compared to untreated cells and cells treated with 750 μM PBN **48** (maximum non-toxic dose), reduced expression of the senescence associated genes *p16* and *p21* was observed.

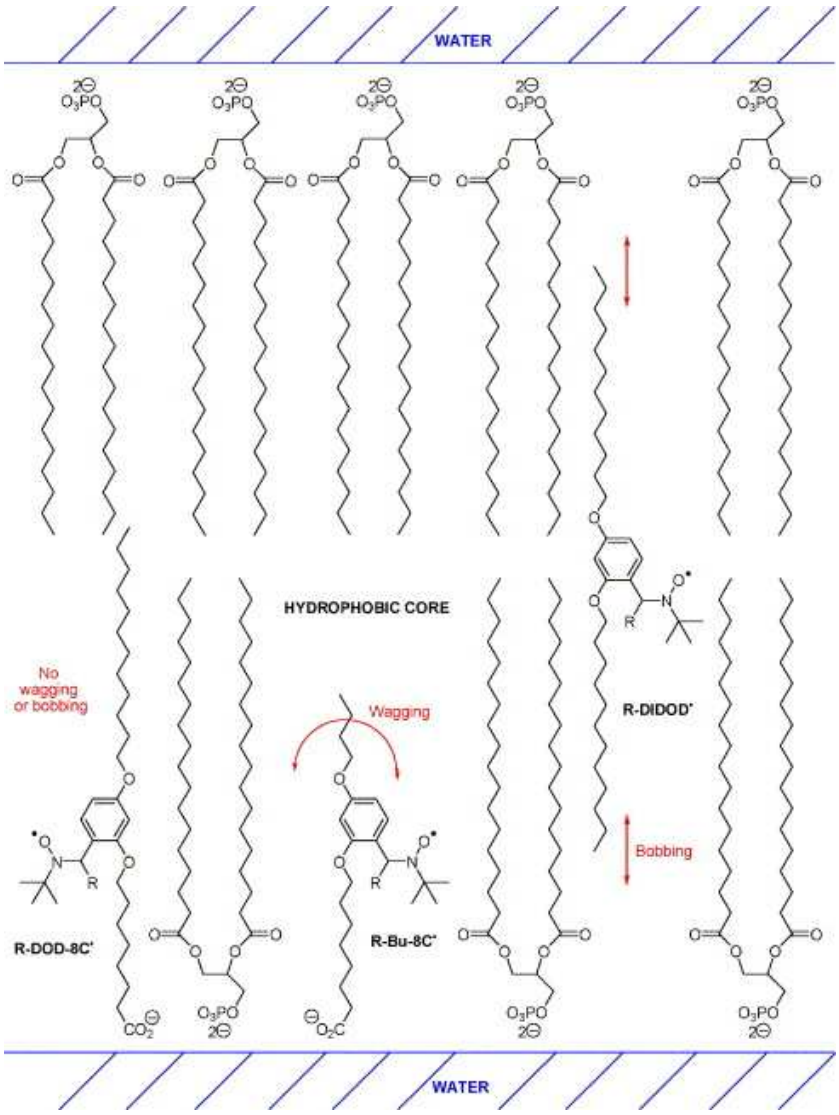

Figure 29: Localisation of alkyl derivatives in lipid membranes

The cyclic pyrroline-*N*-oxides such as DMPO **49** are much more efficient at trapping the oxygen-centred radicals $HO^{\bullet}$ and $O_2^{\bullet-}$ to form detectable adducts. However, the DMPO-OOH adduct **84** can undergo decomposition to form an acyclic by-product **85** and a hydroxyl radical, which can then be trapped by another molecule of DMPO **51** to form DMPO-OH adduct **86** (Scheme 25).[46]

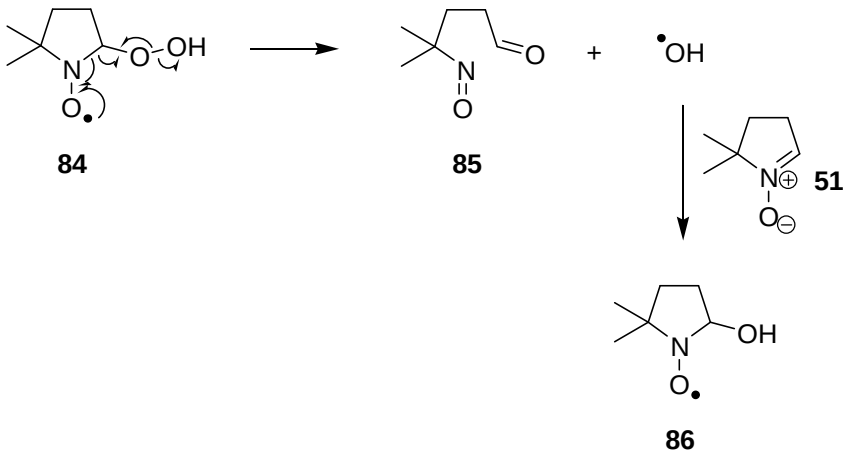

Scheme 25: Decomposition of the DMPO-OOH adduct **84**

Therefore, detection of the hydroxyl radical using DMPO **49** may be an artefact of this decomposition rather than actual $HO^{\bullet}$ production. Using similar strategies to those used with the PBN-type nitrones attempts have been made to find analogues which would increase the stability of the adducts to avoid this problem. Phosphorylated analogues such as DEPMPO **87** show improved stability of the $HO^{\bullet}$ and $O_2^{\bullet-}$ adducts due to the electron-withdrawing phosphonate group.[68] Other derivatives CMPO **88**[69], EMPO **89**[50] and BMPO **90** also show improved stability. Interestingly, CMPO is selective for the detection of the $HO^{\bullet}$ radical and either does not trap superoxide or forms an unstable adduct. There has been very little investigation of cyclic spin traps as therapeutics.

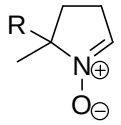

51, R = Me
87, R = $P(O)(OEt)_2$
88, R = COOH
89, R = COOEt
90, R = COO^tBu

Figure 30: Structure of DMPO analogues

2.5 Nitroso spin traps

Nitroso compounds can also be used as spin traps where they undergo the general reaction shown in Scheme 26 to form nitroxides.

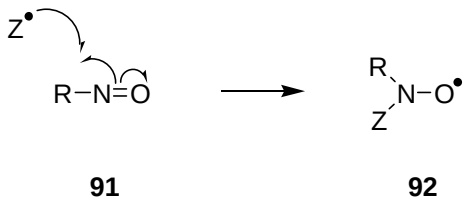

91 **92**

Scheme 26: Nitroso spin trapping

The most common nitroso spin traps are MNP (2-methyl-2-nitrosopropane) **93**, nitrosobenzene **94** and DBNBS (3,5-dibromo-4-nitrosobenzene sulphonate) **95** (Figure 31).[70]

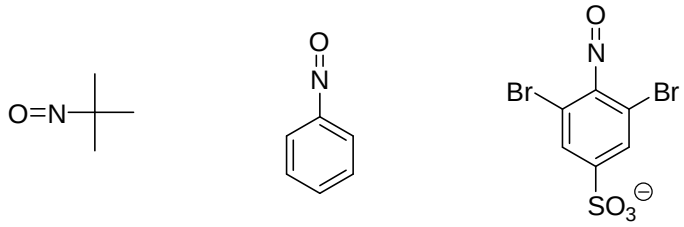

93 **94** **95**

Figure 31: Structures of nitroso spin traps

However compared to nitrones, nitroso compounds have been much less widely used as spin traps. This is largely due to their tendency to undergo side reactions which also form nitroxides and the very short lifetimes of their oxygen-centred radical adducts. They are also poorly water-soluble and tend to form dimers, with the exception of DBNBS **95**. In addition to this, nitroso compounds are known to be cytotoxic and mutagenic, therefore their use is largely limited to cell free studies.

2.6 Conclusion

Both hydrogen atom transfer agents and spin traps are useful EPR probes for detecting radicals. Hydrogen atom transfer agents give a very stable signal that is quantifiable but give no information on the identity of the reacting radical. The cyclic and acyclic spin traps allow identification of radicals from the EPR spectrum of the resulting adduct but this is not quantifiable. However as has been discussed some adducts are unstable, break down very rapidly and in some cases are undetectable by EPR spectroscopy. In the case of DMPO-OOH **84**, the decomposition of the adduct actually produces harmful ROS and gives a false spectrum. Therefore there is scope for the development of new EPR probes to study oxidative stress. As mitochondria are the major source of ROS production in the body, there is interest in targeting probes to them. By targeting spin traps and hydrogen atom transfer agents to this organelle, identification and quantification of radicals could be achieved. Additionally by converting highly reactive radicals to more stable ones spin traps and hydrogen atom transfer agents can also exert an

antioxidant effect, limiting the damaging reactions initiated by mitochondrial-derived radicals.

Chapter 3: Targeting mitochondria

Much of the ROS production implicated in oxidative stress originates from the mitochondria. For this reason it is desirable to target sensors of oxidative stress and antioxidants to mitochondria preferentially over other parts of the cell. This is desirable for a number of reasons. Targeting sensors to mitochondria allows the study of ROS production at the source, before further ROS-forming reactions can occur. This can give better information on the identity and quantity of ROS generated from the mitochondria and from this, a better understanding of the overall oxidative stress process. Targeting antioxidants to mitochondria allows them to mop up radicals at the source and stop damage occurring to the components of the mitochondria to other parts of the cell.

3.1 Delocalised, lipophilic cations as a mitochondria targeting strategy

As discussed previously mitochondria have a large membrane potential. This can be exploited for targeting purposes. Mitochondrial targeting has been successfully achieved through conjugation with delocalised, lipophilic cations (DLCs).[71] The positive charge is attracted to the negatively-charged mitochondrial matrix and the delocalisation of charge and the lipophilicity allow passage through the cell and mitochondrial membranes. The advantage of using lipophilic cations is that they require no specific uptake mechanism and are easily synthetically accessible. The degree of accumulation is related to the size of the membrane potential and can be calculated using the Nernst equation:

$$\Delta\psi = \frac{RT}{F} \ln \left(\frac{\text{Cation}_{in}}{\text{Cation}_{out}} \right)$$

where $\Delta\psi$ = membrane potential, R = gas constant, T = temperature and F = Faraday constant.

Converting to $\log_{10}$ gives:

$$\Delta\psi = \frac{2.303\ RT}{F} \log_{10} \left(\frac{\text{Cation}_{in}}{\text{Cation}_{out}} \right)$$

Replacing R,T and F gives a useful form of the equation for monovalent cations:

$$\Delta\psi = 61.5 \log_{10} \left(\frac{\text{Cation}_{in}}{\text{Cation}_{out}} \right)$$

The typical values given for the mitochondrial membrane potential range from 140-180 mV, which gives an accumulation of ~200-300 fold within mitochondria compared to the cytoplasm (Figure 32).

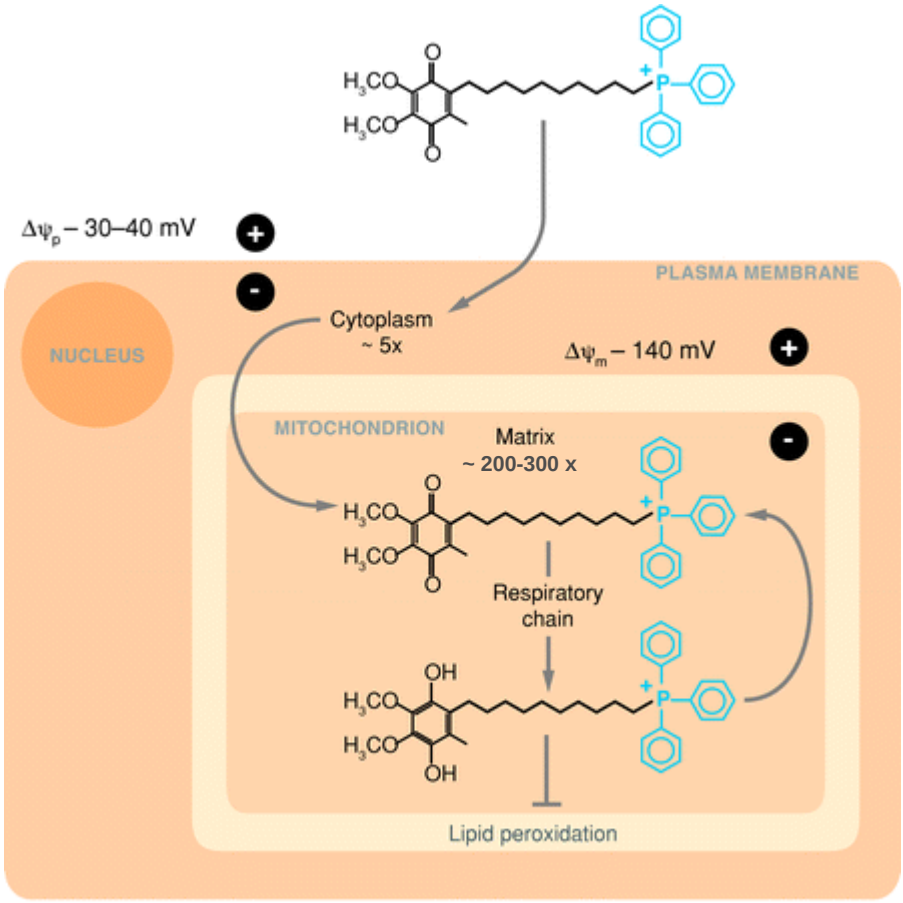

Figure 32: Mitochondrial targeting with DLCs (taken from Murphy and Smith[71])

The most widely used and well-characterised DLC for targeting molecules to the mitochondria is the triphenylphosphonium (TPP) cation which was originally used to investigate the mitochondrial membrane potential. Its use in targeting antioxidant compounds to mitochondria was developed by the groups of Murphy and Smith, but has subsequently been used by others. Other DLCs including alkylpyridinium cations have been used to target mitochondria (but rarely for the study of oxidative stress) and fluorescent lipophilic cations such as rhodamine

have been used for mitochondrial staining. In the discussion of the literature that follows the anionic counter ion is omitted from structures as this is exchangeable *in vivo*, can change from step to step in a synthesis and can be set by ion exchange at the end of a synthesis.

3.2 Antioxidants targeted with triphenylphosphonium cations

A number of known antioxidants targeted to mitochondria by the TPP group have been synthesised and their structures are shown in Figure 33. MitoE_2 **96** is a targeted version of d-α-tocopherol **23** that scavenges radicals in the same way (Chapter 1, Scheme 11). MitoE_2 was shown to be more effective at preventing lipid peroxidation in isolated mitochondria than d-α-tocopherol **23** itself.[72]

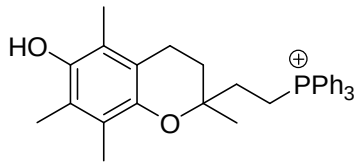

MitoE_2 **96**

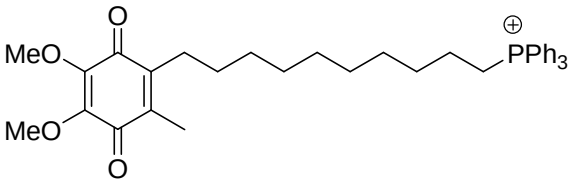

MitoQ **97**

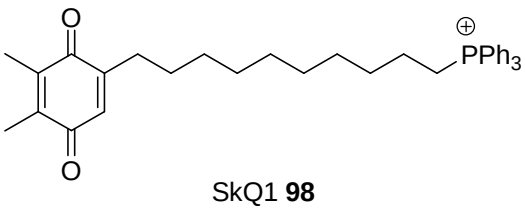

SkQ1 **98**

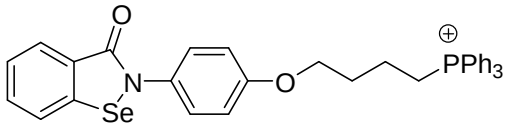

MitoPeroxidase **99**

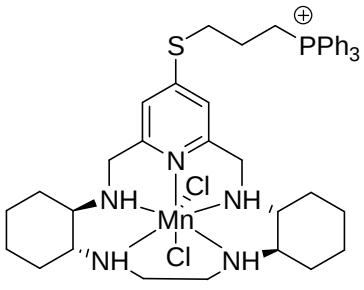

MitoSOD **100**

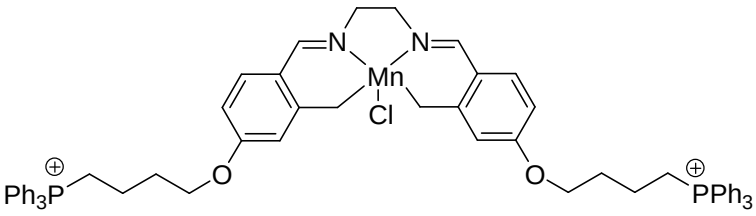

JD-29 **101**

Figure 33: Antioxidants targeted to mitochondria using TPP

MitoQ **97** is a mitochondria-targeted version of ubiquinone **1** that contains a 10-carbon linker between the ubiquinone and the TPP moiety.[73] This chain length

was chosen specifically to sink the ubiquinone group into the mitochondrial inner membrane at a specified depth. The positively charged head group remains embedded at the inside surface of the mitochondrial inner membrane while the lipophilic alkyl chain can enter the membrane, inserting the ubiquinone to a known depth. This depth is the region where it is believed that most ROS are produced and where the anti-oxidant would be most effective. Once in the membrane, MitoQ **97** is reduced *in situ* by complex II of the ETC to form ubiquinol **102** (Figure 34) which reacts with and terminates radical species, forming a radical intermediate which is then recycled back to MitoQ **97**.[74]

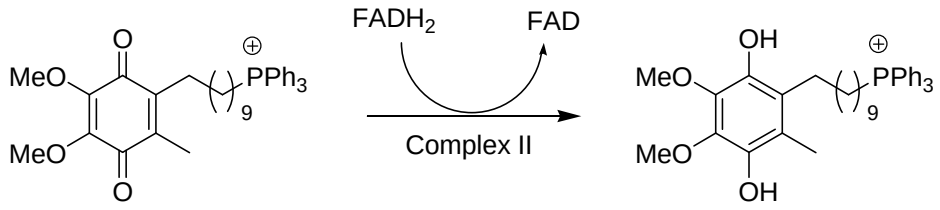

MitoQ **97** **102**

Figure 34: MitoQ **97** is reduced to **102** by the mitochondrial electron transport chain

MitoQ **97** has been shown to exert an antioxidant effect in a number of mitochondria and cell models, primarily by preventing lipid peroxidation.[71] MitoQ **97** is currently in clinical trials for the treatment of hepatic inflammatory disorders caused by oxidative stress, including non-alcoholic steatohepatitis (NASH), and for dermatological applications.[75]

As part of a large collaborative "megaproject" started in 2003 at the Lomonosov Moscow State University in Russia, a number of mitochondria-targeted antioxidants structurally related to MitoQ **97** have been reported.[76] In 2008 a series of 5 articles were published detailing the results of studies on the antioxidant and therapeutic properties of these compounds.[77,78,79,80,81] SkQ1 **98** is the most successful example and incorporates a plastoquinone moiety rather than a ubiquinone one. Plastoquinone is the chloroplast equivalent of ubiquinone **1**. SkQ1 functions as an antioxidant at very low concentrations via a similar mechanism to that of MitoQ **97**, forming the reduced compound $SkQ1H_2$. SkQ1 **98** protected human fibroblasts from H_2O_2-induced apoptosis and mitochondrial fragmentation at lower concentrations than that required by MitoQ. It was also effective against cancer, suppressing tumour formation in p53 null mice. SkQ1 **98** also prevented the development of age-induced cataracts and retinopathies in a

rat model of progeria (accelerated ageing). A number of eye diseases, including age-dependant cataracts, retinopathy and glaucoma, were also successfully treated in a number of animals by direct administration of SkQ1 solutions to the eyes. Finally, SkQ1 **98** has been shown to prolong the lifespan of 4 species, including mice. SkQ1 **98** appears extremely promising as a therapeutic antioxidant for the treatment of age-related conditions, particularly considering that MitoQ is already in clinical development.

MitoPeroxidase **99**, a mitochondria-targeted version of the peroxidase mimetic ebselen **103** has been reported.[82] Ebselen **103** functions as a peroxidase mimetic due to the presence of the selenium atom in its structure. The catalytic cycle is shown in Scheme 27.

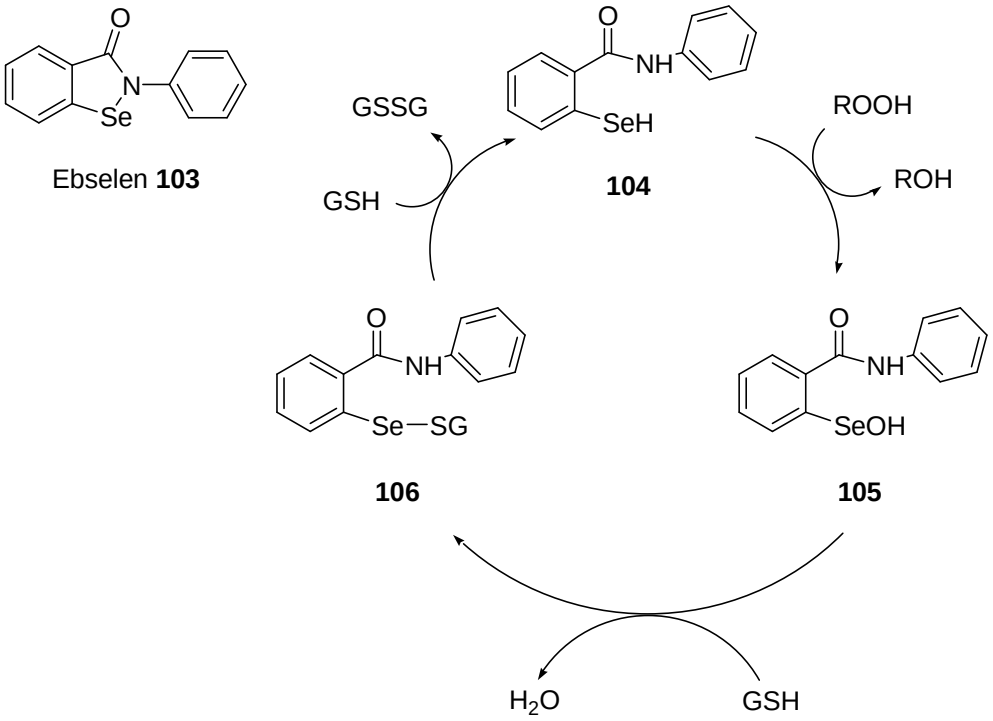

Scheme 27: Catalytic cycle of peroxidase activity of ebselen **103** [83]

The catalytically active species is ebselen selenol **104** which is oxidised to the selenenic acid **105** with simultaneous reduction of a peroxide substrate. In the next step, GSH **20** displaces the -OH group of the acid to form ebselen selenosulphide **106** with the release of water. Finally, a second molecule of GSH **20** enters, producing a molecule of GSSG **21** and regenerating ebselen selenol **104**. MitoPeroxidase **99** functions as a peroxidase and protected isolated mitochondria from lipid peroxidation under oxidative stress induced by H_2O_2 addition.

MitoSOD **100** is a mitochondria-targeted version of the SOD mimetic M40403 which is currently in clinical development for the treatment of radiation-induced oral mucositis, a side effect of cancer radiation therapy.[84] Another SOD mimetic, the salen-manganese complex EUK-134, was targeted to mitochondria by conjugation with a TPP cation to form JD-29 **101**. JD-29 **101** was tested in HeLa cells for its ability to prevent apoptosis when treated with either staurosporine or sodium selenite.[85] Unfortunately, in this study both JD-29 **101** and untargeted EUK-134 were ineffective against staurosporine-induced apoptosis and performed equally against sodium selenite-induced apoptosis.

3.3 Nitroxides targeted with TPP cations

The nitroxides TEMPOL **107** and CP **45** have been targeted to mitochondria by conjugation with TPP cations to form TEMPOL-TPP **108**, MitoTEMPOL **109** and MitoCP **110** (Figure 35).

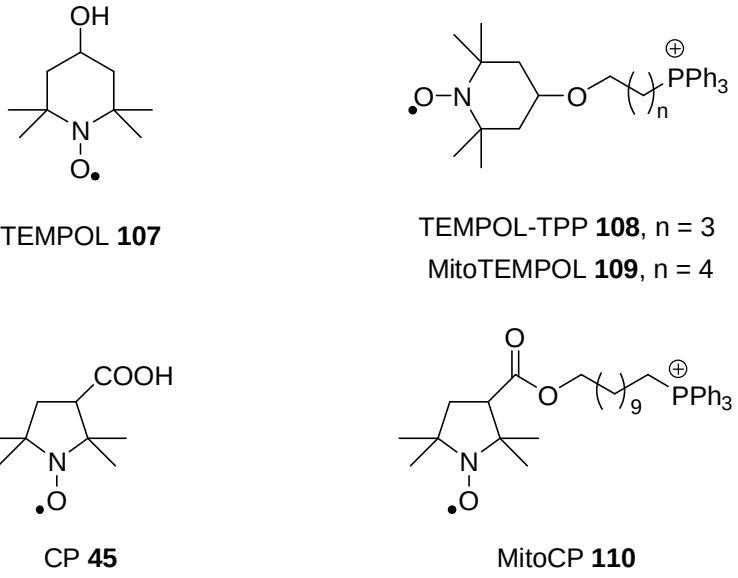

TEMPOL **107**

TEMPOL-TPP **108**, n = 3
MitoTEMPOL **109**, n = 4

CP **45**

MitoCP **110**

Figure 35: Nitroxides targeted to mitochondria using TPP and their parent nitroxides

TEMPOL-TPP **108** was reported in 2002 by Dessolin *et al.* who studied its ability to prevent apoptosis in HeLa cells treated with either staurosporine or sodium selenite in the same study as JD-29 **101**.[85] In this study, both TEMPOL-TPP **108** and TEMPOL **107** were ineffective against staurosporine-induced apoptosis and performed equally against sodium selenite-induced apoptosis. The authors argued that there were a number of possible reasons for these results, including inefficient targeting by TPP, however they never tested this hypothesis. In 2008 Murphy and co-workers reported the synthesis of MitoTEMPOL **109** which is very

close in structure to TEMPOL-TPP **108** and confirmed its accumulation in mitochondria.[86] They found that MitoTEMPOL **109** was reduced to its corresponding hydroxylamine MitoTEMPOL-H **111** in mitochondria by ubiquinol **3**, (Scheme 28). In this form, MitoTEMPOL-H **111** performs as an antioxidant. MitoTEMPOL **109**, like other piperidine nitroxides, can act as a SOD mimetic (Chapter 2, Scheme 17) and is also capable of oxidising Fe(II) to Fe(III), reducing the capacity of a system to produce $HO^{\bullet}$ through Fenton chemistry (Chapter 1, Scheme 1). MitoTEMPOL-H **111** was incapable of either of these functions and exerts its antioxidant activity through hydrogen atom transfer.[87] This was demonstrated by the ability of MitoTEMPOL-H **111** to protect against lipid peroxidation significantly better than MitoTEMPOL **109**. Finally, MitoTEMPOL **109** can prevent oxidative damage to mitochondrial DNA (mtDNA) in cultured murine C2C12 cells. Oxidative stress was induced by addition of menadione, a compound which stimulates superoxide production, and the mtDNA damage was measured by amplification using quantitative PCR (polymerase chain reaction). The presence of MitoTEMPOL **109** decreased the damage caused, demonstrating its ability to act as an antioxidant, most likely as the hydroxylamine MitoTEMPOL-H **111**.

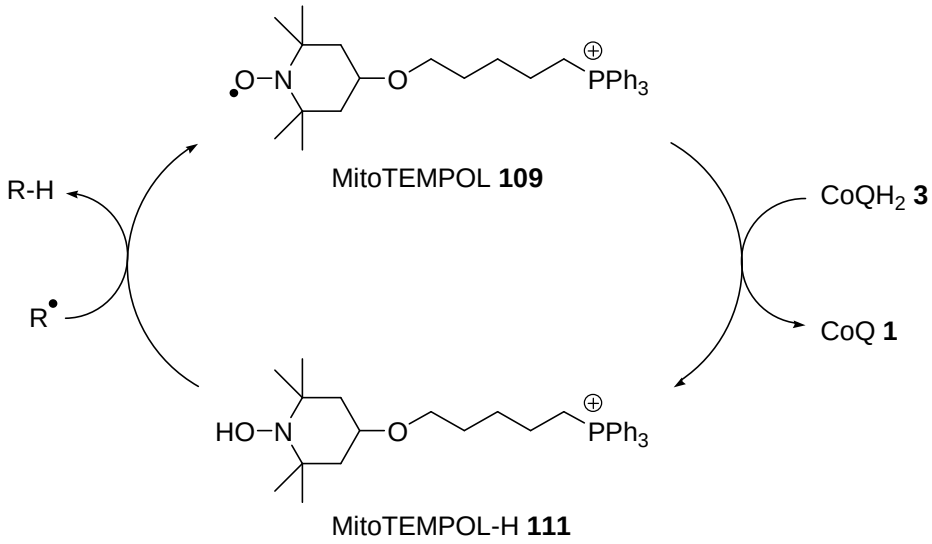

Scheme 28: MitoTEMPOL **109** and MitoTEMPOL-H **111** cycling

The mitochondria-targeted nitroxide MitoCP **110** was reported in 2005 and shown to protect bovine aortic endothelial cells from peroxide-induced oxidative damage and apoptosis.[88] MitoCP **110** has been used in a few subsequent studies including for the prevention of nerve growth factor (NGF)-induced apoptosis and also prevented mitochondrial dysfunction in motor neurons with a SOD1

mutation.[89,90] There is also a patent application for its use as a mitochondrial specific MRI contrast agent.[91]

As discussed in Chapter 2, the pyrrolidine nitroxide CP **45** is significantly less susceptible to reduction to the corresponding hydroxylamine compared with the piperidine nitroxide TEMPONE **43**. Due to this, CP **45,** and other pyrrolidine nitroxides such as MitoCP **110,** predominantly undergo the alternative antioxidant cycling process where they are oxidised by superoxide to the oxoammonium ion and then reduced by superoxide to regenerate the nitroxide, thus behaving as SOD-mimetics.[87] Due to these differences in antioxidant mechanism, comparison of MitoTEMPOL **109** and MitoCP **110** would be useful for the elucidation of the role of hydroxylamines in the antioxidant activity of nitroxides.[86]

3.4 Nitrones targeted with TPP cations

Four examples of mitochondria-targeted nitrone spin traps have been reported and are shown in Figure 36. MitoPBN **112** is an acyclic PBN-derivative[92], MitoDEPMPO **113**[93] and MitoBMPO **114**[94] are targeted versions of existing cyclic spin traps and MitoSpin **115** is a fused ring cyclic nitrone spin trap.[95]

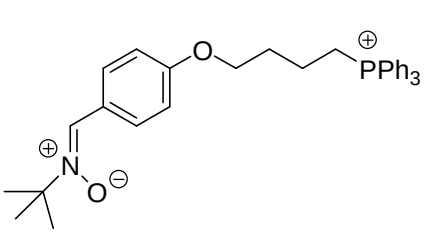

MitoPBN **112**

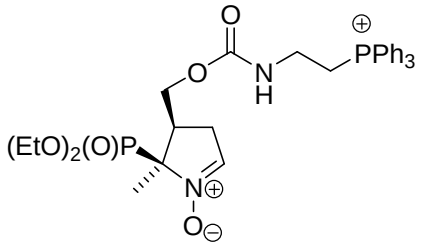

MitoDEPMPO **113**

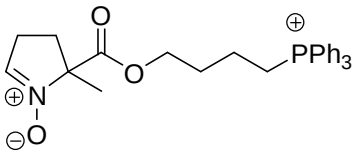

MitoBMPO **114**

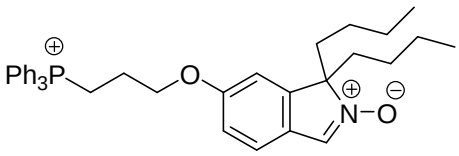

MitoSpin **115**

Figure 36: Nitrones targeted to mitochondria using TPP

Uncoupling proteins (UCPs) can be activated in mitochondria by superoxide and lipid peroxidation products such as 4-HNE **10**. MitoPBN **112** was synthesised and used to probe these pathways to elucidate whether activation by superoxide and by the peroxidation product are independent of each other, or if they are different

parts of a common pathway of UCP activation.[92] MitoPBN **112** was found to block the activation of all mammalian UCPs when superoxide was the initiator but not when 4-HNE **10** was used. This led to two possible mechanisms; either superoxide is required to form lipid peroxidation products downstream, or the two work via different pathways. It was argued that MitoPBN **112** does not react with superoxide or lipid peroxidation products, but it does react with carbon-centred radicals derived from 2,2'-azobis(2-methylpropionamidine) dihydrochloride (AAPH) and can block the initiation of lipid peroxidation by these radicals. It was proposed that there is a single pathway, where superoxide initiates the production of carbon-centred radicals which in turn initiate lipid peroxidation and activiate UCPs. MitoPBN **112** blocks the formation of these radicals so lipid peroxidation cannot occur. However it was unable to prevent activation with 4-HNE **10**, as these products appear further downstream in the pathway. Supporting this hypothesis, carbon-centred radicals formed by AAPH were shown to activate UCPs. MitoPBN **112** was considered crucial to this investigation due to its specific reaction with carbon-centred radicals. However, it must be remembered that the absence of a detectable, stable nitroxide adduct from superoxide and lipid peroxyl radicals does not rule out their transient formation and fragmentation.

Mitochondria-targeted cyclic nitrone spin traps MitoDEPMPO **113** and MitoBMPO **114** have also been published and shown to trap radicals. MitoDEPMPO **113** traps $O_2^{\bullet-}$, $HO^{\bullet}$ and glutathiyl radicals, with the MitoDEPMPO-OOH and MitoDEPMPO-SG adducts having longer half-lives compared to the corresponding DEPMPO **51** adducts.[96] In isolated mitochondria, MitoDEPMPO **113** trapped a mixture of $O_2^{\bullet-}$, $HO^{\bullet}$ and alkyl radicals, whereas DEPMPO **51** only exhibited a weak signal from the $HO^{\bullet}$ adduct. MitoBMPO **114** traps a variety of radicals, including $O_2^{\bullet-}$, $HO^{\bullet}$ and $^{\bullet}CH_2OH$. No decomposition of the MitoBMPO-OOH adduct to the MitoBMPO-OH adduct was seen, but the MitoBMPO-OOH adduct has a shorter half life than that of BMPO-OOH.

MitoSpin **115** is a cyclic nitrone spin trap that accumulates in mitochondria. It was designed to function as a traditional nitrone spin trap, however when attempts were made to trap $HO^{\bullet}$ radicals generated under Fenton conditions, an unexpected three line EPR spectrum was observed. After further investigation it appears that the MitoSpin-OH **116** adduct was rapidly converted to the nitroxide MitoSpinOx **118** via the hydroxylamine **117** (Scheme 29). This means that MitoSpin **115,** while not useful for identifying specific radicals, can function as a

targeted probe for general oxidative stress and also potentially as a targeted therapeutic.[95]

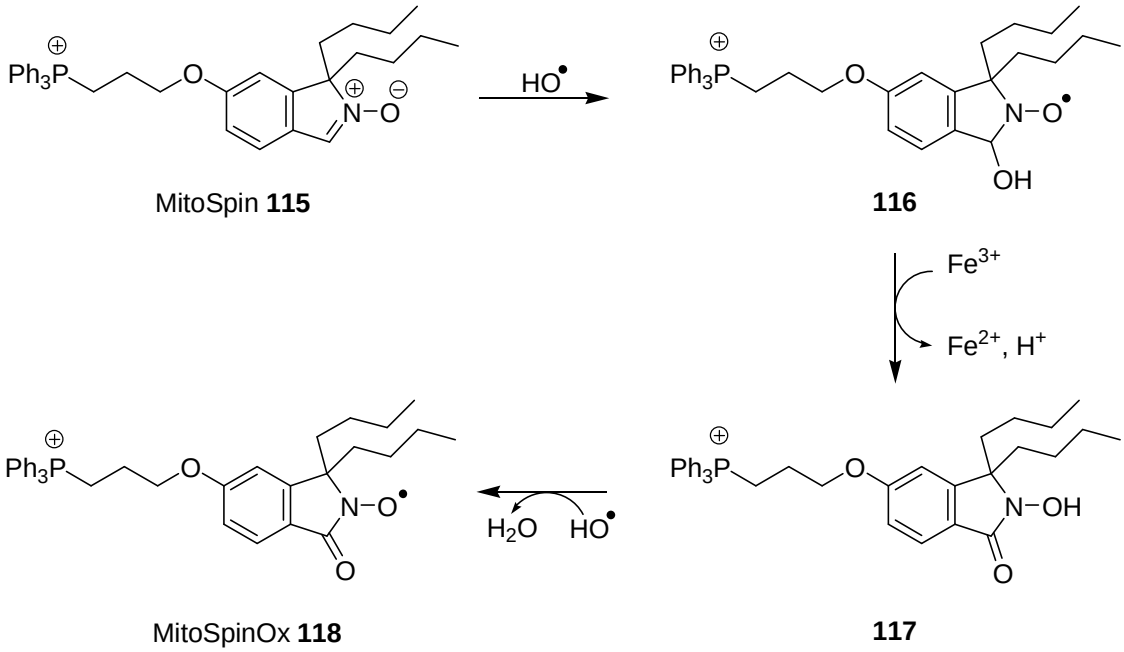

Scheme 29: Oxidation of MitoSpin **115** to MitoSpinOx **118**

Of the four reported TPP-conjugated nitrone spin traps, only the acyclic MitoPBN **112** and the cyclic MitoDEPMPO **113** have been used in isolated mitochondria and as yet there have been no reports of their use as therapeutics.

3.5 Fluorescent sensors targeted with TPP cations

MitoSOX™Red (or MitoHE) **120** is a commercially available fluorescent probe for mitochondrial superoxide which incorporates a TPP cation in its structure. It is a mitochondria-targeted version of the superoxide probe hydroethidium (HE) **119** and is selectively taken up by mitochondria.[97] Both MitoSOX™Red **120** and HE **119** exhibit fluorescence when excited at 510 nm, however this fluorescence has been attributed to both a specific superoxide oxidation product, HO-Mito-Etd$^+$ **122** and a non-specific oxidation product, Mito-Etd$^+$ **124** (Scheme 30).

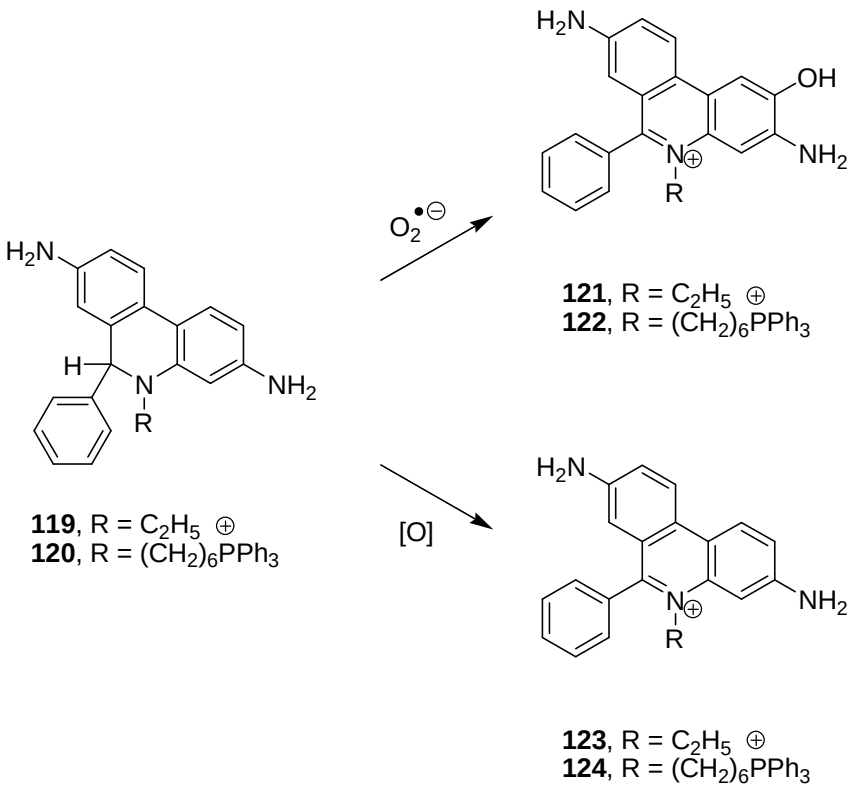

Scheme 30: Specific and non-specific oxidation of the superoxide probes HE **119** and MitoSOX™Red **120**

Robinson *et al.* reported that excitation at 396 nm improved results as the resulting fluorescence is only due to the specific superoxide oxidation products HO-Eth$^+$ **121** or HO-Mito-Eth$^+$ **122**.[97] Recently the TPP-conjugated fluorescent H_2O_2 probe MitoPy1 **125** was reported.[98] This probe will be discussed in detail in Chapter 6.

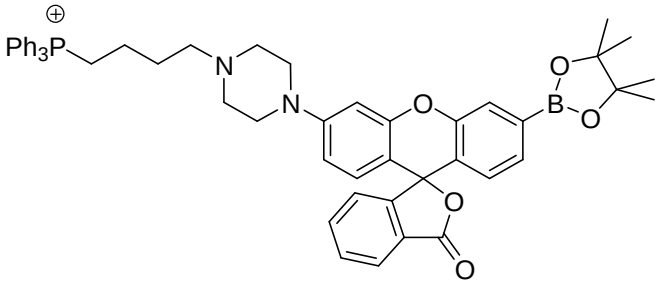

125

Figure 37: MitoPy1 **125**

3.6 Synthesis of TPP salts

The presence of a TPP cation can dramatically reduce the solubility of compounds in organic solvents, making them difficult to handle, difficult to purify and limiting the feasibility of further synthetic steps. Because of this, they are best introduced into a molecule as late in the synthetic scheme as possible. There are two main

ways of introducing a TPP cation into a molecule, both of which can be carried out towards the end of a synthetic route. The first is to directly displace a halide by heating with triphenylphosphine. This strategy was used in the synthesis of MitoQ **97**, shown in Scheme 31.[73]

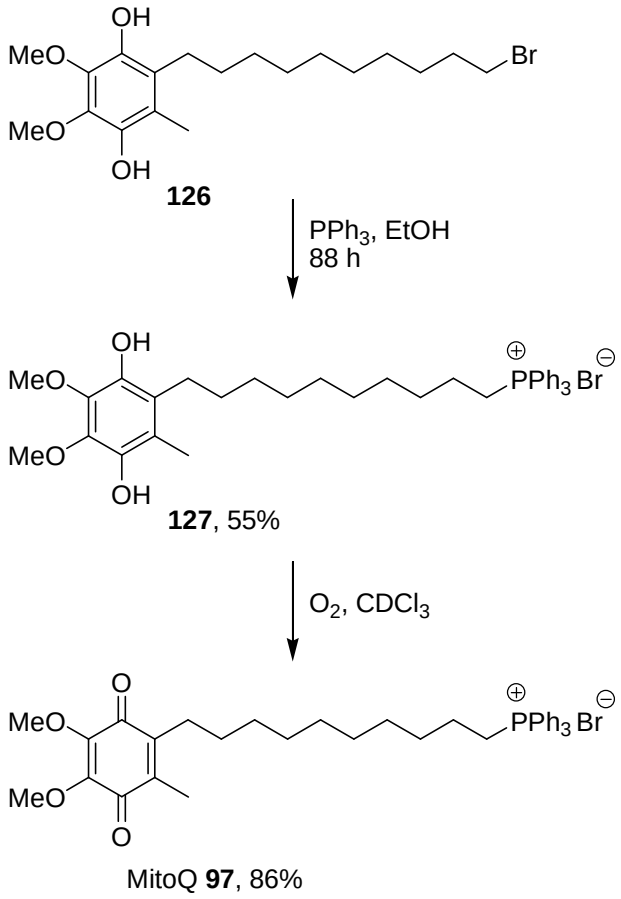

Scheme 31: Triphenylphosphine displacing a halide in the synthesis of MitoQ **97**

As is common for this displacement reaction, synthesis of TPP salt **127** requires a long reaction time at high temperature (88 h at 85 ℃) which is not always tolerated by the substrate. However, if the reaction is carried out in a relatively non-polar organic solvent, such as toluene, the product is insoluble and precipitates out of the solution. This drives equilibrium in favour of product formation and can make purification easier. However, there is often triphenylphosphine contamination which can prove difficult to remove and if more than one halide is present in the molecule there will be selectivity problems.

Alternatively, the TPP salt may be formed by displacement of a halide on another moiety and coupled to the portion of the molecule containing functionality in the final stages of the synthesis. This method allows removal of the TPP contaminants at an earlier stage of the synthesis and reaction times are generally

shorter. Scheme 32 shows the synthesis of MitoPBN **112** in which this strategy was utilised to attach 4-iodobutyl triphenylphosphonium iodide **129** through the phenol group of 4-hydroxybenzaldehyde **128** to introduce the TPP cation via an ether linkage.[92] The ether linkage is stable to biological cleavage and the yield of the coupling step was high. The authors were concerned about the potential sensitivity of the nitrone functionality, therefore they chose to introduce it in the final step of the synthesis via reductive condensation of 2-methyl-2-nitropropane with aldehyde **130**.

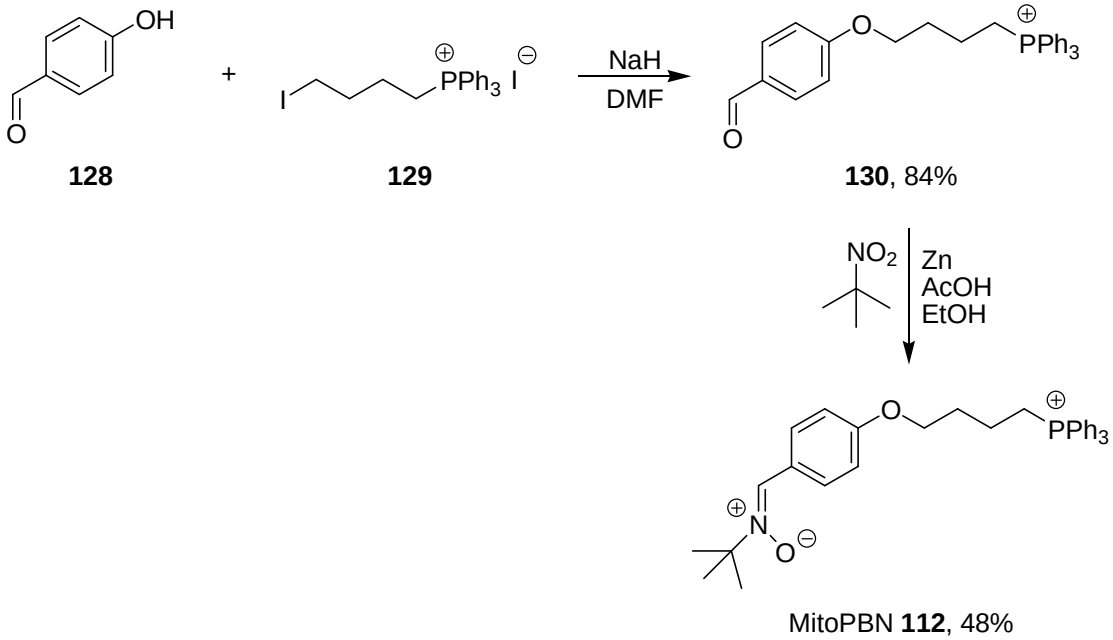

128 **129** **130**, 84%

MitoPBN **112**, 48%

Scheme 32: Synthesis of MitoPBN **112**

Other linkages such as esters can be used, however these may be susceptible to enzymatic cleavage if used in biological systems. In the final step of the synthesis of MitoDEPMPO **113** a carbamate linkage is formed by reaction between carbonate **131** and 2-aminoethyltriphenylphosphonium bromide **132** to introduce the TPP group (Scheme 33). Like esters, the carbamate group may be susceptible to enzymatic cleavage *in vivo*, however spin trap **113** has not been used with cells either *in vitro* or *in vivo*.

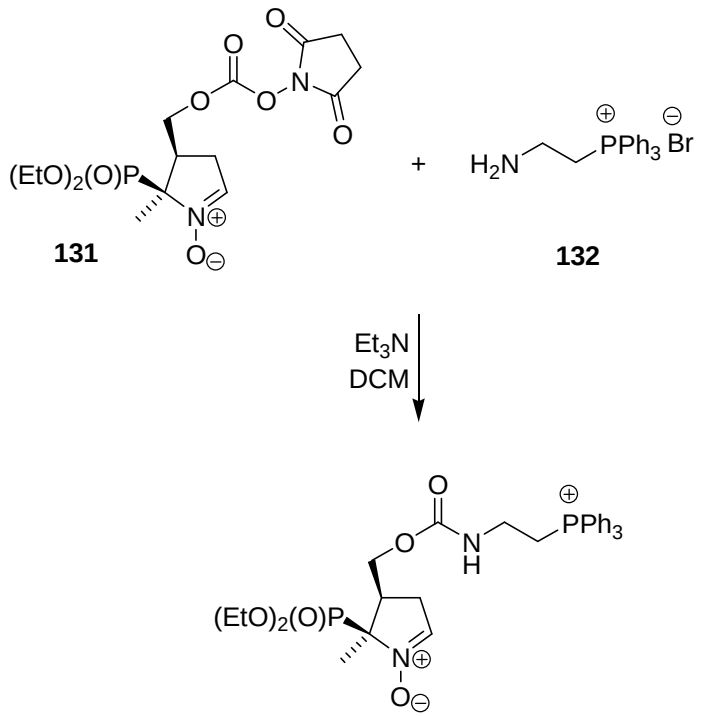

MitoDEPMPO **113**, 69%

Scheme 33: Final step of MitoDEPMPO **113** synthesis

The synthesis of TPP-conjugated nitroxides is important to our work, and TEMPOL-TPP **108** and MitoCP **110** each demonstrate the use of one of a different one of the above approaches. The synthesis of TEMPOL-TPP **108** is shown in Scheme 34.

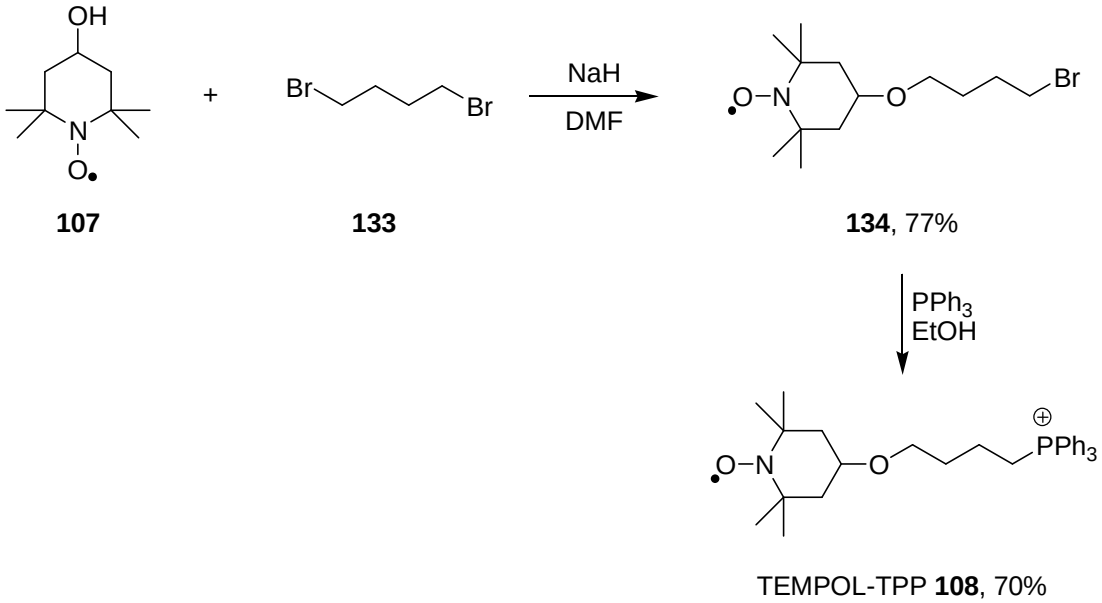

107 **133** **134**, 77%

TEMPOL-TPP **108**, 70%

Scheme 34: Synthesis of TEMPOL-TPP **108**

Deprotonation of TEMPOL **107** using NaH followed by introduction of 1,4-dibromobutane **133** gave butyl bromide **134** in a high yield. An ethanolic solution

of the alkyl bromide **134** and triphenylphosphine was heated at reflux for 72 h to give TEMPOL-TPP **108** in good yield. In this synthesis the TPP cation was introduced in the final step by displacement of a halide and is connected to the nitroxide moiety via a robust ether linkage.

The alternative strategy was adopted for the synthesis of MitoCP **110** which begins with the synthesis of 1-hydroxyundecanyltriphenylphosphonium bromide **136** (Scheme 35). The acid chloride **137** was formed by treatment of CP **46** with $SOCl_2$ and coupling to alcohol **136** gave MitoCP **110**. Like in the synthesis of TEMPOL-TPP **108**, the TPP cation was introduced into the molecule in the final step of the synthesis. However, in MitoCP **110** the linkage between the nitroxide and TPP moieties is an ester which may be susceptible to enzymatic cleavage.

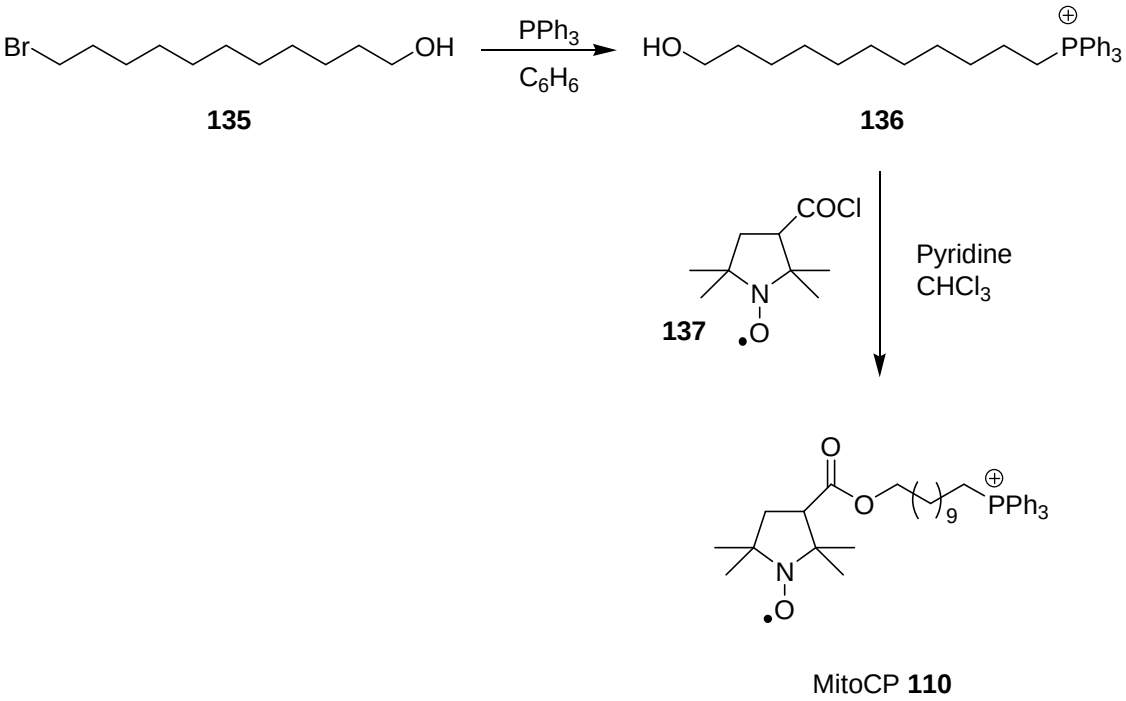

Scheme 35: Synthesis of MitoCP **110**

To conclude, introduction of the TPP cation of TPP-conjugated compounds is via two routes; direct displacement of halide or coupling of a TPP-containing compound. All the examples shown in this section use one of these methods and the cation is generally introduced in the final step of the synthesis, unless there are specific reasons not to, such as in the synthesis of MitoPBN **112**.

3.7. Other lipophilic cations for studying oxidative stress

Other lipophilic cations that accumulate in mitochondria have been used in the study of oxidative stress. Some examples of these are shown in Figure 38.

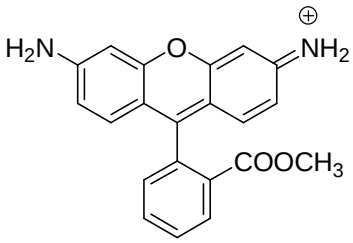

138

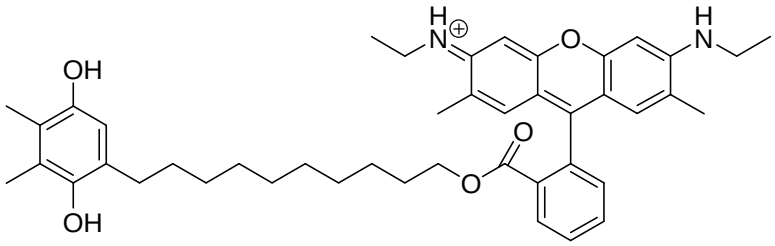

SkQR1 **139**

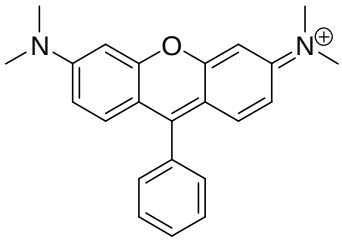

140

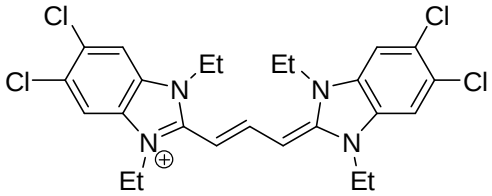

JC-1 **141**

Figure 38: Mitochondria-targeted fluorescent dyes

Rhodamine-123 **138** is a member of the rhodamine dye family and contains a positively charged nitrogen atom which enables its selective accumulation in mitochondria. Rhodamine-123 **138** has been used for a number of years as a fluorescent stain for mitochondria and has also been used to measure mitochondrial membrane potentials.[99,100] As part of the previously mentioned Russian collaborative project, a plastoquinone derivative called SkQR1 **139** was synthesised.[76] Like the previously discussed SkQ1 **98**, SkQR1 **139** is a derivative of plastiquinone and exhibited similar antioxidant capabilities to that of SkQ1 **98**.[77-81] However, SkQR1 **139** contained a rhodamine group for targeting to mitochondria which enabled its movement to be tracked by fluorescence. Other cationic mitochondria-targeted dyes are available, including Invitrogen's patented series of MitoTracker dyes which allow staining of mitochondria and can be retained after cell fixation, unlike rhodamine-123 **138**.[101] One example,

MitoTracker Orange **140**, is shown in Figure 38. Another example of a cationic fluorescent dye that selectively accumulates in mitochondria is the cyanine JC-1 **141**.[102]

3.8. Alternative mitochondria-targeting groups

There are alternative strategies that have been used for mitochondria targeting. L-Carnitine **142** is a biosynthesised quaternary ammonium salt used to transport fatty acids into mitochondria via the carnitine translocase system.[103] Carnitine-conjugated cisplatin derivatives (mitoplatins) have been patented for use as anticancer agents.[104] The Hartley group have recently published the synthesis of a carnitine conjugated nitrone spin trap, CarnDOD-7C **143**, designed to accumulate in mitochondria (carnitine portion shown in red, Figure 39).[105]

The Szeto-Schiller (SS) peptides are a series of cationic tetrapeptides that accumulate in the mitochondrial inner membrane (example **144**, Figure 40).[106] It was initially assumed that since protonation of the amino groups and the arginine side chain would give these molecules a positive charge, uptake would be via the same mechanism as DLCs, although the positive charge normally needs to be insulated for this to happen. However the mitochondrial accumulation of the SS peptides is independent of mitochondrial membrane potential and the mechanism remains unknown. These peptides can also exert an antioxidant effect by scavenging H_2O_2 and inhibiting linoleic acid oxidation.[107] A pentapeptide fragment of the mitochondrial membrane-targeting antibiotic Gramicidin S has also been used to target the nitroxide TEMPO **36** to mitochondria (see nitroxide **145**, Figure 39).[108]

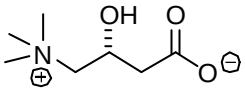

Carnitine **142**

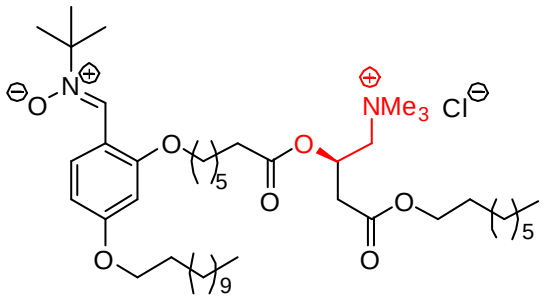

CarnDOD-7C **143**

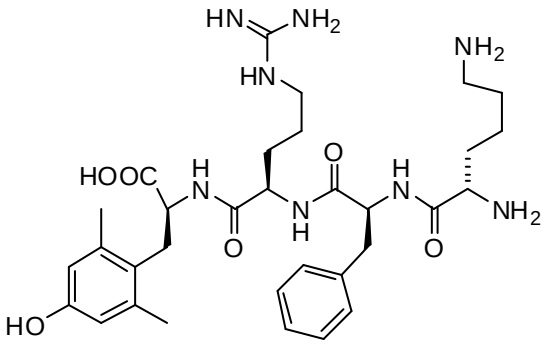

SS-02 **144**

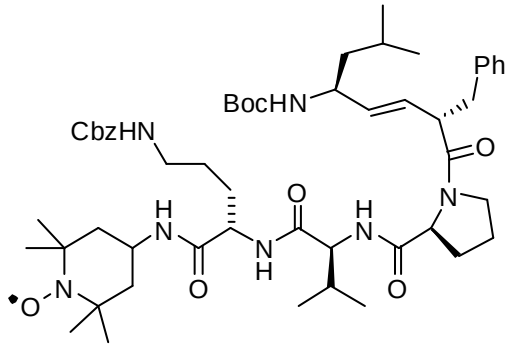

145

Figure 39: Mitochondrial targeting groups and targeted antioxidants

3.9 Conclusion

In conclusion, targeting sensors of oxidative stress to mitochondria in theory allows ROS to be detected at their main production site. In many cases there is also an antioxidant effect exerted by these compounds due to their conversion of highly reactive species into relatively stable species.

I have carried out three research projects which aim to build upon current work into mitochondrial targeted molecules for the study of oxidative stress. The first two use DLCs as mitochondrial targeting agents while the third shows proof of principle and is currently being developed to incorporate mitochondrial targeting.

Chapter 4: Synthesis of a mitochondria-targeted *N*-hydroxyisoindoline

Targeting a hydroxylamine derivative to mitochondria would be useful for assessing whether oxidative stress originating from this organelle is significant in disease and ageing processes. As discussed in Chapter 2, the adducts formed through spin-trapping of radicals by nitrones are useful for identification of the reacting ROS by EPR spectroscopy, but are unsuitable for quantification due to their instability. On the other hand, hydroxylamines react quickly with radicals to form the same nitroxide radical regardless of the reacting species. As this nitroxide is stable, the EPR signals are strong and quantifiable. Thus, hydroxylamines and the nitroxides they produce are good probes for overall oxidative stress. Reduction of nitroxides by cellular ascorbate causes a decline in their EPR signal and regenerates the original hydroxylamine (e.g. TEMPONE **43** is reduced to TEMPONE-H **42**). This reduction is undesirable when quantification is required, so it would be useful to have more sterically hindered hydroxylamines. These could react with smaller ROS but sterics would make it difficult for the larger reductant molecules to reduce the resulting nitroxides. We considered *N*-hydroxy-isoindolines as probes, as hydrogen atom abstraction from these hydroxylamines produces isoindoline nitroxides which have been well studied.

4.1 Isoindoline nitroxides

The first examples of isoindoline nitroxides were tetraethyl substituted analogues such as TEIO (1,1,3,3-tetraethylisoindolin-2-yloxyl radical) **146** reported by Rozantsev and co-workers in the late 1960's.[109] Rassat and co-workers expanded upon this work, publishing a number of papers on diradical derivatives of TEIO in the 1970's.[110]

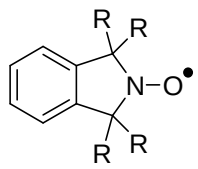

TEIO **146**, R = Et
TMIO **147**, R = Me

Figure 40: First examples of isoindoline nitroxides

However it was not until after 1979, when Rizzardo and Solomon introduced the concept of radical trapping, that isoindoline nitroxides found widespread application. [111] Radical trapping involves the reaction of a stable radical (generally a nitroxide) with a carbon-centred radical in a system to form a spin-paired adduct (Scheme 36). These adducts can then be separated and identified using normal methods of structure determination.

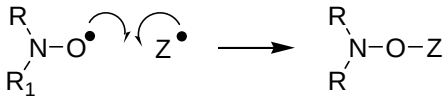

35 **148**

Scheme 36: Radical trapping

The first scavenger radical used in radical trapping experiments was the piperidine nitroxide TEMPO **36**. However, the tetraalkylisoindoline nitroxides offer a number of advantages over the piperidine nitroxides for this application. When separating complex mixtures of adducts, HPLC with UV detection is often utilised, but many TEMPO adducts have poor UV absorbance at around 215 nm, similar to solvent.[112] In contrast, the nitroxide TMIO **147** (1,1,3,3-tetramethylisoindolin-2-yloxyl radical) has a λ_{max} at 435 nm in hexane, much more suitable for UV detection.[113] The TMIO system also exhibits excellent thermal and chemical stability over a variety of conditions.[114] Furthermore, TMIO-type radicals have superior EPR line-widths compared with the piperidine nitroxides, a property not essential for radical trapping, but useful for other applications such as spin-labelling. TMIO **147** was introduced as a radical scavenger to probe polymerisation mechanisms using radical trapping experiments.[115] Since then TMIO **147** has been primarily employed as a radical trapping agent for the study of many systems. Other nitroxides have been used in biological systems as spin probes and spin labels. However, the poor water-solubility of the isoindoline nitroxides limited their use for these applications. A few substituted analogues of TMIO **147** and TEIO **146** existed but it was not until the late 1990's that the first water-soluble analogues, CTMIO **149**,[116] **150**[116] and NaTMIOS **151**[117] were published, enabling biological studies (Figure 41).

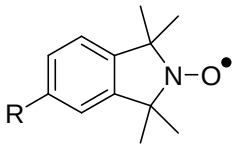

149, R = CO_2H
150, R = $Me_3N^+I^-$
151, R = $SO_3^-Na^+$

Figure 41: Water-soluble TMIO derivatives

Of these water soluble derivatives, CTMIO **149** has enjoyed the most success as a probe and has also demonstrated the ability to delay tumours in ataxia telangiectasia by exerting an antioxidant effect.[118] Other CTMIO analogues are currently being tested as therapeutic antioxidants.

In 2000, Rassat and co-workers published the synthesis of water-soluble TEIO nitroxides **152** and **153** and used them along with TEIO **146** and nitroxide **150** in a comparative study on their rate of reduction by ascorbate.[119] Tetraethyl substitution was found to confer a much greater resistance to reduction by ascorbate likely due to increased steric hindrance around the radical.

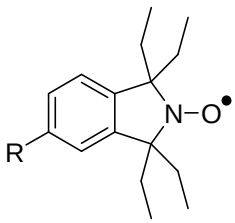

152, R = $Me_3N^+I^-$
153, R = $SO_3^-Na^+$

Figure 42: TEIO nitroxides published by the group of Rassat

The same group also published the diradical TEIO nitroxide **154** as a "spin-labelled spin trap" for EPR studies.[120] In this molecule, the two nitroxide moeties are closer than 500 pm apart and so a broad line is seen in the EPR spectrum due to a large dipolar interaction (Scheme 37, A). Reaction between nitric oxide and the aryl nitroxide of **154** abolishes this interaction, forming TEIO nitroxides **155**-**158**, and leaving only the single EPR signal observed from these compounds (Scheme 37, B), which do not react with nitric oxide. Even at low concentration of monoradical this signal appears as a narrow line and is detectable in the presence of the broad signal resulting from a much higher concentration of the diradical **154**.

As expected, when bisnitroxide **154** was exposed to ascorbate, the aryl nitroxide was rapidly reduced, while the TEIO nitroxide was reduced slowly.

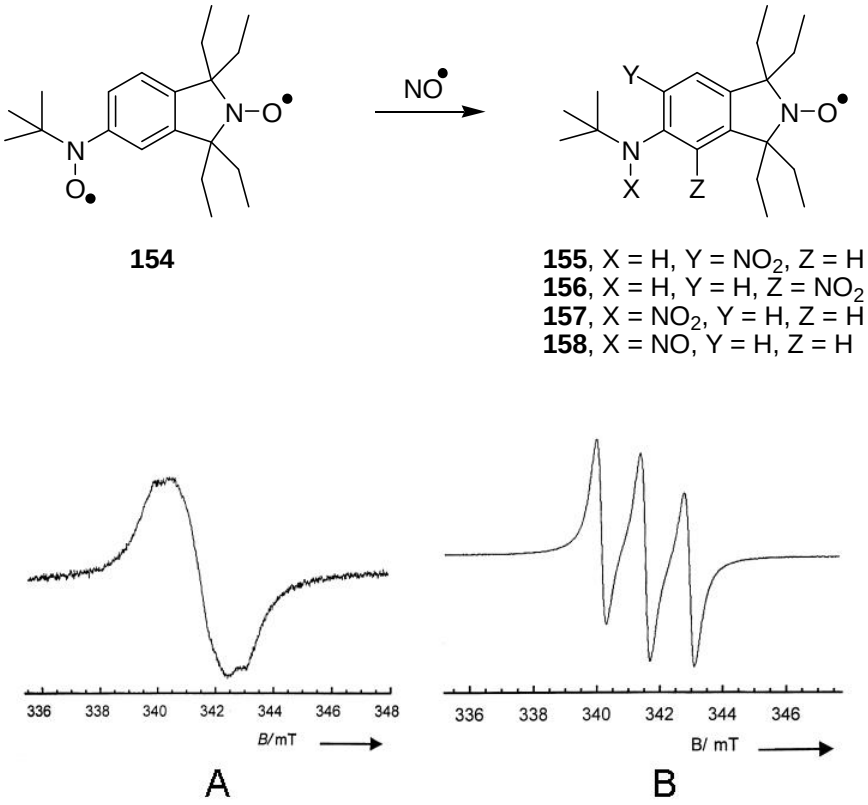

154

155, X = H, Y = NO_2, Z = H
156, X = H, Y = H, Z = NO_2
157, X = NO_2, Y = H, Z = H
158, X = NO, Y = H, Z = H

Scheme 37: Reaction of **154** with $NO^{\bullet}$ and resulting EPR spectra

TMINO **159**, a cyclic nitrone spin trap based on the TMIO scaffold has been reported.[121] The fused ring structure of this scaffold and the lack of a hydrogen atom on the carbon of the nitrone limits the decomposition of spin adducts of this nitrone via the pathways that DMPO is susceptible to (see Chapter 2, Scheme 25). TMINO reacts with oxygen and carbon-centred radicals, but is selective for $HO^{\bullet}$ over $O_2^{\bullet-}$.

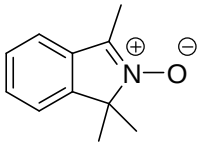

159

Figure 43: TMINO **159**

4.2 Synthesis of isolindoline nitroxides

The first full synthesis of TMIO **147** was published by Griffiths *et al.* in 1983 and is shown in Scheme 38.[122] Since then TMIO **147** has been primarily employed as a

radical trapping agent for the study of many systems. The synthetic route begins with the tetramethylation of *N*-benzylphthalimide **160** using a Grignard reagent, which proceeded in moderate yield to give *N*-benzylisoindoline **161**. Removal of the benzyl group by hydrogenolysis gave isoindoline **162** in excellent yield. The final oxidation step was carried out using sodium tungstate and H_2O_2, and proceeded smoothly to yield TMIO **147**.

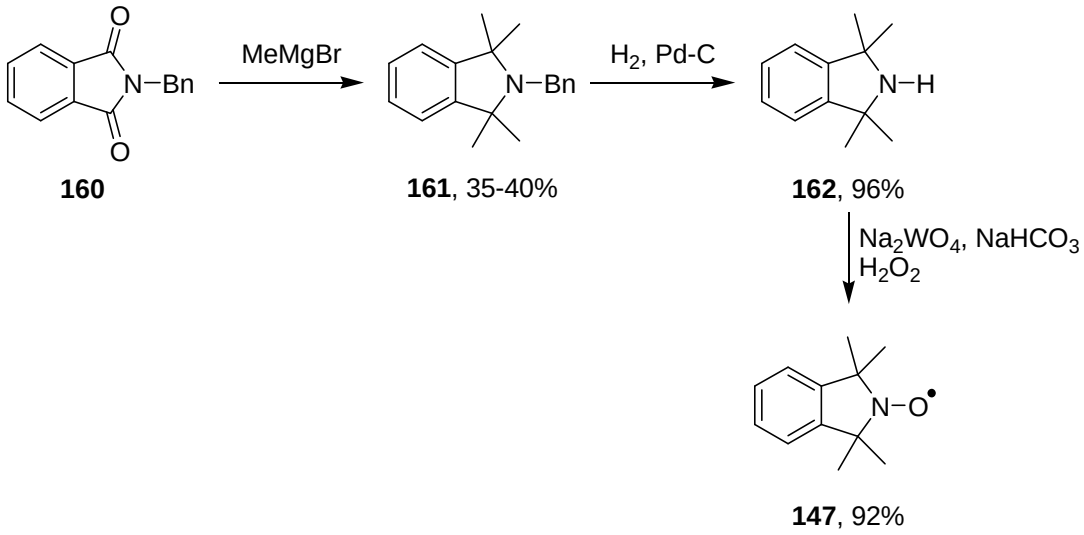

160 **161**, 35-40% **162**, 96%

147, 92%

Scheme 38: Griffiths' synthesis of TMIO **147**

The Bottle group used Griffiths' methodology to synthesise isoindoline **162**, then developed a bromination procedure to access functionalised isoindolines. Using 6 equivalents of bromine, the dibrominated compound **163** was accessed. Tribrominated **164** was synthesised by increasing the equivalents to 15.[123] Isoindoline **163** was utilised in the synthesis of CTMIO **149** (Scheme 39).[124] They also reported a procedure for converting TMIO **147** into its hydroxylamine hydrochloride **166** by treatment with HCl gas in dry EtOH (Scheme 40).[116]

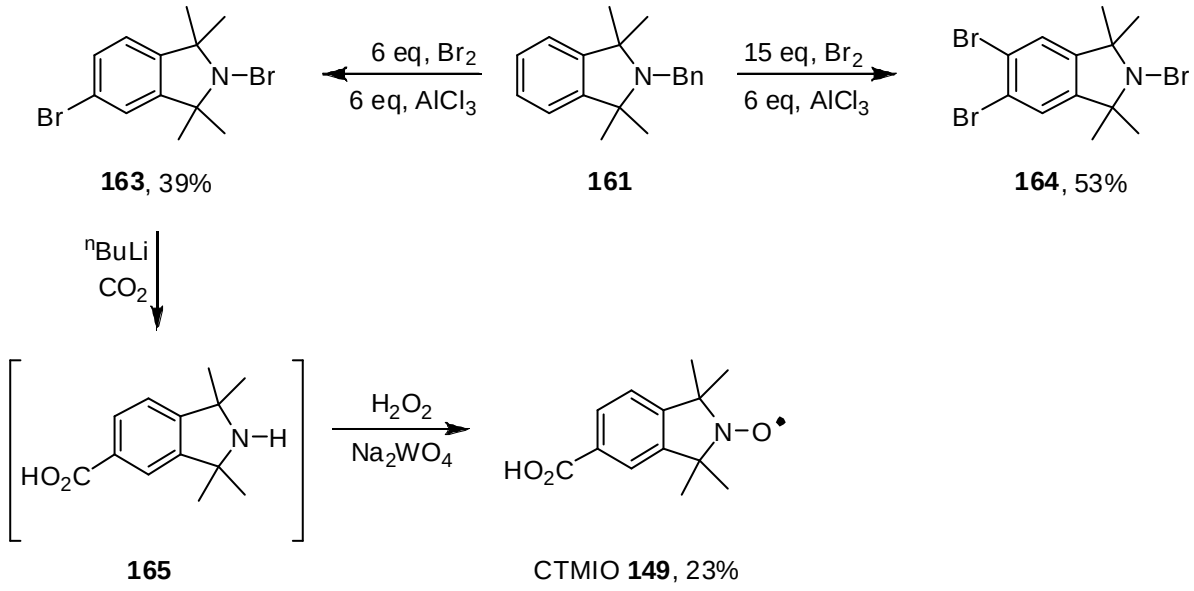

Scheme 39: Bottle's synthesis of brominated isoindolines

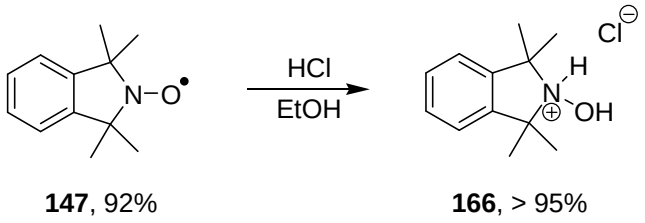

Scheme 40: Conversion of TMIO **147** into its hydroxylamine hydrochloride **166**

The route that Marx and Rassat used for the synthesis of diradical isoindoline **154** also required a brominated isoindoline but their synthesis differed from that of Bottle (Scheme 41). They began with phthalic anhydride **167** and introduced a single aryl bromide by treatment with bromine to yield anhydride **168**. This differs significantly from the Bottle route where bromination was delayed until after alkylation. Treatment with *N*-benzylamine gave benzyl phthalimide **169**. It was only at this stage that the Grignard reaction was carried out, introducing the four ethyl groups to give tetraethylisoindoline **170**. Lithium-bromine exchange, followed by reaction with 2-nitroso-2-methylpropane, gave isoindoline **171**. The benzyl group was cleaved by hydrogenolysis which also reduced the *N*-hydroxyl group. Oxidation with mCPBA oxidised both amine moeties to their corresponding nitroxides and gave the final product **173**.

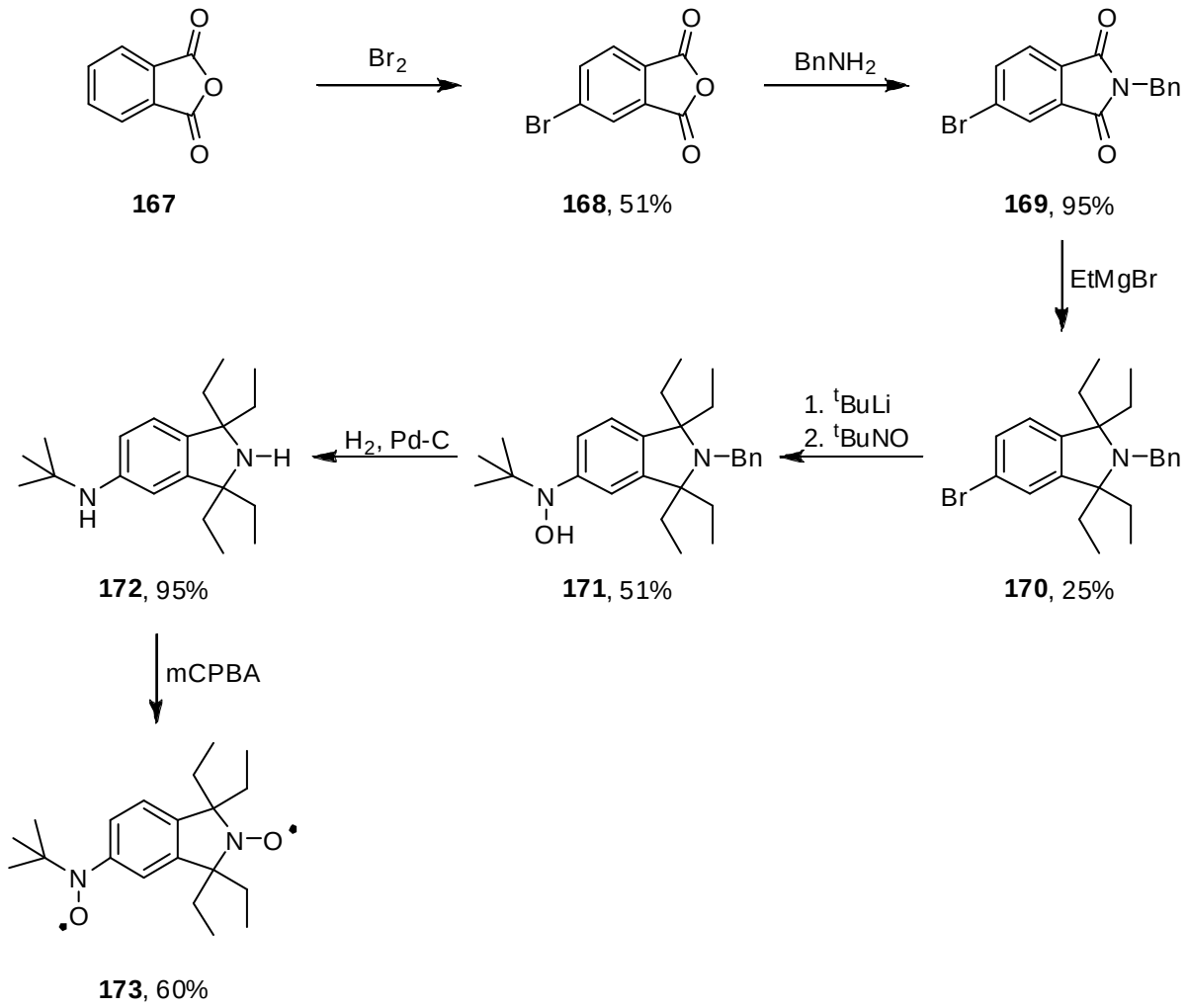

Scheme 41: Marx and Rassat's route to diradical isoindoline **154**

4.3 Novel probe design

Our first target hydrogen atom transfer probe was hydroxylamine **174** (Figure 44). This molecule features a TPP cation mitochondria-targeting group, a linking alkyl chain to determine the depth of penetration into membranes and a robust C-C bond attaching this chain to the isoindoline core. The hydroxylamine is chemically reactive and can be oxidised to the nitroxide **175**, but is sterically hindered by the presence of the tetraethyl substitution (Scheme 42). This will reduce interactions with cellular machinery, restricting access so that oxidation of the hydroxylamine **174** is only possible by small oxidising agents such as ROS. Also, reduction of nitroxide **175** by the cell's antioxidant defence systems should be slowed or prevented. It is also possible that the product nitroxide **175** would be a good antioxidant as it could act as a SOD mimetic (as previously described, see Chapter 2, Scheme 17), but should not be reduced to the hydroxylamine, which cannot function in this way.

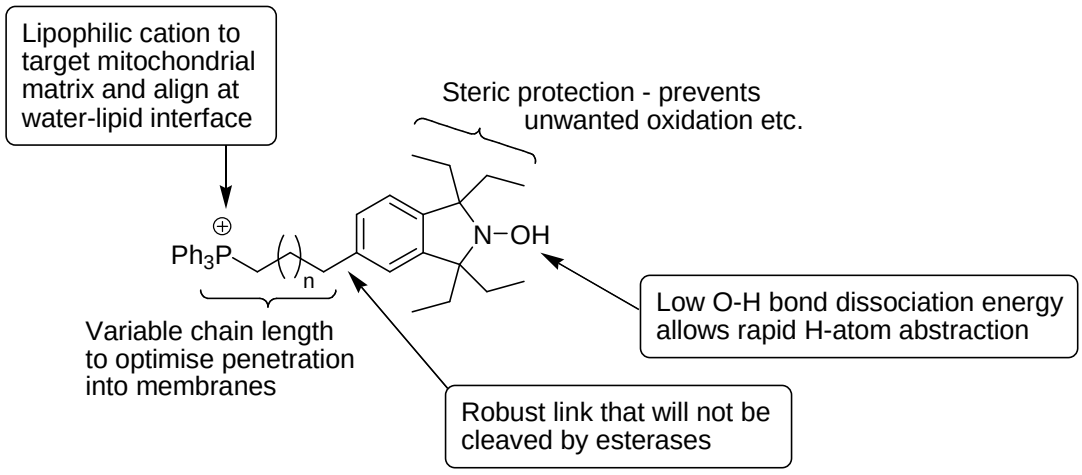

174

Figure 44: Design of target isoindoline hydroxylamine **174**

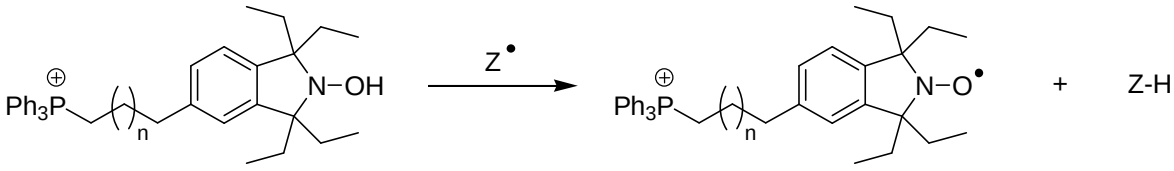

174 **175**

Scheme 42: Mode of action of target hydroxylamine **174**

4.4 Proposed synthesis of target hydroxylamine 174

The retrosynthetic analysis of target hydroxylamine **174** is shown in Scheme 43. Functional group interconversion leads from target molecule **174** back to nitroxide **175**, with a further functional group interconversion giving amine **176**. Reconnection of the *N*-benzyl protecting group leads back to benzylamine **177**. Disconnection of the alkyl TPP chain leads back to brominated isoindoline **178**. Disconnection of the four ethyl groups leads back to phthalimide **179**, which could be made from the corresponding brominated anhydride **180**. Disconnection of the bromine then reveals phthalic anhydride **181** as the starting material for the scheme.

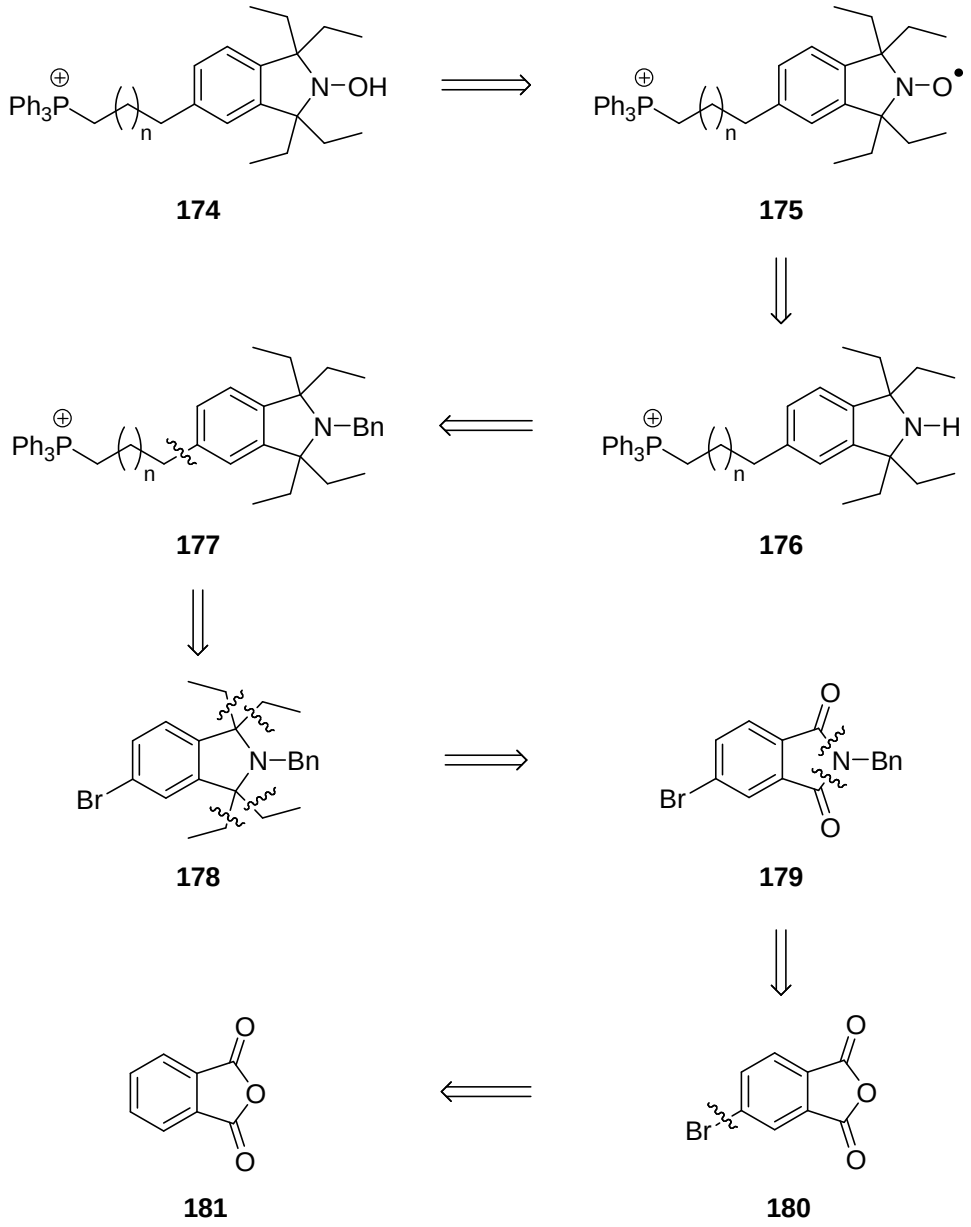

Scheme 43: Retrosynthesis

The proposed forward synthetic route is shown in Scheme 44. Following the route of Marx and Rassat[120] (Scheme 41), phthalic anhydride **181** would be converted into tetraethylisoindoline **178** by bromination, conversion of anhydride **180** to N-benzyl phthalimide **179** and tetraalkylation using a Grignard reaction. This route was chosen over the Bottle approach,[116] involving simultaneous bromination and debenzylation, which at the time of this work had only been demonstrated on TMIO derivatives. Continuing the route, the alkyl chain could be introduced by alkenyl-aryl cross-coupling by boronation followed by treatment with an alkenyl halide and $PdCl_2$(dppf) to give **182**.[125] Hydrogenolysis would cause double deprotection of the benzyl groups and saturation of the alkenyl chain to give amine **183**, which could then be oxidised to nitroxide **184** by *m*CPBA or by H_2O_2 in the

presence of Na_2WO_4 as catalyst. Finally, mesylation and reaction with triphenylphosphine should give TPP-conjugated nitroxide **175** which would be converted into the hydrochloride salt **185** of hydroxylamine **174**.

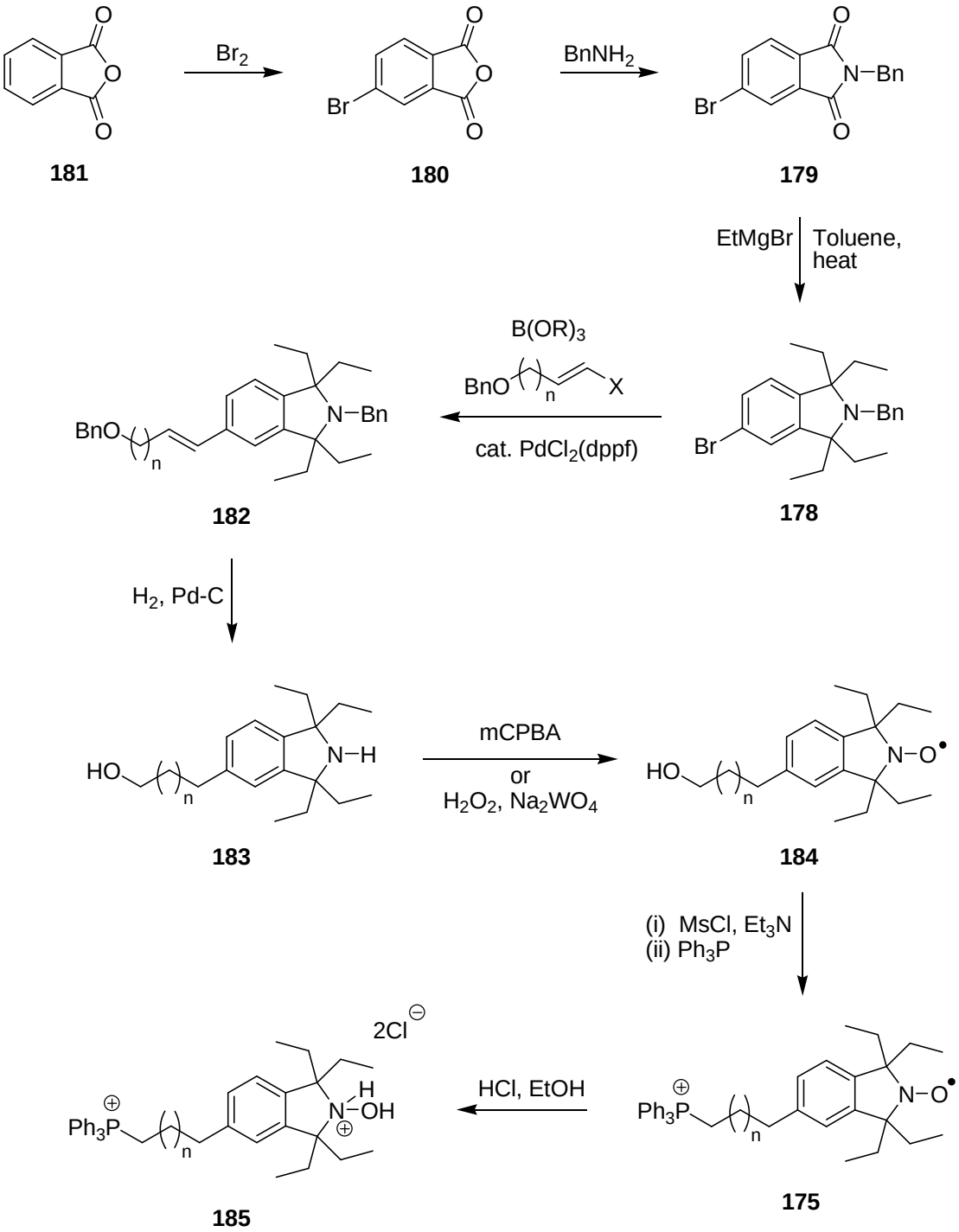

Scheme 44: Proposed synthetic route to **185**

Initially, it was assumed that bromination of phthalic anhydride **181** could be achieved through simple reaction with bromine in chloroform. However, this was unsuccessful and gave only starting material. Upon reflection, it was concluded that the two carbonyl groups present in the anhydride ring were both deactivating

the aromatic ring to electrophilic substitution, to the extent that no product was formed. When the reaction was conducted using bromine in 3 M aqueous sodium hydroxide, the anhydride ring was opened and the disodium acid salt **186** was formed. The carboxylate groups do not deactivate the aromatic ring and bromination was successful under these conditions. The crude brominated salt was treated with excess thionyl chloride to reform the anhydride ring and gave 3-bromophthalic anhydride **180**. (Purification at this stage proved difficult.) There was an unbrominated impurity visible in the ^{1}H NMR spectrum with an R_f value identical to the product. Crystallisation proved impossible so it was decided to carry this crude material on to the next stage with the hope of synthesising a crystalline product. Fortunately, when crude anhydride **180** was treated with one equivalent of benzylamine, the resulting solid was easily recrystallisable to give phthalimide **179** in a good yield from **186** (Scheme 45).

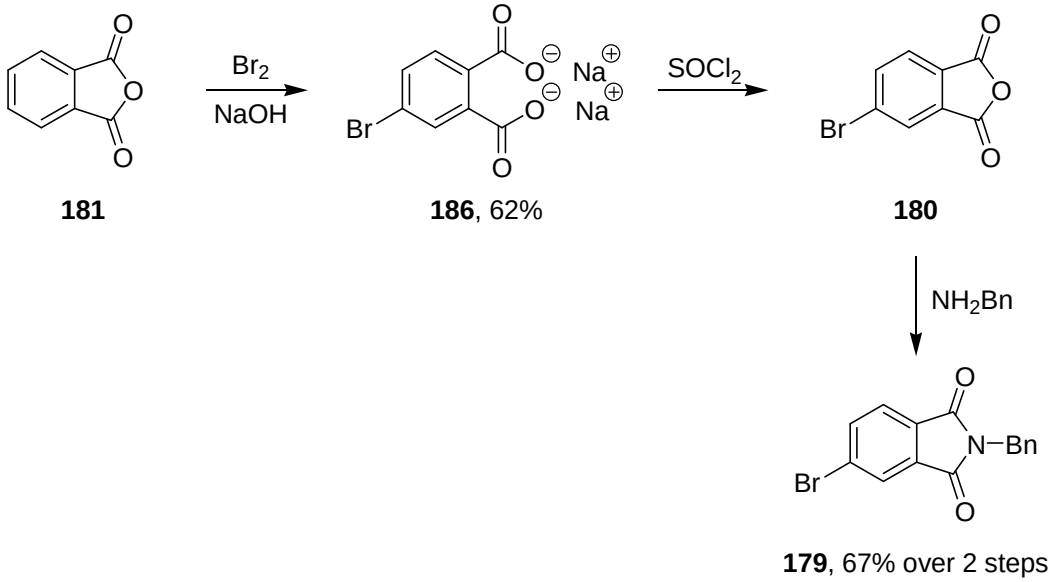

181 **186**, 62% **180**

179, 67% over 2 steps

Scheme 45

An alternative strategy was also tried where bromination would be delayed until after phthalimide formation. When phthalic anhydride **181** was treated with an excess of benzylamine, the dibenzylated product **187** was formed (Scheme 46). When exactly one equivalent of benzylamine was used and the reaction conducted in the microwave, clean conversion to phthalimide **188** was achieved. However, when undertaken using conventional heating methods, the reaction was not as clean. Since our microwave reactor is not suitable for large scale reactions and a large quantity of phthalimide **188** was needed, this approach was

abandoned once synthesis of bromophthalimide **179** had been achieved via the original strategy.

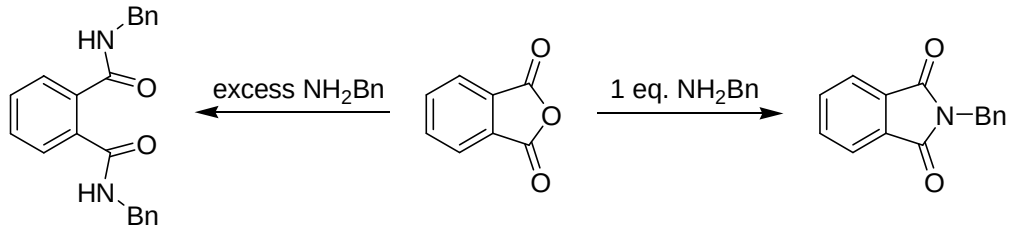

187, 99% **181** **188**, 58%

Scheme 46

With phthalimide **179** in hand, a Grignard reaction was used to simultaneously introduce the four ethyl groups (Scheme 47). The most recent paper that carried out this reaction reported a 25% yield but did not detail the full experimental procedure.[120] Therefore, the reaction conditions were investigated in an attempt to optimise the reaction. The conditions used are summarised in Table 1.

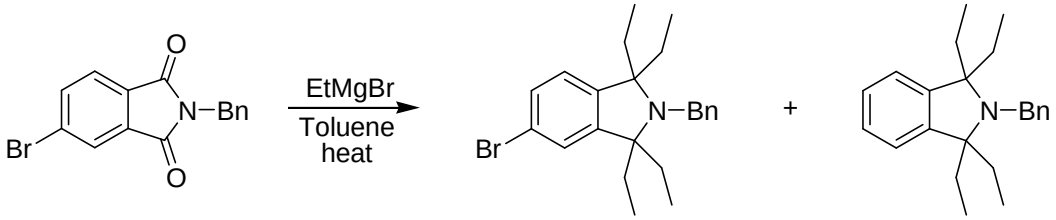

179 **178** **189**

Scheme 47

Entry	Reagent	Temp	Time	Solvent	Combined isolated yield of 178 & 189	Ratio (178:189)
1	EtMgBr, 6 eq.	130 ℃	4 h	Toluene	5% crude	-
2	EtMgBr, 8 eq. , $BF_3.O(CH_2CH_3)_2$	90 ℃	4 h	Toluene	0%	-
3	EtMgBr, 8 eq.	Reflux	o/n	Diethyl ether	0%	-
4	EtMgBr, 8 eq. (Schlenk tube)	75 ℃	o/n	DME	0%	-
5	EtMgBr, 11 eq. Concentrated	120 ℃	o/n	Toluene	32%	1:1
6	EtMgBr, 11 eq. Concentrated	120 ℃	4 h	Toluene	26%	1:1
7	EtMgBr, 11 eq. Concentrated	120 ℃	1.5 h	Toluene	61%	4:1

Table 1: Attempted reaction conditions for alkylation of phthalimide **179**

Initially the alkylation was unsuccessful. In entries 1-4 the ethereal EtMgBr solution was used at 3 M as supplied. Although no product was formed, monitoring by TLC showed the disappearance of starting material. Experimental details for a similar reaction, using MeMgBr, suggested concentrating the Grignard reagent by distilling off the ether before adding the substrate.[116] This technique was used for entries 5-7. Entry 7 shows the most successful reaction conditions giving a 4:1 ratio of the desired alkylated product **178** and a debrominated product **189** in a 61% yield of the mixture (ratio determined by integration of the CH_2 peak of the benzyl group). The unbrominated product **189** was presumably formed by metal-halogen exchange to give aryl Grignard reagent **190**, which protonates on quenching with water (Scheme 48).

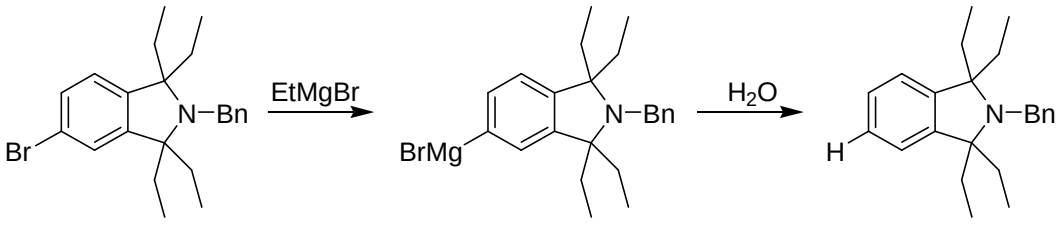

178 **190** **189**

Scheme 48: Formation of unbrominated side product **189**

Disappointingly **178** and **189** proved to be inseparable and so the material carried forward contained both products. On scale up to 40 g, the yield for the tetraalkylation reaction dropped to 27% and the product was a 2:1 ratio of brominated and debrominated products. This yield may seem low, however when looking at the mechanism, shown in Scheme 49, it is understandable. The tetraalkylation is a multi-step reaction and after each step there is the potential for side reactions such as ring opening to occur, yielding undesired products. Therefore a yield of 27% of this mixture is acceptable and the 61% obtained on smaller scale actually fairly high when this is considered.

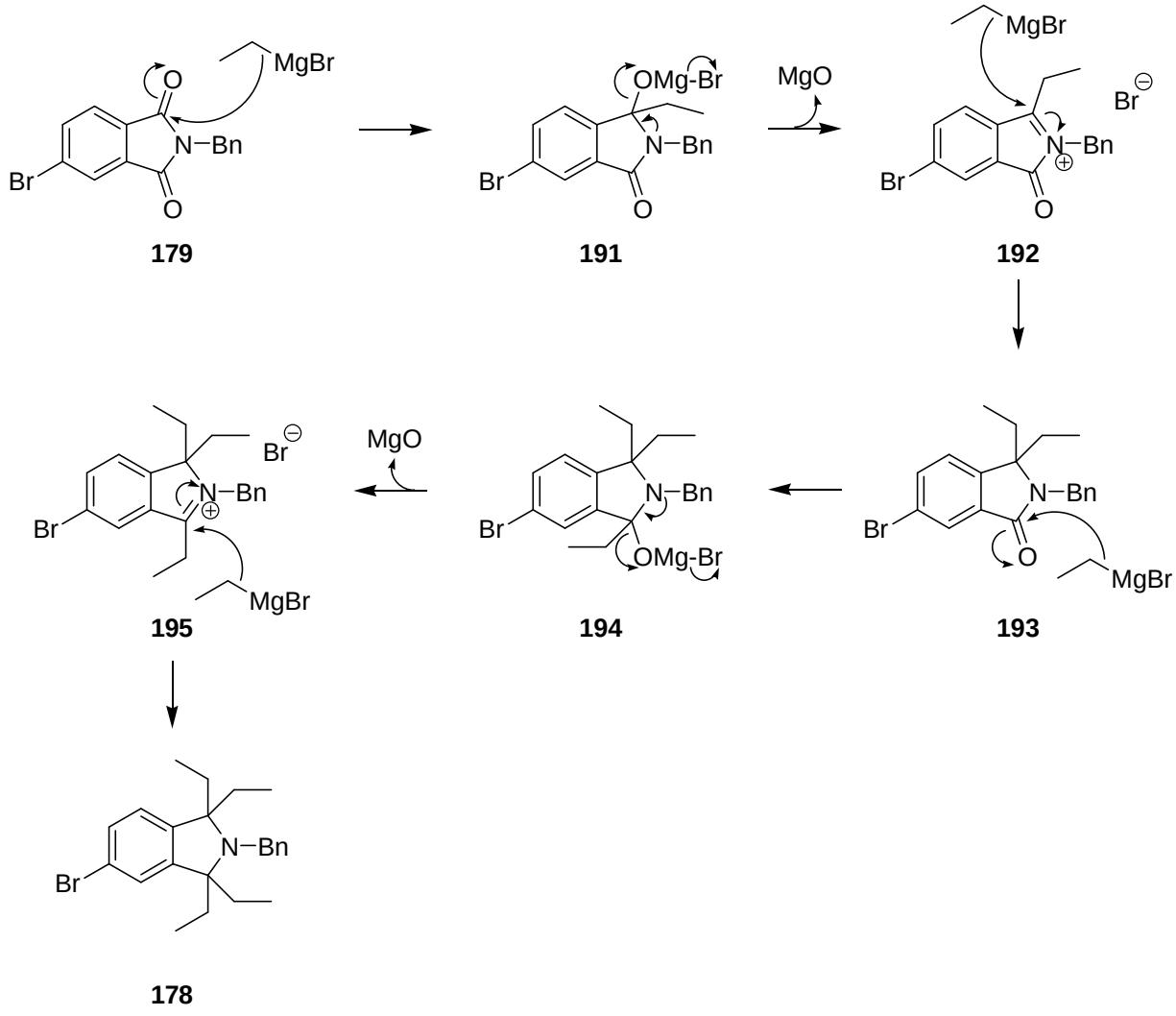

Scheme 49: Mechanism of Grignard reaction

At this stage of the synthesis, it was planned to introduce the alkyl chain using a Suzuki coupling (Scheme 50). Conversion of bromide **178** to boronate **197** was successful as judged from the ^{1}H NMR spectrum of the crude material which showed correct integration of the CH_3 peak of the boronate group when compared with the signals for the aromatic and benzyl group protons. However when column chromatography was performed, the boronate decomposed. Due to this result, the

Suzuki coupling was not attempted. We had planned to use an alkenyl halide in this cross-coupling reaction, followed by a hydrogenation reaction to give the desired alkyl chain. The reason for this becomes apparent when considering the cross-coupling reaction mechanism.

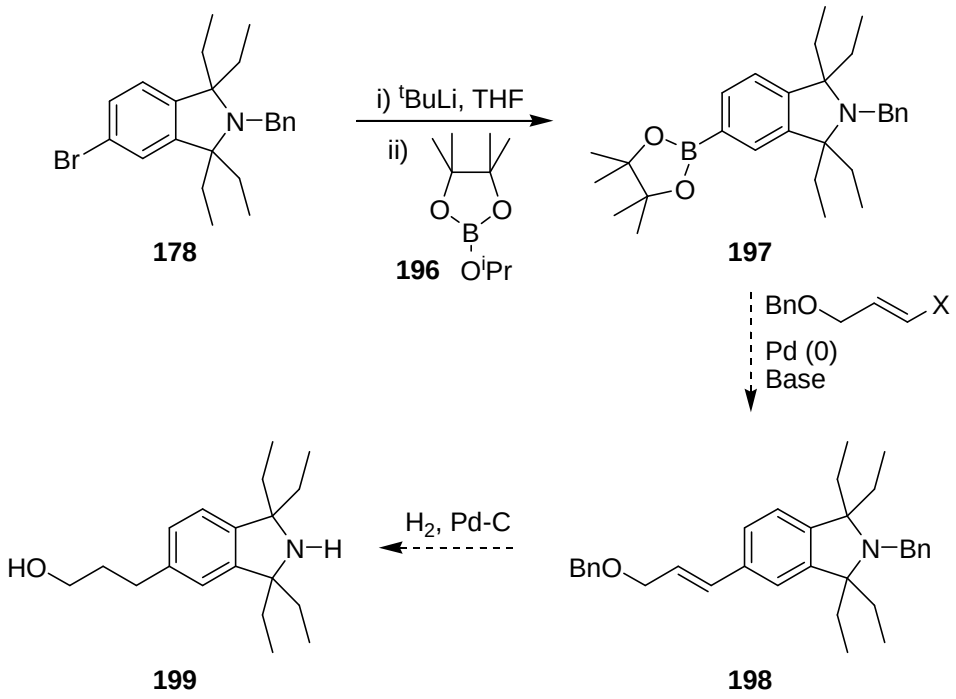

178 **196** **197** **199** **198**

Scheme 50: Planned Suzuki coupling strategy

The reaction follows the general catalytic cycle for palladium-catalysed coupling reactions (Scheme 51). Oxidative addition of the alkenyl halide **201** to coordinatively unsaturated palladium complex **200** gives square planar palladium(II) complex **202**. Transmetallation gives another palladium(II) complex **205** and reductive elimination gives the product **206** and regenerates the catalyst **200**. In this catalytic cycle, the transmetallation step is slow and reductive elimination is fast. If R^1 has β-hydrogens it can undergo a side reaction following oxidative addition, known as β-elimination which occurs faster than transmetallation (Scheme 52). In the Suzuki coupling, we planned to use an alkenyl halide as β-elimination from alkenes to form alkynes is slow.

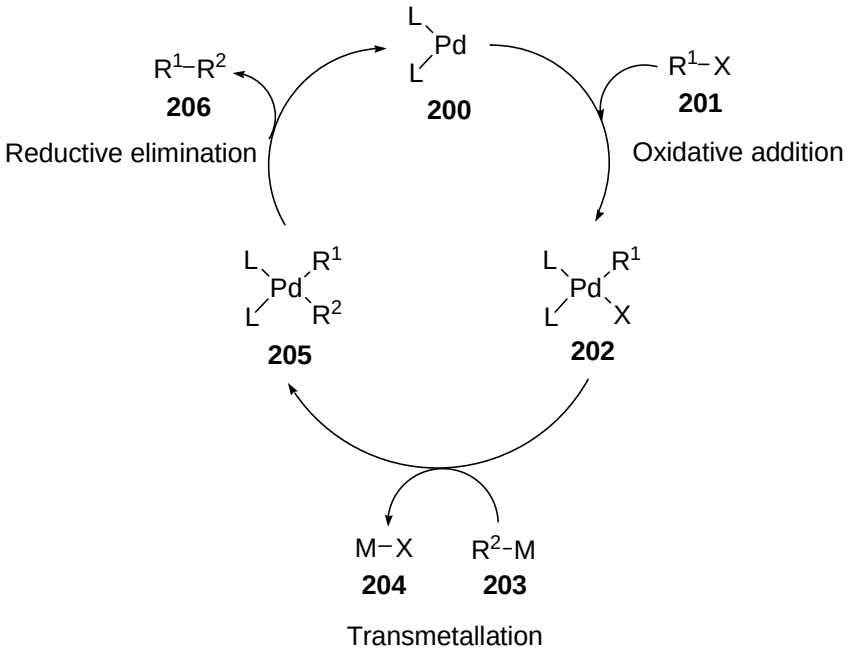

Scheme 51: General catalytic cycle for palladium cross-couplings[126]

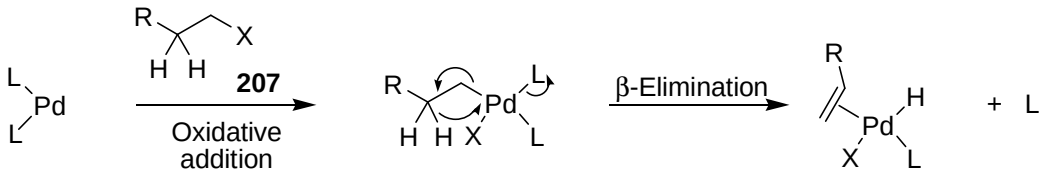

Scheme 52: β-Elimination

Although the Suzuki coupling was not carried out, the fact that boronate formation was achieved led us to our next, successful strategy. We decided to use aryl boronation to introduce an ether link and changed our target molecule to hydroxylamine **210**.

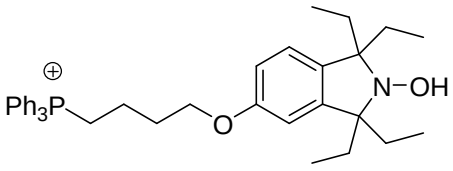

210

Figure 45

The mixture of brominated product **178** and unbrominated product **189** was treated with ^{t}BuLi, followed by 2-isopropoxy-4,4,5,5-tetramethyl-1,3,2-dioxaborolane **196**, and finally with hydrogen peroxide and base. This converted **178** into phenol **211** and left unbrominated **189** untouched (Scheme 53).

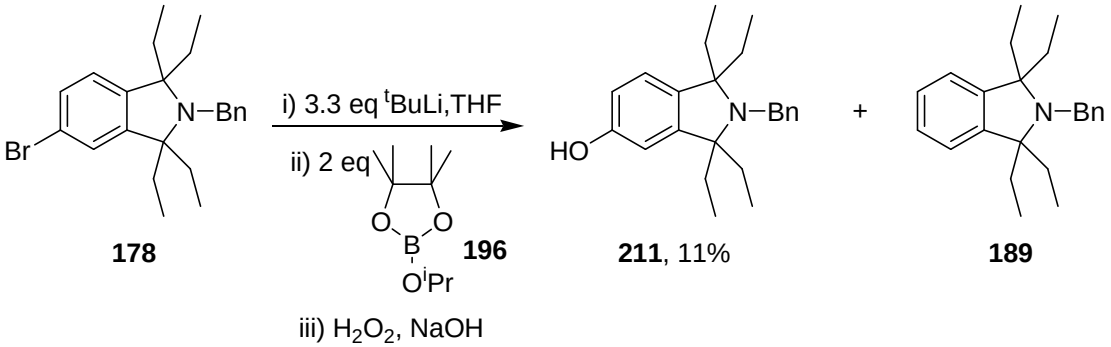

178 **196** **211**, 11% **189**

Scheme 53

As the arylboronates were previously found to be unstable on silica, purification was delayed until phenol **211** was in hand. Fortunately, the difference in R_f value was now sufficient to separate phenol **211** from unbrominated compound **189** by column chromatography, but the yield was poor. The reaction sequence was repeated a number of times but unwanted side products were formed that had to be carried through the route, most notably the unbrominated compound **189**. Because of this, a modified route was proposed where the oxygen atom required for ether formation was already in place prior to the introduction of the four ethyl groups (Scheme 54).

4.5 Second route to target hydroxylamine 210 – Methoxy precursor

The second route begins with the oxidation of 3,4-dimethylanisole **212** to give diacid **213**. Initially a literature procedure using ZnO was used,[127] however when applied to 3,4-dimethylanisole **212**, only starting material was recovered after 24 h. An alternative procedure using $KMnO_4$[128] was employed successfully to give clean diacid **213** in reasonable yield up to 34 g scale. Once this oxidation was achieved, the route proceeded in a similar manner to the previous one. Anhydride **214** was formed using $SOCl_2$ and treated with benzylamine to give phthalimide **215** in moderate yield from the diacid. Once again, purification at this stage was achieved by crystallisation. Tetraethylation was carried out as previously to give isoindoline **216** in 29% yield on 6 g scale. At this stage, phenol **211** was easily formed in good yield by demethylation of ether **216** using BBr_3.

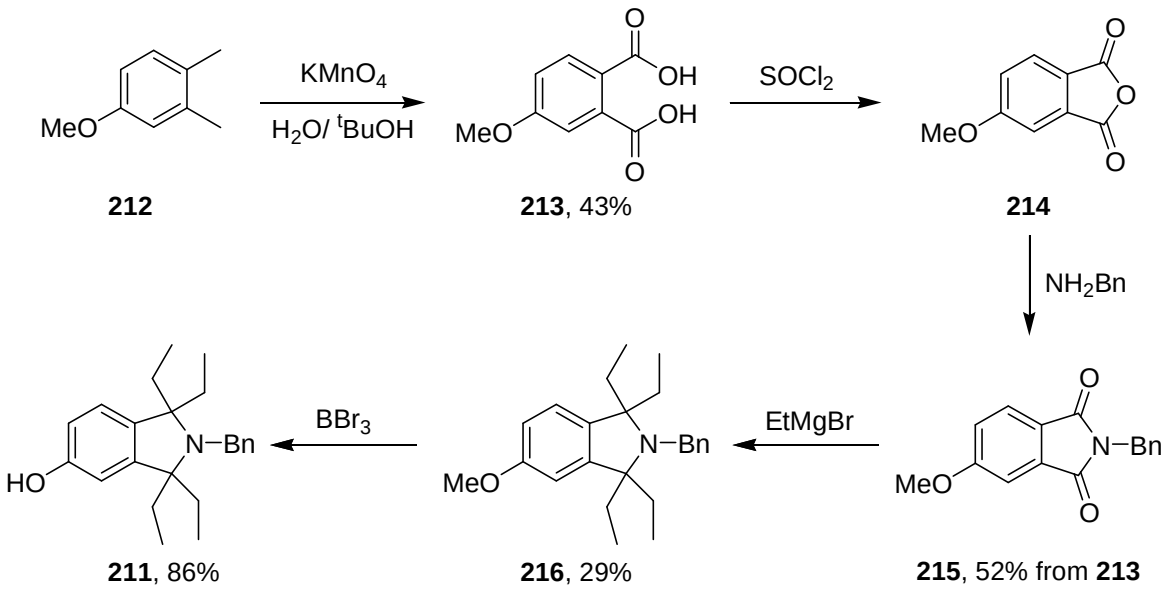

212 **213**, 43% **214**

211, 86% **216**, 29% **215**, 52% from **213**

Scheme 54

The yields for this synthetic route are comparable to the previous one. However, in this route there were no unwanted side products carried through and, unlike the bromo group, the methoxy group did not cleave under the conditions of the Grignard reaction. Also, the phenol-forming step is much simpler and higher yielding in the second route. With phenol **211** in hand via two different routes, the next step was introduction of the TPP cation using the hydroxyl group. Phenol **211** and (3-iodopropyl) triphenylphosphonium iodide **217** (previously synthesised in the group by S. El Fangour) were dried by azeotroping with toluene, then dissolved in anhydrous methanol. Cesium carbonate was used as the base and the reaction was heated at 55 ℃ for 48 h (Scheme 55).

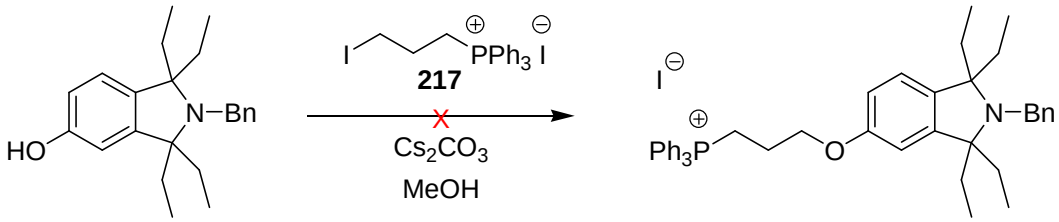

211 **218**

Scheme 55

It was established from the ^{1}H NMR spectrum of the crude product that the desired product had not been formed. There was no new CH_2 peak with ^{1}H-^{31}P coupling and also no new OCH_2 peak, expected at around 4-5 ppm. It is unclear why this reaction was unsuccessful, but it may be that the electron-withdrawing effect of the TPP cation encouraged E2 elimination of the iodide (Scheme 56).

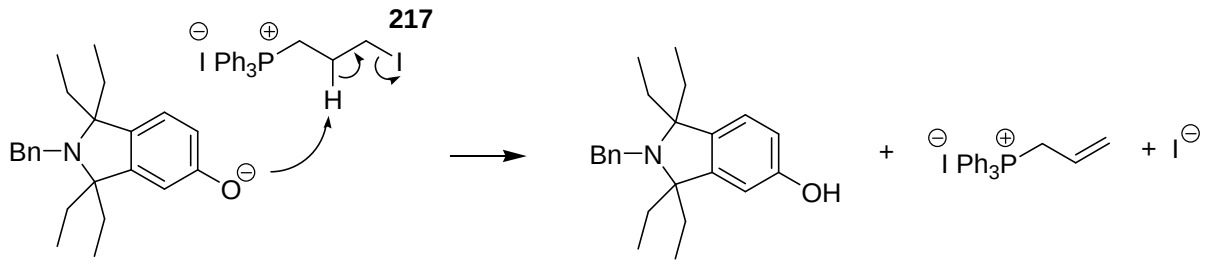

219 **211** **220**

Scheme 56

This theory is supported by the fact that the reaction was successful when carried out using commercially available 4-bromobutylphosphonium bromide **221** (Scheme 57).

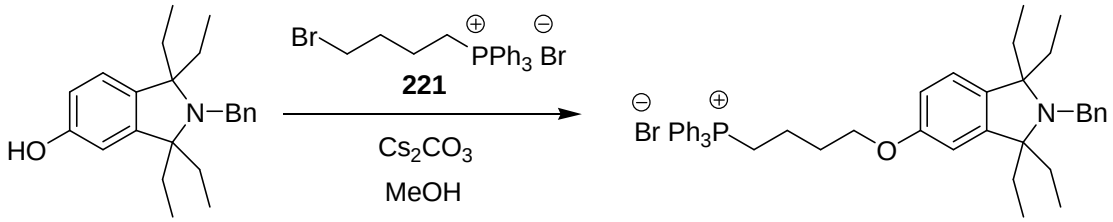

211 **222**, 30%

+

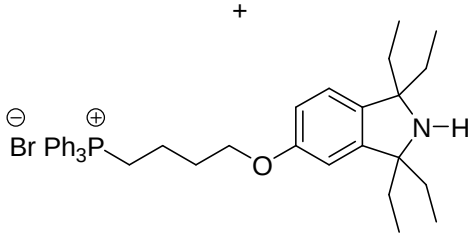

223, 15%

Scheme 57

In alkyl bromide **221** the extra carbon atom means that the electron-withdrawing TPP group is further away from the protons β to the bromine atom. The crude phosphonium salt **222** was purified by two subsequent rounds of column chromatography. Disappointingly, elimination of triphenylphosphine was seen on the column and the overall yield for the reaction after purification was low. Unexpectedly a small amount of deprotected amine **223** was also isolated from the column despite not being present in the crude mixture.

After successfully introducing the TPP group, all that remained was to remove the benzyl group and oxidise the resulting amine to form a nitroxide, which could be

treated with HCl to form the salt of hydroxylamine **210**. The debrominated side product **189** isolated in the first route was used to optimise these steps to avoid loss of the TPP compound **222**, which was difficult to purify. Also, by optimising the procedures to minimise side reactions and maximise yields, it was hoped that minimal purification would be needed when the TPP compounds were used.

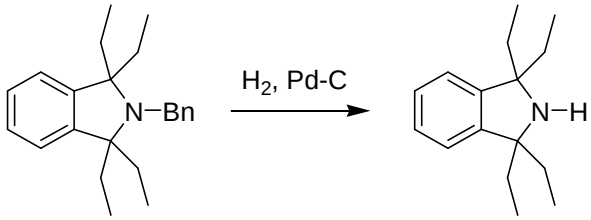

189 **224**, 93%

Scheme 58

Hydrogenation of benzylamine **189** using Pd-C catalyst proceeded smoothly in high yield. This success was encouraging as a number of features of the reaction procedure were compatible with TPP-containing compounds. It was carried out in ethanol, one of only a few solvents that phosphonium salt **222** was fully soluble in. The work-up was a simple filtration followed by concentration of the reaction mixture, eliminating the need for an aqueous work-up and potential partitioning of the TPP salt. Finally, the reaction proceeded to completion with no other side products formed, eliminating the need to separate multiple TPP-containing compounds. With this encouraging result, the procedure was applied to phosphonium salt **222**. Unfortunately, only starting material was recovered, even after repeating the reaction. Fortunately this was overcome by addition of HBr to the reaction mixture. The deprotection then occurred in an excellent yield, with no purification required to give the HBr salt **225** (Scheme 59).

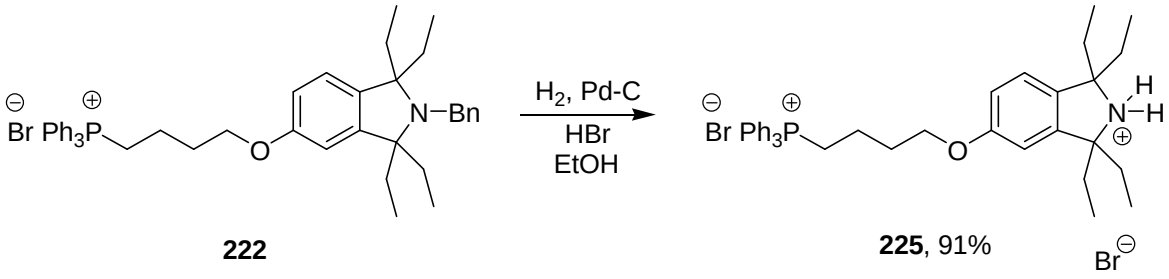

222 **225**, 91%

Scheme 59

The next step was oxidation to introduce the nitroxide functionality. The amine **224** derived from the debrominated side product **189** was used to optimise this step. In the synthesis of nitroxide **154**, Marx and Rassat used *m*-CPBA as the oxidising agent,[120] however their paper contained no experimental procedure so an alternative method was chosen. This method employed H_2O_2 and Na_2WO_4 and has been used previously in the synthesis of TMIO and analogues with very high yields.[122] Disappointingly, in our hands the reaction had little success. ^{1}H NMR spectra showed starting material, sometimes with slight broadening suggesting a small amount of nitroxide but nowhere near the yields achieved previously (near quantitative). Reasoning that this may be due to the increased steric bulk around our amine due to tetraethyl substitution, we turned our attention to *m*-CPBA instead. Treatment with *m*-CPBA gave more extensive broadening of the NMR signals, indicating the presence of significant amounts of radical. However lack of experience in dealing with the isolation and characterisation of stable radicals made it difficult for us to determine whether or not the reaction had been a success.

An alternative route was also tried using *N*-hydroxyphthalimide **226** as the starting material (Scheme 60). This route appeared promising as the hydroxylamine functionality was already in place and could potentially be unmasked by a simple hydrogenation. *N*-Hydroxyphthalimide **226** was benzyl protected in good yield. However, reaction with ethylmagnesiumbromide did not give the tetraethyl compound **228** so this route was not pursued further.

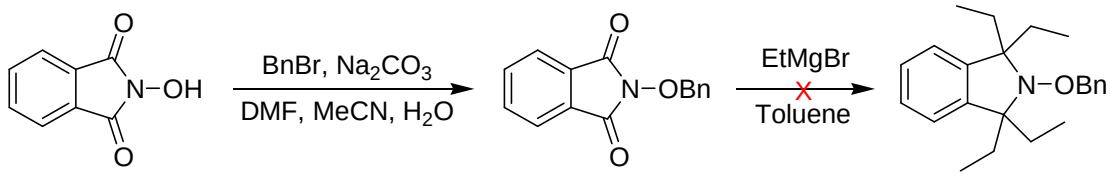

226 **227**, 88% **228**

Scheme 60

At this early stage in my PhD a second project (discussed in Chapter 5) was begun and proved successful. Since isolation of the nitroxide was proving problematic, this area of work was stopped and was only resumed in the last month of my PhD. While attending the SPIN2008 conference I met Dr Lucien Marx who kindly provided me with further experimental details for the synthesis of nitroxide **154**.[129] These proved invaluable in the handling of this reaction. It was

decided to use Dr Marx's procedure on the phosphonium salt **225** as we were confident it would be successful due to the high similarity of our desired nitroxide **229** to nitroxide **154**. Salt **225** was neutralised with $NaHCO_3$ before following the provided procedure. *m*-CPBA was added to a solution of amine **223** and stirred at 25 ℃ (Scheme 61). The progress of the reaction was monitored using EPR spectroscopy by the appearance of a triplet due to the nitroxide radical (Figure 46).

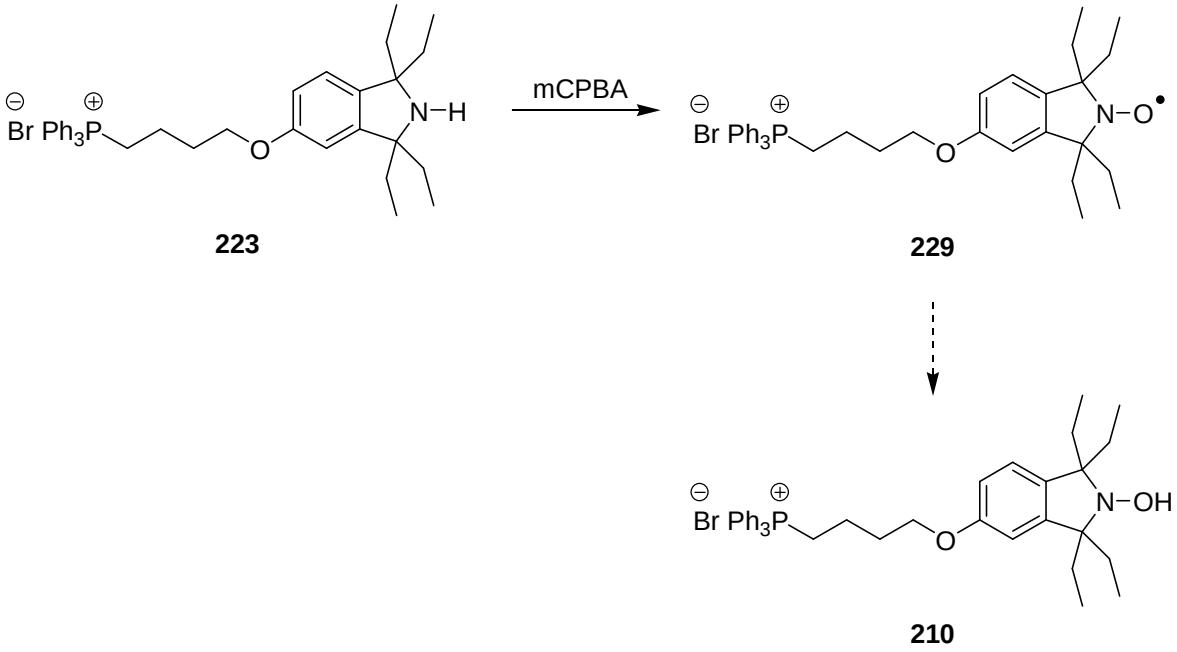

223 **229** **210**

Scheme 61

The reaction was quenched when the triplet showed no further increase in intensity. The appearance of a strong EPR signal indicates that nitroxide **229** was successfully formed. Unfortunately, TLC showed more than one compound present in the sample and, due to the problems encountered when chromatographing the previous TPP salt **222**, it was decided that reverse-phase HPLC purification would be the best course of action. This was not available to me within the time of this research, but will be carried out by another member of the group in the future. It is anticipated that pure nitroxide **229** will be isolated so that completion of the scheme to yield the target hydroxylamine **210** will be possible.

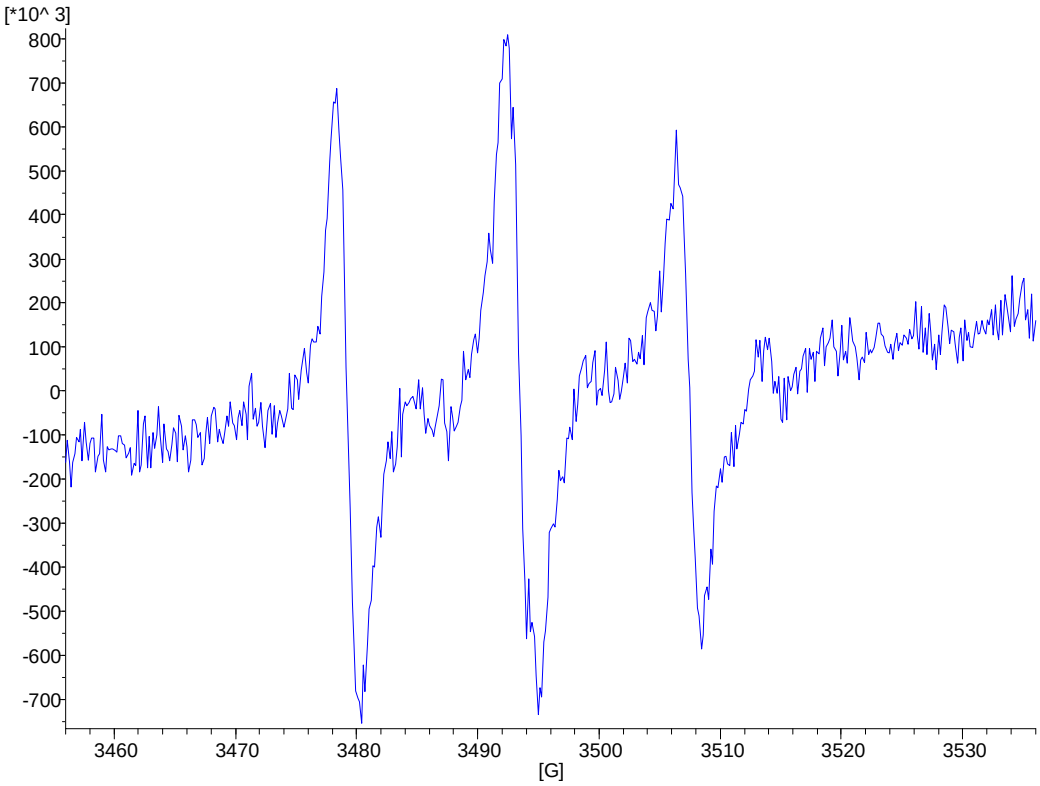

Figure 46: EPR spectrum of nitroxide **229**

g = 2.0059, A_N = 14.10 G (t).

4.6 Conclusion

In summary, the synthesis of an isoindoline hydroxylamine **210** bearing a TPP group proved problematic when an aryl bromide **179** was used as the precursor for introduction of the targeting group. An improved synthesis in which an ether link is used instead of a C-C link proved much more successful. Lack of experience in synthesising radicals played a large part in the difficulties encountered with the penultimate oxidation step in this second route. However, evidence from EPR spectroscopy makes us confident that nitroxide **229** was successfully formed.

To conclude, we achieved the synthesis and full characterisation of an isoindoline bearing a TPP group as its HBr salt **225**, a late-stage precursor to hydroxylamine **210**. Nitroxide **229** was probably prepared and would represent the first example of a mitochondria-targeted isoindoline nitroxide which may be a useful SOD mimic and is the oxidised form of our target hydroxylamine.

Chapter 5: Synthesis of Pyridinium Salt Nitrone Spin Traps

5.1 Pyridinium salts

As discussed in Chapter 3, the use of delocalised lipophilic cations (DLCs) is a highly effective strategy for mitochondrial targeting.[130] For this purpose, the most widely used DLC is the TPP cation, however there are limitations to using this cation. Due to its cone shape, the TPP group could disrupt membrane structure by favouring a convex shape over the desired concave shape of the inside of the mitochondrial inner membrane.[131] This may be responsible for the toxic limit of TPP-targeted compounds. Also, the TPP group has a high molecular weight which is a disadvantage for any potential pharmaceutical applications. To conform to Lipinski's rules for good pharmacokinetics, the entire molecule should have a molecular weight of < 500.[132] Because of these issues we have considered *N*-arylpyridinium cations as alternatives to the TPP cation. These are still DLCs but are not cone-shaped so would be less likely to disrupt the membrane structure and they have lower molecular weights.

There are a number of literature examples of pyridinium cations targeting compounds to mitochondria. Rhodacyanine dyes, such as MKT-077 **230** have been shown to selectively accumulate in mitochondria.[133] F16 **231**,[134] an inhibitor of tumour growth, dequalinium **232**,[135] and pyridinium salt derivatives of ceramides (examples **233** and **234**)[136] have all been shown to be selective for mitochondria (Figure 47). These all contain *N*-alkyl rather than *N*-aryl pyridinium cations. Our choice of *N*-arylpyridinium ions was aimed at increasing the hydrophobic surface in the region of the cation (note that the cation is only formally on nitrogen, actually the positive charge is distributed over the other atoms and the electronegative nitrogen will bear a partial negative charge).

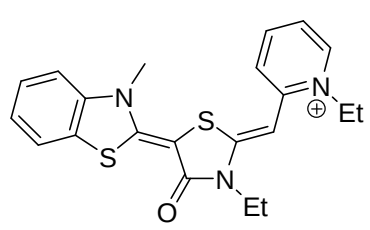

230

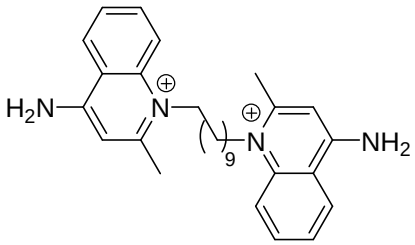

231

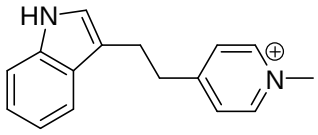

232

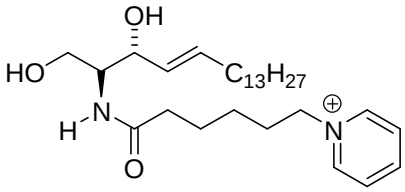

233

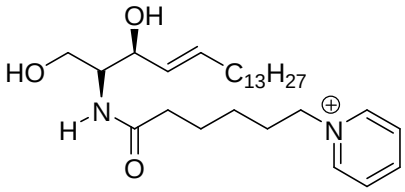

234

Figure 47: Examples of pyridinium ions that accumulate in mitochondria

Pyridinium salts can be made in a variety of ways. The most common ones are discussed in this section.

5.2 Pyridinium salts by the Menschutkin reaction and S_NAr

N-Alkylpyridinium salts **237** are commonly made using pyridines **235** as nucleophiles to displace the halogen atom of an alkyl halide **236** (Scheme 62). Mesylate or tosylate groups can also be displaced to give pyridinium salts **237**.[137] This is known as the Menschutkin reaction.[138] Substitution of a halide on an asymmetric carbon can result in racemisation by S_N1 when this can compete with the S_N2 process.[139] There are also problems associated with the use of secondary and tertiary alkyl halides or sulfonates, as there can be competing side reactions such as elimination.

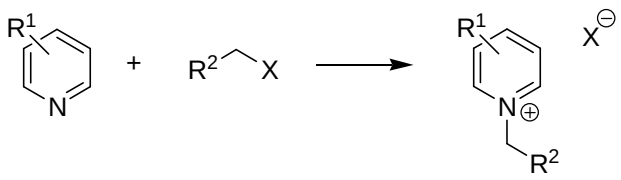

235 **236** **237**

Scheme 62

N-Arylpyridinium salts cannot be made by S_N1 or S_N2 reactions, but can be accessed through S_NAr where a nucleophilic pyridine displaces a good leaving group from an electron-poor aromatic ring by an addition/elimination mechanism. An excellent example is the formation of *N*-2,4-dinitrophenylpyridinium salts, or Zincke salts **239**. These salts are made by nucleophilic substitution of chloride from 1-chloro-2,4,-dinitrobenzene **238** using pyridines **235** as the nucleophiles (Scheme 63). The reaction is very efficient due to the presence of the electron-withdrawing nitro groups. Unfortunately, S_NAr only allows the synthesis of *N*-arylpyridinium salts with very electron-poor aryl substituents.

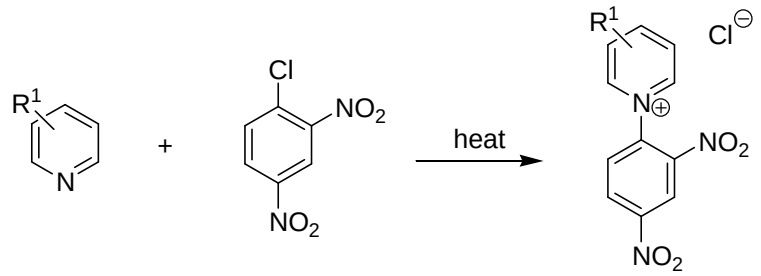

235 **238** **239**

Scheme 63: Formation of Zincke salts

5.3 Furaldehyde reaction

N-Aryl-3-hydroxypyridinium salts **242** can be made via the reaction of aniline **241** or a derivative, HCl and furaldehyde **240** (Scheme 64).[140] A conjugated intermediate, known as a Stenhouse or König salt and analogous to salt **253**, is formed. This salt then cyclises to give the pyridinium salt **242**. This is a useful reaction for the synthesis of 3-hydroxypyridinium salts but cannot be applied to the synthesis of *N*-arylpyridinium salts lacking the hydroxy substituent.

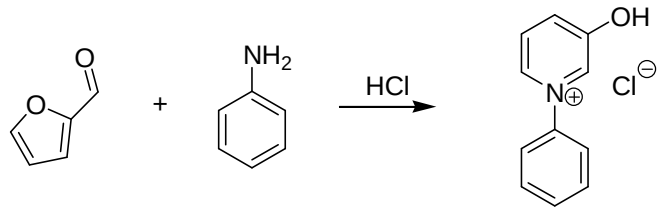

240 **241** **242**

Scheme 64: Formation of 3-hydroxypyridinium salt **242** from furaldehyde **240**

5.4 Zincke reaction

The Zincke reaction, first reported in 1903 makes pyridinium salts from the corresponding amines.[141] The general scheme for the reaction is shown in Scheme 65. The Zincke reaction is an amine exchange that converts *N*-(2,4-dinitrophenyl)pyridinium salts **239** to *N*-alkylpyridinium salts **243** or *N*-arylpyridinium salts **244** and 2,4-dinitroaniline **245**. There are some variations possible by using different nitrogen nucleophiles. Reaction with hydroxylamines yields the corresponding pyridine *N*-oxides and treatment with hydrazines gives *N*-amino pyridinium salts. *N*-iminopyridinium ylides can also be made using this type of reaction. In the context of this thesis we will concentrate on its use in making *N*-arylpyridinium salts **244**.

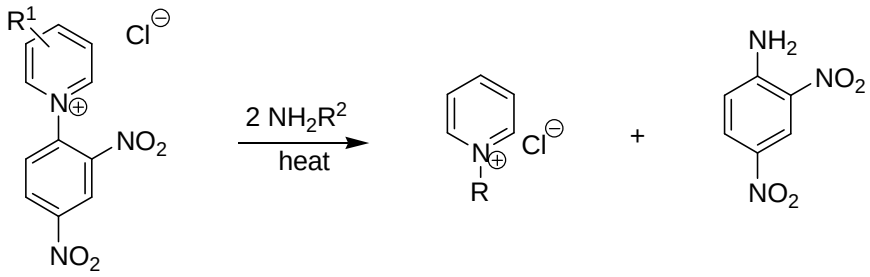

239 **243**, R = alkyl **244**, R = aryl **245**

Scheme 65: The Zincke reaction

It offers two significant advantages over the nucleophilic substitution method; it occurs with retention of stereochemistry when a chiral aliphatic amine is used and does not require electron-withdrawing groups on the reacting aryl group when *N*-arylpyridinium salts are being prepared. The reaction can be used to make a wide range of substituted *N*-alkyl and *N*-aryl pyridinium salts and is not restricted to the synthesis of 3-hydroxypyridinium compounds, so in this respect it offers an advantage over the use of the furaldehyde reaction. It has been used for a number of applications, including synthesis of natural products,[142] solid-supported synthesis[143] and the synthesis of NADH analogues.[144] In this section only the mechanism and the effect of ring-substituents will be discussed. However there are comprehensive reviews of the reaction and its applications in recent literature.[139, 145]

The Zincke salts **239** are prepared by S_NAr reaction between pyridines **235** and 1-chloro-2,4-dinitrobenzene **238** as shown in Scheme 63. Once prepared, this salt is reacted at room temperature with at least 2 equivalents of an aniline derivative

246. The mechanism is shown for the reaction of the simplest Zincke salt **247** with an aniline **246** (Scheme 66). At first sight, the overall reaction appears to require only 1 equivalent of the aniline **246.** Attack by aniline **246** occurs at the carbon atom adjacent to the nitrogen atom, followed by deprotonation with a second equivalent of aniline **246**. Electrocyclic ring opening occurs to give the conjugated intermediate **251**. Formation of the König salt **253** is first order with respect to the Zincke salt **247**, but second order with respect to the aniline **246** (or first order in aniline and first order in added base) and this provides evidence for the electrocyclic mechanism shown. The structure of König salt **253** demonstrates the need for two equivalents of aniline **246**. Protonation of open intermediate **250** allows bond rotation to give the all *E* geometry. The aniline **246** then attacks for a second time, proton transfer occurs and 2,4-dinitroaniline **245** is eliminated to give the conjugated iminium intermediate, or König salt **253**. *E-Z* interconversion and deprotonation by aniline **246** gives the free imine **254** which cyclises through an electrocyclic ring closure. This process can be accelerated by the addition of base to encourage formation of the free imine **254**. Protonation of imine **254** encourages elimination of one equivalent of aniline **246**, restoring aromaticity and forming the desired *N*-arylpyridinium salt **244**.

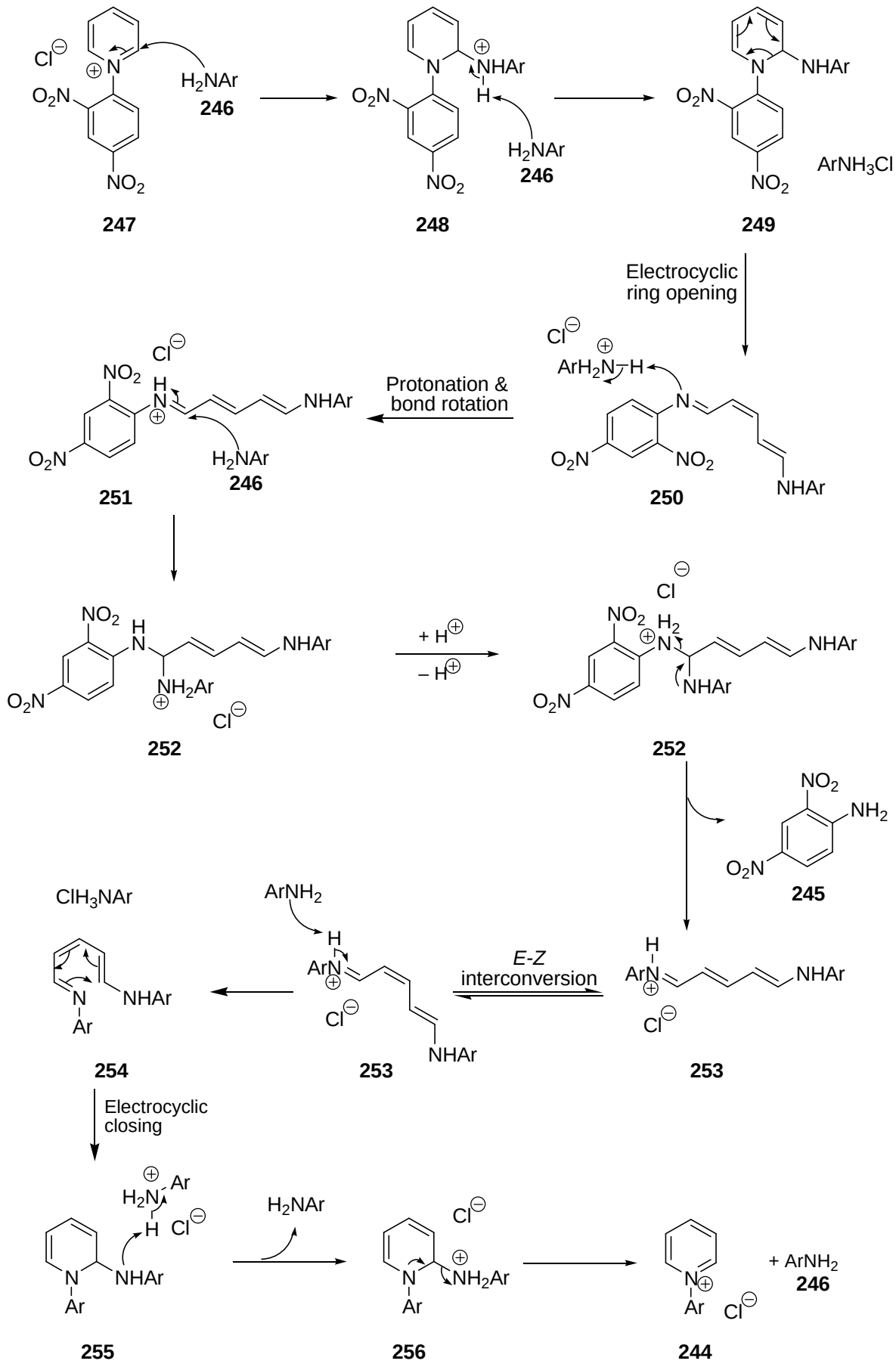

Scheme 66: Mechanism of Zincke reaction

A large number of *N*-arylpyridinium salts have been prepared by the Zincke reaction. These can have substituents on the pyridinium ring, the aryl group, or both rings. Substituent effects play a huge role in determining the success of the S_NAr reaction to generate the Zincke salt **239** (Scheme 63), and in the Zincke reaction itself (Scheme 65) and are discussed in further detail.

Firstly, let us consider substituents on the pyridines **236** used to prepare the Zincke salts **239** (Scheme 63). There are two factors to consider when thinking about how the structure of the pyridines **236** will affect the overall reaction. Firstly, pyridines **236** must be nucleophilic enough to form the starting Zincke salts **239**, and this means that substituents cannot be very electron-withdrawing. However in general, electron-withdrawing substituents on the pyridinium ring of the resulting Zincke salts **239** increase the rate of ring-opening in the Zincke reaction and if the Zincke salts are too electron-rich the reaction is slowed or stopped. Therefore, a balance between these two conflicting requirements is essential for the combination of salt formation and the subsequent Zincke reaction to be successful.

Substituents on the aryl ring also affect the Zincke reaction. The Zincke salts **239** themselves have nitro groups in the 2 and 4 positions of the aryl ring. This enables the salts **239** to be easily formed via nucleophilic substitution of a chloride and also makes a good leaving group, 2,4-dinitroaniline **245**, which is eliminated in the Zincke reaction. There are a number of Zincke salts reported in the literature that have extra substituents on the *N*-aryl ring but all contain the 2,4-dinitro substitution pattern.

Finally, substituents on the reacting aniline **246** can dramatically influence the reaction. Very electron-poor anilines are not good substrates for the Zincke reaction. If they are more electron-poor than 2,4-dinitroaniline **245** then it is likely that they will be eliminated in the final ring closing step, resulting in reformation of the starting material. However, such electron-poor *N*-arylpyridinium salts can usually be formed through S_NAr of an electron-poor aryl halide by a pyridine derivative, as described for Zincke salt formation.

Mildly electron-deficient anilines, electron-rich anilines, and aniline itself, are excellent substrates for the Zincke reaction, forming salts that would be impossible to form by S_NAr, for example *N*-phenylpyridinium salt **259** (Scheme 67).

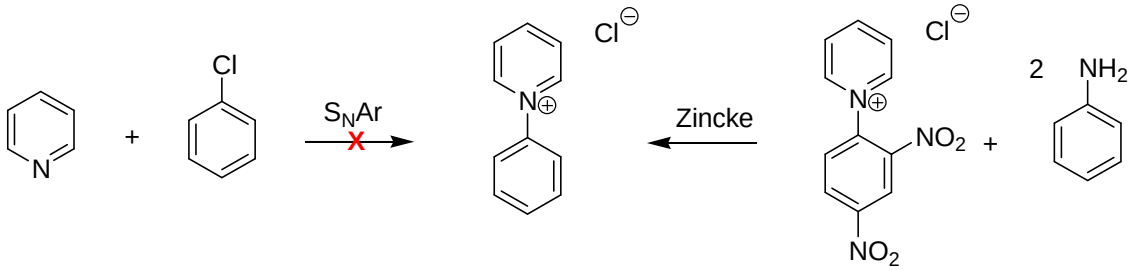

Scheme 67: Comparison of S_NAr and Zincke reaction to form pyridinium salt **259**

5.5 Design of new spin traps

We aimed to prepare the first examples of spin traps bearing *N*-arylpyridinium ions with the general structure shown in Scheme 68. PBN analogues were chosen for their simplicity of synthesis and their known efficacy as biological antioxidants. The nitrone spin traps **261** would react with radicals ($Y^{\bullet}$) to give sterically-protected nitroxides **262**.

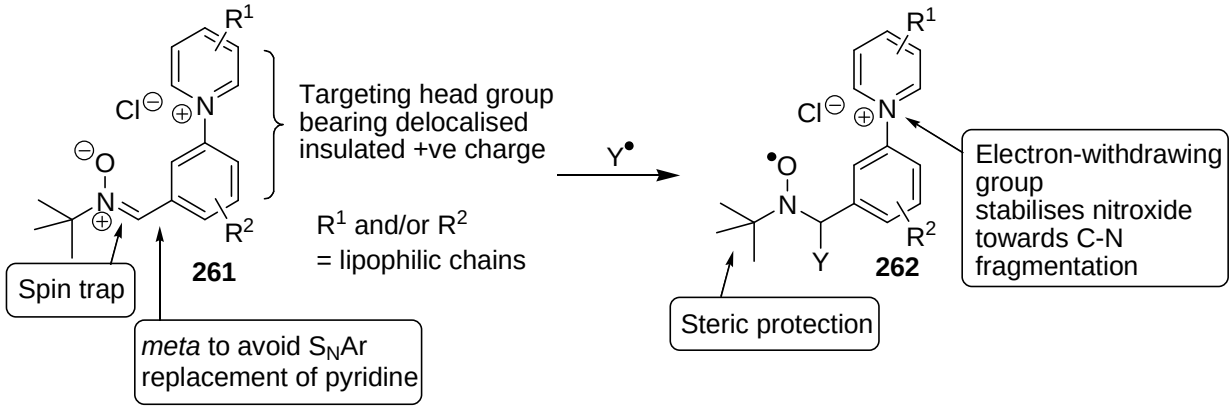

Scheme 68: Design of nitrones **261**

The presence of the pyridinium ion is expected to stabilise the nitroxide adduct to some degree by disfavouring C-N fragmentation which would involve a benzylic cation (see Chapter 2). More importantly, the pyridinium ion is a delocalised cation further insulated by the presence of the second aromatic ring. It could therefore act as a mitochondria-targeting group in the same way as the *N*-alkylpyridinium groups in compounds **230**-**234** (Figure 47), particularly when lipophilicity is increased by the incorporation of alkyl chains on either or both aromatic rings. The nitrone group is located on the *N*-aryl ring rather than on the pyridinium ring as it is an electron-withdrawing group and would encourage nucleophilic addition to the pyridinium ring if it were attached to it (Figure 48). This may also encourage reduction under biological conditions.

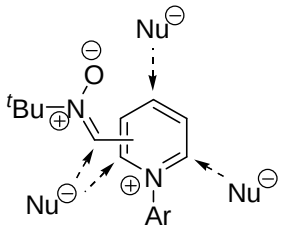

263

Figure 48

Indeed, the biological co-factor nicotinamide adenine dinucleotide (NAD^+) **264** has an electron-withdrawing amide group on an *N*-alkylpyridinium ring and is easily reduced to NADH **265** (Scheme 69).

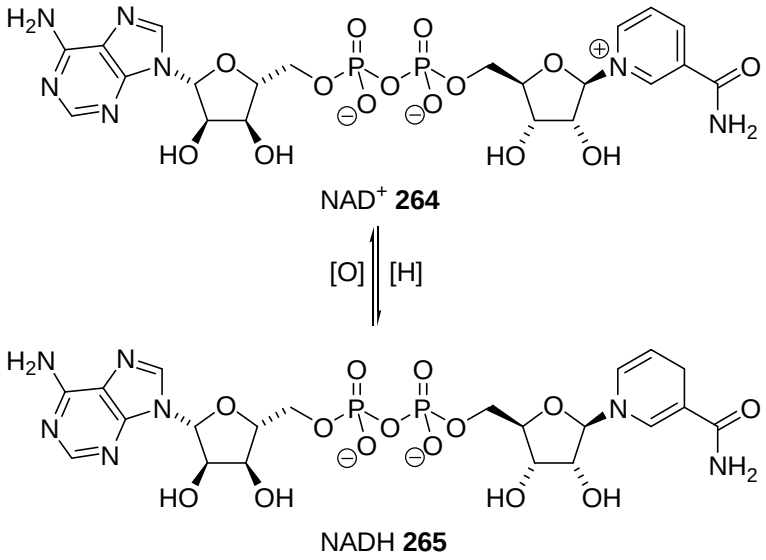

NAD^+ **264**

[O] [H]

NADH **265**

Scheme 69: Reduction of NAD^+ **264** to NADH **265**

Although direct attachment of the nitrone to the pyridinium ring would increase the stability of spin adducts, this position has a further disadvantage. It is possible that it could encourage nucleophilic addition of water to the nitrone to give a hydroxylamine, which upon auto-oxidation would give the same nitroxide as would result from addition of a hydroxyl radical to the nitrone. Finally, the *N*-pyridyl substituent is placed *meta* to the nitrone on the benzene ring to avoid any chance of this mitochondria-targeting group being lost by S_NAr. A nitrone **266** with an *ortho N*-pyridyl substituent might be particularly susceptible to such a process (Scheme 70). The *meta* substitution pattern was also expected to be less problematic in the Zincke reaction.

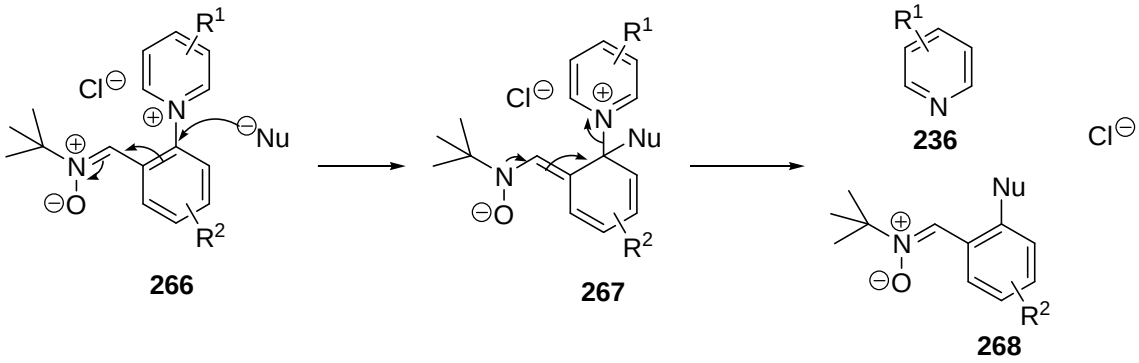

Scheme 70

5.6 First target N-arylpyridinium salt 269

Our first target was nitrone **269** which constitutes the head group alone and was expected to be water soluble. After establishing a successful route to this product it was adapted to incorporate alkyl chains (R^1 and/or R^2) to improve the lipophilicity.

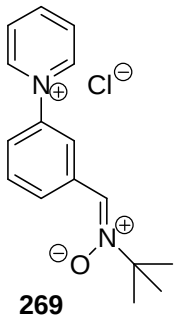

269

Figure 49

Three different strategies were attempted for the synthesis of spin trap **269**. Two of these routes were unsuccessful and the progress made with them will be discussed, along with the failings, before presenting the successful route. All strategies required the formation of Zincke's salt **247** by S_NAr, as shown for the generalised Zincke salts **239** in Scheme 63. Zincke's salt **247** was easily made in excellent yield on a 12 g scale by nucleophilic attack of pyridine **257** on 1-chloro-2,4-dinitrobenzene **238**. No solvent was required as aryl chloride **238** fully dissolved in pyridine and the reaction solidified after 1 h, indicating product formation.

5.6.1 Route via a benzylic alcohol

The first route proposed for the synthesis of nitrone **269** is shown in Scheme 71. It involved formation of a benzylic alcohol bearing a pyridinium salt **271**, oxidation to

the aldehyde **272** and conversion to the nitrone **269**. The Zincke reaction between 3-aminobenzyl alcohol **270** and Zincke salt **247** proceeded cleanly to give salt **271** in good yield. The work-up that was established for the Zincke reaction mixtures was very efficient at giving clean products. The aqueous layer was washed a number of times with EtOAc or DCM to remove the non-ionic organic side products and then the water was removed under reduced pressure to give the pyridinium salt. This method generally resulted in products which needed no further purification and was used for all Zincke reactions carried out in this project.

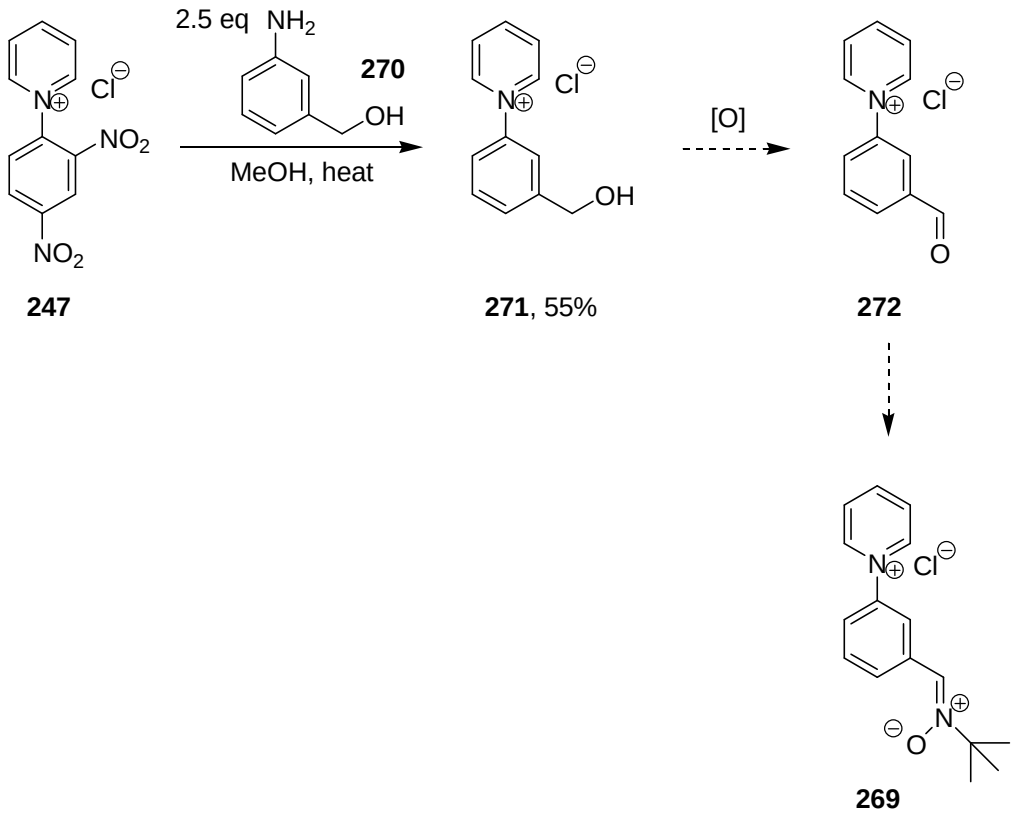

Scheme 71: Oxidation route to pyridinium salt spin traps

With salt **271** in hand, we attempted a number of oxidations to the aldehyde **272**. Pyridinium salt **271** had limited solubility (H_2O, DMSO, DMF, MeOH and EtOH) so we were restricted in our choice of oxidation method. The methods tried are summarised in Table 2.

Entry	Reagent	Conditions	Result
1	MnO_2[146]	H_2O, rt, 18 h	SM
2	MnO_2	H_2O, 110 °C, 18 h	SM
3	Py-SO_3, NEt_3, DMSO[147]	0 °C → rt, 18 h	SM
4	$(COCl)_2$, NEt_3, DMSO[148]	0 °C → rt, 18 h	SM
5	KI, I_2, K_2CO_3[149]	H_2O, 90 °C, 45 min	SM
6	KI, I_2, K_2CO_3	H_2O, 90 °C, 18 h	SM
7	H_2O_2, $FeBr_3$[150]	rt, 18 h	SM
8	sIBX, DMSO[151]	rt, 2 h	Possibly aldehyde but mostly SM
9	sIBX, DMSO	rt, 18 h	Possibly aldehyde but mostly SM
10	sIBX, DMSO	50 °C, 18 h	Possibly aldehyde but mostly SM
11	sIBX, DMSO, fluorobenzene[152]	85 °C, 18 h	Possibly aldehyde but mostly SM
12	$Pd(OAc)_2$, DMSO, $NaHCO_3$[153]	80 °C, 72 h	SM

Table 2: Oxidation conditions for the synthesis of **272**

In most of the reactions only starting material was recovered. MnO_2 is clearly not a powerful enough oxidant to oxidise a benzylic alcohol to an electron poor aldehyde (entries 1 & 2). Parikh-Doering oxidation also failed (entry 3). The Swern oxidation procedure (entry 4) was adapted to use DMSO as the solvent instead of DCM, due to the solubility issues, but therefore it was not possible to cool to -78 ℃ in this solvent system, possibly a reason for its failure. The potassium iodide/iodine/potassium carbonate system was also unsuccessful (entries 5 & 6), as was $FeBr_3$ and H_2O_2 (entry 7). When stabilised 2-iodoxybenzoic acid (sIBX) (entries 8-11) was used some traces of an aldehyde were seen in the ^{1}H NMR spectrum but these were a very minor component and it was unclear whether or not it was the desired aldehyde. sIBX also proved very difficult to separate from pyridinium salts. Palladium catalysed oxidation also

failed (entry 12). The Kornblum oxidation converts primary halides to aldehydes using sodium bicarbonate in DMSO.[154] Using the procedure of Shao and co-workers,[155] alcohol **271** was treated with neat thionyl chloride and gave benzylic chloride **273** in an excellent yield (Scheme 72).

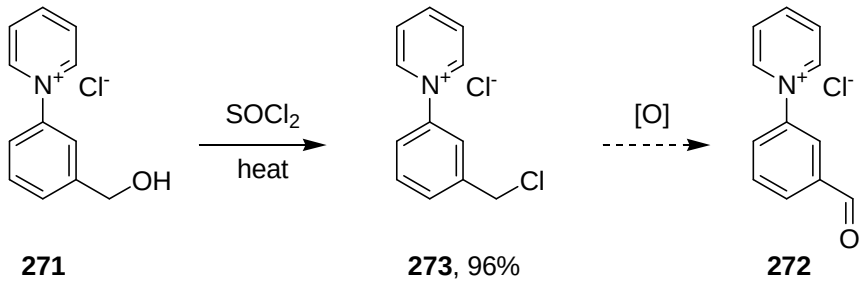

271 **273**, 96% **272**

Scheme 72: Alternative oxidation route via benzylic chloride

Unfortunately oxidation using this method was unsuccessful and gave only starting materials. We also synthesised the methyl pyridinium salt **275** in excellent yield using the Zincke reaction. Attempts to oxidise this using either SeO_2 or sIBX also proved unsuccessful (Scheme 73). At this point the oxidation route was considered not viable and other routes to nitrone **269** were explored.

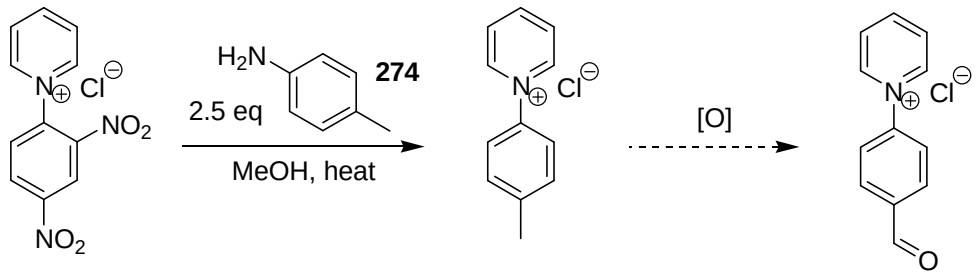

247 **275**, 96% **276**

Scheme 73: Alternative oxidation route

5.6.2 Route employing acetal protecting groups

The second route proposed for the synthesis of nitrone **269** is shown in Scheme 74. This route begins with the protection of 3-nitrobenzaldehyde **277** as acetals **278** and **279**, followed by reduction to the corresponding anilines **280** and **281**. Zincke reaction would form salts **282** and **283** which would be deprotected to give aldehyde **272**. Conversion to the nitrone would then give the first spin trap **269**. *Para*-substituted analogues were also investigated.

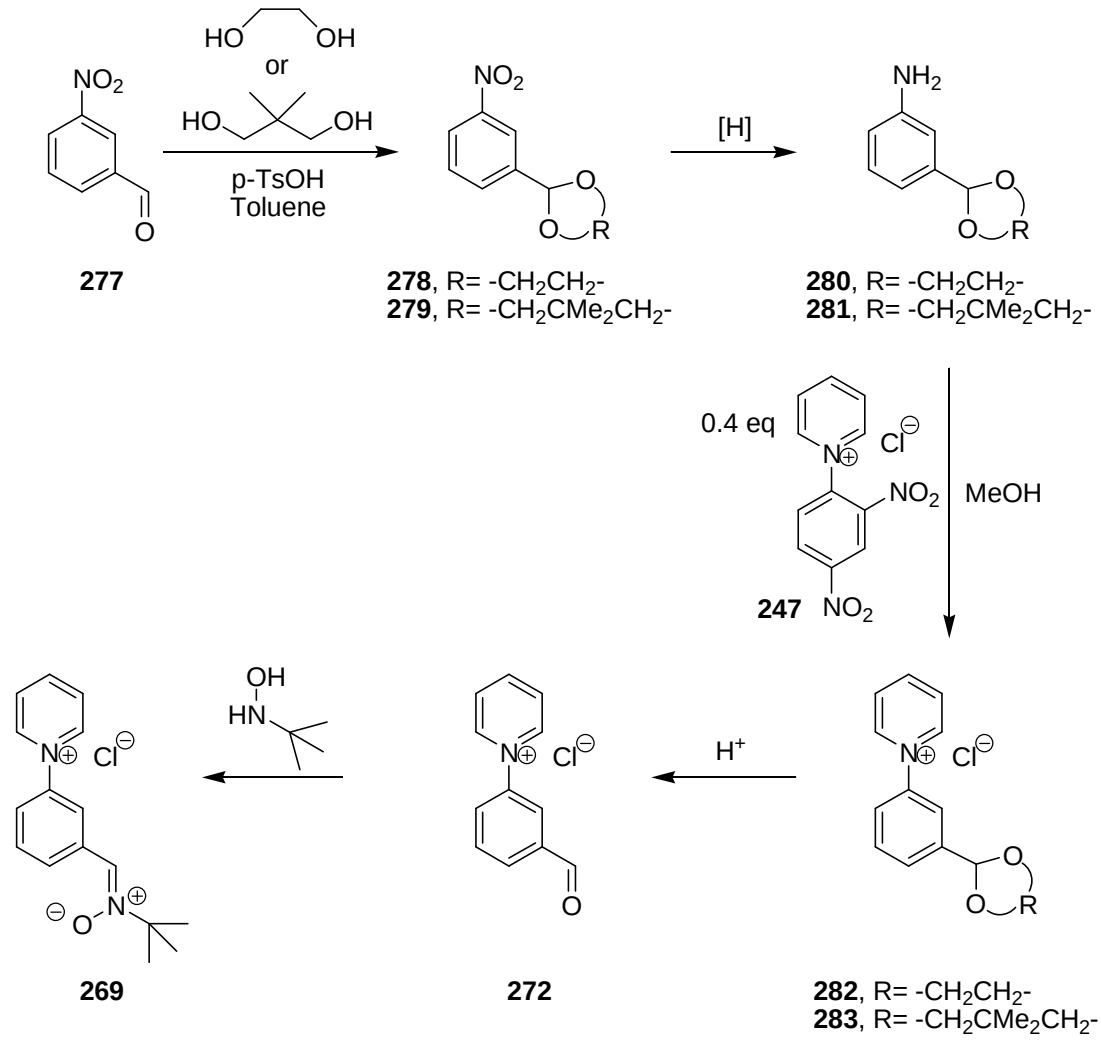

Scheme 74: Proposed route to pyridinium salt spin trap **269** using acetal intermediates

Acetals **278**, **279**, **284** and **285** (Figure 50) were synthesised from the corresponding aldehydes under Dean-Stark conditions with catalytic *p*-toluene sulfonic acid and the appropriate diol, in 96%, 95%, 90% and 99% yield respectively.

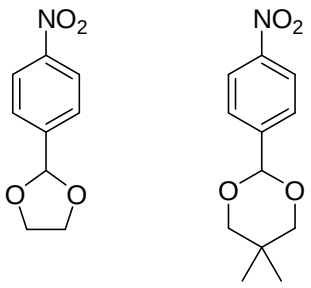

284 **285**

Figure 50

In contrast to this, the success of the subsequent reduction step varied hugely. In the case of dioxolane **284**, reduction to aniline **286** was attempted using iron and

ammonium chloride, but the only product formed was an insoluble yellow solid believed to be a polymer. Next, hydrogenation using the H-Cube® automated hydrogenator and palladium on carbon (Pd/C) as the catalyst was tried (Scheme 75). However, concentration of the solution at the end gave only an insoluble yellow solid again. The reaction was then tried using transfer hydrogenation reaction conditions with ammonium formate and Pd/C[156] but the solid was formed again. Another procedure[157] was attempted using $NaBH_4$ and Pd/C but gave the same product. It was thought that this solid was poly-imine **288**, the result of polymerisation of 4-aminobenzaldehyde **287**, formed through reduction to **286** and removal of the acetal (Scheme 75). Pd/C can contain some residual HCl because it is manufactured by reduction of $PdCl_2$ and it was thought that this was causing the cleavage of the acetal. For this reason a reduction method was tried that did not use this catalyst.

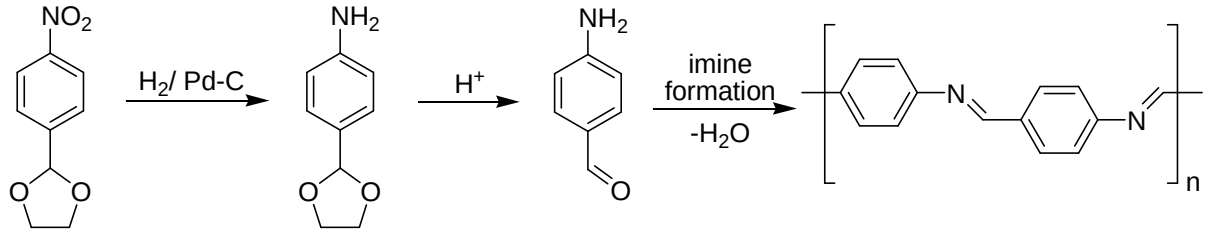

284 **286** **287** **288**

Scheme 75: Proposed polymerisation

Platinum(IV) oxide was then investigated as it is an effective hydrogenation catalyst but does not have the acidity associated with palladium on carbon. Nitro compound **278** was successfully reduced to aniline **280** (Scheme 76). Nonetheless, dioxolane **280** also had a tendency to polymerise (Scheme 75) upon concentration, so was not isolated but was used as a solution in the Zincke reaction. 5,5-Dimethyl-1,3-dioxanes **279** and **285** did not give rise to any problems but were successfully reduced by hydrogenation with platinum(IV) oxide as the catalyst to give anilines **281** and **289** in excellent yield (Schemes 77 and 78). These results were surprising as 5,5-dimethyl-1,3-dioxanes are reported to be slightly less stable to acid than dioxolanes, and benzylic acetals with a *para* amino substituent would be expected to be more susceptible to hydrolysis than when the substituent is *meta*.[158]

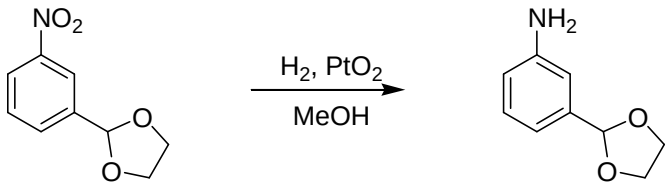

278 **280**, unstable

Scheme 76

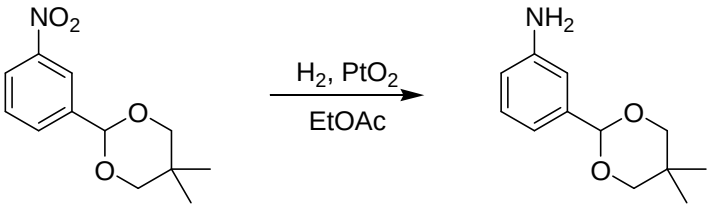

279 **281**, 99%

Scheme 77

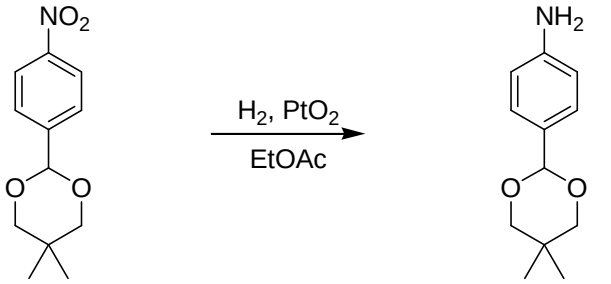

285 **289**, 100%

Scheme 78

The Zincke reaction (Scheme 65) between Zincke's salt **247** and anilines **280**, **281** and **289** was used to form the pyridinium salts **282**, **283** and **290** respectively. Salt **283** was formed cleanly and in excellent yield based on Zincke's salt **247** (Scheme 79, note that 2.5 equivalents of aniline are used).

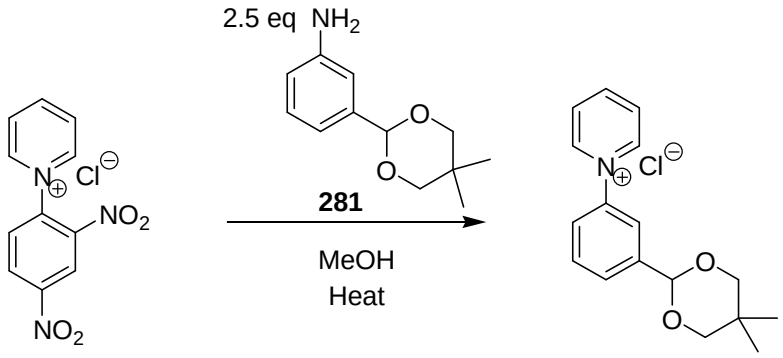

247 **283**, 90%

Scheme 79

Salt **282** was more challenging to make. When a small sample was removed from the hydrogenation of nitro compound **278** in EtOAc for analysis by NMR spectroscopy, it was clear that the reaction had been successful and aniline **280** had formed, determined by the loss the aldehyde peak. However, over time this solution turned orange and a solid began to precipitate. It was suspected that polymerisation was occurring. The solvent used in the hydrogenation was changed from EtOAc to methanol and instead of concentrating the reaction mixture at the end of the hydrogenation, the catalyst was filtered off and the filtrate was immediately added to Zincke salt **247** to perform the Zincke reaction. This method gave salt **282** in excellent yield based on Zincke salt **247** (Scheme 80). In the case of salt **290**, the reaction appeared successful from the aromatic region of the ^{1}H NMR spectrum but could not be purified in the standard way so it is unclear whether this actually formed (Scheme 81).

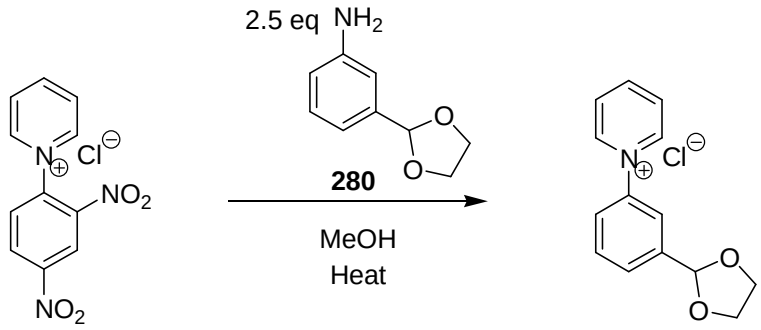

247 **282**, 92%

Scheme 80

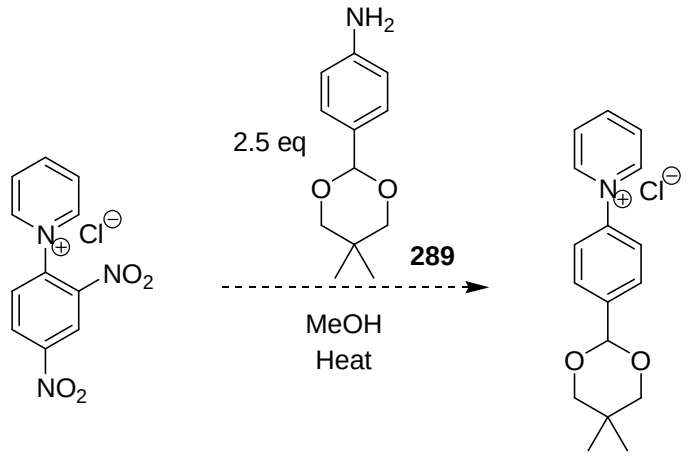

247 **290**

Scheme 81

Deprotection reactions were performed on salts **282** and **283**. Due to the aforementioned impurities, salt **290** was not used. 5,5-Dimethyl-1,3-dioxane **283** was treated with 6M HCl at room temperature for 24 h, but showed no deprotection. It was then heated at reflux in 6M HCl but there was still no deprotection and only starting material was seen. Due to the apparent inertness of this compound under harsh conditions, it was concluded that the acetal on salt **283** was too stable for deprotection. Dioxolane **282** was also treated with 6M HCl at room temperature for 22 h. The ^{1}H NMR spectrum showed the appearance of a small aldehyde peak so the reaction was heated at reflux for a further 22 h. However, there was still a large amount of starting material in the reaction and attempts to separate the two salts by recrystallisation did not give aldehyde **272** cleanly.

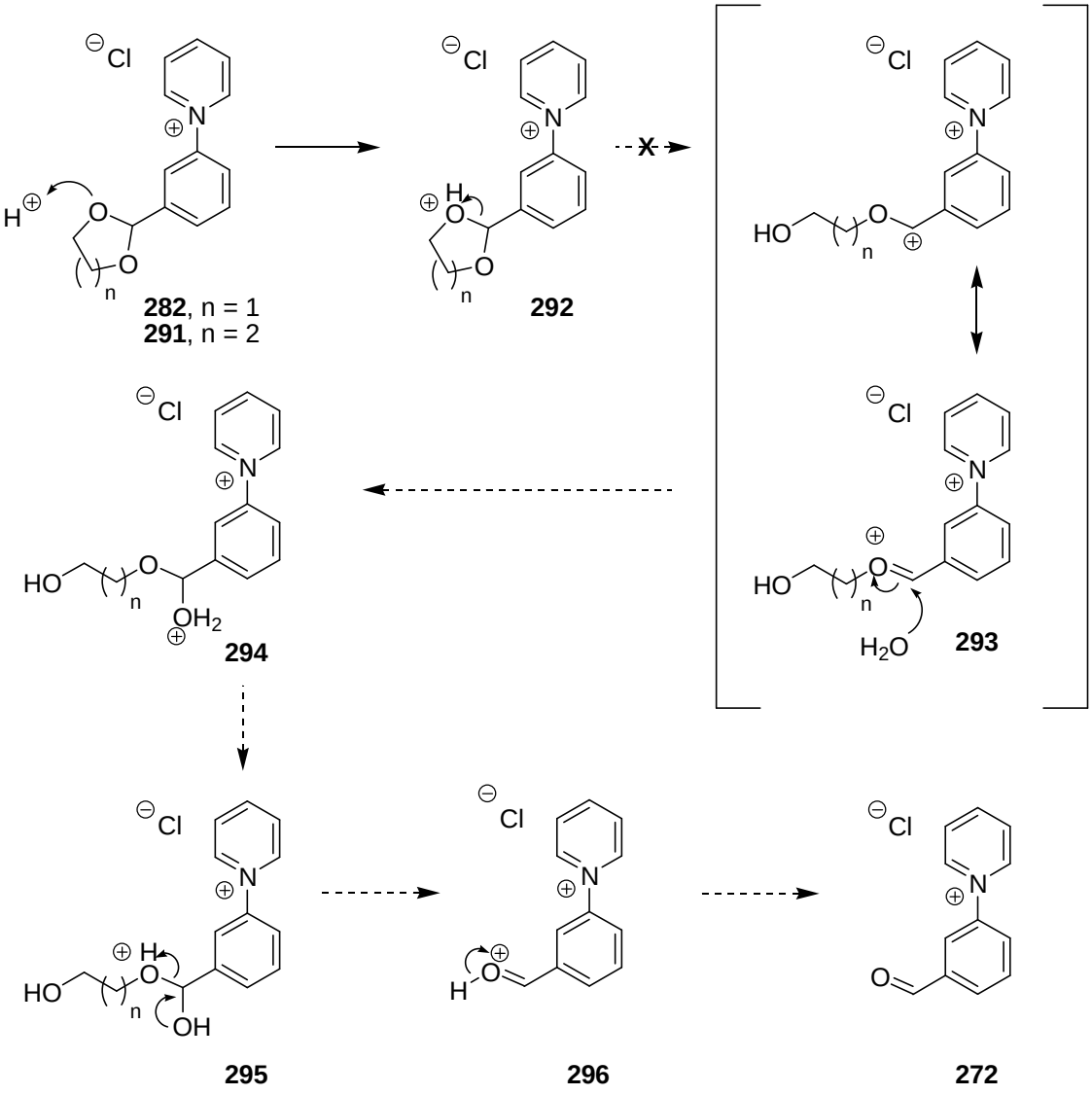

Scheme 82: Mechanism of acid-catalysed acetal hydrolysis

The stability of the acetals to acid-catalysed hydrolysis is not surprising given the mechanism of the reaction (Scheme 82). The rate determining step is the opening of the acetal to form dication **293**. This is disfavoured for pyridinium salt acetals as the cation formed by opening of the acetal is conjugated to the aromatic ring bearing the electron-withdrawing pyridyl group, disfavouring the formation of dication **293**.

Fortunately, at this time the nitrone route that was being tested proved successful so the acetal route was abandoned.

5.6.3 Chemoselective route using a pre-formed nitrone

The successful route to spin trap **269** is shown in Scheme 83. The key to the success of this route was the formation of the pyridinium salt in the final step, because the Zincke reaction proceeds in high yield and purity there was no need to separate multiple pyridinium salts. There were also no restrictions on reagents or conditions used due to the limited solubility of the pyridinium salts.

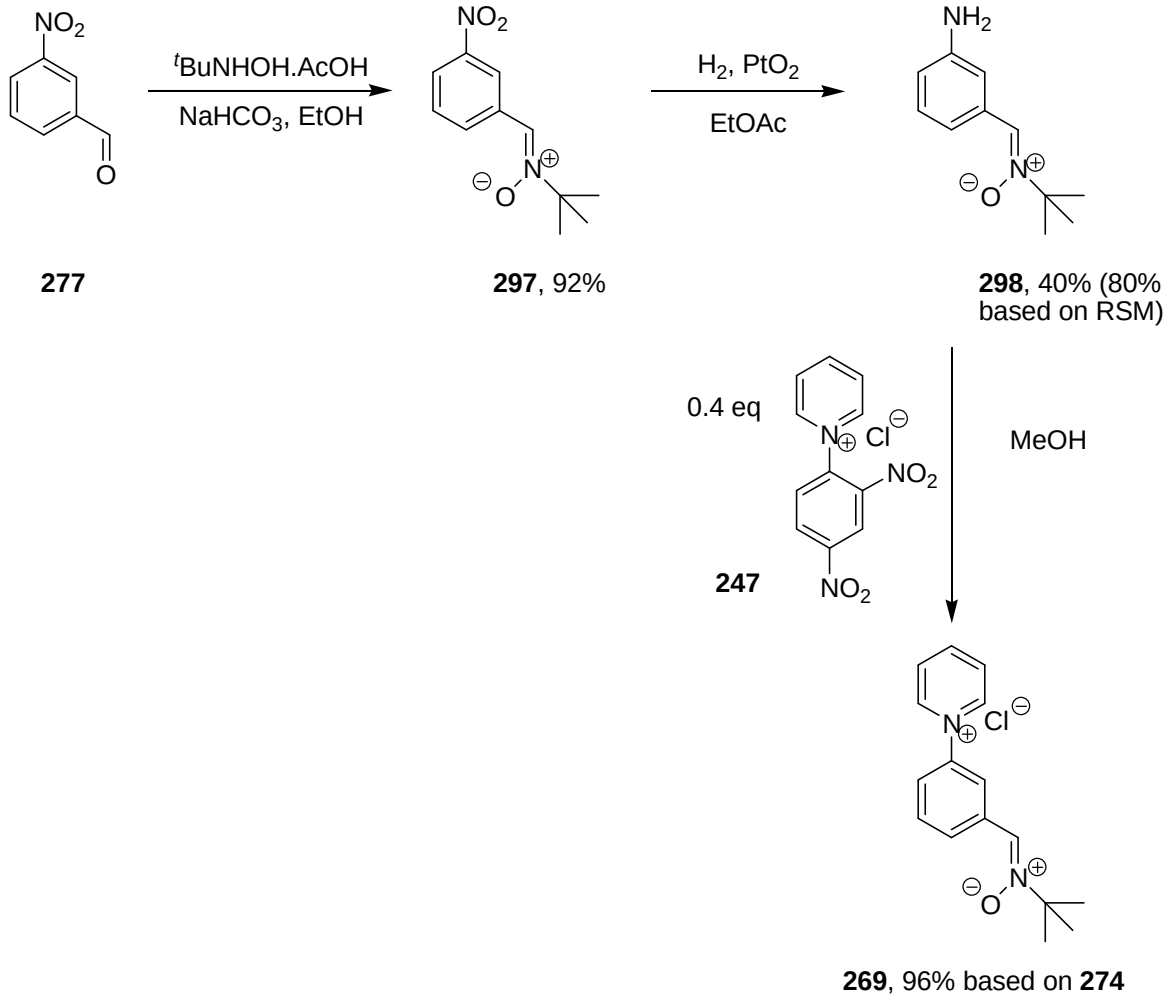

Scheme 83: Successful route to pyridinium salt spin trap **269**

3-nitrobenzaldehyde **277** was smoothly converted into *N*-*tert*-butylnitrone **297** in excellent yield with no need for purification. Upon completion, if the reaction mixture was poured into water and allowed to stand for approximately 1 h, the product crystallised out as bright yellow needles. The highly crystalline nature of this compound was advantageous in the next stage of the synthesis.

The reduction of the nitro group was similar to that of the previous synthesis so the issue with using Pd/C in the presence of the acid-sensitive nitrone group was anticipated. For this reason, platinum(IV) oxide was again selected as the hydrogenation catalyst. It was also unknown whether hydrogenation would be selective for the nitro group over the nitrone in compound **297**. Fortunately, hydrogenation occurred at the nitro group first, but if the reaction was allowed to continue to completion some reduction of the nitrone was observed. If nitrone contaminated with the over-reduction product was used in the subsequent Zincke reaction, a small impurity was seen in the final ^{1}H NMR spectrum of the product that could not be removed. An extra singlet *tert*-butyl peak indicated that this impurity also contained a *tert*-butyl group. EPR data (see later in this chapter) indicated that this impurity was nitroxide **300** produced by autooxidation of hydroxylamine **299** formed from an over-reduced product from the hydrogenation step (Scheme 84).

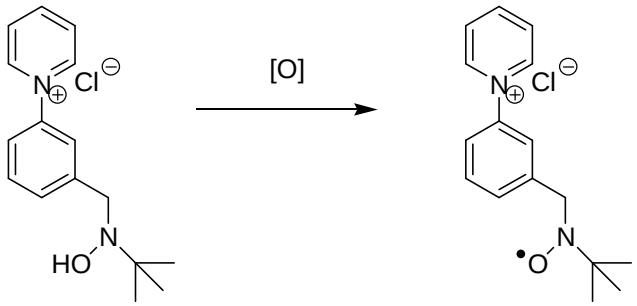

299 **300**

Scheme 84

Efforts were made to prevent this contamination. Firstly, the hydrogenation reaction was stopped after approximately 50% conversion and the mixture of nitrones **297** and **298** was used in the Zincke reaction. This also resulted in some impurities in the final product. The best method that was found for eliminating the over-reduced product was to stop the hydrogenation at ~50% conversion and crystallise the starting nitrone **297** out of the mixture using a methanol/water mixture. This gave a yield of only 40% of nitrone **298** but the yield was 80% based

on recovered starting material **297**. Once the problem of nitrone reduction had been solved, an excellent yield of the spin trap **269** was isolated from the Zincke reaction. The nitrone produced under the optimised procedure was estimated to contain only 2% of the nitroxide **300** impurity, by integration of the ^{1}H NMR signal at δ 1.42 ppm, presumed to result from its *tert*-butyl group.

Salt **269** was soluble in water, DMSO, EtOH, and MeOH, and insoluble in all other organic solvents. This indicated that salt **269** would not be sufficiently lipophilic to pass through cell membranes. Therefore, now that an efficient route to the first salt had been established this route was modified to incorporate lipophilic alkyl groups.

5.7 Synthesis of lipophilic nitrone spin traps

5.7.1 Route using a lipophilic Zincke salt

The first approach to a lipophilic spin trap **304** is shown in Scheme 85. It involved synthesis of a Zincke salt **303** with an alkyl group attached to the pyridinium ring. This route was appealing as it would allow the rest of the synthesis to proceed exactly as in the previous synthesis, using those optimised reactions.

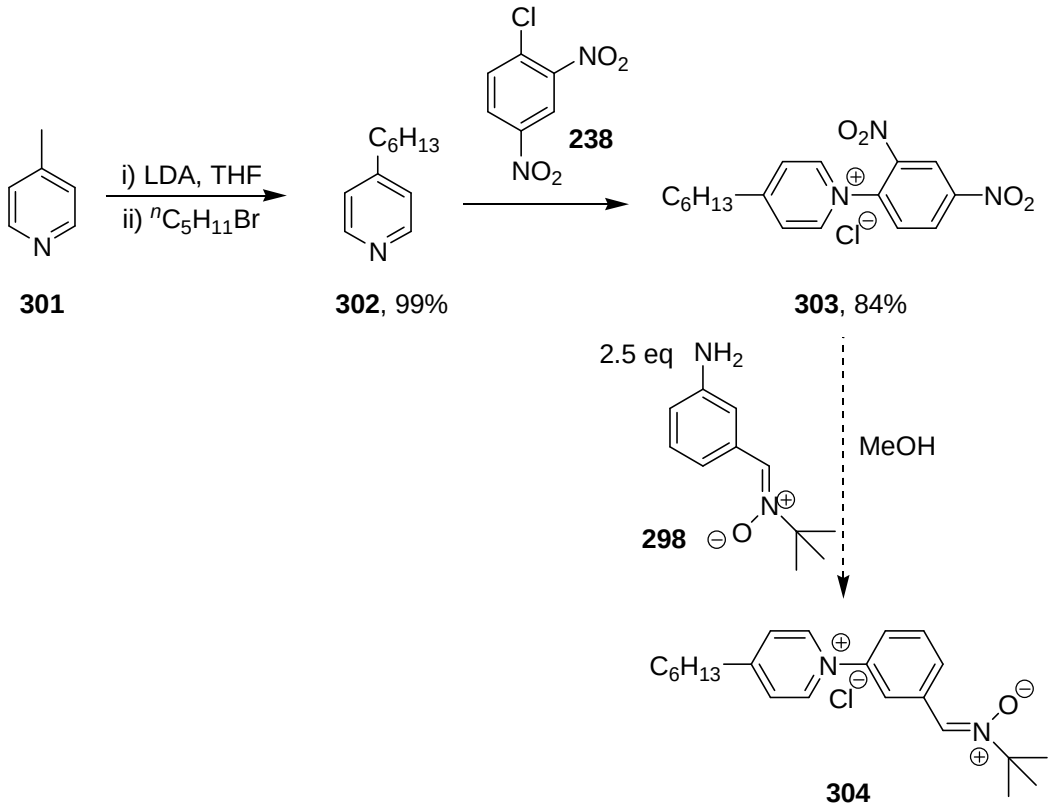

Scheme 85: First route to lipophilic pyridinium salt spin traps

4-Methylpyridine **301** was treated with LDA and reacted with 1-bromopentane to give 4-hexylpyridine **302** in quantitative yield after column chromatography. Nucleophilic attack by pyridine **302** on 1-chloro-2,4-dinitrobenzene **238** gave the lipophilic Zincke salt **303** in a high yield. Unlike the formation of Zincke salt **247**, no solid was formed and the reaction mixture was a brown/black oil. The best purification method involved dissolving the oil in MeOH (minimal) and water, washing with EtOAc until the washings were colourless and then concentrating the aqueous layer to give the salt **303**.

Aniline **298** was made in the same way as previously described and the Zincke reaction between this and salt **303** was attempted. The procedure that was used successfully in previous reactions gave only a mixture of starting materials. Increasing the equivalents of amine from 2.5 to 3 did not change this result. Addition of Et_3N and changing the solvent from MeOH to *n*-butanol/toluene also gave only starting materials.

From this negative result it can be concluded that simply attaching a hexyl group to the pyridinium ring of the Zincke salt makes it too electron-rich to react with electron-deficient aniline **298**. To solve this problem, an alternative route was developed (Scheme 86). The electron-density of the pyridinium ring was decreased by using an unsubstituted pyridine to make the Zincke's salt **247**, and an electron-donating group was attached to the aniline ring to make it more electron-rich. This gives a much better combination for the Zincke reaction.

5.7.2 Route using a lipophilic aniline

The route shown in Scheme 86 involves attaching the alkyl group to the aniline via an ether linkage. A 6 or 12 carbon chain was introduced by alkylation followed by introduction of a nitro group. Alkylation of salicylaldehyde **305** using 1-bromohexane or 1-iodododecane proceeded in excellent yield for both compounds to give ethers **306** and **307**, respectively.

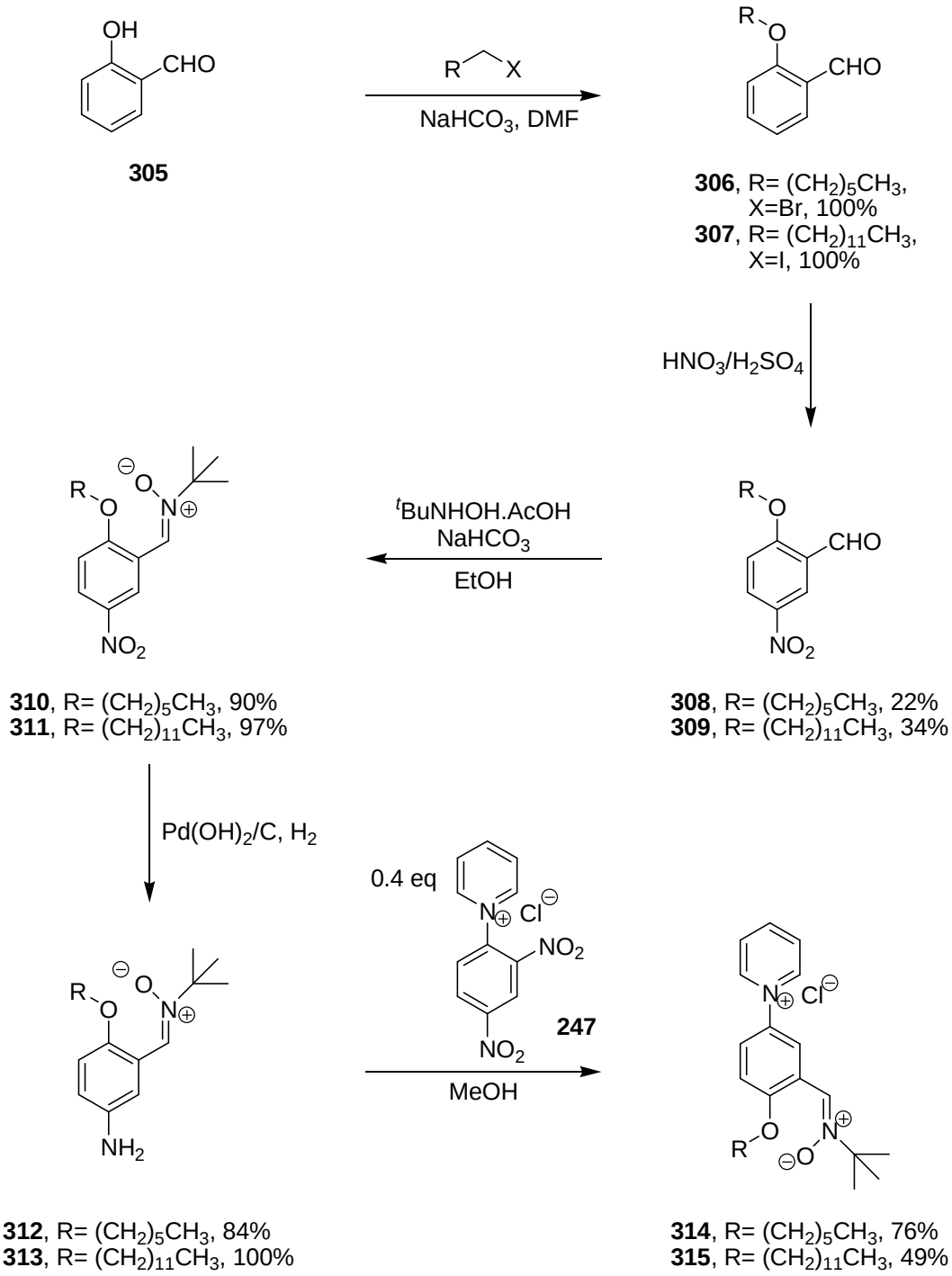

Scheme 86: Successful route to lipophilic pyridinium salt spin traps

The nitro group was introduced with a view to hydrogenating it further along the route to give an amino group. Nitration of 2-hexyloxybenzaldehyde **306** with fuming HNO_3 and concentrated H_2SO_4 gave a mixture of the desired product **308** and side products after 1 h. The products could be separated by recrystallisation, but the isolated yield of hexyl ether **308** was low. Nitration of 2-dodecyloxybenzaldehyde **307** required some alteration of the conditions as using the same conditions as above gave mostly side products and very little of the desired product **309**. Changing from fuming HNO_3 to 70% HNO_3 and lowering the

reaction time to 15 min gave a mixture of products. This mixture was an oil so could not be recrystallised, but column chromatography allowed isolation of the desired compound **309** in a moderate yield. However, enough material was made to allow continuation of the route. Introduction of the *N*-*tert*-butylnitrone groups proceeded in excellent yield for both compounds. Once again, reduction occurred at the nitro group first, but the reaction times for the reduction of nitro compounds **310** and **311** were much shorter (~30-40 min) than for the conversion of nitroarene **297** into aniline **298**, and the starting material could not be crystallised out. This meant that often the nitrone moiety was reduced to some extent and contaminants were seen in the final product. The reaction times varied between different experiments and this was most likely due to inaccurate weighing of platinum(IV) oxide. Platinum(IV) oxide is a very fine, brown powder which is susceptible to a build up of static electricity. It also does not come loaded on carbon which means that much less mass is used, usually under 10 mg per reaction. It was decided to change the catalyst to slow the rate and allow for more accurate weighing of catalyst. By changing to 10% palladium(II) hydroxide on carbon the mass was increased and therefore weighing inaccuracies were minimised. Also, there was no noticeable effect from static electricity so no catalyst was lost on addition to the flask. Changing to palladium(II) hydroxide gave much more reproducible and slightly increased reaction times. Anilines **312** and **313** were formed in high yields, with a small amount of starting material present in the case of aniline **312**. Fortunately, the subsequent Zincke reaction tolerated this starting material and pyridinium salt nitrones **314** and **315** were formed cleanly in moderate to good yield (based on Zincke's salt **247**). The lower yields compared to the preparation of nitrone **269** were attributed to the increased solubility of the salts in organic solvents. The salts were still water soluble, but washing with EtOAc was slow as the layers took much longer to separate. Furthermore, concentration of the aqueous layer was very difficult when larger volumes of water were used to help separation.

Now that all three salts had been synthesised, their spin trapping capabilities were investigated. The ability to trap $HO^{\bullet}$ and $Me^{\bullet}$ radicals was investigated.

5.8 Attempts to trap hydroxyl radicals

The Fenton reaction (Chapter 1, Scheme 1), where Fe(II) ions induce the formation of $HO^{\bullet}$ radicals from H_2O_2, was used in attempts to generate nitroxides **316**, **317** and **318** (Scheme 87). The conditions were adapted from those in the

literature[159] and had been successful with other spin traps synthesised by the group.[160] Nitrones **269**, **314** and **315** were used in a 10-fold excess relative to H_2O_2 and iron(II) ions, in a solution of DMF-H_2O (1:2). They were treated with iron(II) sulfate and H_2O_2, immediately transferred to a quartz flat cell and placed in the EPR spectrometer for analysis. Unfortunately, no EPR signal for nitroxides **316**-**318** were seen when trapping of the $HO^{\bullet}$ radical was attempted. Presumably, fragmentation of the hydroxyl adduct is fast, despite the presence of the electron-withdrawing pyridinium group.

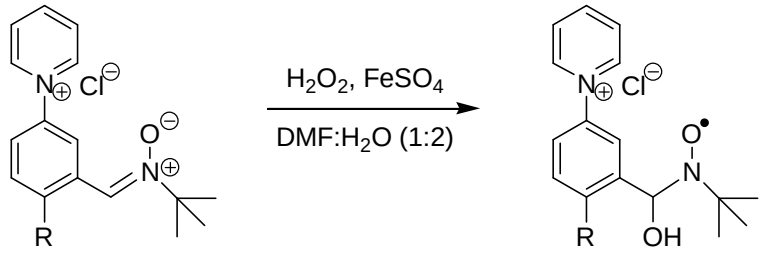

269, R = H
314, R = $O(CH_2)_5CH_3$
315, R = $O(CH_2)_{11}CH_3$

316, R = H
317, R = $O(CH_2)_5CH_3$
318, R = $O(CH_2)_{11}CH_3$

Scheme 87: Reaction of nitrones with $HO^{\bullet}$ radicals

5.9 Trapping of methyl radicals

Similar conditions can be used for the generation of methyl radicals except using DMSO instead of DMF. Reaction between DMSO and $HO^{\bullet}$ radicals gives rise to methyl radicals by the mechanism shown in Scheme 88. An $HO^{\bullet}$ radical reacts with DMSO to form the resonance stabilised radical **320**. This radical can fragment to give sulfinic acid **321** and a methyl radical.

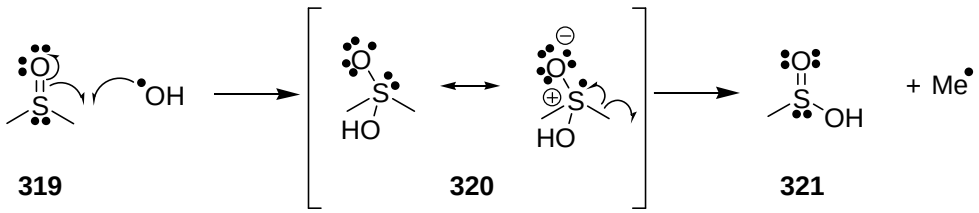

319 **320** **321**

Scheme 88: Generation of methyl radicals from DMSO

Generation of $HO^{\bullet}$ radicals by the reaction of iron(II) sulfate and H_2O_2 in DMSO gives $Me^{\bullet}$ radicals as the overwhelmingly predominant radical, provided the concentration of the reagents is chosen correctly.[161] Replicating conditions that had been used successfully in the group previously,[160] 0.33 mM H_2O_2 and 0.33 mM iron(II) sulphate in DMSO:water (1:2) were reacted with 2.5 equivalents of

nitrone **269** or 10 equivalents of nitrone **314** or **315**. The EPR spectra were recorded immediately and signals were observed that were consistent with nitroxides **322**, **323** and **324**.

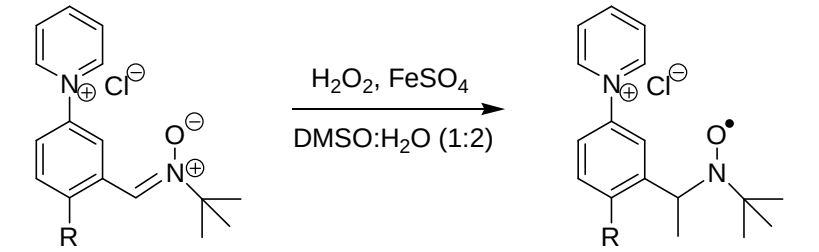

269, R = H
314, R = $O(CH_2)_5CH_3$
315, R = $O(CH_2)_{11}CH_3$

322, R = H
323, R = $O(CH_2)_5CH_3$
324, R = $O(CH_2)_{11}CH_3$

Scheme 89: Reaction of nitrones with $Me^{\bullet}$ radicals

EPR spectra and simulations are shown in Figures 52-54. Each of these spectra shows a triplet of doublets. The large triplet splitting is due to the nitrogen (spin 1) and the doublet splitting is due to the α-hydrogen (spin 1/2). The high field lines are broadened due to m_1-dependent linewidth effects and incomplete averaging of the anisotropic components caused by restricted tumbling of the spin adducts. It was expected that adducts of spin trap **315** would exhibit some broadening due to the dodecyl chains, as this has been observed by Janzen and co-workers for *N*-alkylpyridinium salt **67** (Chapter 2, Figure 26).[55]

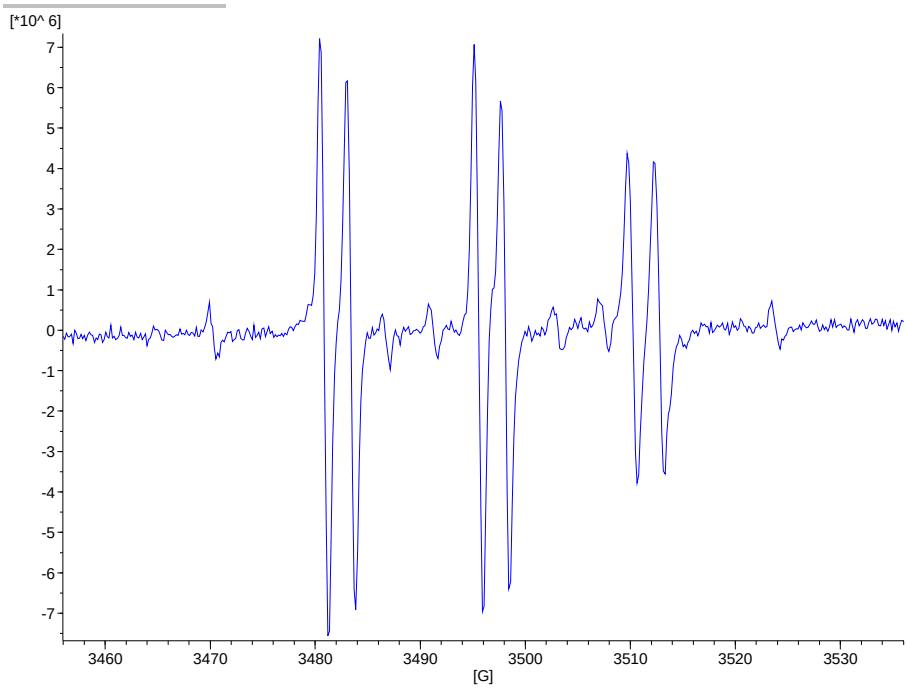

Figure 52a: EPR spectrum of methyl adduct **322**

g = 2.0069, $A_{N\,=}$ 14.70 G (t), A_H = 2.45 G (d)

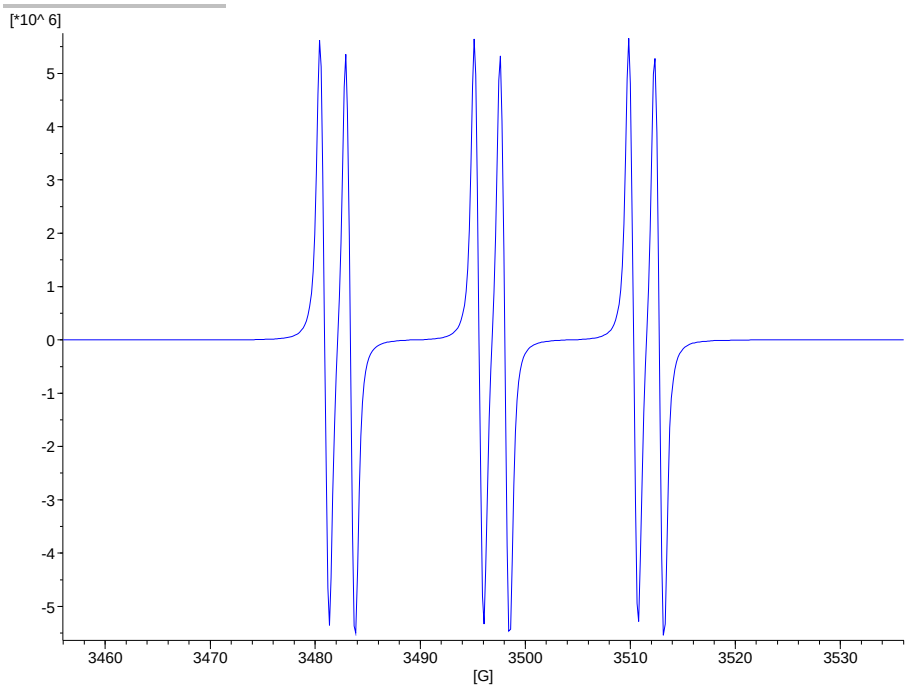

Figure 52b: Simulation of spectrum

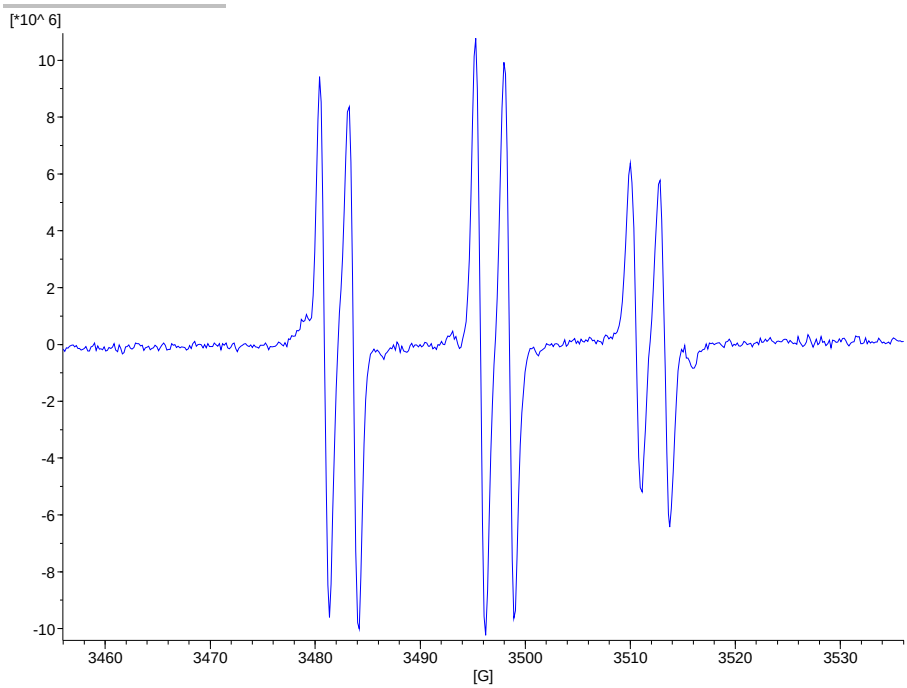

Figure 53a: EPR spectrum of methyl adduct **323**

g = 2.0057, A_N = 14.83 G (t), A_H = 2.70 G (d).

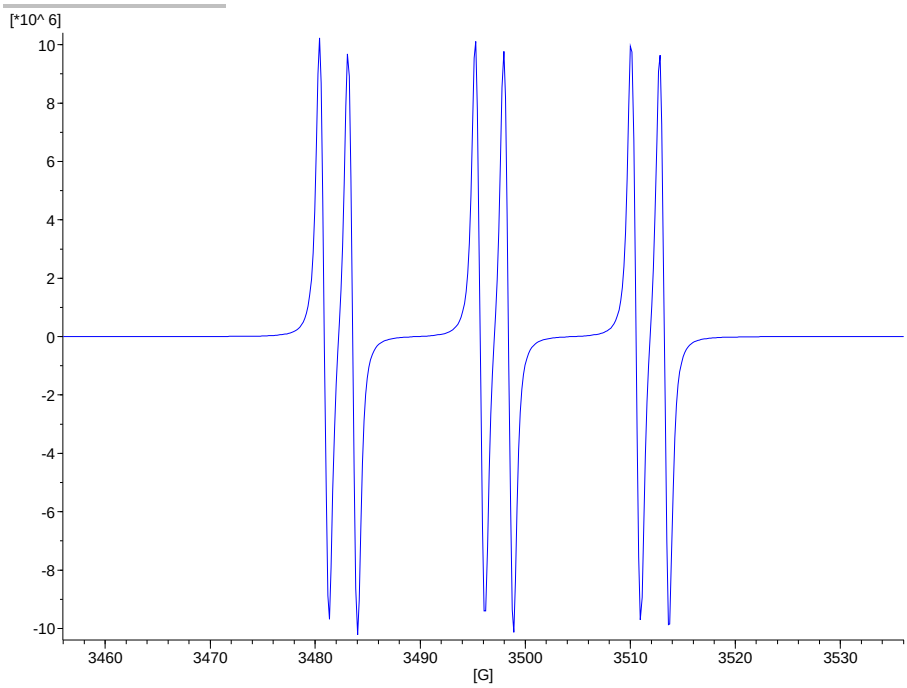

Figure 53b: Simulation of spectrum

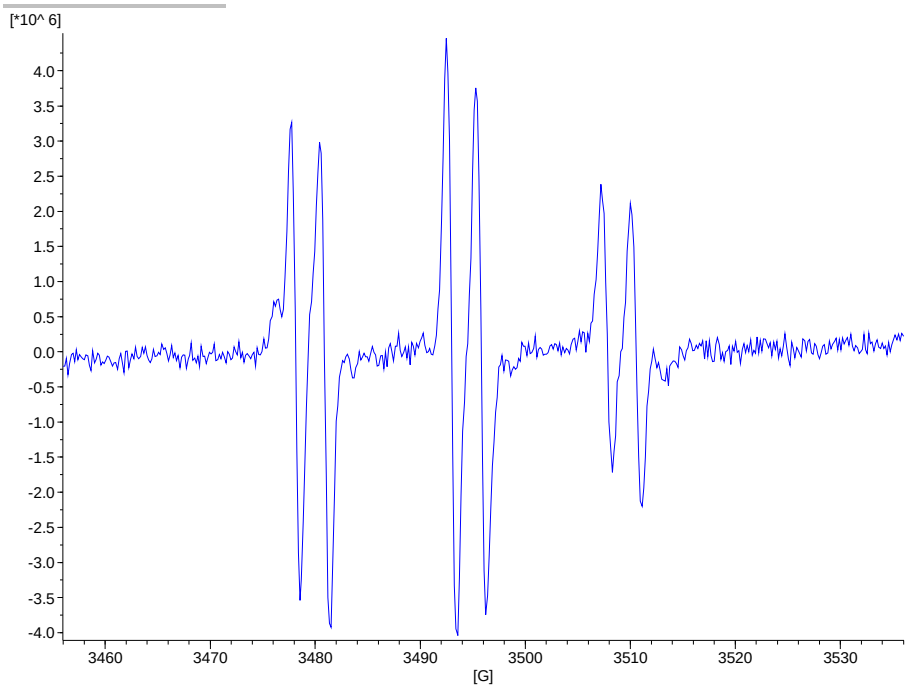

Figure 54a: EPR spectrum of methyl adduct **324**
g = 2.0057, A_N = 14.90 G (t), A_H = 2.75 G (d).

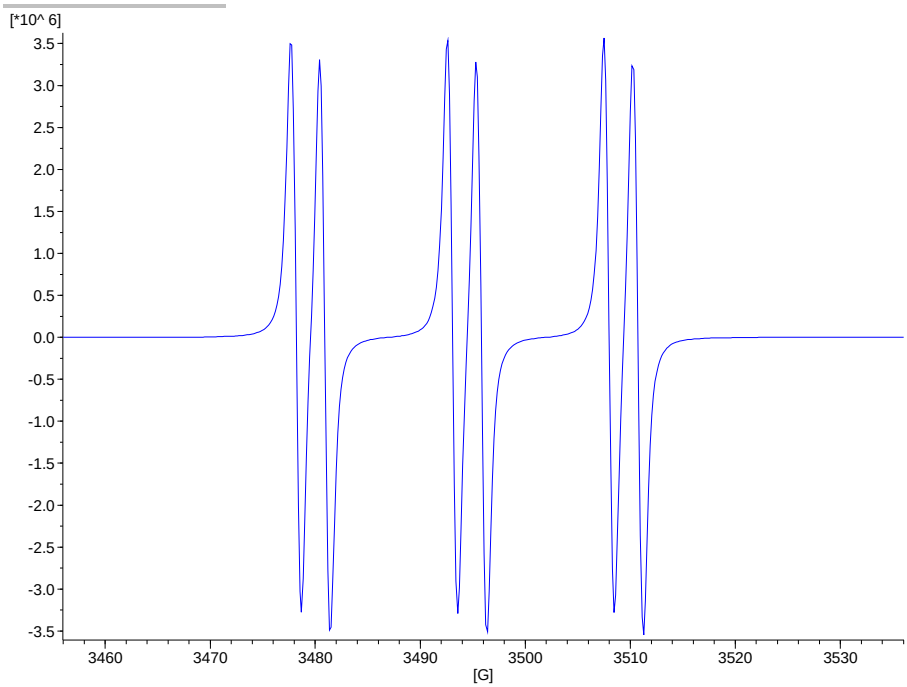

Figure 54b: Simulation of spectrum

A weak background signal was observed when samples of spin trap **269** were dissolved in DMSO/H_2O due to contaminent nitroxide **300** (Scheme 84). The background spectrum alone is shown in Figure 55.

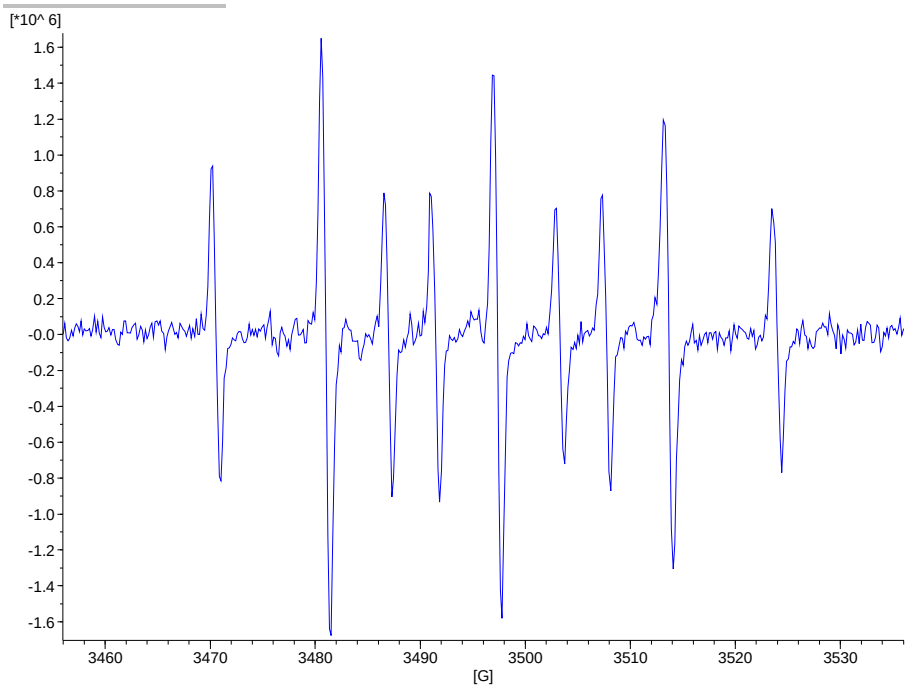

Figure 55a: Blank EPR spectrum of spin trap **269**

g = 2.0056, A_N = 16.32 G (t), A_H = 10.35 G (t).

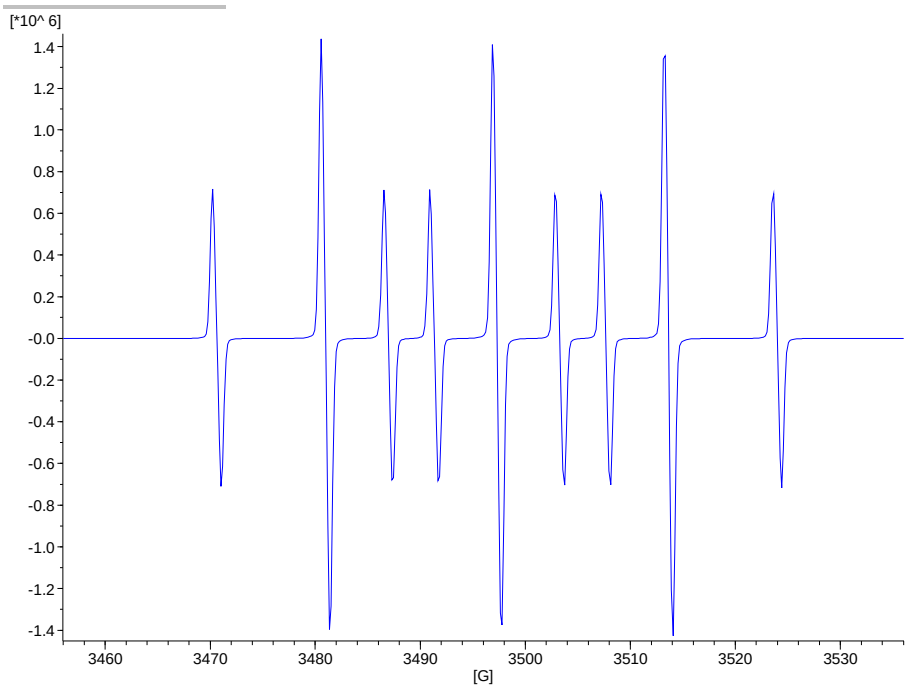

Figure 55b: Simulation of spectrum

Even though the nitroxide impurity **300** is only 2% of the sample of nitrone **269**, its EPR spectrum is visible in the spectrum of the methyl adduct **322**. This is partly because EPR spectroscopy is an extremely sensitive technique. Also, the nitrone **269** is used in excess so that, while nitroxide impurity **300** is already present, not all the nitrone **269** is converted into the nitroxide **322**. The signal from nitroxide impurity **300** is a triple triplet, consistent with the presence of two hydrogen atoms

on the carbon atom attached to the nitroxide. To minimise this signal in the trapping experiments, only 2.5 equivalents of spin trap **269** relative to H_2O_2 were used, compared with 10 equivalents of spin traps **314** and **315**. As yet, the mitochondrial accumulation of these pyridinium salts has not been tested. This could be carried out in collaboration with Dr Mike Murphy in Cambridge.

5.10 Conclusion

After investigation of two unsuccessful strategies, a short route was developed to new *N*-arylpyridinium nitrone spin traps and used in the synthesis of three new spin traps **269**, **314** and **315**. The water-soluble spin trap **269** was synthesised in 3 steps and two lipophilic versions, **314** and **315**, were synthesised in 5 steps. The key reaction in this synthesis was the Zincke reaction to incorporate the nitrone functionality into the *N*-arylpyridinium salt. This work represents the first example of using nitrones in the Zincke reaction and demonstrates their compatibility. Additionally, selective reduction of nitro groups in the presence of nitrones has been achieved with careful reaction monitoring. The ability of the three nitrones **269**, **314** and **315** to trap methyl radicals has been demonstrated. The $HO^{\bullet}$ radical adducts of these traps are not detectable by EPR spectroscopy, which is not uncommon for acyclic nitrones. Spin traps **269**, **314** and **315** may be useful for the detection of carbon-centred radicals in mitochondria, or as therapeutic antioxidants targeted to the main endogenous source of ROS.

Chapter 6: Synthesis of selective uncoupling molecules

The work discussed so far has focussed on the synthesis of compounds designed to react non-specifically with ROS and the carbon-centred radicals that they generate. These allow us to study oxidative stress by EPR spectroscopy and the compounds may also, to some extent, ameliorate oxidative stress as they are converting highly reactive radicals to radical adducts which are less reactive species. The next piece of work I will discuss has a different aim. In this section, the synthesis of compounds that are designed to react specifically with H_2O_2 to release a mitochondrial uncoupler is presented. Firstly, mitochondrial uncoupling is introduced before explaining the rationale and literature precedent for our compounds.

6.1 Mitochondrial uncoupling

As discussed in Chapter 1, the mitochondrial electron transport chain (Figure 6) provides the energy to drive ATP synthesis. It does this by pumping protons into the intermembrane space and only allowing these protons to pass back into the mitochondrial matrix through the ATP synthase complex. The energy released during this process drives the formation of ATP. Uncouplers (UC) allow the protons to bypass ATP synthase and enter the matrix via another pathway, so that electron transport occurs without ATP production i.e. the two processes are uncoupled (Figure 51). The energy is then lost as heat. As the protons are able to move across the membrane in uncoupled mitochondria, an abolition of the mitochondrial membrane potential is observed.[12]

The protein UCP1 (uncoupling protein 1; also known as thermogenin) has been shown to carry out uncoupling very efficiently in the mitochondria of brown adipose tissue.[162] Hibernating mammals and newborn babies use UCP1-mediated uncoupling to produce heat, in a process known as nonshivering thermogenesis. UCP1 forms a pore through which protons can pass back into the matrix, bypassing ATP synthase and thus causing uncoupling. There is some uncertainty about the activation of UCP1-mediated uncoupling, however there is no disputing the fact that it is highly effective.[163] Two other proteins, UCP2 and UCP3, have been identified as having a role in uncoupling and can be activated by superoxide.[164,165] The uncoupling function of these proteins appears to be less direct than that of UCP1 and is not fully understood.

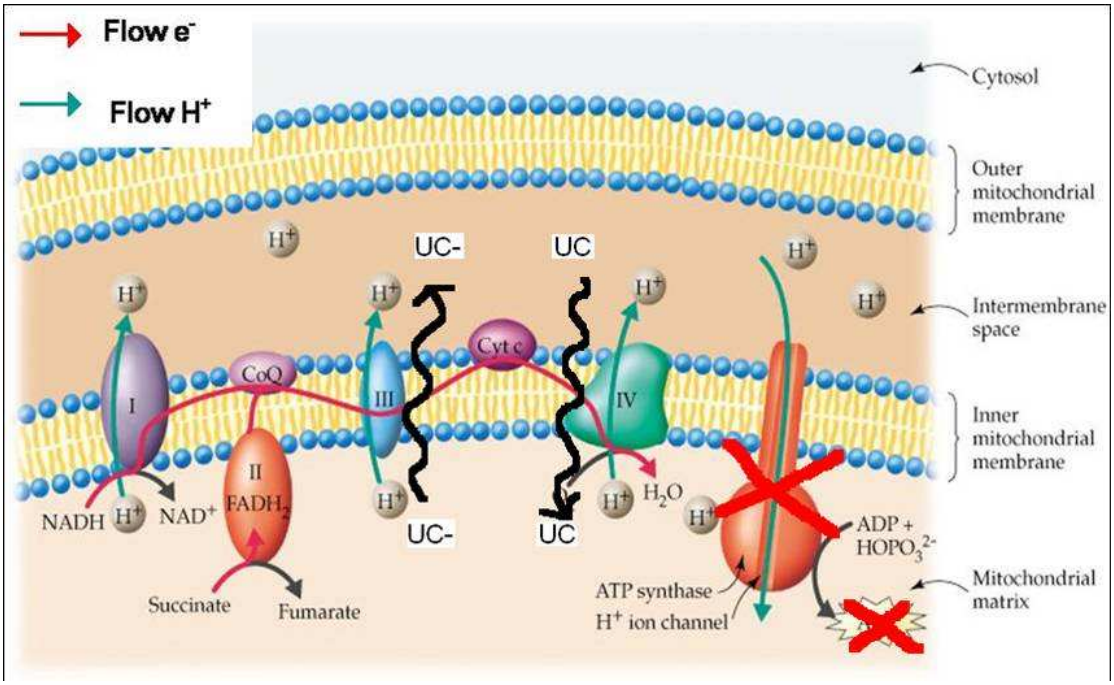

Figure 51: Mitochondrial uncoupling (adapted from McMurry[11]). UC and UC⁻ are uncouplers in their protonated and unprotonated states, respectively.

Small molecules can also induce uncoupling. There are two features that must be present to allow a molecule to uncouple mitochondria successfully. It must have a dissociable proton to allow it to exist in both its protonated and unprotoned forms at physiological pH and it must be sufficiently hydrophobic to allow passage through the mitochondrial membrane in both its ionised and unionised forms. The uncoupler becomes deprotonated in the alkaline mitochondrial matrix (approx. pH 8.3), diffuses across the mitochondrial inner membrane in its anionic form, picks up a proton from the intermembrane space and returns to the matrix. Thus it translocates protons from the intermembrane space to the matrix without the involvement of ATP synthase.

The most commonly used uncouplers in biological studies are 2,4-dinitrophenol (DNP) **325** and carbonyl cyanide 4-(trifluoromethoxy) phenylhydrazone (FCCP) **327** (pKa 4.1[166] and 5.8[167] respectively) (Figure 52). These compounds uncouple mitochondria by being protonated in the intermembrane space as DNP **325** and FCCP **327**, diffusing across the inner membrane and losing this proton again (Figure 51). DNP⁻ **326** and FCCP⁻ **328** can then diffuse out of the matrix and can then repeat this cycle up to 1000 times per second.[168]

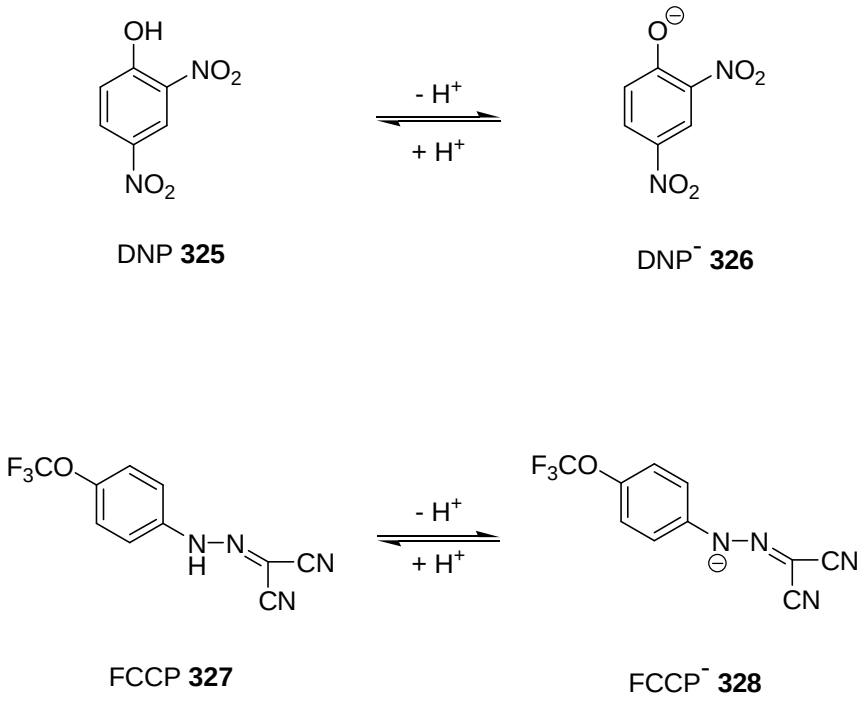

Figure 52: Chemical uncouplers of mitochondria

6.2 Aim of the project

The aim of the project was to synthesise selective uncoupling molecules (SUMs) derived from the two uncouplers DNP **325** and FCCP **327**. These SUMs are inactive, 'caged' versions of the uncouplers that would undergo reaction in the presence of H_2O_2, i.e. when a mitochondrion is under oxidative stress, to release the active uncoupler. This would then reduce the potential across the mitochondrial inner membrane, therefore lowering ROS production (Figure 53). The trigger for release of the uncoupler would utilise the arylboronate functional group and its reaction with H_2O_2 to give a phenol. There are a number of literature examples demonstrating the feasibility of this mechanism for biological probes, which shall be discussed below.

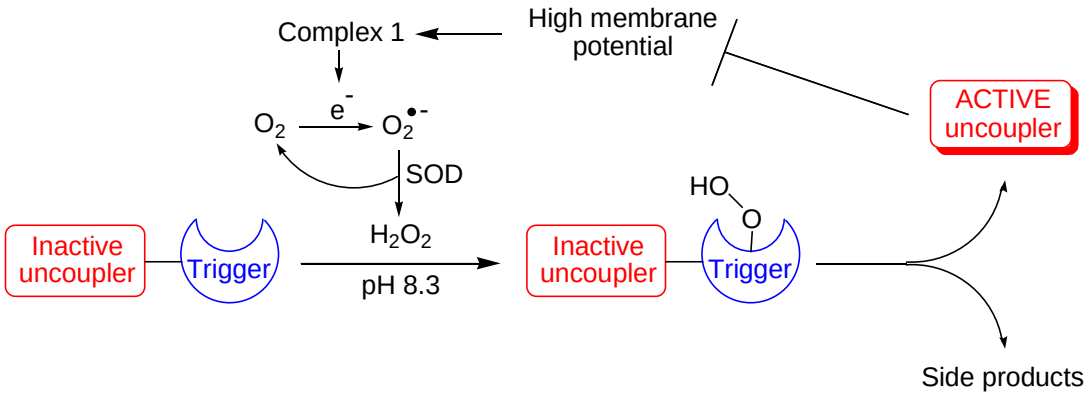

Figure 53: Schematic diagram of caged uncoupler mechanism

6.3 Reaction of Boronates with H_2O_2

The oxidation of a boronate or boronic acid **329** with H_2O_2 under basic conditions gives an alcohol or phenol **330** (Scheme 90).

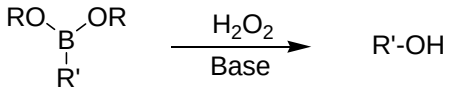

329 **330**

R = H or alkyl
R' = alkyl or aryl

Scheme 90: Boronate oxidation with H_2O_2

The mechanism of this reaction to form phenol **337** is shown in Scheme 91. The hydroperoxide anion nucleophilically attacks the empty p-orbital of the boron atom in arylboronate **331**. This is followed by migration of the aromatic ring from the boron atom to the oxygen atom to give borate ester **333** with loss of a hydroxide ion. The hydroxide ion then attacks the boron atom and the boron-oxygen bond breaks, releasing the phenoxide anion **336** which can be readily protonated to form phenol **337**. This reaction is commonly used in the Brown hydroboration-oxidation to form anti-Markovnikov alcohols from alkenes.[169] Recently it has also been exploited as a sensor for H_2O_2 due to the chemoselectivity of the reaction. Traditional H_2O_2 sensors have used enzymes or fluorescent molecules activated by alternative mechanisms, but are often non-specific and background fluorescence arises from reaction with other ROS.[32]

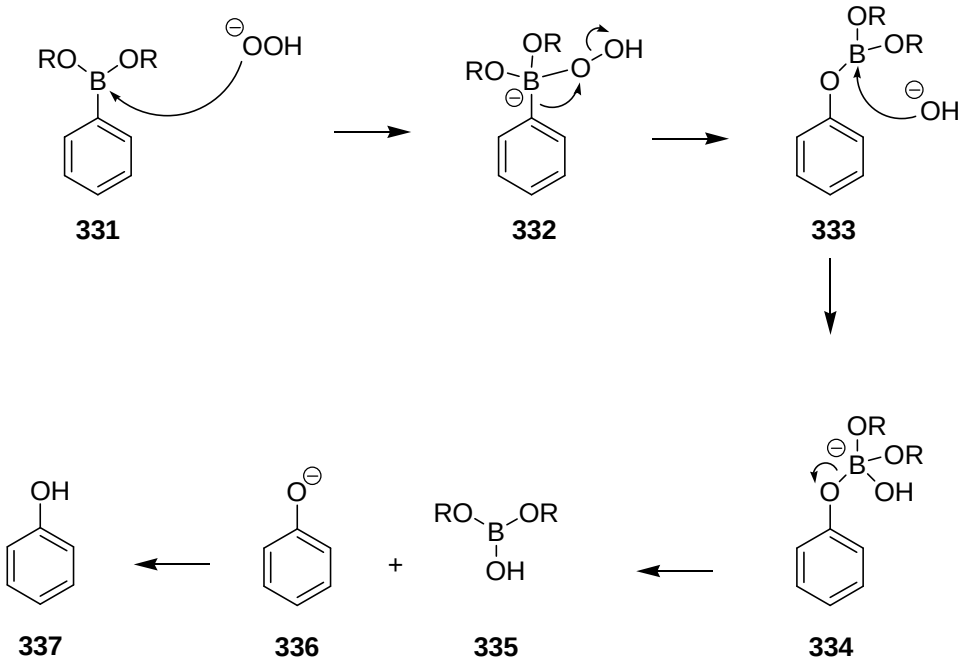

Scheme 91: Mechanism of boronate oxidation

6.4 Literature examples

In 2003, Lo and Chu reported the synthesis of boronates **338** and **339**, as boronate-containing probes for H_2O_2 (Figure 54).[170]

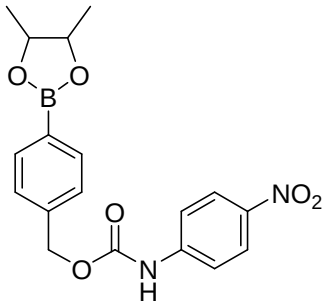

338

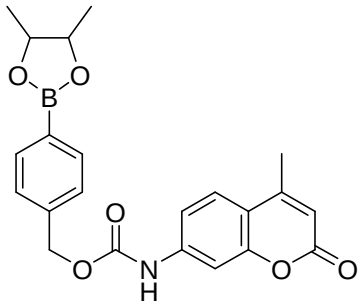

339

Figure 54: Lo and Chu's boronate probes

These probes were designed to react with H_2O_2 and release a chromophore or fluorophore in a two-step mechanism. The first step is reaction with H_2O_2 to form a phenoxide ion **341**. This then rearranges to release a reporter **342**, which is either a chromophoric *p*-nitronaniline group (in the case of **338**) or a fluorophoric 7-amino-4-methylcoumarin group (in the case of **339**) via the mechanism shown in Scheme 92. A quinone methide **343** is also released, which reacts rapidly with water to give benzylic alcohol **344**.

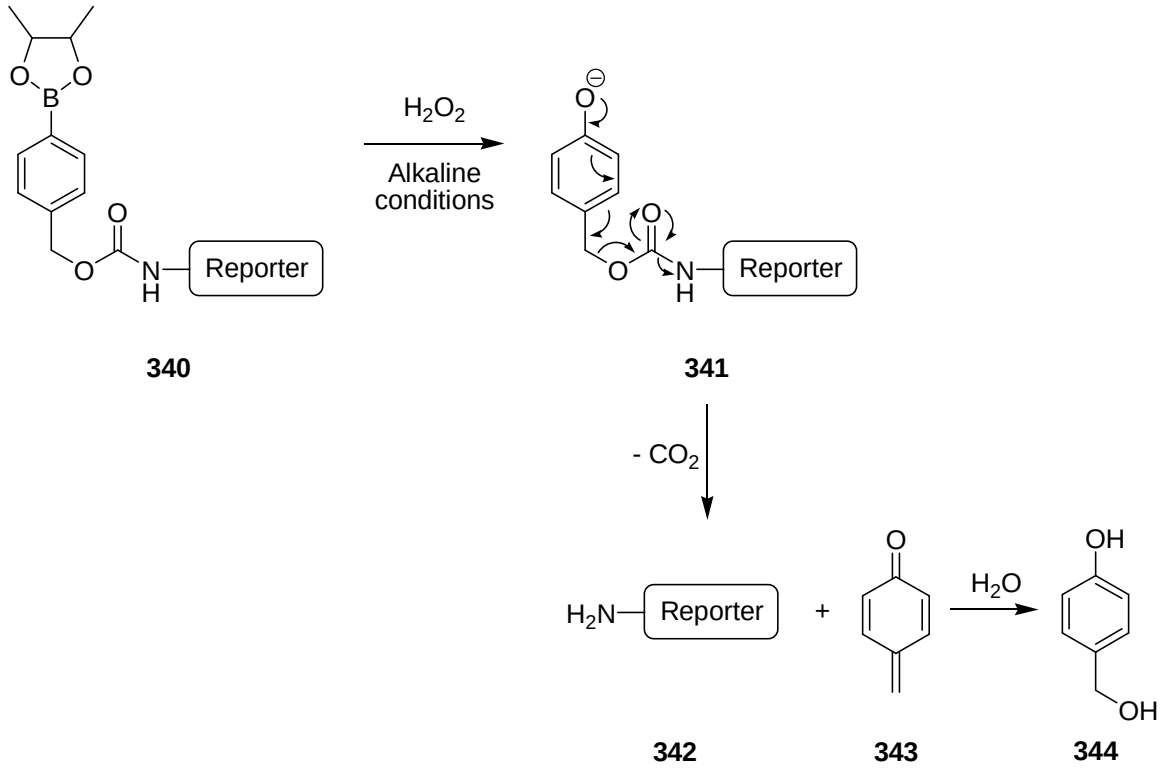

Scheme 92: The two-step mechanism of reporter formation

After incubation with H_2O_2 at pH 8.3, the production of the reporter was measured using a UV-vis spectrophotometer or a fluorimeter. Lo and Chu found that their probes reacted as expected with H_2O_2 to produce the reporter molecules. They observed a good linear correlation between the absorbance after 90 min (i.e. amount of reporter produced) and H_2O_2 concentration. These preliminary results showed that this two-step mechanism is a successful way to release a molecule in response to H_2O_2.

Later the Chang group reported the synthesis of peroxy lucifer 1, or PL1 **345**, which reacts via the same two-step mechanism as shown in Scheme 93.[171] This probe was designed as a ratiometric probe, i.e. there is a signal in both the presence and absence of H_2O_2. As it is the ratio of these signals that is observed, inconsistencies relating to probe distribution and emission intensity are eliminated. PL1 **345** is blue-fluorescent (emission maximum 475 nm) in the absence of H_2O_2. However, upon reaction with H_2O_2, the boronate cleaves and the molecule fragments to form green-fluorescent aniline **347** (emission maximum 540 nm). The ratio F_{540}/F_{475} is then measured in each experiment.

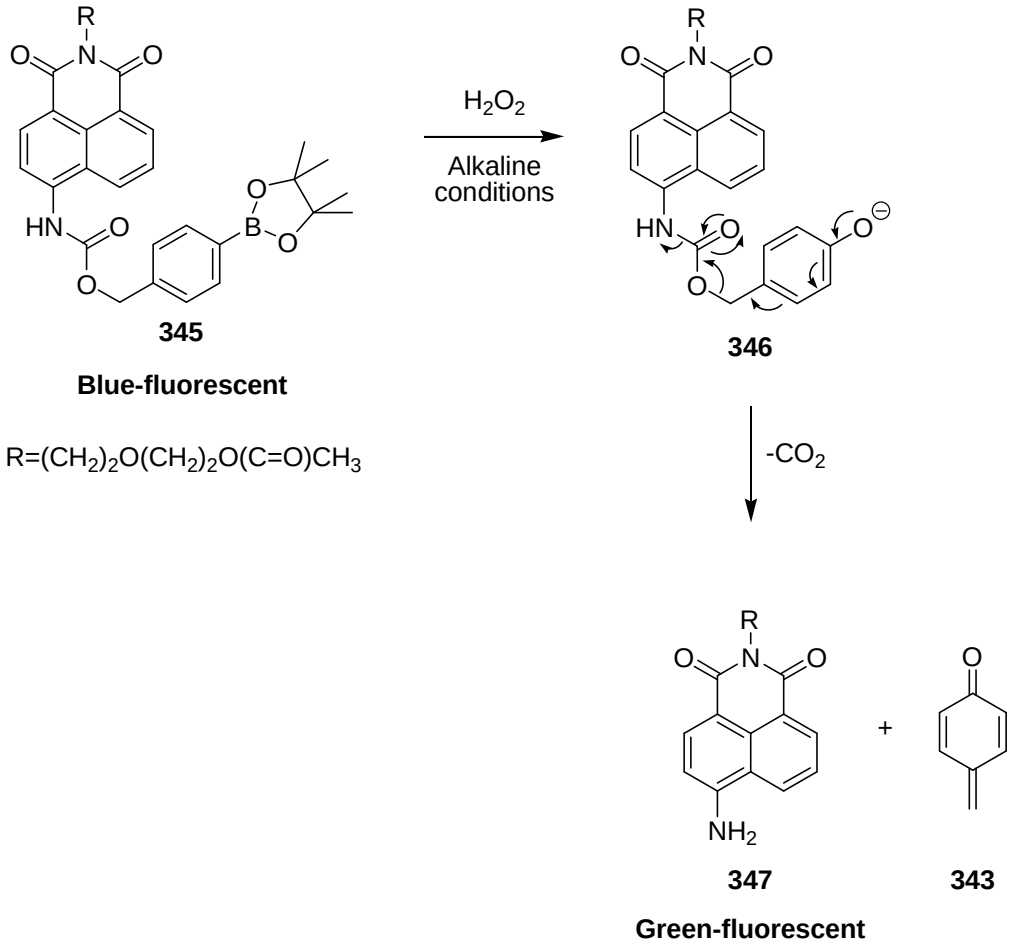

Scheme 93: PL1 reaction with H_2O_2

The probe showed a 12-fold increase in the ratio F_{540}/F_{475} upon reaction with H_2O_2 and did not react significantly with other ROS. Using two-photon microscopy, they demonstrated the probe functioning within macrophages and human embryonic kidney cells treated with H_2O_2. The probe was also successful in detecting H_2O_2 bursts produced by the macrophages when stimulated with phorbol myristate acetate, which induces phagocytosis-assisted H_2O_2 generation.

Chang and co-workers have further developed the concept of H_2O_2 sensing via the reaction of arylboronates. In 2004 they reported the synthesis of peroxyfluor-1, or PF1 **348**, a probe that is converted to green-fluorescent fluoroscein **352** upon reaction with H_2O_2.[172] In 2005 they expanded this family, reporting peroxyresorufin-1 (PR1) **349** which is converted to red-fluorescent resorufin and peroxyxanthone-1 (PX1) **350** which is converted to blue-fluorescent 3,6-dihydroxyxanthone.[173]

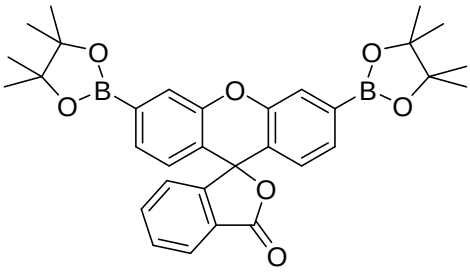

348

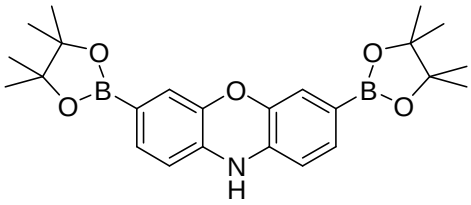

349

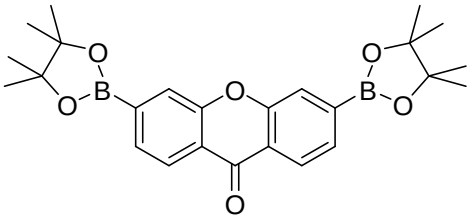

350

Figure 55: Chang probes

The mechanism of reaction of these probes differs from those previously discussed as the activated probe does not fragment to release a reporter following phenoxide generation, but rather the phenol produced is part of the fluorescent reporter. In the case of probes **349** and **350** the reporter is generated directly, while probe **348** reacts with H_2O_2 to form a phenoxide **351** which then rearranges to form the reporter **352** (Scheme 94).

All of these compounds were found to react well with H_2O_2 in similar experiments to Lo and Chu but more importantly, were found to be selective for H_2O_2 over a number of other ROS. The Chang group used confocal microscopy (for arylboronates **348** and **349**) and two-photon microscopy (for arylboronate **350**) to demonstrate that these probes are cell permeable and function successfully in cultured HEK cells. Finally they showed PF1 **348** functioning in live rat hippocampal neurons. In both these systems there was virtually no background fluorescence, which is a significant advantage over probes used to detect H_2O_2 in the past.

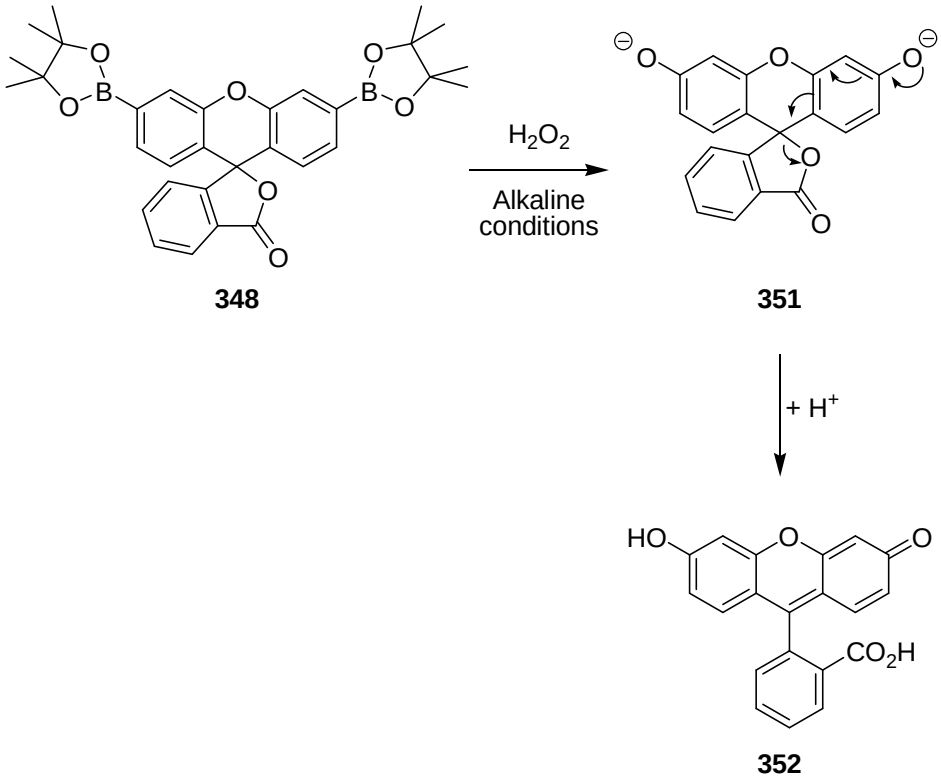

348 **351** **352**

Scheme 94: The one-step mechanism of reporter formation

Most recently the Chang group reported mitochondria peroxy yellow 1, or MitoPY1 **353**, a mitochondria-targeted H_2O_2 probe.[98] This molecule is structurally related to PF1 **348** and undergoes a similar reaction with H_2O_2 to produce a fluorophore, MitoPy1ox **355** (Scheme 95). However, it also contains a TPP cation for targeting to mitochondria. They showed using co-localisation confocal microscopy studies that MitoPy1 **353** localises in the mitochondria of 4 different cell types. HeLa cells were treated with paraquat **356**, an inducer of oxidative stress, and using confocal microscopy an increase in the fluorescence within the mitochondria was observed.

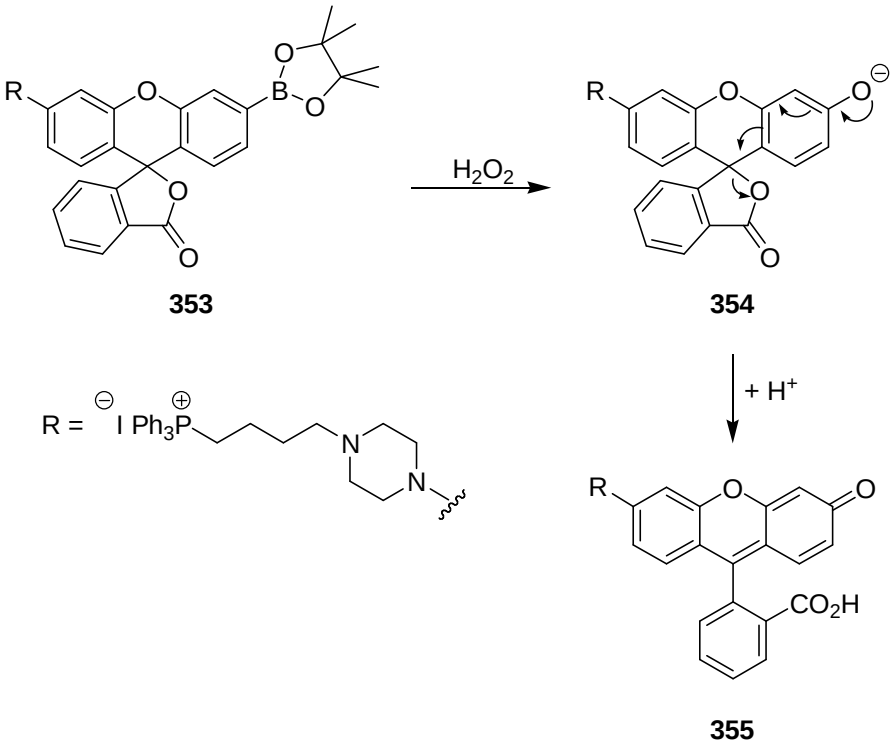

Scheme 95: MitoPY1 **353** reaction with H_2O_2

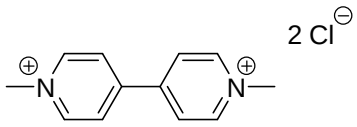

356

Figure 56: Structure of paraquat **356**

Utilising the oxidation of arylboronates, Germain and Knapp developed a protocol for detection of H_2O_2, benzoyl peroxide and triacetone triperoxide, all common explosives.[174] When H_2O_2 was added to a solution of non-fluorescent prochelator **357** and $Zn(OAc)_2$, the boronic acid was cleaved to form diphenoxide **358**, which chelates the Zn^{2+} ions and forms complex **359** which is highly fluorescent (Scheme 96). The other peroxides were first converted into H_2O_2 then detected in the same way. A detectable increase in fluorescence was achieved using nM concentrations of peroxides. This technique has the potential for further development as a detection method in the field due to its simplicity, short reaction time (20 min) and high sensitivity.

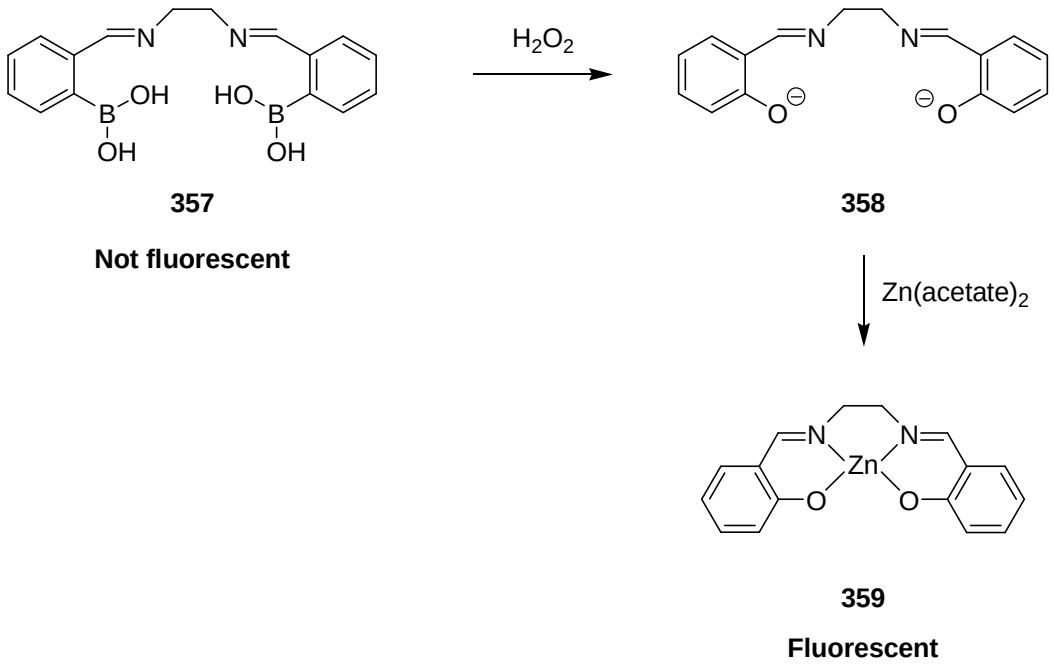

357

Not fluorescent

358

359

Fluorescent

Scheme 96: Germain and Knapp's probe - reaction with H_2O_2

6.5 Synthesis of selective uncoupling molecules (SUMs)

Initially non-targeted versions of the SUMs were synthesised to study their reaction with H_2O_2. Once the reaction of these was fully characterised, the synthesis of mitochondria-targeted versions of the best compounds was planned to follow. MitoPY1 **353** demonstrated the compatibility of the boronate and TPP functional groups within the same molecule and showed that the boronate oxidation can occur within mitochondria for the specific detection of H_2O_2. These factors were important in the idea of our masked uncouplers.

*6.5.1 Synthesis of DNP-SUM **360***

The first target compound synthesised was the simplest DNP-SUM: 2,4-dinitrophenyl-4',4',5',5'-tetramethyl-1',3',2'-dioxaborolane **360**. This was designed to form the uncoupler, DNP^- **326**, directly by oxidation of the arylboronate in a similar way to the activation of Chang's probes **349** and **350** (Scheme 97).

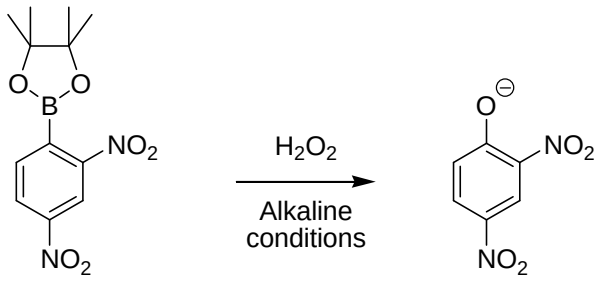

360 **326**

Scheme 97: Caged DNP reaction with H_2O_2

Initially, introduction of the boronate was attempted directly on iodide **361** using the Miyaura borylation reaction, which uses bis(pinacolato)diboron and Pd(dppf)Cl_2 (Scheme 98).[175] However, the major product of this reaction was DNP **325**, identified by ^{1}H NMR data and a low resolution mass spectrum with a molecular ion peak at 184 amu. The successful synthetic route to this molecule is shown in Scheme 99.

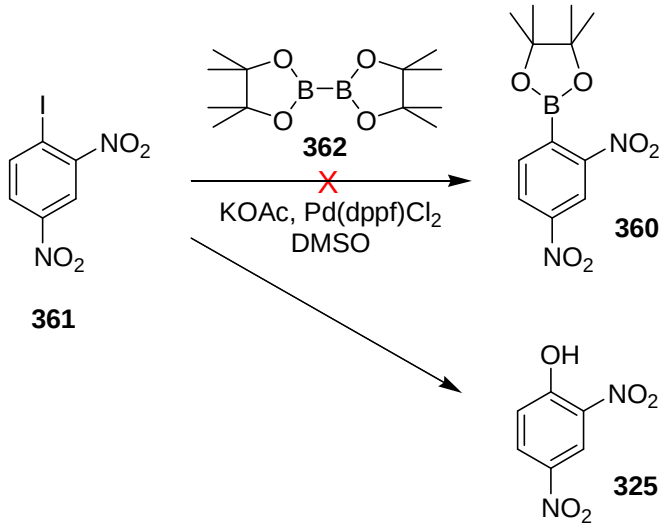

Scheme 98: Attempted Miyaura borylation

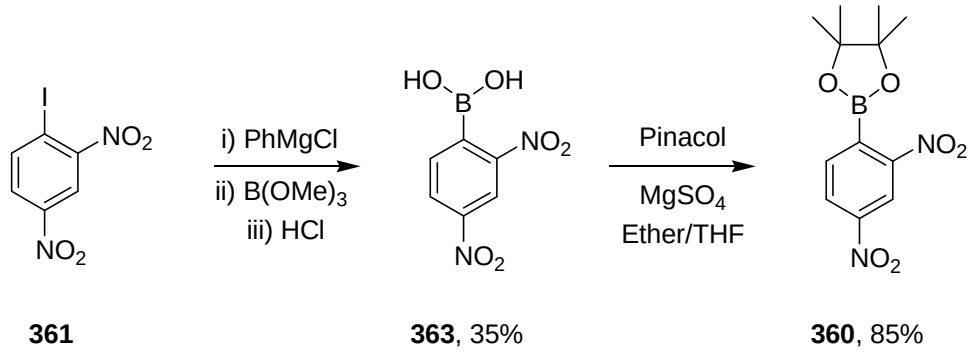

361 **363**, 35% **360**, 85%

Scheme 99: Synthesis of Caged DNP

Phenylmagnesium chloride was used to form a dinitrophenyl Grignard reagent by metal-halogen exchange which was reacted with trimethyl borate. Treatment with HCl gave boronic acid **363**. The same reaction had been reported in the literature with a 75% yield.[176] The reaction was replicated on an identical scale to the paper, using 1.18 g of the starting iodo compound **361**. The reaction was also monitored extremely carefully to ensure the temperature never rose above –60 ºC. Under these conditions, iodo-2,4-dinitrobenzene **361** was successfully converted into 2,4-dinitrophenylboronic acid **363**, but in a low yield. With the boronic acid **363** in hand, the boronate was formed by condensation with pinacol in ether-THF. THF was required to fully dissolve boronic acid **363**. Oven-dried magnesium sulfate was added to the reaction to remove the water formed and the reaction proceeded in an excellent yield to give DNP-SUM **360**. The scheme was straightforward and could potentially be adapted to incorporate a TPP cation by using a diol bearing a TPP group in the second step.

6.5.2 Synthesis of FCCP-SUMs

The next target compound was a derivative of the uncoupler FCCP **327**. Its structure and proposed reaction with H_2O_2 are shown in Scheme 100. It was expected to react via the fragmentation mechanism introduced by Lo and Chu for probes **338** and **339**, where oxidation gives phenoxide **365** which then releases $FCCP^-$ **328**.

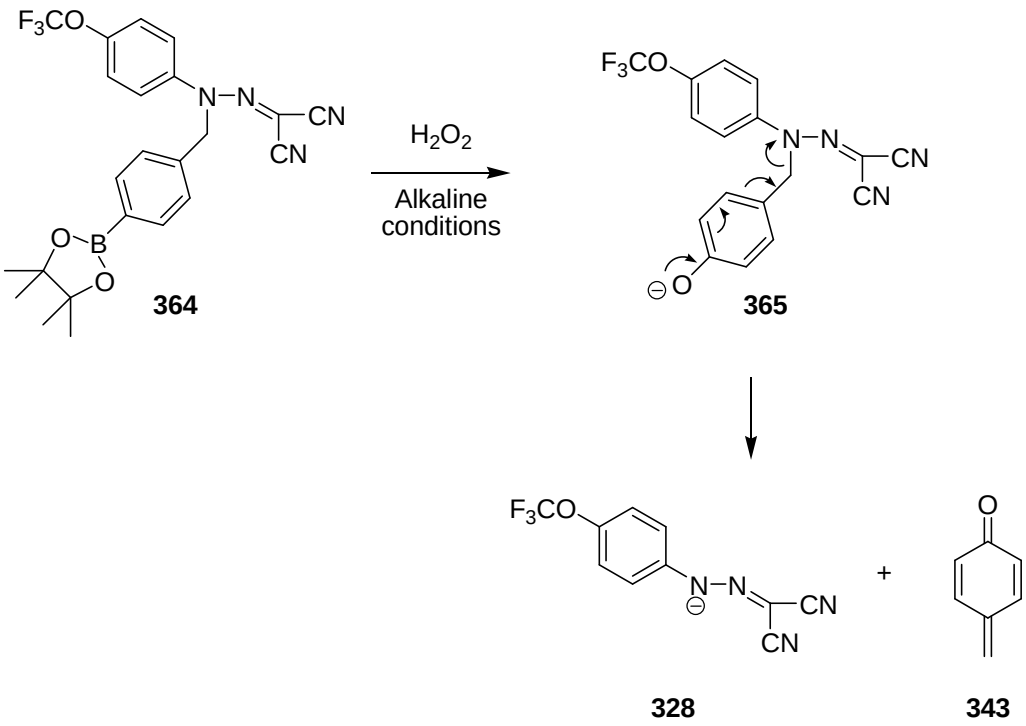

Scheme 100: Proposed release of FCCP⁻ **328**

The kinetic experiments and synthetic route to boronate **364** both required FCCP **327**. This compound is commercially available from Sigma-Aldrich® but is extremely expensive - £241 for 50 mg. Instead it was synthesised in a single step from 4-trifluoromethoxyaniline **366** using the standard method for forming hydrazones of this type.[177] Diazotisation followed by reaction with malononitrile gave FCCP **327** in a good yield (Scheme 101).

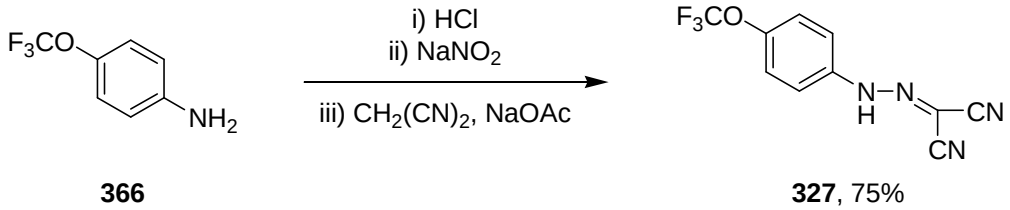

Scheme 101: Synthesis of FCCP **327**

The original synthetic scheme proposed for the synthesis of the FCCP derivative **364** is shown in Scheme 102. The boronate was introduced through lithium-halogen exchange followed by reaction with 2-isopropoxy-4,4,5,5-tetramethyl-1,3,2-dioxaborolane **196** and gave arylboronate **368** in good yield. Originally the reaction was carried out using *tert*-butyllithium and 3.3 equivalents of borate **196** but *n*-butyllithium and only 2 equivalents of the borate was found to give similar yields. Excess borate **196** was removed by Kugelrohr distillation or on the rotary evaporator. Bromination of the benzylic methyl group of arylboronate **368** was

achieved under radical bromination conditions using *N*-bromosuccinamide (NBS) **374** and benzoyl peroxide **370** (Scheme 103). Peroxide **370** is the initiator of the radical bromination and undergoes homolysis when heated to give two identical radicals **371**. Each of these radicals can abstract a hydrogen atom from arylboronate **368** to form benzoic acid **372** and a benzylic radical **373**. This radical **373** reacts with NBS **374** to form the desired product bromide **369** and the succinamide radical **375**. Propagation of the reaction can occur as the succinamide radical **375** can abstract a hydrogen atom from arylboronate **368**, generating benzylic radical **373** which can react with another molecule of NBS **374**.

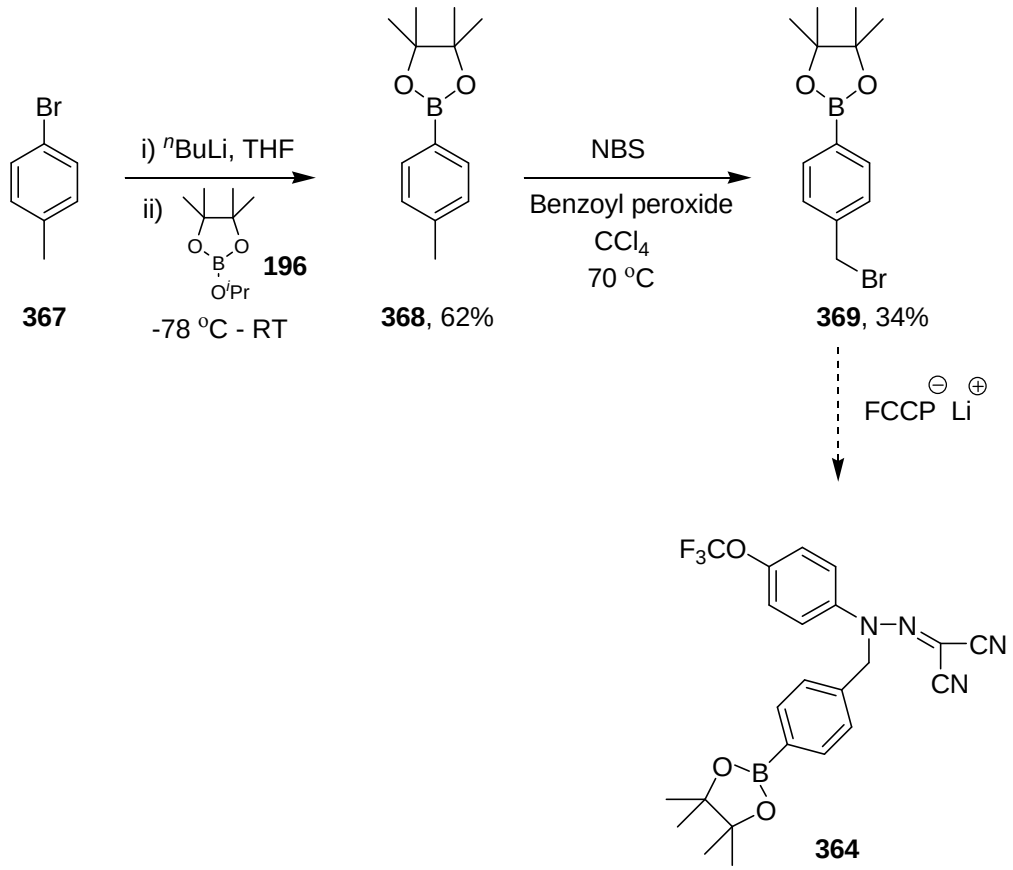

Scheme 102

Initiation:

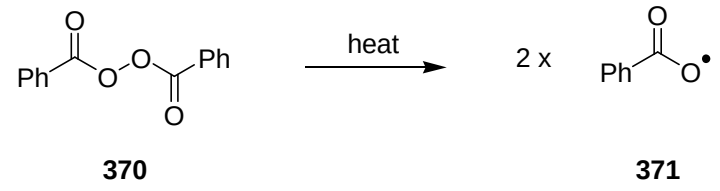

370 **371**

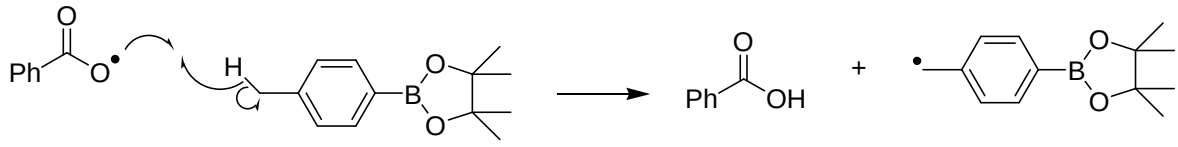

371 **368** **372** **373**

Propagation:

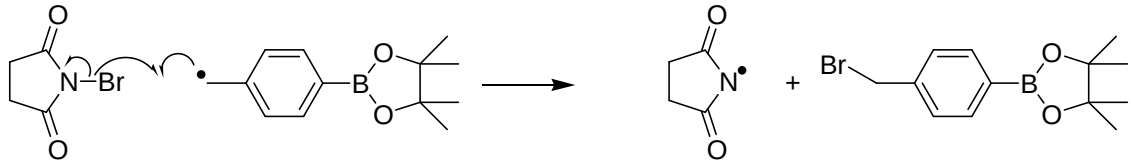

374 **373** **375** **369**

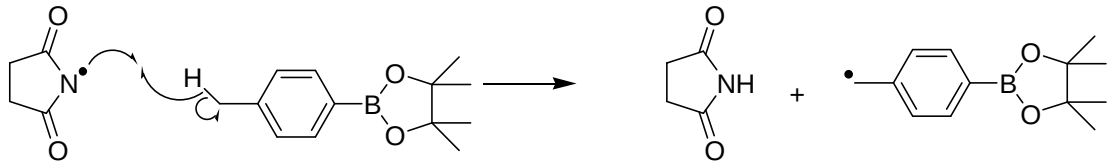

375 **368** **376** **373**

Scheme 103: Mechanism of radical bromination

When the reaction was left for one night, a mini-workup showed the presence of starting material. The reaction was left on for a further night but another product was visible in the ^{1}H NMR spectrum, presumed to be compound **377**. These two compounds were not separable by TLC so column chromatography could not be used as a means of purification.

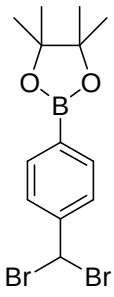

377

Figure 56: Dibrominated side product

Recrystallisation from EtOAc-hexane successfully gave desired product **369**. However, a lot of material was lost in this procedure, resulting in the poor yield. Optimisation of this reaction was not carried out, but this yield could be potentially improved by altering the reaction time, equivalents of NBS or equivalents of benzoyl peroxide. Even with this poor yielding step we had some bromide **369** in hand and coupling was attempted by deprotonating FCCP **327** with LDA (in THF–heptane–ethylbenzene) followed by reaction with bromide **369**. Unfortunately, the crude mixture contained many compounds by TLC and the ^{1}H NMR spectrum was very messy. This was most likely due to the use of commercial LDA and could possibly be improved by *in situ* generation of fresh LDA. NaH was also used as base but no reaction was observed and the ^{1}H NMR spectrum showed only a mixture of the two starting materials. Due to this disappointing result an alternative route to a modified FCCP-SUM structure **380** was undertaken (Scheme 104).

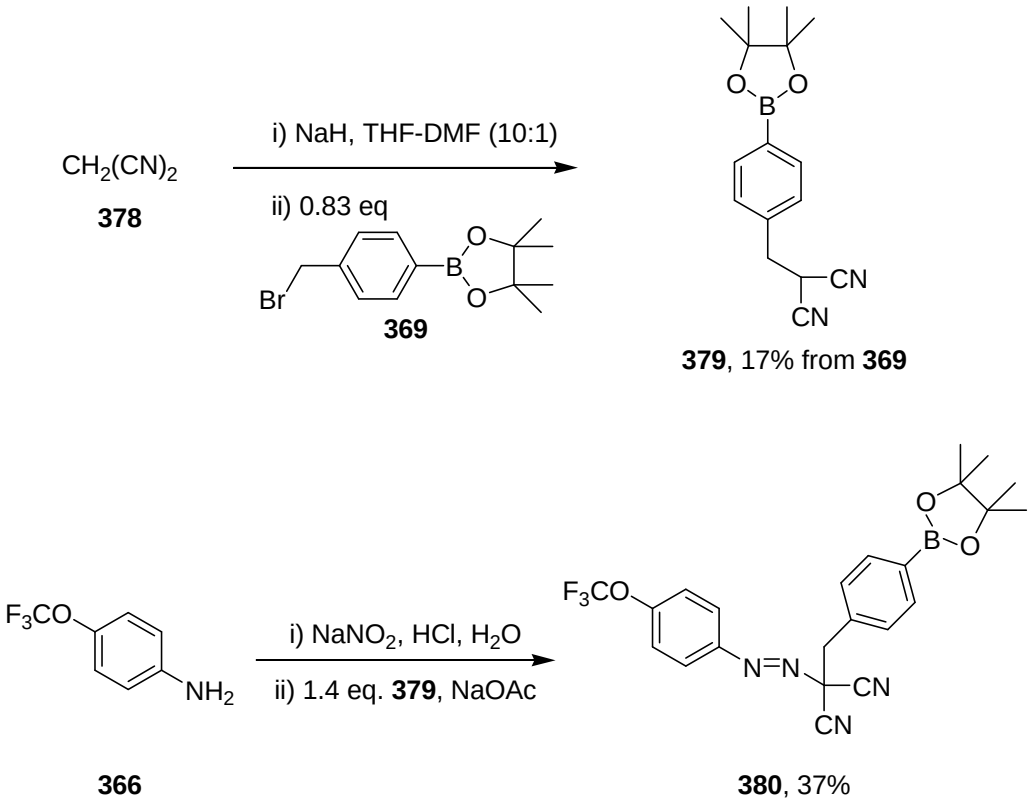

Scheme 104: Route to FCCP-SUM **380**

Malononitrile **378** was deprotonated with NaH in THF-DMF and reacted with benzylic bromide **369** to give nitrile **379** in a low yield. This yield was poor because of the presence of an undesired side product formed by addition of two molecules of bromide **369** to the same molecule of malononitrile **378**. Fortunately

the two products were separable by crystallisation and the reaction was not repeated due to time constraints. Potentially the yield could be improved by using a greater excess of deprotonated malononitrile. The final step in the reaction was analogous to FCCP **327** formation (Scheme 101). Diazotisation of 4-trifluoromethoxyaniline **366** was followed by reaction with nitrile **379** in the presence of a mild base, sodium acetate, to give FCCP-SUM **380** in modest yield.

6.6 Kinetic Experiments with DNP-SUM 360

We planned to use UV spectrophotometry to study the reactions between DNP-SUM **360** and H_2O_2. This method required a significant difference between the UV spectrum of DNP^- **326** and that of DNP-SUM **360**. All UV spectra and subsequent reactions were run at 37 ℃ (body temperature) and pH 8.3 (the approximate pH of the mitochondrial matrix). The UV spectrum of 0.2 mM DNP^- **326** [i.e. 0.2 ml of a 1 mM DNP solution in DMF + 0.4 ml of 140 mM $NaHCO_3$ buffer (aq) + 0.4 ml DMF] was taken over the wavelength range of 250-500 nm and is shown in Figure 57. Under the same conditions a spectrum of 0.2 mM DNP-SUM **360** was recorded (Figure 58). 410 nm was chosen as a suitable wavelength for monitoring the production of DNP^- **326** as it strongly absorbs in this region whereas DNP-SUM **360** does not. After 3 h another UV spectrum of DNP-SUM **360** in DMF-buffer solution was measured under identical conditions to the first. An increase in the absorbance at 410 nm was observed and attributed to approximately 5% decomposition of DNP-SUM **360** in DMF solution over this time.

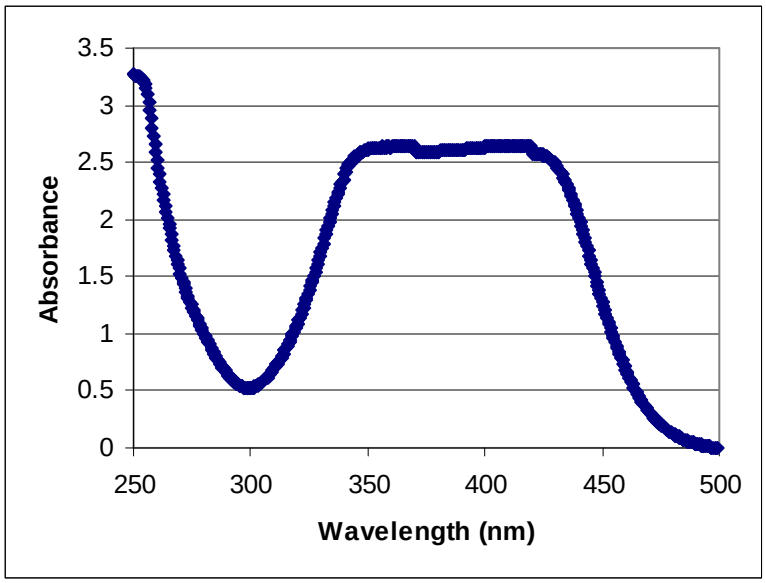

Figure 57: UV spectrum of DNP^- **326**

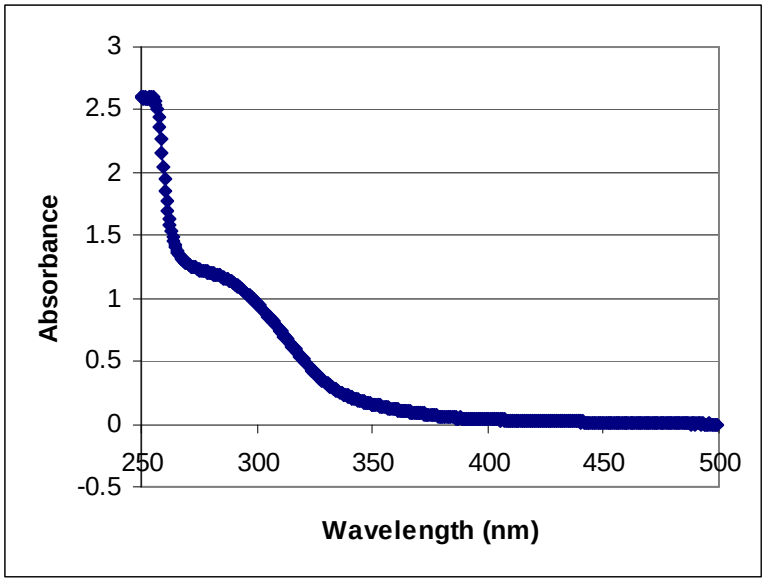

Figure 58: UV spectrum of DNP-SUM **360**

After selecting this wavelength, the subsequent reactions of DNP-SUM **360** with H_2O_2 were monitored at 410 nm over a time course. The reaction would be expected to be second order and have the rate equation:

$$\frac{d[DNP^-]}{dt} = k_2^{DNP}[H_2O_2][\text{DNP-SUM}]$$

Figure 59: Second order rate equation

The second order rate constant of this reaction is difficult to obtain as the concentrations of both H_2O_2 and DNP-SUM **360** would need to be measured simultaneously. A solution to this problem is to use one reagent in excess (in this case DNP-SUM **360**), therefore effectively keeping its concentration constant, and applying the *pseudo*-first order approximation to give the *pseudo*-first order equation:

$$\text{if } [\text{DNP-SUM}] >> [H_2O_2] \text{ then,}$$

$$\frac{d[DNP^-]}{dt} \approx k_1^{DNP}[H_2O_2]$$

Figure 60: *Pseudo*-first order rate equation

By applying this approximation the concentration of H_2O_2 could be used to calculate a *pseudo*-first order rate constant, k_1^{DNP}, for the reaction. Dividing this by

the concentration of DNP-SUM **360** gives a good approximation of the second order rate constant, k_2^{DNP}.

For the time course experiments the UV spectrophotometer measured two absorbances simultaneously, a sample and a reference. In the sample cuvette, 0.5 ml DNP-SUM **360** solution (1mM in DMF) and 0.5 ml $NaHCO_3$ buffer (140mM in H_2O) were mixed. 0.1 ml of H_2O_2 solution (1mM in H_2O) was added and the A_{410} was monitored over 2000 s. The reference cuvette contained 0.5 ml DNP-SUM **360** solution and 0.6 ml $NaHCO_3$ buffer. The graph in Figure 61 shows the results averaged over two identical runs.

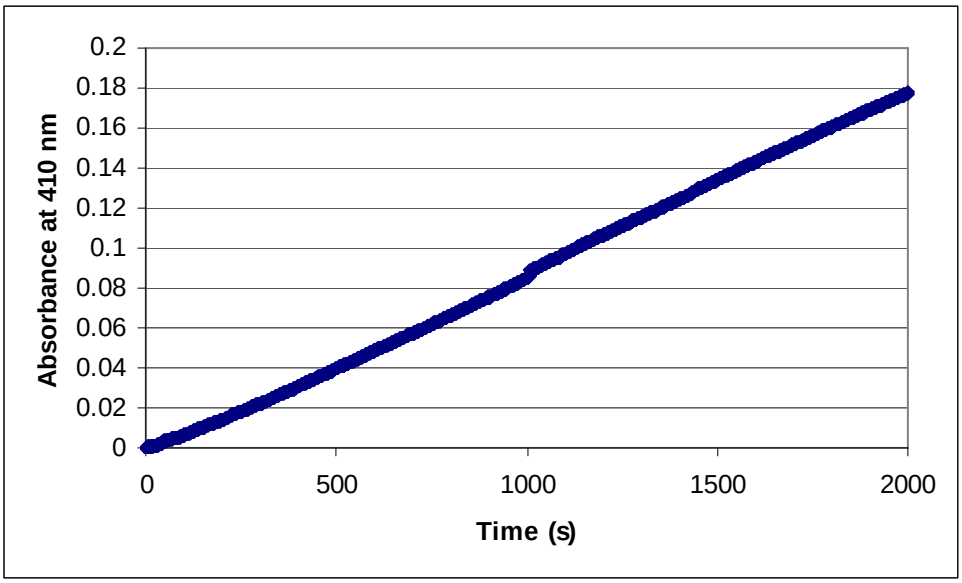

Figure 61: Caged DNP **360** (final conc. 454 μM) reaction with H_2O_2 (final conc. 91 μM)

From curve-fitting, the average *pseudo*-first order rate constant, k_1^{DNP}, for this reaction was calculated to be 9.17×10^{-5} s^{-1}. Dividing this by the concentration of DNP-SUM **360**, 4.54×10^{-4} M gives an average second order rate constant of 0.20 M^{-1} s^{-1}. For good *pseudo*-first order kinetics, this graph should appear as a curve that plateaus to a constant value rather than a straight line. The observed graph shows very slow reaction between DNP-SUM **360** and H_2O_2. For complete reaction with the H_2O_2 the final A_{410} value should be 1.06, however after 2000 s it is only 0.18. This means that only 17% of the DNP-SUM **360** is being converted into DNP **360** after 2000 s. This slow reaction could be explained by examining the mechanism of the reaction (Scheme 105). The reaction between the electron-poor arylboronate **360** and H_2O_2 to give borate anion **381** is expected to be fast, so the slow reaction rate is probably the result of slow migration of the aryl group from

the boron atom to the oxygen atom. This migration would be slowed by the electron-withdrawing nitro groups.

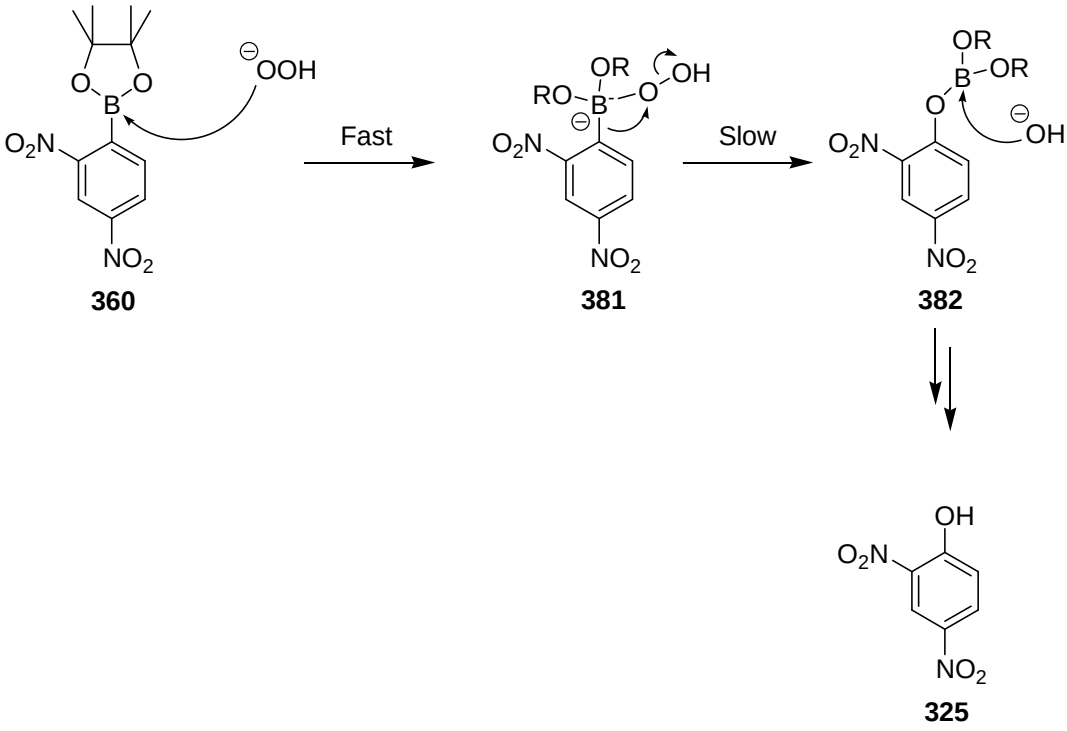

Scheme 105

6.7 Kinetic experiments with FCCP-SUM 380

A similar approach was taken for the investigation of the kinetics of FCCP-SUM **380**. Once again all UV spectra were measured at 37 ℃ and pH 8.3 (using 140 mM $NaHCO_3$ buffer solution). The UV spectra of $FCCP^-$ **328** and FCCP-SUM **380** are shown in Figures 62 and 63 respectively. The wavelength selected for monitoring in the subsequent kinetic experiments was 385 nm.

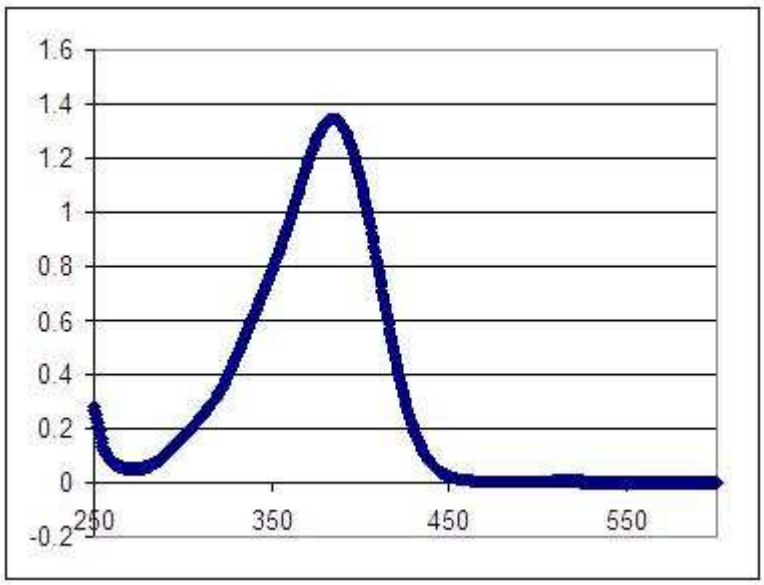

Figure 62: UV spectrum of $FCCP^-$ **328** [50 μM in DMF-$NaHCO_3$ buffer (aq) (1:1)]

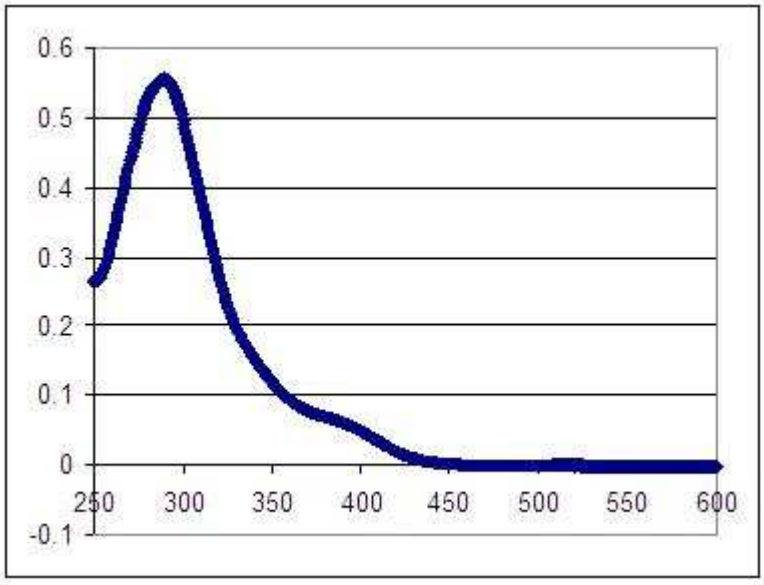

Figure 63: UV spectrum of FCCP-SUM **380** [50 μM in DMF-$NaHCO_3$ buffer (aq) (1:1)]

To eliminate the possibility that the incomplete reactions observed for DNP-SUM **360** were due to decomposition of H_2O_2, the concentration of the H_2O_2 stock solution was determined accurately before performing time course experiments with FCCP-SUM **380**. The standard method of determining H_2O_2 concentration is by titration against $KMnO_4$.[178] The reaction is shown in Scheme 106.

$$2\ MnO_4^- + 5\ H_2O_2 + 6\ H^+ \rightarrow 2\ Mn^{2+} + 5\ O_2 + 8\ H_2O$$

Scheme 106: Reaction between H_2O_2 and $KMnO_4$

Time course experiments of the reaction between FCCP-SUM **380** and H_2O_2 were performed under similar conditions to those for the reaction of DNP-SUM **360**.

Once again *pseudo*-first order conditions were used and the concentration of FCCP-SUM **380** was in excess. In the sample cuvette, 0.5 ml $NaHCO_3$ buffer (140 mM aq), 0.495 ml DMF and 0.005 ml FCCP-SUM **380** (10 mM in DMF, final concentration 50 μM) were mixed. 20 μl of 0.5 mM H_2O_2 (final concentration 10 μM) was added and A_{385} was monitored over 1000 s. The reference cuvette contained an identical mixture of buffer-DMF-FCCP-SUM, but no H_2O_2. In contrast to DNP-SUM **360**, FCCP-SUM **380** gave a good *pseudo*-first order kinetic profile that was replicated for a second time. To confirm that the reaction was conforming to *pseudo*-first order kinetics, experiments were conducted using the same conditions but adding only 10 μl of 0.5 mM H_2O_2, to give a final concentration of 5 μM. For good *pseudo*-first order kinetics the *pseudo*-first order rate constant should be the same for different concentrations of H_2O_2. Figure 64 shows the averaged results for 10 μM and 5 μM H_2O_2.

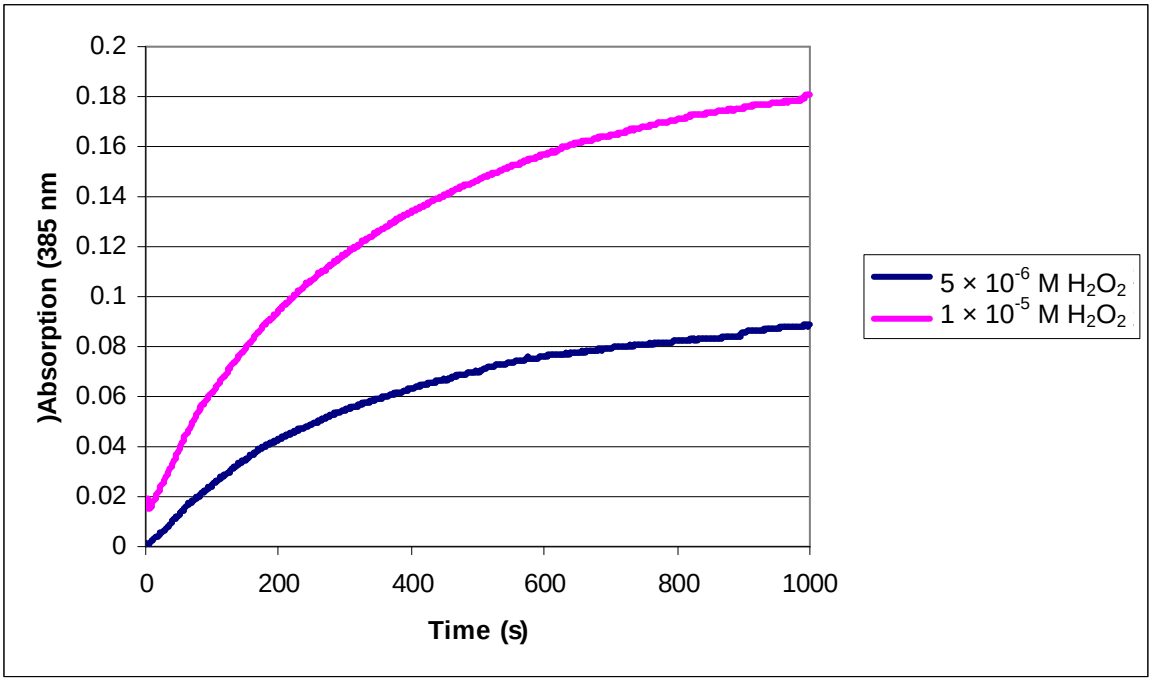

Figure 64: FCCP-SUM **380** reaction with H_2O_2. Blue line - 5 μM H_2O_2 and is averaged over 3 runs; purple line - 10 μM H_2O_2 and is averaged over 2 runs.

10 μM H_2O_2 *Pseudo*-first order rate constant: 0.00315 s^{-1}

5 μM H_2O_2 *Pseudo*-first order rate constant: 0.00327 s^{-1}

Average first order rate constant: 0.00321 s^{-1}

Average second order rate constant: 64 M^{-1} s^{-1}

The *pseudo*-first order rate constants derived from experiments using 10 μM and 5 μM H_2O_2 were close in value, indicating that *pseudo*-first order kinetics were being followed. These results show that FCCP-SUM **380** reacts with H_2O_2 faster than DNP-SUM **360** and release of $FCCP^-$ **328** is proportional to the amount of H_2O_2. However, a 1:1 reaction stoichiometry between H_2O_2 and FCCP-SUM **380** was not observed. In the 10 μM experiments only 56% of the expected $FCCP^-$ **328** was produced and 60% in the 5 μM experiments. This could be explained by preferential trapping of the quinone methide **343** by the hydroperoxide ion rather than water (Scheme 107). If this is the case, some of the H_2O_2 will be used up in this side reaction rather than oxidising the boronate group of FCCP-SUM **380**. The peroxide anion **385** may be formed and could potentially take the place of H_2O_2 in the boronate oxidation. However, the pKa of the benzylic peroxide **384** may be higher than than that of H_2O_2.

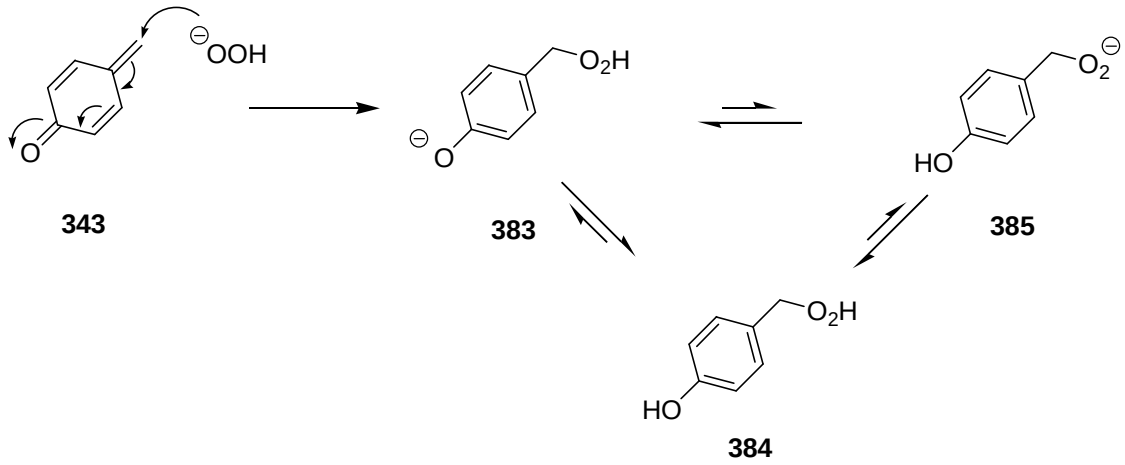

Scheme 107

FCCP-SUM **380** was susceptible to breakdown in the 1:1 DMF-buffer mixture. After 1000s there is a large amount of non-specific breakdown, ~14% of the total probe. However it should be noted that in all experiments this is accounted for in the blank reference cuvette and the $FCCP^-$ **328** production shown in Figure 64 is over and above this level.

6.8 Conclusions from kinetic experiments

In summary, DNP-SUM **360** reacts extremely slowly relative to FCCP-SUM **380** and would be unable to release DNP rapidly in response to changes in H_2O_2 concentration. FCCP-SUM **380** does release the free uncoupler molecule in an H_2O_2-dependant manner. However, the reaction has a >1:1 stoichiometry for

H_2O_2-probe **380**, which suggests the sequestering of H_2O_2 by competing side reactions. Both compounds undergo some non-selective decomposition, which limits their usefulness *in vivo*, and some structural changes may be necessary to increase their stability.

6.9 Synthesis of a mitochondrial targeted FCCP-SUM

The synthesis of boronate **390** containing a TPP group was also begun (Scheme 108).

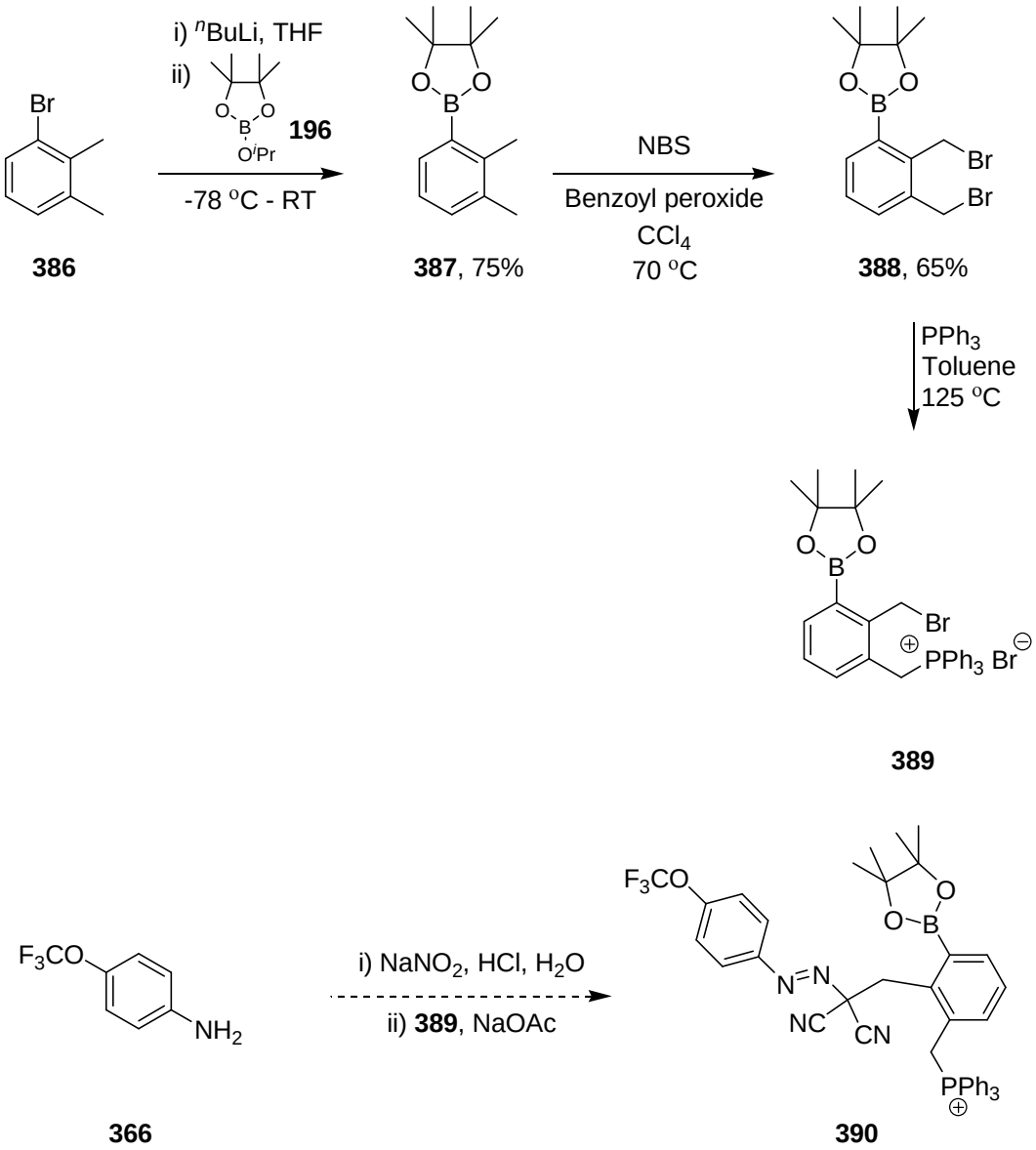

Scheme 108

Starting with 3-bromo-*ortho*-xylene **386**, boronation and bromination were carried out in the same way as in the previous syntheses. Bromide **388** contained a small impurity that could not be removed, thought to be a tribrominated compound.

However, it was thought that purification may be easier at the next stage so the synthesis was continued. Dibromide **388** was reacted with triphenylphosphine in an attempt to form phosphonium salt **389** with sterics controlling the regiochemistry. The ^{1}H NMR spectrum of the crude mixture after work up showed the presence of the desired product, indicated by a splitting of the CH_2 peak at 5.06 ppm, but contained impurities. Attempts to purify this compound by washing with various solvents proved unsuccessful and no further work was carried out on this route, though it may be exploited by other members of the group.

6.10 Future direction of the project

Work is currently ongoing within the Hartley group on the synthesis of mitochondria-targeted derivatives of FCCP-SUM **380**. The TPP cation must be attached to a part of the molecule that is not incorporated into the released uncoupler, otherwise this would interfere with its ability to diffuse across the mitochondrial inner membrane. A potential point of attachment may be on the aromatic ring containing the boronate (e.g. **390**). Alternatively it may be possible to attach the TPP cation to one of the alkyl groups on the boronate itself (e.g. **391**, Figure 65).

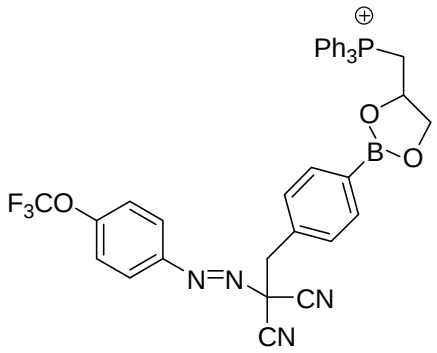

391

Figure 65: Alternative structure for mitochondria-targeted FCCP-SUM

6.11 Conclusion

Two novel caged uncouplers have been synthesised that utilise the boronate functionality to release an active uncoupler in the presence of H_2O_2. The kinetic results from initial experiments with these compounds show that they release the desired molecule successfully under the reaction conditions, with FCCP-SUM **380** reacting much faster. However, both compounds are susceptible to decomposition in solution to some extent.

Chapter 7: Experimental

7.1 General experimental

All reactions under an inert atmosphere were carried out using oven dried or flame dried glassware. Solutions were added via syringe. Diethyl ether, tetrahydrofuran, dichloromethane and toluene were dried where necessary using a Puresolv™ 400-5MD solvent purification system (Innovative Technology, Inc). Methanol was dried by distillation from magnesium and iodine, and then stored over 3 Å molecular sieves. Reagents were obtained from commercial suppliers and used without further purification unless otherwise stated.

^{1}H and ^{13}C NMR spectra were obtained on a Bruker DPX/400 spectrometer operating at 400 and 100 MHz, respectively. All coupling constants are measured in hertz. DEPT was used to assign the signals in the ^{13}C NMR spectra as C, CH, CH_2 or CH_3. Mass spectra (MS) were recorded on a Jeol JMS700 (MStation) spectrometer. Infra-red (IR) spectra were obtained using attenuated total reflectance (ATR) on a Shimadzu FTIR-8400S spectrometer.

Flash column chromatography was carried out using Fisher Matrex silica 60. Macherey-Nagel aluminium backed plates pre-coated with silica gel 60 (UV_{254}) were used for thin layer chromatography.

7.2 Synthesis

2-Benzyl-5-bromo-1,1,3,3-tetraethylisoindoline 178

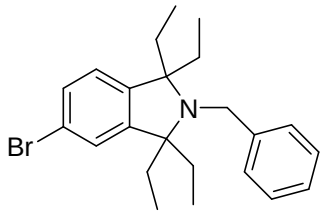

Ethylmagnesium bromide (3 M in diethyl ether, 23.5 mL, 70.5 mmol) was cannulated into a 3-necked round bottomed flask, fitted with a reflux condenser and distillation apparatus, under argon. The solution was stirred at 80 ℃ until no more ether was removed. The distillation apparatus was replaced with a stopper and a solution of phthalimide **179** (2.01 g, 6.33 mmol) in anhydrous toluene (15 mL) was added dropwise via syringe. The reaction mixture was heated at 120 ℃

for 1.5 h, then cooled and quenched by careful addition of H_2O, followed by dilution with EtOAc. The aqueous layer was extracted with EtOAc (× 3). The combined organic extracts were washed with brine, concentrated *in vacuo,* and the resulting solid was dissolved in petroleum ether (bp 40-60 ℃). The solution was filtered and the organic extracts were dried over $MgSO_4$, filtered and concentrated *in vacuo*. The crude mixture was washed through a plug of neutral alumina using petroleum ether (bp 40-60 ℃) to yiel d an inseparable 4:1 mixture of product **178** and unbrominated material **189** as a yellow oil (1.48 g, 61%). Data derived for bromide **178**: δ_H (400 MHz, $CDCl_3$): 0.75 (12H, q, *J* 7.2 Hz, 4 × CH_3), 1.46-1.56 (4H, m, 4 × C*H*$_a$H$_b$), 1.83-1.93 (4H, m, 4 × CH$_a$*H*$_b$), 3.96 (2H, s, CH_2), 6.90 (1H, d, *J* 8.4 Hz, H-7), 7.17 (1H, d, *J* 1.9 Hz, H-4) 7.22-7.32 (4H, m, 3 × Ar-H and H-6), 7.40-7.43 (2H, m, 2 × Ar-H).

2-Benzyl-5-bromo-isoindole-1,3-dione 179[179]

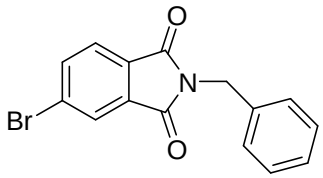

Thionyl chloride (17 mL, 233 mmol) was added to dicarboxylate salt **186** (8.42 g, 31.5 mmol). The reaction mixture was placed under argon and stirred at 85 ℃ for 2.5 h. Excess thionyl chloride was removed *in vacuo* and the residue dissolved in hot EtOAc. The hot solution was filtered and the filtrate concentrated to yield an orange solid. This solid was dissolved in hot EtOAc and filtered again to yield crude anhydride **180** as an orange solid. Benzylamine (3.2 mL, 29.3 mmol) was added to crude anhydride **180** and the mixture stirred at 155 ℃ for 23 h. Upon cooling a brown solid formed which was dissolved in EtOAc and dropped into stirring 2 M HCl (aq). The precipitate formed was left stirring for 2 h then collected by filtration. The precipitate was recrystallised from hexane to give pure phthalimide **179** as light yellow needles (6.23 g, 63%). Mp 119-121 ℃. δ_H (400 MHz, $CDCl_3$): 4.85 (2H, s, CH_2), 7.27-7.36 (3H, m, 3 × Ar-H), 7.43-7.45 (2H, m, 2 × Ar-H), 7.72 (1H, d, *J* 8.0 Hz, H-7), 7.85 (1H, dd, *J* 8.0 and 1.6 Hz, H-6), 7.98 (1H, d, *J* 1.4 Hz, H-4). δ_C (100 MHz, $CDCl_3$): 41.95 (CH_2), 124.83 (CH), 126.84 (CH), 128.07 (CH), 128.75 (CH), 128.84 (CH), 129.01 (C), 130.74 (C), 133.86 (C), 136.14 (C), 137.09 (CH), 166.76 (C), 167.30 (C). LRMS (EI$^+$) 317 (M$^{+\bullet}$, ^{81}Br,

63%), 315 ($M^{+\bullet}$, ^{79}Br, 63), 28 (100). HRMS: 316.9883 and 314.9899, $C_{15}H_{10}O_2{}^{81}Br$ requires 316.9876 and $C_{15}H_{10}O_2{}^{79}Br$ requires 314.9895. ν_{max} (ATR) 1697 (C=O) cm^{-1}.

^1H and ^{13}C NMR data consistent with literature.

4-Bromophthalic acid disodium salt 186

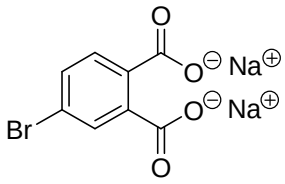

Following the published procedure,[180] bromine (3.6 mL, 78 mmol) was added to a stirred solution of phthalic anhydride **181** (11.07 g, 74.7 mmol) in 3 M NaOH (aq) (45 mL). The reaction mixture was stirred at 90 ℃ for 5 h open to the atmosphere. Additional bromine (1.7 mL, 33 mmol) and 3 M NaOH (aq) (10 mL) were added and the reaction mixture stirred at 90 °C for a further 20 h. The resulting white solid was filtered and washed with 20% $Na_2S_2O_3$ (aq) to give bromide **186** as an off-white solid (11.74 g, 54%). Mp. (decomp.) 280 ℃. δ_H (400 MHz, DMSO-d_6): 7.73 (1H, dd, *J* 8.4 and 2.2 Hz, H-5), 8.11 (1H, d, *J* 8.4 Hz, H-6), 8.29 (1H, d, *J* 2.1 Hz, H-3). ν_{max} (ATR) 1715 (C=O) cm^{-1}.

***N*,*N*-Dibenzylbenzene-1,2-diamide 187**

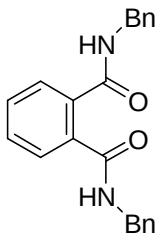

Phthalic anhydride **181** (1.003 g, 6.77 mmol) and benzylamine (10 mL, 91.55 mmol) were stirred at 200 ℃ for 24 h. Upon coolin g, the mixture formed a white solid which was dissolved in EtOAc and dropped into stirring 2 M HCl (aq). The resulting precipitate was filtered and dried *in vacuo* to give diamide **187** as a white solid (2.30 g, 99%). Mp 162-164 ℃ (lit. 168 °C) [181]. δ_H (400 MHz, $CDCl_3$): 4.52 (4H, d, *J* 5.8 Hz CH_2), 7.00 (2H, br s, 2× NH), 7.27-7.36 (10H, m, 10 × Ar-H), 7.50

(2H, dd, *J* 5.7 Hz and 3.3 Hz, H-4 and H-5), 7.60 (2H, dd, *J* 5.5 Hz and 3.1 Hz, H-3 and H-6). δ_C (100 MHz, $CDCl_3$): 40.87 (CH_2), 127.75 (CH), 128.00 (CH), 128.53 (CH), 128.91 (CH), 130.51 (CH), 134.64 (C), 137.86 (C), 169.10 (C). LRMS (EI^+) 344 ($M^{+\bullet}$, 4%), 277 (34), 262 (65), 73 (100). HRMS: 344.1528, $C_{22}H_{20}O_2N_2$ requires 344.1525. ν_{max} (ATR) 3283 (NH), 3032 (CH), 1628 (C=O) cm^{-1}.
No other literature data available.

_N_-Benzylphthalimide 188[182]

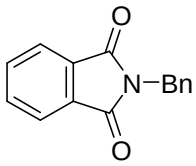

Phthalic anhydride **181** (161 mg, 1.08 mmol) and benzylamine (116 mg, 1.08 mmol) were placed in an open 5 ml microwave tube. The mixture was heated under 300 W of microwave irradiation. The temperature was increased to 155 ℃ over 5 min and was maintained at that temperature for 5 min. Upon cooling, the mixture formed a white solid which was dissolved in EtOAc and dropped into stirring 2 M HCl (aq). The resulting precipitate was filtered and dried *in vacuo* to give the phthalimide **181** as a white solid (151 mg, 58%). Mp 107-110 ℃. (lit. 111-112 ℃) [183]. δ_H (400 MHz, $CDCl_3$): 4.85 (2H, s, CH_2), 7.28-7.34 (3H, m, 3 × Ar-H), 7.43-7.45 (2H, m, 2 × Ar-H), 7.71 (2H, dd, *J* 5.5 Hz and 3.1 Hz, H-4 and H-5), 7.85 (2H, dd, *J* 5.5 Hz and 3.1 Hz, H-3 and H-6). δ_C (100 MHz, DMSO-d_6): 40.87 (CH_2), 123.27 (CH), 127.37 (CH), 127.44 (CH), 128.62 (CH), 131.57 (C), 134.62 (CH), 136.69 (C), 167.77 (C).
Mp, ^1H and ^{13}C NMR data consistent with literature.

2-Benzyl-1,1,3,3-tetraethylisoindoline 189[184]

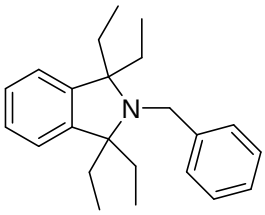

Isoindoline **189** was also isolated from chromatography following method 1. R_f [EtOAc-hexane (1:4)] 0.66. δ_H (400 MHz, $CDCl_3$): 0.68 (12H, t, *J* 7.4 Hz, 4 × CH_3), 1.40-1.49 (4H, m, 4 × C*H*^{a}H^b), 1.79-1.88 (4H, m, 4 × CH^a*H*^{b}), 3.91 (2H, s, CH_2), 6.97 (2H, dd, *J* 5.6 and 3.2 Hz, H-6 and H-7), 7.11 (2H, dd, *J* 5.6 and 3.2 Hz, H-5 and H-8), 7.15-7.23 (3H, m, 3 × Ar-H), 7.36-7.38 (2H, m, 2 × Ar-H).
^{1}H NMR data similar to literature but peaks are shifted, solvent not stated in literature.

2-Benzyl-5-hydroxy-1,1,3,3-tetraethylisoindoline 211

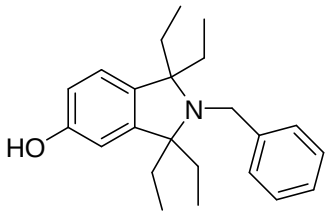

Method 1: A solution of benzylamine **178** (3.62 g, 9.03 mmol) in anhydrous THF (40 mL) was cooled to -78 ℃ and stirred for 15 min . *tert*-Butyllithium (1.05 M in pentane, 17.2 mL, 18.06 mmol) was added dropwise and the reaction mixture was stirred at -78 ℃ for a further 15 min. 2-Isopropo xy-4,4,5,5-tetramethyl-1,3,2-dioxaborolane **196** (6.08 mL, 29.8 mmol) was added dropwise and the reaction mixture was stirred at -78 ºC for a further 1.5 h before being allowed to warm to rt and stirred at rt overnight. The reaction mixture was quenched with H_2O and extracted with DCM (× 3). The combined organic extracts were washed with water (× 1), then brine (× 1), dried over $MgSO_4$ and concentrated. Excess dioxaborolane **196** was removed *in vacuo* to leave a brown oil which was dissolved in anhydrous THF (20 mL). NaOH (aq) (3M, 12.1 mL) was added, followed by dropwise addition of H_2O_2 (50% wt. in H_2O, 2.2 mL). The reaction mixture was heated at 55 ℃ for 3 h then cooled and extracted with DCM (× 3). The combined organic extracts were dried over $MgSO_4$, filtered and concentrated *in vacuo*. The crude residue was chromatographed [SiO_2, Et_2O-hexane (1:19)] to give phenol **211** as a yellow oil (313 mg, 11%).

Method 2: BBr_3 (18.7 mL, 18.7 mmol) was added via syringe to a solution of methoxy compound **216** (2.19 g, 6.24 mmol) in anhydrous DCM (50 mL) at -78 ℃. The reaction mixture was warmed to rt and stirred for 24 h. The mixture was

concentrated and the residue chromatographed [SiO_2, Et_2O-hexane (3:97)] to give phenol **211** as a yellow oil (1.81 g, 86%).

R_f [EtOAc-hexane (1:4)] 0.26. δ_H (400 MHz, $CDCl_3$): 0.65-0.69 (12H, m, 4 × CH_3), 1.35-1.45 (4H, m, 4 × C$H_a$$H_b$Me), 1.73-1.80 (4H, m, 4 × $CH_a$$H_b$Me), 3.88 (2H, s, CH_2), 6.45 (1H, d, *J* 2.0 Hz, H-4), 6.59 (1H, dd, *J* 8.2 and 2.0 Hz, H-6), 6.79 (1H, d, *J* 8.2 Hz, H-7), 7.14-7.22 (3H, m, 3 × Ar-H), 7.34-7.36 (2H, m, 2 × Ar-H). δ_C (100 MHz, $CDCl_3$): 9.69 (CH_3), 30.44 (CH_2), 46.90 (CH_2), 70.97 (C), 71.33 (C), 110.36 (CH), 113.18 (CH), 124.28 (CH), 126.65 (CH), 127.88 (CH), 129.38 (CH), 136.97 (C), 142.50 (C), 146.53 (C), 153.98 (C). LRMS (CI^+) 394 [$(M + C_4H_9)^+$, 98%], 338 [$(M+H)^+$, 58], 308 (100). HRMS: 338.2470, $C_{23}H_{32}ON$ requires $(M+H)^+$ 338.2484. ν_{max} (ATR) 3296 (br, OH), 2967 (CH), 2933 (CH) cm^{-1}.

4-Methoxyphthalic acid 213[185]

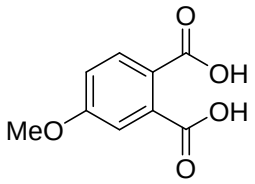

Following the procedure of Wentzel *et al.*[186], 3,4-dimethylanisole **212** (3.5 mL, 25.0 mmol) and potassium permanganate (25 g, 158 mmol) were dissolved in H_2O-*t*-BuOH (70:30) (140 mL). The reaction mixture was stirred at 100 ℃ for 21 h open to the atmosphere. The reaction was quenched by addition of ethanol (50 mL) and the alcohols were removed *in vacuo*. The resulting residue was filtered through celite and washed through with H_2O (300 mL). The aqueous filtrate was concentrated *in vacuo* to approximately 100 mL, conc. HCl was added and a white crystalline solid precipitated out. This was collected by filtration, dissolved in ethanol and filtered. The filtrate was concentrated *in vacuo* to yield 4-methoxyphthalic acid **213** as a white solid (1.90 g, 43%). Mp 146-148 ℃ (lit. 160-165 ℃ [187]). δ_H (400 MHz, DMSO-d_6): 3.83 (3H, s, OCH_3), 7.04 (1H, d, *J* 2.6 Hz, H-3), 7.08 (1H, dd, *J* 8.5 and 2.6 Hz, H-5), 7.73 (1H, d, *J* 8.5 Hz, H-6). δ_C (100 MHz, MeOD): 65.2 (CH_3), 122.5 (CH), 124.6 (CH), 132.2 (C), 140.8 (CH), 146.6 (C), 170.9 (C), 176.9 (C), 178.7 (C). ν_{max} (ATR) 2928 (br, OH), 1670 (C=O) cm^{-1}.
^{1}H NMR data consistent with literature (no ^{13}C NMR data available).

2-Benzyl-5-methoxyisoindoline-1,3-dione 215

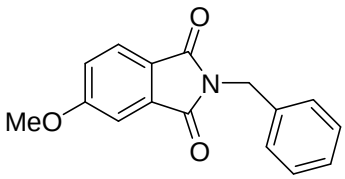

Thionyl chloride (9.5 mL, 130 mmol) was added to phthalic acid **213** (1.90 g, 9.69 mmol). The reaction mixture was placed under argon and stirred at 85 ℃ for 2.5 h. Excess thionyl chloride was removed *in vacuo* to give crude anhydride **214**. Benzylamine (1.06 mL, 9.69 mmol) was added to crude anhydride **214** and the mixture was stirred at 155 ℃ under argon for 24 h. Upon cooling a brown solid formed, which was dissolved in EtOAc and dropped into stirring 2 M HCl (aq). A precipitate formed and the suspension was left stirring for 2 h and then filtered to give phthalimide **215** as an off-white solid (1.34 g, 52%). Mp 169-170 ℃. δ_H (400 MHz, $CDCl_3$): 3.93 (3H, s, CH_3), 4.84 (2H, s, CH_2), 7.16 (1H, dd, *J* 8.3 and 2.3 Hz, H-7), 7.27-7.35 (4H, m, 3 × Ar-H and H-6), 7.43-7.45 (2H, m, 2 × Ar-H), 7.76 (1H, d, *J* 8.2 Hz, H-4). δ_C (100 MHz, $CDCl_3$): 41.58 (CH_2), 56.07 (CH_3), 108.29 (CH), 119.79 (CH), 124.14 (C), 125.16 (CH), 127.86 (CH), 128.64 (CH), 128.76 (CH), 134.86 (C), 136.66 (C), 164.79 (C), 167.95 (C), 167.97 (C). LRMS (EI^+) 267 ($M^{+\bullet}$) 100%. HRMS: 267.0896, $C_{16}H_{13}O_3N$ requires 267.0895. ν_{max} (ATR) 1695 (C=O) cm^{-1}.

2-Benzyl-5-methoxy-1,1,3,3-tetraethylisoindoline 216

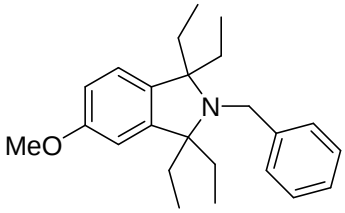

Ethylmagnesium bromide (3 M in diethyl ether, 87 mL, 261 mmol) was cannulated into a 3-necked round bottomed flask, fitted with a reflux condenser and distillation apparatus, under argon. The solution was stirred at 80 ℃ until no more ether was removed. The distillation apparatus was replaced with a stopper and a solution of phthalimide **215** (5.93 g, 22.2 mmol) in anhydrous toluene (50 mL) was added dropwise via syringe. The reaction mixture was stirred at 120 ℃ for 24 h, then

cooled and quenched by careful addition of H_2O, followed by dilution with EtOAc. The aqueous layer was extracted with EtOAc (× 3). The combined organic extracts were washed with brine, dried over $MgSO_4$, filtered and concentrated *in vacuo*. The crude residue was chromatographed [SiO_2, Et_2O-hexane (1:19)] to yield benzylamine **216** as a brown oil (2.19 g, 29%). R_f [EtOAc-hexane (1:4]) 0.58. δ_H (400 MHz, $CDCl_3$): 0.77 (12H, q, *J* 7.4 Hz, 4 × CH_3), 1.45-1.54 (4H, m, 4 × C*H*^{a}H^{b}Me), 1.83-1.92 (4H, m, 4 × CH^a*H*^{b}Me), 3.81 (3H, s, OCH_3), 3.98 (2H, s, CH_2), 6.59 (1H, d, *J* 2.4 Hz, H-4), 6.76 (1H, dd, *J* 8.3 and 2.5 Hz, H-6), 6.94 (1H, d, *J* 8.3 Hz, H-7), 7.21-7.31 (3H, m, 3 × Ar-H), 7.43-7.45 (2H, m, 2 × Ar-H). δ_C (100 MHz, $CDCl_3$): 9.78 (CH_3), 29.86 (CH_2), 30.52 (CH_2), 46.93 (CH_2), 55.50 (CH_3), 70.93 (C), 71.41 (C), 109.10 (CH), 111.40 (CH), 124.12 (CH), 126.65 (CH), 127.89 (CH), 129.40 (CH), 136.99 (C), 142.52 (C), 146.25 (C), 158.17 (C). LRMS (CI^+) 409 [(M + C_4H_9)$^+$, 100%], 352 [(M+H)$^+$, 46]. HRMS: 352.2642, $C_{24}H_{34}ON$ requires (M+H)$^+$ 352.2640. ν_{max} (ATR) 2963 (CH), 2934 (CH), 1612 (aromatic) cm^{-1}.

4-(2'-Benzyl-1',1',3',3'-tetraethylisoindolin-5'-oxy)butyltriphenylphosphonium bromide 222

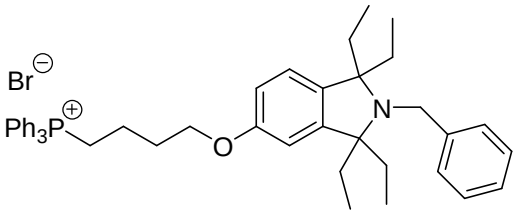

A stirred solution of phenol **211** (70 mg, 0.207 mmol), 4-bromobutyltriphenylphosphonium bromide (198 mg, 0.414 mmol) and cesium carbonate (68 mg, 0.21 mmol) in MeOD (1.5 mL) was heated at 55 ℃ for 24 h. The reaction mixture was filtered and concentrated *in vacuo*. DCM was added and the mixture was filtered. The filtrate was concentrated, dissolved in minimal DCM and Et_2O added. A precipitate formed. The solution was filtered and the filtrate concentrated *in vacuo*. This crude material was chromatographed [SiO_2, MeOH-DCM (1:19)], then chromatographed a second time [SiO_2, MeOH-$CHCl_3$ (1:9)] to give salt **222** as an off-white foamy solid (45 mg, 30%). R_f [MeOH-$CHCl_3$ 1:9]) 0.11. δ_H (400 MHz, $CDCl_3$): 0.74 (12H, t, *J* 7.3 Hz, 4 × CH_3), 1.46-1.52 (2H, m, CH_2), 1.81-1.89 (10H, m, 5 × CH_2), 2.22-2.25 (2H, m, CH_2), 3.96 (2H, s, CH_2Ph), 4.04 (2H, t, *J* 5.5 Hz, OCH_2), 6.48 (1H, d, *J* 2.4 Hz, H-4'), 6.68 (1H, dd, *J*

8.3 and 2.4 Hz, H-6'), 6.90 (1H, d, *J* 8.3 Hz, H-7'), 7.22-7.43 (5H, m, CH_2Ph), 7.64-7.78 (15H, m, PPh_3). δ_C (100 MHz, $CDCl_3$): 9.36 (CH_3), 9.47 (CH_3), 19.34 (CH_2), 22.39 (d, *J* 50.7 Hz, CH_2), 29.25 (d, *J* 16.5 Hz, CH_2), 30.08 (CH_2), 30.15 (CH_2), 46.54 (CH_2), 66.27 (CH_2), 70.57 (C), 71.02 (C), 108.96 (CH), 111.80 (CH), 117.97 (d, *J* 85.9 Hz, C), 123.8 (CH), 126.29 (CH), 127.51 (CH), 128.98 (CH), 130.30 (d, *J* 12.5 Hz, CH), 133.44 (d, *J* 10.0 Hz, CH), 134.85 (d, *J* 2.8 Hz, CH), 136.75 (C), 142.05 (C), 145.92 (C), 156.97 (C). LRMS (FAB^+) 654 (M^+, PPh_3 cation, 100%). HRMS: 654.3868, $C_{45}H_{53}ONP$ requires 654.3865. ν_{max} (ATR) 2963 (CH), 2924 (CH), 2876 (CH), 1113 (C-O) cm^{-1}.

4-(1',1',3',3'-tetraethylisoindolin-5'-oxy)butyltriphenylphosphonium bromide 223

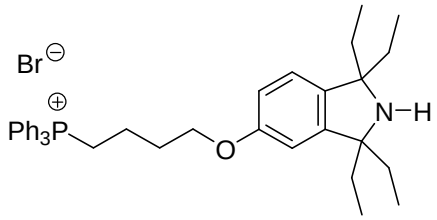

The same reaction gave salt **223** as an off-white foamy solid (20 mg, 15%) after the second round of chromatography [SiO_2, MeOH-$CHCl_3$ (1:9). R_f [MeOH-$CHCl_3$ (1:9)] 0.10. δ_H (400 MHz, $CDCl_3$): 0.90-0.96 (12H, m, 4 × CH_3), 1.87-2.01 (10H, m, 5 × CH_2), 2.19-2.29 (2H, m, CH_2), 3.96-4.03 (2H, m, CH_2), 4.11 (2H, t, *J* 5.5 Hz, OCH_2), 6.57 (1H, d, *J* 2.0 Hz, H-4'), 6.78 (1H, br d, *J* 6.6 Hz, H-6'), 6.97 (1H, d, *J* 8.4 Hz, H-7'), 7.67-7.96 (15H, m, 15 × Ar-H). δ_C (100 MHz, $CDCl_3$): 8.99 (CH_3), 9.04 (CH_3), 19.58 (CH_2), 22.19 (d, *J* 50.5 Hz, CH_2), 29.49 (d, *J* 16.5 Hz, CH_2), 32.90 (CH_2), 66.79 (CH_2), 108.60 (CH), 118.44 (d, *J* 86.0 Hz, C), 123.47 (CH), 130.55 (d, *J* 12.5 Hz, CH), 133.84 (d, *J* 10.0 Hz, CH), 135.07 (d, *J* 2.9 Hz, CH), 158.59 (C).

1,1,3,3-Tetraethylisoindoline 224[188]

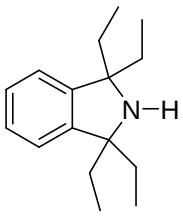

2-Benzyl-1,1,3,3-tetraethylisoindoline **189** (1.08 g, 3.36 mmol) and 10% palladium on carbon (92 mg) were dissolved in EtOH (25 mL). The solution was flushed with hydrogen then placed under a hydrogen atmosphere and stirred at 70 °C for 48 h. The reaction had not gone to completion so a further 200 mg of catalyst was added and the reaction mixture heated for a further 24 h. The reaction mixture was cooled, centrifuged (× 2) and the supernatant was decanted off. The supernatant was filtered through cotton wool and the solution was concentrated *in vacuo* to give 1,1,3,3-tetraethylisoindoline **224** as a pink oil (719 mg, 93%). δ_H (400 MHz, $CDCl_3$): 0.87 (12H, t, *J* 7.4 Hz, 4 × CH_3), 1.62-1.79 (8H, m, 4 × CH_2), 7.07 (2H, dd, *J* 5.6 and 3.2 Hz, H-5 and H-6), 7.21 (2H, dd, *J* 5.6 and 3.1 Hz, H-4 and H-7). δ_C (100 MHz, $CDCl_3$): 9.03 (CH_3), 33.90 (CH_2), 68.40 (C), 122.56 (CH), 126.63 (CH), 147.59 (C). LRMS (CI^+) 232 [$(M+H)^+$, 51%], 85 (63), 73 (100). HRMS: 232.2061, $C_{16}H_{26}N$ requires 232.2065. ν_{max} (ATR) 2963 (CH), 2926 (CH), 1458 (aromatic) cm^{-1}.
^1H and ^{13}C NMR data consistent with literature.

4-(1',1',3',3'-Tetraethylisoindolin-5'-oxy)butyltriphenylphosphonium bromide, hydrobromide salt 225

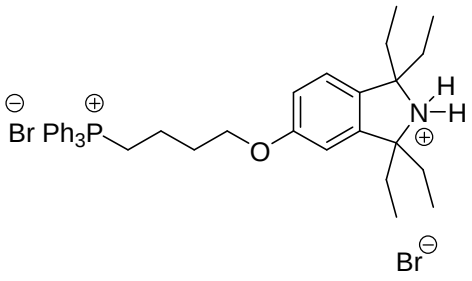

Salt **222** (127 mg, 0.173 mmol), HBr (45% in acetic acid, 31 µL) and 10% palladium on carbon (45 mg, 0.25 mol%) were dissolved in EtOH (0.85 mL). The solution was flushed with hydrogen then placed under a hydrogen atmosphere and

stirred at rt for 20 h. The catalyst was removed by filtration through cotton wool and the solution was concentrated *in vacuo* to give salt **225** as a yellow, foamy solid (114 mg, 91%). δ_H (400 MHz, MeOD): 0.99-1.11 (12H, m, 4 × CH_3), 1.82-1.93 (2H, m, CH_2), 2.03-2.16 (10H, m, 5 × CH_2), 3.58-3.65 (2H, m, CH_2), 4.13 (2H, t, *J* 5.6 Hz, O-CH_2), 6.85 (1H, d, *J* 1.6 Hz, Ar H-3), 6.98 (1H, dd, *J* 8.4 and 1.6 Hz, Ar H-5), 7.23 (1H, d, *J* 8.8 Hz, Ar H-6), 7.73-7.87 (15H, m, 15 × Ar-H). δ_C (100 MHz, MeOD): 8.68 (CH_3), 8.75 (CH_3), 20.24 (CH_2), 22.31 (d, *J* 51.3 Hz, CH_2), 30.70 (d, *J* 16.5 Hz, CH_2), 31.42 (CH_2), 31.36 (CH_2), 68.13 (CH_2), 76.97 (C), 76.70 (C), 110.07 (CH), 116.99 (CH), 119.79 (d, *J* 86.0 Hz, C), 125.63 (CH), 131.48 (d, *J* 12.5 Hz, CH), 133.31 (C), 134.82 (d, *J* 10.0 Hz, CH), 136.18 (d, *J* 2.7 Hz, CH), 142.96 (C), 161.11 (C). LRMS (FAB^+) 565 [M^+ (phosphonium ion), 100%]. HRMS: 564.3392, $C_{38}H_{47}NOP$ requires 564.3395. ν_{max} (ATR) 2969 (CH), 2936 (CH), 2876 (CH), 1112 (C-O) cm^{-1}.

2-Benzyloxyisoindoline-1,3-dione 227[189]

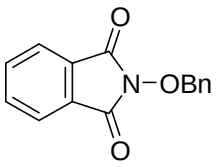

Benzyl bromide (3.56 mL, 30.0 mmol) was added via syringe to a stirred solution of *N*-hydroxyphthalimide **226** (4.90 g, 28.1 mmol) and sodium carbonate (8.55 g, 80.7 mmol) in a mixture of DMF (40 mL), MeCN (7.5 mL) and H_2O (40 mL). After 4 h the reaction mixture was filtered, washed with H2O (× 2) and ice cold MeCN (× 1). The remaining solid was dried by azeotrope with toluene (× 3) giving compound **227** as a pink powder (6.65 g, 88%). δ_H (400 MHz, $CDCl_3$): 5.21 (2H, s, CH_2), 7.37-7.40 (3H, m, 3 × Ar-H), 7.53-7.55 (2H, m, 2 × Ar-H), 7.73 (2H, dd, *J* 5.4 and 3.2 Hz, H-5 and H-6), 7.81 (2H, dd, J 5.5 and 3.1 Hz, H-4 and H-7). δ_C (100 MHz, $CDCl_3$): 79.90 (CH_2), 123.53 (CH), 128.60 (CH), 128.86 (C), 129.40 (CH), 129.94 (CH), 133.72 (C), 134.51 (CH), 163.53 (C). LRMS (CI^+) 254 [$(M+H)^+$, 100%]. HRMS: 254.0818, $C_{15}H_{12}O_3N$ requires $(M+H)^+$ 254.0817. ν_{max} (ATR) 1726 (C=O) cm^{-1}.

^1H and ^{13}C NMR data consistent with literature.

4-(2'-Oxy-1',1',3',3'-tetraethylisoindolin-5'-oxy)butyltriphenylphosphonium bromide 229

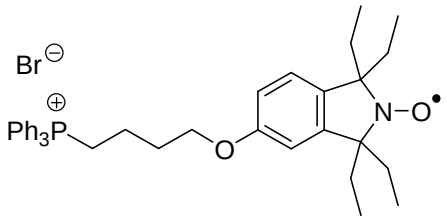

A solution of salt **225** (114 mg, 0.158 mmol), *m*-chloroperbenzoic acid (70%, 78 mg, 0.316 mmol) and sodium hydrogen carbonate (13 mg, 0.158 mmol) in anhydrous methanol (6.1 mL) was stirred at rt for 3 h. The reaction mixture was concentrated and dissolved in anhydrous MeOH (1 mL) and a second portion of *m*-chloroperbenzoic acid (70%, 78 mg, 0.316 mmol) was added. The reaction mixture was stirred at rt for 21 h. An EPR spectrum of the reaction mixture showed a strong signal so the reaction was quenched by addition of 5% Na_2CO_3 (aq) (5 mL). A yellow oil separated and was dissolved in DCM. Upon concentration of the DCM solution an off-white, foamy solid was formed. (10 mg, 10%).

N-(2',4'-Dinitrophenyl)pyridinium chloride 247[190]

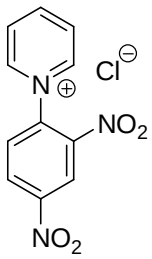

Pyridine **257** (4.0 mL, 49 mmol) and 1-chloro-2,4-dinitrobenzene **238** (10.01 g, 49.4 mmol) were heated together at 95 ℃ for 1 h. T he resulting yellow solid was triturated with acetone until no further colour was removed, to give pyridinium salt **247** as an off-white solid (12.6 g, 91%). Mp 193–195 °C. δ_H (400 MHz, MeOD): 8.39 (1H, d, *J* 8.7 Hz, H-6'), 8.47 (2H, dd, *J* 7.9 and 6.8 Hz, H-3 and H-5), 8.97 (1H, dd, *J* 8.7 and 2.5 Hz, H-5'), 9.02 (1H, tt, *J* 7.9 and 1.3 Hz, H-4), 9.31 (1H, d, *J* 2.5 Hz, H-3'), 9.40 (2H, dd, *J* 6.9 and 1.3 Hz, H-2 and H-6). δ_C (100 MHz, MeOD): 121.35 (CH), 128.01 (CH), 130.20 (CH), 132.01 (CH), 138.72 (C), 143.05 (C),

146.08 (CH), 148.79 (CH), 149.00 (C). LRMS (FAB^+) 246 [M^+ (pyridinium cation), 100%]. HRMS: 246.0514, $C_{11}H_8N_3O_4$ requires 246.0515. ν_{max} (KBr) 3117, 3057, 1610 (aromatic), 1542 (NO_2), 1473 (aromatic), 1342 (NO_2) cm^{-1}.
^1H and ^{13}C NMR data consistent with literature data obtained in $(CD_3)_2SO$.

N-tert-Butyl-α-[3-(pyrid-1'-yl)phenyl]nitrone chloride 269

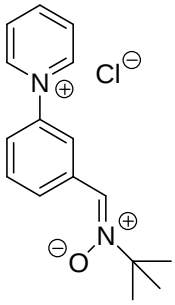

N-tert-Butyl-α-(3-aminophenyl)nitrone **298** (80 mg, 0.44 mmol) was added to a stirred solution of N-(2',4'-dinitrophenyl)pyridinium chloride **247** (42 mg, 0.15 mmol) in anhydrous methanol (4 mL) under argon at rt. After 2 h the resulting red mixture was heated to reflux for 18 h until the red colour disappeared. The mixture was cooled, diluted with H_2O and washed with EtOAc until no further colour was removed from the aqueous layer. The aqueous portion was concentrated *in vacuo* to give pyridinium salt **269** as a brown oil (40 mg, 96%). δ_H (400 MHz, MeOD): 1.68 (9H, s, 3 × CH_3), 7.87 (1H, t, *J* 8.0 Hz, H-5), 7.97 (1H, ddd, *J* 8.1, 2.4 and 0.9 Hz, H-6), 8.21 (1H, s, CH=N), 8.37 (2H, dd, *J* 7.9 and 6.9 Hz, H-3' and H-5'), 8.49 (1H, dt, *J* 7.9 and 1.4 Hz, H-4), 8.87 (1H, tt, *J* 7.9 and 1.3 Hz, H-4'), 9.16 (1H, dd, *J* 2.0 and 1.8 Hz, H-2), 9.35 (2H, dd, *J* 6.9 and 1.4 Hz, H-2' and H-6'). δ_C (100 MHz, MeOD): 28.37 (CH_3), 73.17 (C), 125.14 (CH), 127.13 (CH),129.67 (CH),131.72 (CH),132.00 (CH),133.42 (CH), 134.57 (C), 144.38 (C), 146.12 (CH), 148.18 (CH). LRMS (FAB^+) 255 [M^+ (pyridinium cation), 100%]. HRMS: 255.1501, $C_{16}H_{19}N_2O$ requires 255.1497. ν_{max} (ATR) 3074 (CH), 2980 (CH), 2934 (CH), 1628 (Ar), 1583 (Ar), 1472 (Ar), 1190 (nitrone) cm^{-1}.

N-(3'-Hydroxymethylphenyl)pyridinium chloride 271

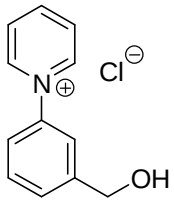

3-Aminobenzyl alcohol **270** (2.74 g, 22.3 mmol) was added to a stirred solution of *N*-(2',4'-dinitrophenyl)pyridinium chloride **247** (2.50 g, 8.90 mmol) in anhydrous methanol (60 mL) under argon at rt. After 24 h, the resulting red mixture was heated to reflux for 48 h until the red colour disappeared. The mixture was cooled, diluted with H_2O and washed with EtOAc until no further colour was removed from the aqueous layer. The aqueous layer was concentrated *in vacuo* to give a brown solid that was recrystallised from ^{i}PrOH–acetone to give pyridinium salt **271** as brown cubes (1.08 g, 55%). Mp 107–109 ℃. δ_H (400 MHz, MeOD): 4.83 (2H, s, CH_2OH), 7.75–7.79 (3H, m, H-4', H-5' and H-6'), 7.85 (1H, br s, H-2'), 8.33 (2H, dd, *J* 7.8 and 6.8 Hz, H-3 and H-5), 8.84 (1H, tt, *J* 7.8 and 1.3 Hz, H-4), 9.30 (2H, dd, *J* 6.9 and 1.4 Hz, H-2 and H-6). δ_C (100 MHz, MeOD): 62.41 (CH_2), 121.96 (CH), 122.54 (CH), 128.07 (CH), 129.14 (CH), 130.14 (CH), 143.08 (C), 144.59 (CH), 145.13 (C), 146.39 (CH). LRMS (FAB$^+$) 186 [M^+ (pyridinium cation), 100%]. HRMS: 186.0916, $C_{12}H_{12}NO$ requires 186.0919. ν_{max} (ATR) 3295 (OH), 2916 (CH), 2851 (CH), 1614 (aromatic), 1471 (aromatic) cm^{-1}.

N-(3'-Chloromethylphenyl)pyridinium chloride 273

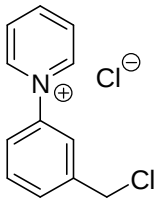

A mixture of *N*-(3'-hydroxymethylphenyl)pyridinium chloride **271** (300 mg, 1.61 mmol) and $SOCl_2$ (3.0 mL, 40.6 mmol) was heated at 95 ℃ under argo n for 18 h. The reaction was cooled and the excess $SOCl_2$ was quenched by slow addition of H_2O. The reaction mixture was washed with $CHCl_3$ and the aqueous portion was concentrated *in vacuo* to give pyridinium salt **273** as a brown oil (310 mg, 96%).

δ_H (400 MHz, MeOD): 4.88 (2H, s, CH_2Cl), 7.79–7.89 (3H, m, H-4', H-5' and H-6'), 8.01 (1H, s, H-2'), 8.36 (2H, m, H-3 and H-5), 8.86 (1H, t, *J* 7.7 Hz, H-4), 9.32 (2H, d, *J* 6.1 Hz, H-2 and H-6). δ_C (100 MHz, MeOD): 45.49 (CH_2), 125.42 (CH), 125.77 (CH), 129.66 (CH), 132.12 (CH), 132.85 (CH), 142.41 (CH), 144.53 (C), 146.12 (C), 148.10 (CH). LRMS (FAB^+) 204 [M^+ (^{35}Cl, pyridinium cation), 100%], 206 [M^+ (^{37}Cl, pyridinium cation), 33%]. HRMS: 204.0579 and 206.0553. $C_{12}H_{11}{}^{35}ClN$ requires 204.0580 and $C_{12}H_{11}{}^{37}ClN$ requires 206.0553. ν_{max} (ATR) 3032 (CH), 2958 (CH), 1627 (aromatic), 1473 (aromatic) cm^{-1}.

N-(4'-Methylphenyl)pyridinium chloride 275

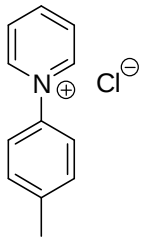

p-Toluidine **274** (471 mg, 4.45 mmol) was added to a stirred solution of *N*-(2',4'-dinitrophenyl)pyridinium chloride **247** (500 mg, 1.78 mmol) in anhydrous methanol (15 mL) under argon at rt. After 2 h, the resulting red mixture was heated to reflux for 24 h until the red colour disappeared. The mixture was cooled, diluted with H_2O and washed with EtOAc until no further colour was removed from the aqueous layer. The aqueous layer was concentrated *in vacuo* to give pyridinium salt **275** as a yellow oil (352 mg, 96%). δ_H (400 MHz, MeOD): 2.55 (3H, s, CH_3), 7.61 (2H, d, *J* 8.0 Hz, H-3' and H-5'), 7.77 (2H, d, *J* 8.4 Hz, H-2' & H-6'), 8.32 (2H, dd, *J* 7.5 and 6.9 Hz, H-3 and H-5), 8.82 (1H, tt, *J* 7.8 and 1.2 Hz, H-4), 9.27-9.29 (2H, m, H-2 and H-6). δ_C (100 MHz, MeOD): 21.16 (CH_3), 125.23 (CH), 129.55 (CH), 132.16 (CH), 142.22 (C), 143.73 (C), 146.01 (CH), 147.63 (CH). LRMS (FAB^+) 171 [M^+ (pyridinium cation), 100%]. HRMS: 170.0972, $C_{12}H_{12}N$ requires 170.0970. ν_{max} (ATR) 3053 (CH), 1628 (Ar), 1477 (Ar) cm^{-1}.

Literature mp available for tetrafluoroborate salt but not chloride salt.[191]

2-(3'-Nitrophenyl)-1,3-dioxolane 278[192]

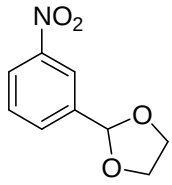

3-Nitrobenzaldehyde **277** (1.32 g, 8.74 mmol), ethylene glycol (1.0 mL, 16 mmol) and p-toluenesulphonic acid (30 mg, 0.16 mmol) were dissolved in anhydrous toluene (30 mL). The reaction was heated under argon in a Dean-Stark apparatus at 140 ℃ for 24 h. Upon completion, the mixture was cooled, washed with saturated aqueous $NaHCO_3$ (× 3), H_2O and brine. The organic extracts were combined, dried over $MgSO_4$, and concentrated *in vacuo* to give a yellow solid which was recrystallised from Et_2O-hexane to give acetal **278** as yellow needles (1.63 g, 96%). Mp 49-50 ℃, lit. 56-58 ℃. δ_H (400 MHz, $CDCl_3$): 3.98-4.09 (4H, m, 2 × CH_2), 5.81 (1H, s, CH_2O), 7.49 (1H, t, *J* 8.0 Hz, H-5'), 7.74 (1H, d, *J* 7.7 Hz, H-4'), 8.14 (1H, ddd, *J* 8.2, 2.3 and 1.1 Hz, H-6'), 8.27 (1H, t, *J* 1.9 Hz, H-2'). δ_C (100 MHz, $CDCl_3$): 65.35 (CH_2), 102.01 (CH), 121.44 (CH), 123.79 (CH), 129.31 (CH), 132.62 (CH), 140.27 (C), 148.04 (C). LRMS (CI^+) 196 [$(M+H)^+$, 88%], 166 (28), 69 (100). HRMS: 196.0613, $C_9H_{10}NO_4$ requires 196.0610. ν_{max} (ATR) 2889 (CH), 1522 (NO_2), 1479 (aromatic), 1344 (NO_2), 1082 (C-O stretch) cm^{-1}.
^1H and ^{13}C NMR data consistent with literature.

5,5-Dimethyl-2-(3'-nitrophenyl)-1,3-dioxane 279[193]

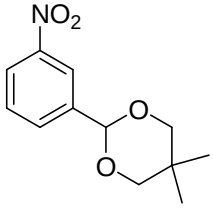

3-Nitrobenzaldehyde **277** (1.00 g, 6.62 mmol), 2,2-dimethyl-1,3-propanediol (1.41 g, 13.6 mmol) and p-toluenesulfonic acid (24 mg, 0.12 mmol) were dissolved in anhydrous toluene (23 mL). The reaction was heated under argon in a Dean–Stark apparatus at 140 ℃ for 24 h. Upon completion, the mixture was cooled, washed with $NaHCO_3$ (× 3), H_2O and brine. The organic extracts were combined, dried over $MgSO_4$, and concentrated *in vacuo* to give acetal **279** as a yellow oil (1.50 g,

95%) that solidified on standing. Mp 46–48 ℃. δ_H (400 MHz, $CDCl_3$): 0.81 (3H, s, CH_3), 1.27 (3H, s, CH_3), 3.67 (2H, d, *J* 10.6 Hz, CH_2O–), 3.78 (2H, d, *J* 10.1 Hz, CH_2O–), 5.45 (1H, s, CHO_2), 7.53 (1H, t, *J* 8.0 Hz, H-5'), 7.81–7.83 (1H, m, H-4'), 8.18 (1H, ddd, *J* 1.0, 2.3 and 8.2 Hz, H-6'), 8.37 (1H, t, *J* 1.9 Hz, H-2'). δ_C (100 MHz, $CDCl_3$): 21.86 (CH_3), 23.07 (CH_3), 30.31 (C), 77.70 (CH_2), 99.92 (CH), 121.62 (CH), 123.69 (CH), 129.30 (CH), 132.49 (CH), 140.61 (C), 148.23 (C). LRMS (CI^+) 238 [$(M+H)^+$, 78%], 79 (100). HRMS: 238.1078, $C_{12}H_{16}NO_4$ requires $(M+H)^+$, 238.1079. ν_{max} (ATR) 2955 (CH), 2870 (CH), 1529 (NO_2), 1460 (aromatic), 1348 (NO_2), 1082 (C–O stretch) cm^{-1}.
^{1}H NMR and mp not in agreement with literature.

2-(3'-Aminophenyl)-5,5-dimethyl-1,3-dioxane 281

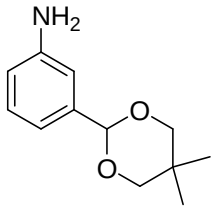

5,5-Dimethyl-2-(3'-nitro-phenyl)-[1,3]dioxane **279** (825 mg, 3.48 mmol) and platinum(IV) oxide (16 mg, 5 mol %) were dissolved in EtOAc (16.5 mL). The solution was flushed with hydrogen then placed under a hydrogen atmosphere and stirred at rt for 20 h. The catalyst was removed by filtration through cotton wool and the solution was concentrated *in vacuo* to give amine **281** as an orange-brown solid (720 mg, 100%). Mp 60–61 ℃. δ_H (400 MHz, $CDCl_3$) 0.78 (3H, s, CH_3), 1.30 (3H, s, CH_3), 3.58–3.64 (4H, m, NH_2 + CH_2), 3.74–3.77 (2H, m, CH_2), 5.30 (1H, s, CHO_2), 6.61 (1H, ddd, *J* 0.9, 2.4 and 7.9 Hz, H-6'), 6.83 (1H, t, *J* 2.0 Hz, H-2'), 6.86–6.89 (1H, m, H-4'), 7.13 (1H, t, *J* 7.8 Hz, H-5'). δ_C (100 MHz, $CDCl_3$): 21.84 (CH_3), 23.06 (CH_3), 30.19 (C), 77.58 (CH_2), 101.78 (CH), 112.67 (CH), 115.61 (CH), 116.31 (CH), 129.18 (CH), 139.55 (C), 146.53 (C). LRMS (EI^+) 207 ($M^{+\bullet}$, 90%),121 (100). HRMS: 207.1263, $C_{12}H_{17}NO_2$ requires 207.1259. ν_{max} (ATR) 3381 (NH_2), 3360 (NH_2), 2957 (CH), 1620 (NH_2 bend), 1462 (aromatic), 1385, 1094 (C–O stretch) cm^{-1}.

_N_-[3'-(1",3"-dioxolan-2"-yl)phenyl]pyridinium chloride 282

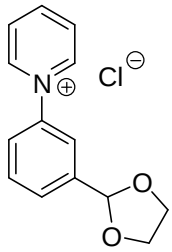

2-(3'-Nitrophenyl)-1,3-dioxolane **278** (3.632g, 18.60 mmol) and platinum(IV) oxide (88 mg, 5 mol %) were dissolved in anhydrous methanol (100 mL). The solution was flushed with hydrogen then placed under a hydrogen atmosphere and stirred at rt for 5 h. A small sample was removed, concentrated and the ^{1}H NMR spectrum was taken to show that amine **280** had been formed [δ_H (400 MHz, $CDCl_3$): 3.97-4.10 (4H, m, 2 × CH_2), 5.73 (1H, s, CH_2O), 6.64 (1H, ddd, *J* 8.0, 2.4 and 1.0 Hz, H-6'), 6.79 (1H, app. t, *J* 2.0 Hz, H-2'), 6.87 (1H, br d, *J* 7.6 Hz, H-4'), 7.16 (1H, t, *J* 7.8 Hz, H-5')]. The solution was filtered directly into a flask containing *N*-(2',4'-dinitrophenyl)pyridinium chloride **247** (1.048 g, 3.72 mmol). The reaction was stirred under argon at RT for 21 h then heated at reflux for 4 h until the red colour disappeared. The mixture was cooled, diluted with H_2O and washed with EtOAc until no further colour was removed from the aqueous layer. The aqueous portion was concentrated *in vacuo* to give **282** as a brown oil (905 mg, 92%). δ_H (400 MHz, MeOD): 4.09-4.21 (4H, m, 2 × CH_2), 5.97 (1H, s, CHO_2), 7.80-7.91 (3H, m, H-4', H-5' & H-6'), 8.00 (1H, broad s, H-2'), 8.34 (2H, dd, *J* 7.8 Hz & 6.8 Hz, H-3 & H-5), 8.84 (1H, tt, *J* 7.9 Hz & 1.3 Hz, H-4), 9.30 (2H, dd, *J* 6.9 Hz & 1.3 Hz, H-2 & H-6). δ_C (100 MHz, MeOD): 66.61 (CH_2), 103.47 (CH), 123.75 (CH), 126.18 (CH), 129.55 (CH), 130.96 (CH), 131.78 (CH), 143.14 (C), 144.49 (C), 146.19 (CH), 148.01 (CH); LRMS (FAB$^+$) 228 [M^+ (pyridinium cation), 100%]. HRMS: 228.1019, $C_{14}H_{14}NO_2$ requires 228.1025. ν_{max} (ATR) 3032 (CH), 2889 (CH), 1626 (aromatic), 1591 (aromatic), 1473 (aromatic) cm^{-1}.

_N_-[3'-(5'',5''-Dimethyl-1'',3''-dioxan-2''-yl)phenyl]-pyridinium chloride 283

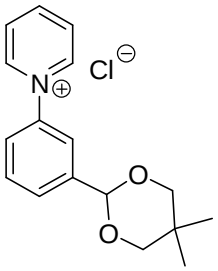

_N_-2',4'-Dinitrophenyl pyridinium chloride **247** (333 mg, 1.18 mmol) was dissolved in anhydrous methanol (12 mL) and amine **281** (613 mg, 2.96 mmol) was added. The reaction was stirred under argon at rt for 20 h and then heated at reflux for 3 h until the red colour disappeared. The mixture was cooled, diluted with H_2O and washed with EtOAc until no further colour was removed from the aqueous layer. The aqueous portion was concentrated *in vacuo* to give pyridinium salt **283** as a yellow oil (326 mg, 90%). δ_H (400 MHz, MeOD): 0.87 (3H, s, CH_3), 1.30 (3H, s, CH_3), 3.81 (4H, s, 2 × CH_2), 5.65 (1H, s, CHO_2), 7.80 (1H, t, *J* 7.6 Hz, H-5'), 7.86 (1H, ddd, *J* 8.0, 2.4 and 1.3 Hz, H-4' or H-6'), 7.91 (1H, dt, *J* 7.6 and 1.5 Hz, H-4' or H-6'), 7.98–8.00 (1H, m, H-2'), 8.32 (2H, dd, *J* 7.9 and 6.9 Hz, H-3 and H-5), 8.83 (1H, tt, *J* 1.4 and 7.9 Hz, H-4), 9.29 (2H, dd, *J* 6.9 and 1.4 Hz, H-2 and H-6). δ_C (100 MHz, MeOD): 21.91 (CH_3), 23.32 (CH_3), 78.57 (CH_2), 101.09 (CH), 123.45 (CH), 125.73 (CH), 129.53 (CH), 130.66 (CH), 131.58 (CH), 143.29 (C), 144.38 (C), 146.20 (CH), 147.97 (CH). LRMS (FAB^+) 270 [M^+ (pyridinium cation), 100%]. HRMS: 270.1488, $C_{17}H_{20}NO_2$ requires 270.1494. ν_{max} (ATR) 3007 (CH), 2949 (CH), 2868 (CH), 1628 (aromatic), 1473 (aromatic) cm^{-1}.

2-(4'-Nitrophenyl)-1,3-dioxolane 284[194]

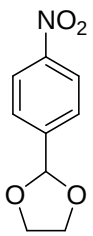

4-Nitrobenzaldehyde (6.60 g, 43.7 mmol), ethylene glycol (5.0 mL, 90 mmol) and *p*-toluenesulfonic acid (153 mg, 0.80 mmol) were dissolved in anhydrous toluene (150 mL). The mixture was heated under argon in a Dean-Stark apparatus at 140

℃ for 48 h. The mixture was then cooled, washed with saturated aqueous $NaHCO_3$ (× 3), H_2O and brine. The organic layer was dried over $MgSO_4$, and concentrated *in vacuo* to give acetal **284** as yellow needles (7.64 g, 90%). Mp 84-86 ℃ (lit. 80-82 ℃). [195] δ_H (400 MHz, $CDCl_3$): 4.06-4.09 (2H, m, 2 × C*H*^{a}H^b), 4.11-4.16 (2H, m, 2 × CH^a*H*^{b}), 5.90 (1H, s, CH), 7.66 (2H, d, *J* 8.6 Hz, H-2' & H-6'), 8.24 (2H, d, *J* 8.8 Hz, H-3' & H-5'). δ_C (100 MHz, $CDCl_3$): 65.57 (CH_2), 102.30 (CH), 123.64 (CH), 127.51 (CH), 145.05 (C), 148.45 (C). LRMS (CI) 196 [$(M+H)^+$, 100%], 166.19 (30). HRMS: 196.0607, $C_9H_{10}NO_4$ requires 196.0610. ν_{max} (ATR) 2895 (CH), 1610 (aromatic), 1519 (NO_2), 1489 (aromatic), 1346 (NO_2), 1076 (C-O stretch) cm^{-1}.

^1H and ^{13}C NMR data consistent with literature.

5,5-Dimethyl-2-(4'-nitrophenyl)-1,3-dioxane 285[196]

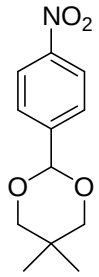

4-Nitrobenzaldehyde (1.00 g, 6.62 mmol), 2,2-dimethyl-1,3-propanediol (1.41 g, 13.6 mmol) and *p*-toluenesulfonic acid (24 mg, 0.12 mmol) were dissolved in anhydrous toluene (23 mL). The mixture was heated under argon in a Dean–Stark apparatus at 140 ℃ for 24 h. Upon completion, the mixture was cooled, washed with $NaHCO_3$ (× 3), H_2O and brine. The organic extracts were combined, dried over $MgSO_4$, and concentrated *in vacuo* to give acetal **285** as a yellow solid (1.53 g, 97%). Mp 78-80 ℃ (lit. 83-85 ℃) [197]. δ_H (400 MHz, $CDCl_3$): 0.82 (3H, s, CH_3), 1.28 (3H, s, CH_3), 3.67 (2H, d, *J* 10.7 Hz, 2 × C*H*^{a}H^b), 3.80 (2H, d, *J* 10.7 Hz, 2 × CH^a*H*^{b}), 5.46 (1H, s, CH), 7.68 (2H, d, *J* 8.8 Hz, H-2' & H-6'), 8.23 (2H, d, *J* 8.8 Hz, H-3' & H-5'). δ_C (100 MHz, $CDCl_3$): 21.96 (CH_3), 23.11 (CH_3), 30.43 (C), 77.82 (CH_2), 100.12 (CH), 123.61 (CH), 127.42 (CH), 145.12 (C), 148.28 (C). LRMS (CI) 238 [$(M+H)^+$, 100%]. HRMS: 238.1078, $C_{12}H_{16}NO_4$ requires $(M+H)^+$ 238.1079. ν_{max} (ATR) 2960 (CH), 2859 (CH), 1519 (NO_2), 1456 (aromatic), 1346 (NO_2), 1092 (C–O stretch) cm^{-1}.

^1H NMR data consistent with literature.

2-(4'-Aminophenyl)-5,5-dimethyl-1,3-dioxane 289[196]

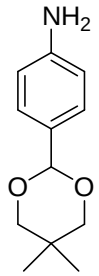

A solution of 5,5-dimethyl-2-(4'-nitrophenyl)-1,3-dioxane **285** (50 mg, 0.21 mmol) in EtOAc (1 mL), containing a suspension of platinum(IV) oxide (1 mg, 5 mol%) was flushed with hydrogen gas then placed under a hydrogen atmosphere and stirred at rt for 5 h. The catalyst was removed by filtration through cotton wool and the solution was concentrated *in vacuo* to give amine **289** as a brown solid (44 mg, 100%). δ_H (400 MHz, $CDCl_3$): 0.78 (3H, s, CH_3), 1.29 (3H, s, CH_3), 3.61-3.64 (4H, m, 2 × C*H*^{a}H^b and NH_2), 3.73-3.76 (2H, m, 2 × CH^a*H*^{b}), 5.29 (1H, s, CH), 6.65 (2H, d, *J* 8.6 Hz, H-2' & H-6'), 7.29 (2H, d, *J* 8.5 Hz, H-3' & H-5'). δ_C (100 MHz, $CDCl_3$): 21.96 (CH_3), 23.13 (CH_3), 30.21 (C), 77.70 (CH_2), 102.10 (CH), 114.78 (CH), 127.32 (CH), 128.91 (C), 147.08 (C). ν_{max} (ATR) 3283 (NH_2), 2870 (CH), 1476 (aromatic), 1391, 1053 (C–O stretch) cm^{-1}.
^{1}H NMR data consistent with literature.

***N-tert*-Butyl-α-(3-nitrophenyl)nitrone 297**[198]

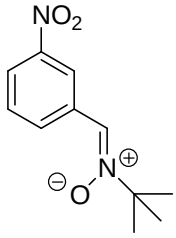

3-Nitrobenzaldehyde **277** (500 mg, 3.31 mmol), *N*-(*tert*-butyl)-hydroxylammonium acetate (740 mg, 4.96 mmol) and sodium hydrogen carbonate (417 mg, 4.96 mmol) were dissolved in ethanol (40 mL). The reaction was heated, with stirring, at 70 ℃ for 48 h. The reaction mixture was poured in to H_2O (120 mL) and left to stand for 1 h. The bright yellow crystals that formed were filtered off to give

nitrone **297** as yellow, feathery crystals (641 mg, 92%). Mp 102–103 ℃ (lit. 108–110 ℃) [198]. δ_H (400 MHz, $CDCl_3$): 1.62 (9H, s, 3 × CH_3), 7.55 (1H, t, *J* 8.1 Hz, H-5), 7.69 (1H, s, CH=N), 8.18 (1H, dd, *J* 8.1 and 1.7 Hz, H-4), 8.57 (1H, dt, *J* 8.0 and 1.48 Hz, H-6), 9.17 (1H, t, *J* 1.7 Hz, H-2). δ_C (100 MHz, $CDCl_3$): 28.31 (CH_3), 71.99 (C), 123.18 (CH), 124.29 (CH), 127.94 (CH), 129.46 (CH), 132.53 (C), 133.99 (CH), 148.18 (C). LRMS (EI^+) 222 ($M^{+\bullet}$, 10%), 84 (30), 57 ($C_4H_9^+$, 100). HRMS: 222.1003, $C_{11}H_{14}N_2O_3$ requires 222.1004. ν_{max} (KBr) 2985 (CH), 2940 (CH), 1556 (aromatic), 1522 (NO_2), 1415 (aromatic), 1366 (NO_2), 1339 (nitrone) cm^{-1}.

^1H NMR data consistent with literature data obtained in $(CD_3)_2SO$.

N-tert-Butyl-α-(3-aminophenyl)nitrone 298

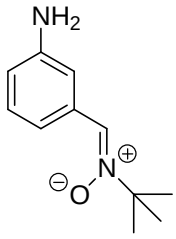

N-tert-Butyl-α-(3-nitrophenyl)nitrone **297** (500 mg, 2.34 mmol) and platinum(IV) oxide (11 mg, 5 mol %) were dissolved in EtOAc (10 mL). The solution was flushed with hydrogen then placed under a hydrogen atmosphere and stirred at rt for 45 min. The catalyst was removed by filtration through Celite and the solution was concentrated *in vacuo* to give a 1:1.4 mixture of the product **298** and starting material **297**. The starting material **297** was removed by precipitation from EtOH–H_2O (× 2) as a crystalline solid. The supernatant was concentrated to give a 10:1 mixture of nitrones **298** and **297** as a yellow oil (108 mg, 40%; 81% based on recovered SM). δ_H (400 MHz, $CDCl_3$): 1.49 (9H, s, 3 × CH_3), 3.73 (2H, br s, NH_2), 6.63 (1H, ddd, *J* 7.9, 2.4 and 0.9 Hz, H-4), 7.07 (1H, t, *J* 7.9 Hz, H-5), 7.19 (1H, d, *J* 7.8 Hz, H-6), 7.37 (1H, s, CH=N), 8.00 (1H, t, *J* 1.9 Hz, H-2).

Material was carried on to next stage with no further purification or analysis due to potential instability.

4-Hexylpyridine 302[199]

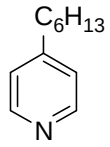

LDA (3.6 mL of 2 M in THF–heptane–ethylbenzene, 7.2 mmol) was added dropwise over 10 min to a stirred solution of 4-picoline **301** (0.5 mL, 5.34 mmol) in anhydrous THF (5 mL) under argon at -78 ℃. After stirring for a further 30 min at -78 ℃, a solution of 1-bromopentane (0.44 mL, 3.6 mmol) in anhydrous THF (5 mL) was added dropwise over 5 min and the mixture allowed to warm to rt and stirred for 20 h. Saturated aqueous NH_4Cl solution (10 mL) and H_2O (10 mL) were added and the mixture was extracted with EtOAc (× 2). The combined organic extracts were with H_2O, dried over $MgSO_4$ and concentrated *in vacuo* to give a yellow oil. The crude residue was chromatographed [SiO_2, EtOAc–hexane (1:9) to give **302** as a yellow oil (579 mg, 100%). R_f [EtOAc–hexane (3:7)] 0.23. δ_H (400 MHz, $CDCl_3$): 0.87 (3H, t, *J* 6.8 Hz, CH_3), 1.23–1.34 (6H, m, 3 × CH_3), 1.57–1.64 (2H, m, CH_2), 2.58 (2H, t, *J* 7.6 Hz, CH_2), 7.10 (2H, d, *J* 5.9 Hz, H-3 and H-5), 8.47 (2H, d, *J* 5.8 Hz, H-2 and H-6). δ_C (100 MHz, $CDCl_3$): 14.17 (CH_3), 22.65 (CH_2), 28.95 (CH_2), 30.37 (CH_2), 31.70 (CH_2), 35.37 (CH_2), 124.08 (CH), 149.52 (CH), 152.12 (C). LRMS (EI^+) 163 ($M^{+\bullet}$, 30%), 93 [$M^{+\bullet}$ - $CH_3(CH_2)_2CH{=}CH_2$, 100]. HRMS: 163.1358, $C_{11}H_{17}N$ requires 163.1361. ν_{max} (ATR) 2955 (CH), 2928 (CH), 2857 (CH), 1603 (aromatic), 1415 (aromatic) cm^{-1}.

^1H NMR data consistent with literature.

4-Hexyl-*N*-(2',4'-dinitrophenyl)pyridinium chloride 303

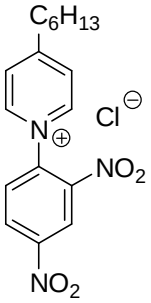

4-Hexylpyridine **302** (2.27 g, 13.9 mmol) and 1-chloro-2,4-dinitrobenzene **238** (5.62 g, 27.8 mmol) were heated together at 95 ℃ for 48 h. The reaction was

cooled, dissolved in H_2O and washed with EtOAc until no further colour was removed from the aqueous layer. The aqueous portion was concentrated *in vacuo* to give **303** as a dark brown oil (4.29 g, 84%). δ_H (400 MHz, MeOD): 1.02 (3H, t, *J* 7.0 Hz, CH_3),1.44–1.60 (6H, m, 3 × CH_2), 1.94–2.01 (2H, m, CH_2), 3.24 (2H, t, *J* 7.6 Hz, CH_2), 8.36 (2H, d, *J* 6.4 Hz, H-3 and H-5), 8.44 (1H, d, *J* 8.7 Hz, H-6'), 8.98 (1H, dd, *J* 8.6 and 2.3 Hz, H-5'), 9.29 (1H, d, *J* 2.4 Hz, H-3'), 9.31 (2H, d, *J* 6.5 Hz, H-2 and H-6). δ_C (100 MHz, MeOD): 14.46 (CH_3), 23.53 (CH_2), 29.92 (CH_2), 30.79 (CH_2), 32.59 (CH_2), 37.24 (CH_2), 124.08 (CH), 129.12 (CH), 131.20 (CH), 132.92 (CH), 139.96 (C), 144.56 (C), 146.11 (CH), 150.82 (C), 169.12 (C). LRMS (FAB^+) 330 [M^+(pyridinium cation), 100%]. HRMS: 330.1452, $C_{17}H_{20}O_4N_3$ requires 330.1454. ν_{max} (ATR) 2928 (CH), 2859 (CH), 1610 (aromatic), 1537 (NO_2), 1462 (aromatic), 1342 (NO_2) cm^{-1}.

2-Hexyloxybenzaldehyde 306[200]

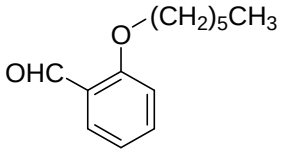

1-Bromohexane (4.7 mL, 0.034 mol) was added to a solution of salicylaldehyde **305** (3.0 mL, 0.028 mol) and K_2CO_3 (4.647 g, 0.034 mol) in DMF (40 mL). The reaction was heated, with stirring, at 130 ℃ for 2 0 h. The reaction was cooled, filtered and diluted with H_2O. The mixture was extracted with EtOAc (× 3) and the combined organic extracts were washed with 1 M KOH. The organic extracts were dried over $MgSO_4$ and concentrated *in vacuo* to give aldehyde **306** as a yellow oil (5.768 g, 99%). δ_H (400 MHz, $CDCl_3$): 0.86–0.89 (3H, m, CH_3), 1.27–1.33 (4H, m, 2 × CH_2), 1.41–1.47 (2H, m, CH_2), 1.76–1.83 (2H, m, CH_2), 4.01 (2H, t, *J* 6.4 Hz, CH_2), 6.93 (1H, d, *J* 8.4 Hz, H-3), 6.94 (1H, t, *J* 7.5 Hz, H-5), 7.47 (1H, ddd, *J* 8.5, 7.4 and 1.8 Hz, H-4), 7.78 (1H, dd, *J* 7.7 and 1.8 Hz, H-6), 10.48 (1H, s, CHO). δ_C (100 MHz, $CDCl_3$): 14.00 (CH_3), 22.57 (CH_2), 25.72 (CH_2), 29.02 (CH_2), 31.50 (CH_2), 68.46 (CH_2), 112.47 (CH), 120.38 (CH), 124.81 (C), 128.05 (CH), 135.92 (CH), 161.56 (C), 189.78 (CH). LRMS (EI+) 206 ($M^{+\bullet}$, 15%), 122 (30), 85 (65), 83 (100). HRMS: 206.1309, $C_{13}H_{18}O_2$ requires 206.1307. ν_{max} (ATR) 2955 (CH), 2859 (CH), 1688 (C=O), 1599 (aromatic), 1456 (aromatic), 1240 (C–O stretch) cm^{-1}.
Literature reports microanalysis only.

2-Dodecyloxybenzaldehyde 307

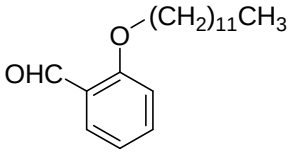

1-Iodododecane (8.38 mL, 0.034 mol) was added to a solution of salicylaldehyde **305** (3.0 mL, 0.028 mol) and K_2CO_3 (4.647 g, 0.034 mol) in DMF (40 mL). The reaction was heated, with stirring, at 130 ℃ for 2 0 h. The reaction was cooled, filtered and diluted with H_2O. The mixture was extracted with EtOAc (× 3) and the combined organic extracts were washed with 1 M KOH. The organic extracts were dried over $MgSO_4$ and concentrated *in vacuo* to give aldehyde **307** as a yellow solid, which melts upon handling (8.0295 g, 99%). δ_H (400 MHz, $CDCl_3$): 0.87 (3H, t, *J* 6.2 Hz, CH_3), 1.22–1.35 (16H, m, 8 × CH_2), 1.43–1.47 (2H, m, CH_2), 1.79–1.86 (2H, m, CH_2), 4.05 (2H, t, *J* 6.4 Hz, CH_2), 6.94–6.99 (2H, m, H-4 and H-5), 7.48–7.52 (1H, m, H-3), 7.81 (1H, d, *J* 7.6 Hz, H-6), 10.50 (1H, s, CHO). δ_C (100 MHz, $CDCl_3$): 14.19 (CH_3), 22.77 (CH_2), 26.13 (CH_2), 29.16 (CH_2), 29.43 (CH_2), 29.54 (CH_2), 29.64 (CH_2), 29.67 (CH_2), 29.71 (CH_2), 29.73 (CH_2), 31.99 (CH_2), 68.57 (CH_2), 112.54 (CH), 120.48 (CH), 124.94 (C), 128.20 (CH), 135.96 (CH), 161.64 (C), 189.90 (CH). LRMS (EI^+) 290 ($M^{+\bullet}$, 60%), 122 (100). HRMS: 290.2244, $C_{19}H_{30}O_2$ requires 290.2246. ν_{max} (ATR) 2922 (CH), 2853 (CH), 1688 (C=O), 1599 (aromatic), 1458 (aromatic), 1240 (C–O stretch) cm^{-1}.

2-Hexyloxy-5-nitrobenzaldehyde 308

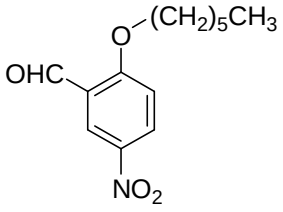

A mixture of fuming nitric acid (100%, *d* = 1.52, 7 mL) and concentrated sulfuric acid (18.1 M, 7 mL) was cooled, with stirring, to -10 ℃. 2-Hexyloxybenzaldehyde **306** (5.55 g, 269 mmol) was added dropwise to the mixture. The reaction was allowed to warm to rt. After 1 h the reaction was poured onto ice. The precipitate formed was filtered, washed with H_2O and dissolved in Et_2O. The ether solution

was washed with H_2O, saturated aqueous $NaHCO_3$ (× 3) and again with H_2O. The organic extracts were dried over $MgSO_4$ and concentrated *in vacuo* to give a yellow solid. This solid was recrystallised three times from Et_2O–hexane to give aldehyde **308** as off-white needles (1.49 g, 22%). Mp 61–62 ℃ (lit. 66–70 ℃) [201]. δ_H (400 MHz, $CDCl_3$): 0.91 (3H, t, *J* 6.8 Hz, CH_3), 1.35–1.38 (4H, m, 2 × CH_2), 1.47–1.52 (2H, m, CH_2), 1.87–1.94 (2H, m, CH_2), 4.21 (2H, t, *J* 6.4 Hz, CH_2), 7.10 (1H, d, *J* 9.2 Hz, H-3), 8.41 (1H, dd, *J* 9.2 and 2.8 Hz, H-4), 8.69 (1H, d, *J* 2.8 Hz, H-6), 10.47 (1H, s, CHO). δ_C (100 MHz, $CDCl_3$): 14.11 (CH_3), 22.65 (CH_2), 25.71 (CH_2), 28.90 (CH_2), 31.52 (CH_2), 70.00 (CH_2), 113.00 (CH), 124.64 (CH), 124.66 (C), 130.78 (CH), 141.49 (C), 165.39 (C), 187.77 (CH). LRMS (EI^+) 251 ($M^{+\bullet}$, 85%), 84 (65), 43 (100). HRMS: 251.1157, $C_{13}H_{17}NO_4$ requires 251.1158. ν_{max} (ATR) 2951 (CH), 2911 (CH), 2843 (CH), 1688 (C=O), 1609 (aromatic), 1512 (NO_2), 1427 (aromatic), 1339 (NO_2), 1273 (C–O stretch) cm^{-1}.

2-Dodecyloxy-5-nitrobenzaldehyde 309

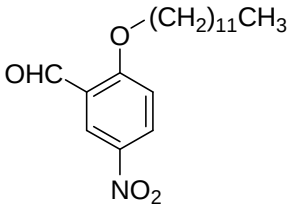

A solution of 2-dodecyloxybenzaldehyde **307** (3.79 g,13 mmol) in concentrated sulphuric acid (3 mL) was cooled, with stirring, to -10 ℃. A mixture of 70% nitric acid (1.3 mL) and concentrated sulfuric acid (18.1 M, 1.3 mL) was also cooled, with stirring, to -10 ℃. The acid mixture was adde d dropwise to the aldehyde solution and the mixture stirred at rt for 15 min. The reaction mixture was poured onto ice. The aqueous layers were extracted with EtOAc (× 3). The combined organic extracts were washed with H_2O (× 3), dried over $MgSO_4$ and concentrated *in vacuo* to give an orange oil. Chromatography [SiO_2, EtOAc–hexane (1:19)] gave **309** as a yellow oil (1.141 g, 34%). R_f [EtOAc–hexane (1:4)] 0.40. δ_H (400 MHz, $CDCl_3$): 0.83 (3H, t, *J* 6.5 Hz, CH_3), 1.22–1.35 (16H, m, 8 × CH_2), 1.44–1.51 (2H, m, CH_2), 1.85–1.92 (2H, m, CH_2), 4.20 (2H, t, *J* 6.5 Hz, CH_2), 7.10 (1H, d, *J* 9.2 Hz, H-3), 8.36 (1H, dd, *J* 9.2 and 2.8 Hz, H-4), 8.60 (1H, d, *J* 2.8 Hz, H-6), 10.42 (1H, s, CHO). δ_C (100 MHz, $CDCl_3$): 14.14 (CH_3), 22.72 (CH_2), 25.94 (CH_2), 28.86 (CH_2), 29.30 (CH_2), 29.38 (CH_2), 29.54 (CH_2), 29.59 (CH_2), 29.66 (CH_2), 31.62

(CH_2), 31.94 (CH_2), 69.99 (CH_2), 113.04 (CH), 124.31 (CH), 124.54 (C), 130.64 (CH), 141.32 (C), 165.35 (C), 187.58 (CH). LRMS (EI^+) 335 ($M^{+\bullet}$, 22%), 318 (45), 97 (49), 85 (70), 71 (88), 57 ($C_4H_9^+$, 100). HRMS: 335.2096, $C_{19}H_{29}NO_4$ requires 335.2097. ν_{max} (ATR) 2924 (CH), 2853 (CH), 1692 (C=O), 1609 (aromatic), 1589 (aromatic), 1522 (NO_2), 1466 (aromatic), 1341 (NO_2), 1271 (C–O stretch) cm^{-1}.

N-tert-Butyl-α-(2-hexyloxy-5-nitrophenyl)nitrone 310

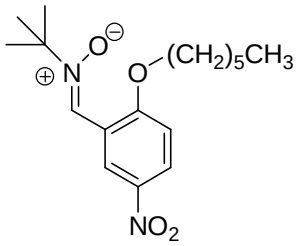

2-Hexyloxy-5-nitrobenzaldehyde **308** (490 mg, 1.95 mmol), *N*-(*tert*-butyl)hydroxylammonium acetate (437 mg, 2.93 mmol) and sodium hydrogen carbonate (246 mg, 2.93 mmol) were dissolved in ethanol (20 mL). The reaction was heated, with stirring, at 70 ℃ for 72 h. The r eaction mixture was poured into H_2O (100 mL) and left to stand for 1 h. The resulting precipitate was filtered and dissolved in EtOAc. The solution was washed with H_2O (× 2) and brine, dried over $MgSO_4$ and concentrated *in vacuo* to give a yellow solid. The solid was recrystallised from Et_2O–hexane to give nitrone **310** as yellow cubes (610 mg, 97%). Mp 102–103 ℃. δ_H (400 MHz, $CDCl_3$): 0.92 (3H, t, *J* 6.7 Hz, CH_3), 1.34–1.39 (4H, m, 2 × CH_2), 1.46–1.54 (2H, m, CH_2), 1.63 (9H, s, 3 × CH_3), 1.85–1.92 (2H, m, CH_2), 4.14 (2H, t, *J* 6.4 Hz, CH_2), 6.95 (1H, d, *J* 9.2 Hz, H-3), 8.16 (1H, s, CH=N), 8.27 (1H, dd, *J* 9.1 and 2.6 Hz, H-4), 10.24 (1H, d, *J* 2.6 Hz, H-6). δ_C (100 MHz, $CDCl_3$): 14.12 (CH_3), 22.73 (CH_2), 25.85 (CH_2), 28.36 (CH_3), 28.98 (CH_2), 31.55 (CH_2), 69.48 (CH_2), 72.04 (C), 110.32 (CH), 120.54 (C), 123.33 (CH), 124.05 (CH), 126.87 (CH), 141.25 (C), 160.95 (C). LRMS (EI^+) 322 ($M^{+\bullet}$, 20%), 266 ($M^{+\bullet}$ - C_4H_8, 70), 57 ($C_4H_9^+$, 100). HRMS: 322.1896, $C_{17}H_{26}N_2O_4$ requires 322.1893. ν_{max} (ATR) 2951 (CH), 2982 (CH), 1609 (aromatic), 1580 (aromatic), 1516 (NO_2), 1466 (aromatic), 1343 (NO_2), 1273 (nitrone), 1248 (C–O stretch) cm^{-1}.

N-tert-Butyl-α-(2-dodecyloxy-5-nitrophenyl)nitrone 311

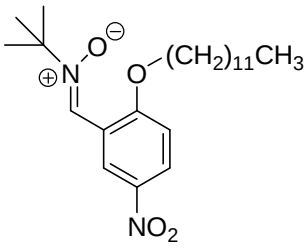

2-Dodecyloxy-5-nitrobenzaldehyde **309** (1.41 g, 4.40 mmol), *N*-(*tert*-butyl)hydroxylammonium acetate (984 mg, 6.60 mmol) and sodium hydrogen carbonate (554 mg, 6.60 mmol) were dissolved in ethanol (40 mL). The reaction was heated, with stirring, at 70 ℃ for 48 h. The r eaction mixture cooled, diluted with H_2O and extracted with EtOAc (× 3). The combined organic extracts were washed with H_2O (× 2) and brine, dried over $MgSO_4$ and concentrated *in vacuo* to give nitrone **311** as a yellow solid (1.60 g, 90%). Mp 39–40 ℃. δ_H (400 MHz, $CDCl_3$): 0.88 (3H, t, *J* 6.4 Hz, CH_3), 1.27–1.40 (16H, m, 8 × CH_2), 1.47–1.52 (2H, m, CH_2), 1.63 (9H, s, 3 × CH_3), 1.85–1.92 (2H, m, CH_2), 4.13 (2H, t, *J* 6.4 Hz, CH_2), 6.93 (1H, d, *J* 9.2 Hz, H-3), 8.09 (1H, s, CH=N), 8.24 (1H, dd, *J* 9.1 and 2.7 Hz, H-4), 10.28 (1H, d, *J* 2.7 Hz, H-6). δ_C (100 MHz, $CDCl_3$): 14.25 (CH_3), 22.81 (CH_2), 26.18 (CH_2), 28.39 (CH_3), 29.03 (CH_2), 29.40 (CH_2), 29.46 (CH_2), 29.68 (CH_2), 29.73 (CH_2), 29.75 (CH_2), 29.77 (CH_2), 32.03 (CH_2), 69.45 (CH_2), 72.01 (C), 110.27 (CH), 120.72 (C), 122.70 (CH), 123.92 (CH), 126.69 (CH), 141.28 (C), 160.87 (C). LRMS (EI^+) 406 ($M^{+\bullet}$, 12%), 350 (70), 318 (65), 182 (73), 57 ($C_4H_9^+$, 100). HRMS: 406.2829, $C_{23}H_{38}N_2O_4$ requires 406.2832. ν_{max} (ATR) 2955 (CH), 2920 (CH), 2851 (CH), 1607 (aromatic), 1518 (NO_2), 1464 (aromatic), 1339 (NO_2), 1271 (nitrone), 1244 (C–O stretch) cm^{-1}.

α-(5-Amino-2-hexyloxyphenyl)-*N-tert*-butylnitrone 312

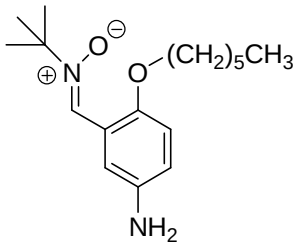

N-tert-Butyl-α-(2-hexyloxy-5-nitrophenyl)nitrone **310** (613 mg, 1.90 mmol) and palladium hydroxide (20% on carbon, 66 mg, 5 mol%) were dissolved in EtOAc (9.5 mL). The solution was flushed with hydrogen then placed under a hydrogen atmosphere and stirred at rt for 30 min. The catalyst was removed by filtration through Celite and the solution was concentrated *in vacuo* to give a 5:1 mixture of α-(5-amino-2-hexyloxyphenyl)-*N-tert*-butylnitrone **312** and nitrone **310** as a yellow oil (556 mg, approx. 82% yield of nitrone **312**). Data derived for nitrone **312**: δ_H (400 MHz, $CDCl_3$): 0.87 (3H, t, *J* 7.1 Hz, CH_3), 1.29–1.34 (4H, m, 2 × CH_2), 1.40–1.47 (2H, m, CH_2), 1.56 (9H, s, 3 × CH_3), 1.70–1.77 (2H, m, CH_2), 3.45 (2 h, br s, NH_2), 3.88 (2H, t, *J* 6.4 Hz, CH_2), 6.64–6.69 (2H, m, H-5 and H-6), 8.01 (1H, s, CH=N), 8.78 (1H, d, *J* 2.6 Hz, H-2). Material was carried on to next stage with no further purification or analysis.

α-(5-Amino-2-dodecyloxyphenyl)-*N-tert*-butylnitrone 313

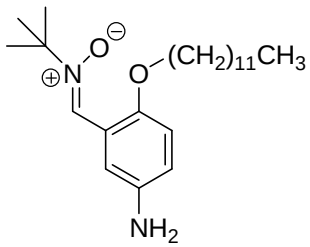

N-tert-Butyl-α-(2-dodecyloxy-5-nitrophenyl)nitrone **311** (563 mg, 1.38 mmol) and palladium hydroxide (20% on carbon, 48 mg, 5 mol %) were dissolved in EtOAc (7.5 mL). The solution was flushed with hydrogen then placed under a hydrogen atmosphere and stirred at room temperature for 50 min. The catalyst was removed by filtration and the solution was concentrated *in vacuo* to give **313** as a brown solid (517 mg, 99%). δ_H (400 MHz, $CDCl_3$): 0.87 (3H, t, *J* 6.3 Hz, CH_3), 1.21–1.34 (16H, m, 8 × CH_2), 1.42–1.47 (2H, m, CH_2), 1.59 (9H, s, 3 × CH_3), 1.73–1.78 (2H, m, CH_2), 3.40 (2H, br s, NH_2), 3.91 (2H, t, *J* 6.4 Hz, CH_2), 6.69–6.73 (2H, m, H-5 and H-6), 8.05 (1H, s, CH=N), 8.82 (1H, d, *J* 2.3 Hz, H-2).

The material was carried onto next stage with no further purification or analysis.

N-tert-Butyl-α-[2-hexyloxy-5-(pyrid-1'-yl)phenyl]nitrone chloride 314

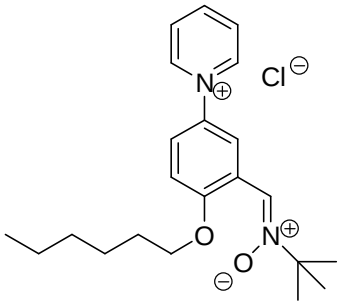

α-(5-Amino-2-hexyloxyphenyl)-*N*-*tert*-butylnitrone **312** [556 mg of a mixture (5:1 mole ratio) of nitrones **312** and **310**, 1.56 mmol] was added to a stirred solution of *N*-(2',4'-dinitrophenyl)pyridinium chloride **247** (180 mg, 0.64 mmol) in anhydrous methanol (14 mL) under argon at rt. After 2 h the resulting red mixture was heated to reflux for 18 h until the red colour disappeared. The mixture was cooled, diluted with H_2O and washed with DCM until no further colour was removed from the aqueous layer. The aqueous portion was concentrated *in vacuo* to give **314** as an orange oil (189 mg, 76%). δ_H (400 MHz, MeOD): 0.93 (3H, t, *J* 6.8 Hz, CH_3), 1.36–1.44 (4H, m, 2 × CH_2),1.52–1.60 (11H, m, 3 × CH_3 and CH_2),1.87–1.94 (2H, m, CH_2), 4.24 (2H, t, *J* 6.2 Hz, CH_2), 7.40 (1H, d, *J* 9.0 Hz, H-3), 7.90 (1H, dd, *J* 9.0 and 3.0 Hz, H-4), 8.32 (1H, s, CH=N), 8.34 (2H, dd, *J* 7.9 and 6.8 Hz, H-3' and H-5'), 8.76 (1H, tt, *J* 7.9 and 1.3 Hz, H-4'), 9.23 (2H, dd, *J* 6.9 and 1.3 Hz, H-2' and H-6'), 9.62 (1H, d, *J* 3.0 Hz, H-6). δ_C (100 MHz, MeOD): 14.42 (CH_3), 23.70 (CH_2), 26.95 (CH_2), 28.37 (CH_3), 29.98 (CH_2), 32.64 (CH_2), 70.72 (CH_2), 73.17 (C), 114.00 (CH), 122.18 (C), 124.66 (CH), 125.99 (CH), 128.73 (CH), 129.63 (CH), 136.72 (C), 145.87 (CH), 147.55 (CH), 160.18 (C). LRMS (FAB^+) 355 [M^+ (pyridinium cation), 100%]. HRMS: 355.2389, $C_{22}H_{31}O_2N_2$ requires 355.2386. ν_{max} (ATR) 2924 (CH), 2855 (CH), 1626 (aromatic), 1479 (aromatic), 1462 (aromatic), 1271 (nitrone), 1230 (C–O stretch) cm^{-1}.

_N_-tert-Butyl-α-[2-dodecyloxy-5-(pyrid-10-yl)phenyl]nitrone chloride 315

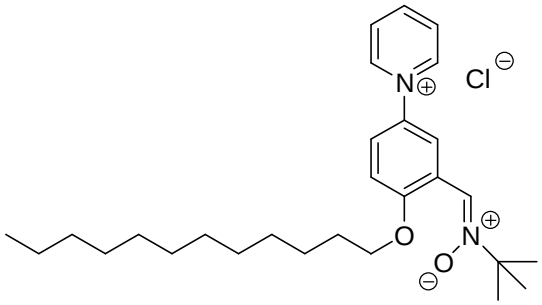

α-(5-Amino-2-dodecyloxyphenyl)-*N*-*tert*-butylnitrone **313** (517 mg, 1.38 mmol) was added to a stirred solution of *N*-(2',4'-dinitrophenyl)pyridinium chloride **247** (156 mg, 0.55 mmol) in anhydrous methanol (12 mL) under argon at rt. After 2 h the resulting red mixture was heated to reflux for 18 h until the red colour disappeared. The mixture was cooled, diluted with H_2O and washed with DCM until no further colour was removed from the aqueous layer. The aqueous portion was concentrated *in vacuo* to give nitrone **315** as an orange oil (129 mg, 49%). δ_H (400 MHz, MeOD): 0.94 (3H, t, *J* 6.7 Hz, CH_3), 1.34–1.67 (27H, m, 3 × CH_3 + 9 × CH_2), 1.93–2.00 (2H, m, CH_2), 4.30 (2H, t, *J* 6.2 Hz, CH_2), 7.46 (1H, d, *J* 9.0 Hz, H-3), 7.95 (1H, dd, *J* 9.0 and 3.0 Hz, H-4), 8.33 (2H, dd, *J* 7.8 and 6.8 Hz, H-3' and H-5'), 8.34 (1H, s, CH=N), 8.82 (1H, tt, *J* 7.8 and 1.3 Hz, H-4'), 9.30 (2H, dd, *J* 6.9 and 1.3 Hz, H-2' and H-6'), 9.69 (1H, d, *J* 3.0 Hz, H-6). δ_C (100 MHz, MeOD): 14.48 (CH_3), 23.74 (CH_2), 27.31 (CH_2), 28.39 (CH_3), 30.06 (CH_2), 30.45 (CH_2), 30.47 (CH_2), 30.71 (CH_2), 30.76 (CH_2), 30.79 (CH_2), 33.79 (CH_2), 70.73 (CH_2), 73.22 (C), 113.97 (CH), 122.21 (C), 124.76 (CH), 126.17 (CH), 128.70 (CH), 129.61 (CH), 136.76 (C), 145.91 (CH), 147.56 (CH), 160.28 (C). (One ^{13}C signal missing due to equivalence.) LRMS (FAB^+) 439 [M^+ (pyridinium cation), 100%]. HRMS: 439.3322, $C_{28}H_{43}O_2N_2$ requires 439.3325. ν_{max} (ATR) 2920 (CH), 2850 (CH), 1626 (aromatic), 1481 (aromatic), 1468 (aromatic), 1271 (nitrone), 1238 (C–O stretch) cm^{-1}.

Carbonyl cyanide 4-(trifluoromethoxy)phenylhydrazone (FCCP) 327[202]

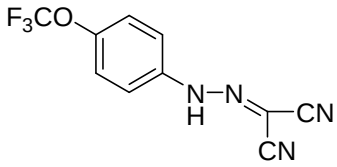

A solution of $NaNO_2$ (350 mg, 5.0 mmol) in H_2O (5 mL) was cooled to 0 ºC. This solution was added dropwise to a solution of 4-trifluoromethoxyaniline **366** (886 mg, 5.0 mmol) and concentrated hydrochloric acid (37%, 4.5 mL) in H_2O (30 mL) at 0 ºC. The mixture was stirred at 0 ºC for 5 min and then added dropwise into a third solution containing malononitrile (0.48 mL, 7.5 mmol) and NaOAc (12.5g, 0.152 mol) in H_2O (50 mL). A yellow precipitate formed and was filtered and washed with ice cold H_2O. The precipitate was dissolved in Et_2O, dried over $MgSO_4$ and concentrated *in vacuo*. The crude residue was recrystallised from EtOAC-hexane to give FCCP **327** as a yellow amorphous solid (951 mg, 75%). Mp (decomp.) 145-148 ºC. δ_H (400 MHz, MeOD): 7.32-7.34 (2H, m, H-3 and H-5), 7.53 (2H, d, 9.2 Hz, H-2 and H-6). δ_C (100 MHz, MeOD): 87.57 (C), 109.85 (C), 114.47 (C), 118.75 (CH), 121.91 (q, *J* 254.1 Hz, CF_3), 123.48 (CH), 141.66 (C), 147.89 (C). ν_{max} (ATR) 3066 (CH), 2226 (CN), 1618 (Ar), 1172 (CF_3), 1153 (CF_3) cm^{-1}.

^1H and ^{13}C NMR data consistent with literature.

2,4-Dinitrophenyl-4',4',5',5'-tetramethyl-1',3',2'-dioxaborolane 360

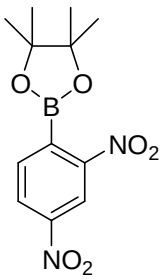

2, 4-Dinitrophenylboronic acid **363** (40 mg, 0.19 mmol), pinacol (22 mg, 0.19 mmol) and oven-dried $MgSO_4$ (22 mg, 0.19 mmol) were dissolved in anhydrous Et_2O (0.5 mL). A few drops of anhydrous THF were added to fully dissolve the acid **363**. The solution was stirred for 20 h at rt, filtered and the residue washed with Et_2O. The combined filtrates were washed with H_2O (× 2), dried over $MgSO_4$

and concentrated *in vacuo* to give arylboronic ester **360** as a yellow powder (50 mg, 89%). Mp 143-145 ºC. δ_H (400 MHz, $CDCl_3$): 1.43 (12H, s, 3 × CH_3), 7.77 (1H, d, *J* 8.0 Hz, H-6'), 8.49 (1H, dd, *J* 8.0 and 2.1 Hz, H-5'), 8.97 (1H, d, *J* 2.0 Hz, H-3'). δ_C (100 MHz, $CDCl_3$): 24.82 (CH_3), 85.57 (C), 118.40 (CH), 127.76 (CH), 134.47 (CH), 149.02 (C), 151.50 (C). LRMS (CI^+) 295 [$(M+H)^+$, ^{11}B, 100%], 294 [$(M+H)^+$, ^{10}B, 25]. HRMS: 294.1131 and 295.1105. $C_{12}H_{16}O_6N_2{}^{10}B$ requires 294.1138 and $C_{12}H_{16}O_6N_2{}^{11}B$ requires 295.1104. ν_{max} (ATR) 2985 (CH), 1593 (Ar), 1528 (NO_2), 1483 (Ar), 1344 (NO_2) cm^{-1}.

2, 4-Dinitrophenylboronic acid 363[203]

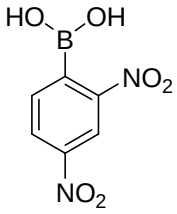

Phenylmagnesium chloride (2 M in THF, 2.2 mL, 4.4 mmol) was added dropwise to a stirred solution of iodo-2,4-dinitrobenzene **361** (1.176 g, 4.0 mmol) in anhydrous THF (4 mL) under argon at –78 ℃. After 15 min, trimethyl borate (0.54 mL, 4.8 mmol) was added dropwise and the solution stirred at –78 ℃ for 30 min. The bath temperature was raised to –20 ℃ and 2 M HCl (aq) (4 mL) was added. The reaction mixture was extracted with Et_2O (× 2). The combined organic extracts were washed with H_2O (× 2), dried over $MgSO_4$ and concentrated *in vacuo* to give a brown solid. The crude solid was washed with hot $CHCl_3$ and filtered to give arylboronic acid **363** as a brown powder (296 mg, 35%). Mp 121-123 ºC. δ_H (400 MHz, $CDCl_3$): 7.74 (1H, d, *J* 8.0 Hz, H-6), 8.54 (1H, dd, *J* 8.0 and 1.9 Hz, H-5), 9.02 (1H, d, *J* 2.0 Hz, H-3). δ_C (100 MHz, $CDCl_3$): 118.49 (CH), 128.41 (CH), 133.32 (CH), 148.72 (C), 150.83 (CH). LRMS (EI^+) 212 [$M^{+\bullet}$ (^{11}B), 100%], 211 [$M^{+\bullet}$ (^{10}B), 26]. HRMS: 211.0279 and 212.0249, $C_6H_5O_6N_2{}^{10}B$ requires 211.0277 and $C_6H_5O_6N_2{}^{11}B$ requires 212.0240. ν_{max} (ATR) 3348 (OH), 1591 (Ar), 1516 (NO_2), 1417 (Ar), 1339 (NO_2) cm^{-1}.

^1H and ^{13}C data consistent with literature.

4'-Methylphenyl-4,4,5,5-tetramethyl-1,3,2-dioxaborolane 368[204]

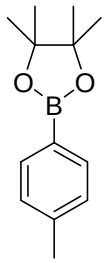

A solution of 4-bromotoluene **367** (2.0 mL, 16 mmol) in anhydrous THF (65 mL) was degassed under argon for 15 min. The solution was cooled to –78 ºC and stirred for 15 min. *n*-Butyllithium (1.9 M in hexanes, 17.2 mL, 32.6 mmol) was added dropwise and the mixture was stirred for a further 15 min. 2-Isopropoxy-4,4,5,5-tetramethyl-1,3,2-dioxaborolane **196** (6.7 mL, 32.6 mmol) was added dropwise and the mixture was stirred at –78 ºC for a further 1.5 h before being allowed to warm to rt overnight. The reaction mixture was quenched with H_2O (50 mL) and extracted with EtOAc (× 2). The combined organic extracts were washed with brine, dried over $MgSO_4$ and concentrated. Excess dioxaborolane was removed *in vacuo* to give arylboronate **368** as an oil which solidified upon standing (2.21 g, 62%). M.p. 50-52 ºC. δ_H (400 MHz, $CDCl_3$): 1.35 (12H, s, 4 × CH_3), 2.37 (3H, s, CH_3), 7.19 (2H, d, *J* 7.7 Hz, H-3' and H-5'), 7.71 (2H, d, *J* 7.7 Hz, H-2' and H-6'). δ_C (100 MHz, $CDCl_3$): 21.87 (CH_3), 24.98 (CH_3), 83.75 (C), 128.66 (CH), 134.93 (CH), 141.54 (C). ν_{max} (ATR) 2978 (CH), 1612 (Ar) cm^{-1}.
IR, ^1H and ^{13}C NMR data consistent with literature.

4'-Bromomethylphenyl-4,4,5,5-tetramethyl-1,3,2-dioxaborolane 369[205]

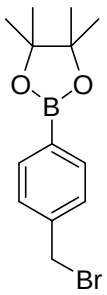

4'-Methylphenyl-4,4,5,5-tetramethyl-1,3,2-dioxaborolane **368** (525 mg, 2.41 mmol), *N*-bromosuccinamide (514 mg, 2.89 mmol) and benzoyl peroxide (12 mg, 48 µmol) were dissolved in CCl_4 (6 mL). The mixture was heated to reflux for 48 h. The

mixture was then cooled, diluted with $CHCl_3$ and washed with $NaHCO_3$ (× 2), H_2O and brine. The organic extracts were dried over $MgSO_4$ and concentrated *in vacuo*. The crude material was recrystallised from Et_2O-hexane to give benzylic bromide **369** as white cubes (243 mg, 34%). Mp 76-78 ºC (lit. 75-77 ℃).[205] δ_H (400 MHz, $CDCl_3$): 1.35 (12H, s, 4 × CH_3), 4.49 (2H, s, CH_2), 7.40 (2H, d, *J* 7.8 Hz, H-3' and H-5'), 7.80 (2H, d, *J* 7.8 Hz, H-2' and H-6'). δ_C (100 MHz, $CDCl_3$): 24.98 (CH_3), 33.45 (CH_2), 84.04 (C), 128.43 (CH), 135.35 (CH), 140.79 (C). LRMS (EI^+): 298 [$M^{+\bullet}$, (^{81}Br), 4%], 296 [$M^{+\bullet}$, (^{79}Br), 4], 217 [$M^{+\bullet}$ – $Br^{\bullet}$, 100]. HRMS: 298.0549 and 296.0567. $C_{13}H_{18}{}^{11}B^{81}BrO_2$ requires $M^{+\bullet}$, 298.0563 and $C_{13}H_{18}{}^{11}B^{79}BrO_2$ requires $M^{+\bullet}$, 296.0583. ν_{max} (ATR) 2978 (CH), 1610 (Ar) cm^{-1}.
NMR data consistent with literature.

2-Cyano-2-[4'-(4'',4'',5'',5''-tetramethyl-1'',3'',2''-dioxaborolan-2''-yl)phenyl] propionitrile 379

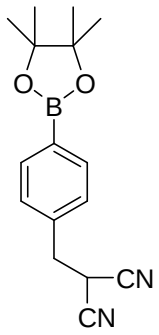

A suspension of NaH (60% in mineral oil, 156 mg, 3.9 mmol) in anhydrous THF (16 mL) and anhydrous DMF (1.6 mL) was stirred at rt under argon. A solution of malononitrile (293 µL, 4.65 mmol) in anhydrous THF (2 mL) was added dropwise to the solution and hydrogen gas was evolved. The reaction was stirred at rt for 30 min then a solution of 4'-bromomethylphenyl-4,4,5,5-tetramethyl-1,3,2-dioxaborolane **369** (1.15 g, 3.9 mmol) in THF (4 mL) was added dropwise. The reaction was stirred at rt overnight. Saturated NH_4Cl (aq) (40 mL) was added to quench the reaction and the mixture was extracted with EtOAc (× 2). The combined organic extracts were washed with H_2O (× 3), dried over $MgSO_4$ and concentrated *in vacuo*. The crude residue was purified chromatographed [SiO_2, EtOAc-hexane (4:1)] R_f = 0.2) followed by recrystallisation from EtOAc/hexane to give bis[4-(4',4',5',5'-tetramethyl-1',3',2'-dioxaborolan-2'-yl)benzyl] malonitrile as a white solid. Mp 229-231 ℃. δ_H (400 MHz, $CDCl_3$): 1.34 (24H, s, 8 × CH_3), 3.29

(4H, s, 2 × CH_2), 7.38 (4H, d, *J* 7.8 Hz, 4 × Ar-H), 7.84 (4H, d, *J* 7.8 Hz, 4 × Ar-H). δ_C (100 MHz, $CDCl_3$): 25.01 (CH_3), 40.87 (C), 43.57 (CH_2), 84.13 (C), 114.90 (CN), 129.76 (CH), 134.90 (C), 135.50 (CH). ν_{max} (ATR) 2980 (CH), 1614 (Ar) cm^{-1}.

The recrystallisation supernatant was concentrated to give **379** as white crystals (188 mg, 17%). Mp 135-137 ºC. δ_H (400 MHz, $CDCl_3$): 1.34 (12H, s, 4 × CH_3), 3.29 (2H, d, *J* 7.0 Hz, CH_2), 3.91 (1H, t, *J* 6.9 Hz, CH), 7.32 (2H, d, *J* 7.7 Hz, H-3 and H-5), 7.84 (2H, d, *J* 7.7 Hz, H-2 and H-6). δ_C (100 MHz, $CDCl_3$): 24.87 (CH_3), 36.62 (CH_2), 84.03 (C), 112.27 (CN), 128.50 (CH), 135.61 (CH), 135.92 (C). LRMS (CI^+) 283 [$(M+H)^+$, ^{11}B, 100%]. HRMS: 283.1613, $C_{16}H_{20}O_2N_2{}^{11}B$ requires 283.1621. ν_{max} (ATR) 2982 (CH), 2361 (CN), 1614 (Ar) cm^{-1}.

2-Cyano-3-[4'-(4'',4'',5'',5''-tetramethyl-1'',3'',2''-dioxaboralan-2''-yl)phenyl]-2-(4'''-trifluoromethoxyphenyldiazeno)propionitrile 380

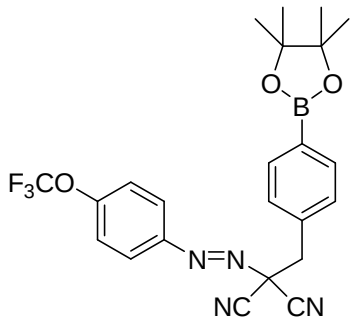

A solution of $NaNO_2$ (16 mg, 0.23 mmol) in H_2O (300 µL) was cooled to 0 ºC. This solution was added dropwise to a solution of 4-trifluoromethoxyaniline **366** (41 mg, 0.231 mmol) and concentrated hydrochloric acid (37%, 0.21 mL) in H_2O (1.5 mL) at 0 ºC. The mixture was stirred at 0 ºC for 5 min and then added dropwise into a third solution containing nitrile **379** (92 mg, 0.33 mmol) and NaOAc (577 mg, 7.03 mmol) in H_2O (1.3 mL), MeOH (1 mL) and EtOH (few drops). A yellow precipitate formed and was filtered and washed with ice cold H_2O. The precipitate was dissolved in EtO_2, dried over $MgSO_4$ and concentrated *in vacuo*. The crude residue was chromatographed [SiO_2, EtOAC-hexane (9:1)] to give **380** as a yellow solid (34 mg, 31%). R_f [SiO_2, EtOAC-hexane (9:1)] 0.42. Mp 120-122 ºC. δ_H (400 MHz, $CDCl_3$): 1.34 (12H, s, 4 × CH_3), 3.69 (2H, s, CH_2), 7.36-7.39 (4H, m, H-2', H-6', H-3''' and H-5'''), 7.82 (2H, d, *J* 8.0 Hz, H-3' and H-5'), 7.90 (2H, d, *J* 9.0 Hz, H-2''' and H-6'''). δ_C (100 MHz, $CDCl_3$): 24.99 (CH_3), 36.62 (CH_2), 69.35 (C), 84.17

(C), 111.85 (CN), 120.38 (q, *J* 259.2 Hz, CF_3)121.48 (CH), 125.81 (CH), 130.15 (CH), 132.86 (C), 135.51 (CH), 147.71 (C), 153.08 (C). LRMS (CI^+) 471 [$(M+H)^+$, ^{11}B, 11%], 446 (39), 337 (40), 283 (95), 219 (91), 189 (100). HRMS 471.1821, $C_{23}H_{23}O_3N_4F_3{}^{11}B$ requires 471.1820. ν_{max} (ATR) 2937 (CH), 2162 (CN), 1614 (Ar) cm^{-1}.

2',3'-Dimethylphenyl-4,4,5,5-tetramethyl-1,3,2-dioxaborolane 387

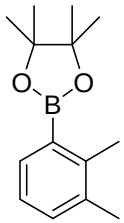

A solution of 3-bromo-*ortho*-xylene **386** (2.0 mL, 15 mmol) in anhydrous THF (60 mL) was degassed under argon for 15 min. The solution was cooled to –78 ºC and stirred for 15 min. *tert*-Butyllithium (1.7 M in pentane, 17.4 mL, 29.5 mmol) was added dropwise and the reaction was stirred for a further 15 min. 2-Isopropoxy-4,4,5,5-tetramethyl-1,3,2-dioxaborolane **196** (9.0 mL, 44 mmol) was added dropwise and the reaction was stirred at –78 ºC for a further 1.5 h before being allowed to warm to rt overnight. The reaction mixture was quenched with H_2O (50 mL) and extracted with EtOAc (× 2). The combined organic extracts were washed with brine, dried over $MgSO_4$ and concentrated *in vacuo*. Excess borate **238** was removed *in vacuo* to give arylboronate **387** as a solid that melted upon handling (2.59 g, 75%). δ_H (400 MHz, $CDCl_3$): 1.33 (12H, s, 4 × CH_3), 2.25 (3H, s, CH_3), 2.47 (3H, s, CH_3), 7.07 (1H, t, *J* 7.4 Hz, H-5'), 7.19 (1H, d, *J* 7.4 Hz, H-4') 7.61 (1H, d, *J* 7.3 Hz, H-6'). δ_C (100 MHz, $CDCl_3$): 18.59 (CH_3), 20.55 (CH_3), 25.00 (CH_3), 83.57 (C), 125.00 (CH), 132.44 (CH), 133.66 (CH), 136.62 (C), 143.17 (C). LRMS (CI^+) 233 [$(M+H)^+$, ^{11}B, 100%], 232 [$(M+H)^+$, ^{10}B, 32]. HRMS: 232.1721 and 233.1713, $C_{14}H_{22}O_2{}^{10}B$ requires 232.1749 and $C_{14}H_{22}O_2{}^{11}B$ requires 233.1716. ν_{max} (ATR) 2976 (CH), 2897 (CH) 1611 (aromatic) cm^{-1}.

2',3'-Dibromomethylphenyl-4,4,5,5-tetramethyl-1,3,2-dioxaborolane 388

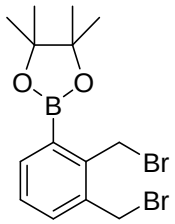

2',3'-Dimethylphenyl-4,4,5,5-tetramethyl-1,3,2-dioxaborolane **387** (717 mg, 3.09 mmol), *N*-bromosuccinamide (1.21 g, 6.80 mmol) and benzoyl peroxide (30 mg, 0.12 mmol) were dissolved in CCl_4 (9 mL). The reaction was heated to reflux for 24 h. The reaction was then cooled, diluted with $CHCl_3$ and washed with $NaHCO_3$ (× 2), H_2O and brine. The organic extracts were dried over $MgSO_4$ and concentrated *in vacuo*. The crude material was chromatographed [SiO_2, EtOAc-hexane (1:19)] to give arylbromide **388** as an oil (783 mg, 65%). R_f [EtOAc-hexane (1:4)] 0.57. δ_H (400 MHz, $CDCl_3$): 1.25 (12H, s, 3 × CH_3), 4.55 (2H, s, CH_2), 5.07 (2H, s, CH_2), 7.15 (1H, t, *J* 7.5 Hz, H-5'), 7.29 (1H, dd, *J* 7.6 and 1.4 Hz, H-4'), 7.71 (1H, dd, *J* 7.5 and 1.4 Hz, H-6'). δ_C (100 MHz, $CDCl_3$) 24.96 (CH_3), 28.94 (CH_2), 30.66 (CH_2), 84.20 (C), 128.48 (CH), 133.87 (CH), 136.92 (C), 137.40 (CH), 143.06 (C). LRMS (CI^+) 389 [$(M+H)^+$, 39%], 311 (77), 309 (72), 231 (100). HRMS: 390.9907, $C_{14}H_{20}O_2{}^{79}Br^{81}Br^{11}B$ requires 390.9906. ν_{max} (ATR) 2978 (CH), 1588 (aromatic) cm^{-1}.

7.3 EPR experiments

Iron(II) sulfate (100 µL of a 1 mM aqueous solution) and hydrogen peroxide (100 µL of a 1 mM aqueous solution) were added to a solution of the nitrone **269**, **314** or **315** in DMSO (100 µL of a 2.5 mM solution in the case of nitrone **269** and a 10 mM solution for nitrones **314** and **315**). The solution [0.83 mM nitrone **269** or 3.33 mM nitrone **314** or **315**, 0.33 mM hydrogen peroxide, 0.33 mM iron(II) sulfate in water–DMSO (2:1)] was then immediately transferred to a quartz flat cell and placed in the EPR spectrometer for analysis. Spectra were acquired on a Bruker e-scan™ bench-top EPR machine with a permanent magnet and a magnetic sweep circuit (centre of field = 0.345 T, sweep width 25 mT) operating at a frequency of 9.8 GHz (X-band). Acquisition parameters: RG 3.99 × 10^3, 2.76mW, MA 0.5 G. g-factors were determined relative to strong pitch. Hyperfine couplings were derived from simulations using WINEPR SimFonia™.

7.4 Kinetic experiments

Titration of hydrogen peroxide[178]: A fresh 0.025 M solution of $KMnO_4$ was made from 1.9755 g of $KMnO_4$ in 500 mL deionised water. A 0.05 M (assumed concentration) H_2O_2 solution was made by dilution of 10 ml 1M (assumed concentration) H_2O_2 stock solution in 190 mL deionised water. 25 mL of 0.05 M H_2O_2 was titrated against $KMnO_4$ until the appearance of the purple MnO_4^- ion indicated complete reaction, and three concurrent titres, 24.3 mL, 24.3 mL and 24.4 mL, were obtained. Calculating the number of mmoles of $KMnO_4$ in each titre gave values of 0.6075, 0.6075 and 0.6010. Since 5 moles of H_2O_2 are required to oxidise 2 moles of $KMnO_4$ the number of moles of H_2O_2 is calculated by multiplying by 5/2, giving 1.51875, 1.51875 and 1.525 mmols. As each titration used 1.25 ml of 1M H_20_2 stock solution, therefore the H_2O_2 stock solution assumed to be 1 M was actually 1.216 M. After determining the accurate concentration, an accurate 1 M solution was prepared.

Kinetic experiments: The stock solutions of SUMs were made up by weight in DMF (FCCP-SUM **380**, 10 mM; DNP-SUM **360**, 1 mM). Reactions were carried out in a 1:1 mixture of DMF and 0.14 M aqueous sodium bicarbonate (pH 8.3). Absorption measurements were made on a JASCO V550 double beam spectrophotometer using matched quartz cuvettes of 1 cm pathlength, with the cuvette compartment maintained at 37 ^{0}C by a circulating water bath. The spectrophotometer was calibrated using a solution of potassium chromate in 0.05 M KOH, whose absorption coefficient at 372 nm is 4830 M^{-1} cm^{-1}.[206] For this standard solution, the measured absorbance was proportional to concentration up to an absorbance of 1.2; all measurements reported in this paper were made with absorbance values less than 1.0. Comparison between the spectra of DNP-SUM **360** and DNP^- **326**, and between FCCP-SUM **380** and $FCCP^-$ **328** showed that the appropriate wavelengths to monitor the reactions were 410 nm and 385 nm respectively, since in each case the starting material showed a very much smaller absorption than the product. The appropriate absorption coefficients for the products (DNP^- **326** at 410 nm and $FCCP^-$ **328** at 385 nm) under the conditions used for the reactions were determined using a parallel dilution approach in which stock solutions of these compounds were diluted into buffer systems where the absorption coefficients had been published,[207,208] and into the buffer system used in the present work. Comparison of the observed absorbance values from these parallel dilutions allowed the appropriate coefficients for our experiments to be

calculated (20 500 $M^{-1}cm^{-1}$ at 410 nm for DNP and 29 700 $M^{-1}cm^{-1}$ at 385 nm for FCCP).

Reactions were initiated by adding small aliquots of H_2O_2 to solutions of DNP-SUM **360** or FCCP-SUM **380** in the DMF/buffer mixture, in a total volume of 1.1 ml or 1 ml, respectively. The blank reaction contained DMF/buffer in place of the H_2O_2. Since the reactions were carried out with the SUMs in considerable excess over H_2O_2, the spontaneous breakdown observed did not affect the observed yields of DNP^- **326** or $FCCP^-$ **328**, although it would have small effects on the calculated second order rate constants. The concentrations of the SUMs and H_2O_2 were chosen to give convenient rates of reaction while maintaining a reasonable approximation to *pseudo*-first order conditions in order to facilitate kinetic analysis. For DNP-SUM **360**, the concentration used was 454 μM and the H_2O_2 concentration was 91 μM. For FCCP-SUM **380**, the concentration used was 50 μM, and the H_2O_2 concentrations were 5 μM and 10 μM. Reactions were performed in triplicate, with the exception of FCCP-SUM **380** with 10 μM H_2O_2 which was performed in duplicate. In each case, the experimental data (absorbance vs. time) were fitted to a first order kinetic process using Microcal Origin software; this gave the end-point (limiting absorbance change) and the first order rate constant. Division of this rate constant by the concentration of the SUM in excess yielded the second-order rate constant for the reaction.

References

1 Sies, H. *Eur. J. Biochem.* **1993**, *215***,** 213-219.

2 Halliwell, B.; Gutteridge, J.M.C. *Free Radicals in Biology & Medicine*, 4th ed., OUP, **2007**.

3 Miwa, S.; Beckman, K.B.; Muller F. *Oxidative Stress in Aging: From Model Systems to Human Diseases*, 1st ed. Humana Press, **2008**.

4 Harman, D. *J. Gerontol.* **1956**, *11*, 298-300.

5 Buettner, G.R. *Arch. Biochem. Biophys.* **1993**, *300*, 535-543.

6 Buetler, T.M.; Krauskopf, A.; Ruegg, U.T. *News Physiol. Sci.* **2004**, *19*, 120-123.

7 Mitchell, P. *FEBS Lett.* **1975**, *56*, 1-6.

8 Fenton, H.J.H. *J. Chem. Soc., Trans.* **1894**, *65*, 899-910.

9 Stohs, S.J.; Baggchi, D. *Free Rad. Biol. Med.* **1995**, *18*, 321-336.

10 http://www.sciencehelpdesk.com/unit/bg3/1 Accessed 6th September 2009.

11 McMurry, J.E. Castellion, M. Fundamentals of General, Organic and Biological Chemistry, 3rd ed., Prentice Hall, **1999**.

12 Berg, J.M.; Tymoczko, J.L.; Stryer, L. *Biochemistry*, 6th ed., W.H.Freeman & Co., **2007**.

13 Murphy, M.P. *Biochem. J.* **2009**, *417*, 1-13.

14 Hirst, J.; Carroll, J.; Fearnley, I.M.; Shannon, R.J.; Walker, J.E. *Biochim. Biophys. Acta* **2003**, *1604*, 135-150.

15 Lodish, H.; Berk, A.; Zipursky, S.L.; Matsudaira, P.; Baltimore, D.; Darnell, J.E. *Molecular Cell Biology*, 4th ed., New York, W. H. Freeman & Co., **1999**.

16 Li, Y.; Huang, T.-T.; Carlson, E.J.; Melov, S.; Ursell, P.C.; Olson, J.L.; Noble, L.J.; Yoshimura, M.P.; Berger, C.; Chan, P.H.; Wallace, D.C.; Epstein, C.J. *Nat. Genet.* **1995**, *11*, 376-381.

17 Suarez, J.; Ranguelova, K.; Jarzecki, A.A.; Manzerova, J.; Krymov, V.; Zhao, X.; Yu, S.; Metlitsky, L.; Gerfen, G.J.; Magliozzo, R.S. *J. Biol. Chem.* **2009**, *284*, 7017-7029.

18 Rebrin, I.; Sohal, R.S. *Adv. Drug Deliv. Rev.* **2008**, *60*, 1545-1552.

19 Burns, J.J. *Nature* **1957** *180*, 553.

20 Krinsky, N.I.; Yeum, K.J. *Biochem. Biophys. Res. Commun.* **2003**, *305*, 754-760.

[21] Hartley, R. C.; Kennedy, M. W. *Trends in Ecology and Evolution* **2004**, *19*, 353-354.

[22] Omenn, G.S.; Goodman, G.E.; Thornquist, M.D.; Balmes, J.; Cullen, M.R.; Glass, A.; Keogh, J.P.; Meyskens, F.L.; Valanis, B.; Williams, J.H.; Barnhart, S.; Hammar, S. *New Engl. J. Med.* **1996**, *334*, 1150-1155.

[23] http://www.ateronon.co.uk/, Accessed on 16th July 2009.

[24] Mullen, W.; Graf, B. A.; Caldwell, S. T.; Hartley, R. C.; Duthie, G. G.; Edwards, C. A.; Lean, M. E. J.; Crozier, A. *J. Agric. Food Chem.*, **2002**, *50*, 6902-6909.

[25] Nath, K.A.; Ngo, E.O.; Hebbel, R.P.; Croatt, A.P.; Zhou, B.; Nutter, L.M. *Am. J. Physiol.* **1995**, *268*, C227-C236.

[26] http://www.un.org/esa/socdev/ageing/popageing.html, Accessed 16th July 2009.

[27] Schriner, S.E.; Linford, N.J.; Martin, G.M.; Treuting, P.; Ogburn, C.E.; Emond, M.; Coskun, P.E.; Ladiges, W.; Wolf, N.; Van Remmen, H.; Wallace, D.C.; Rabinovitch, P.S. *Science* **2005**, *308*, 1909-1911.

[28] Sun, J.; Tower, J. *Mol. Cell. Biol.* **1999**, *19*, 216-228.

[29] Huang, T. T.; Carlson, E. J.; Gillespie, A. M.; Shi, Y.; Epstein, C. J. *J. Gerontol. A: Biol. Sci. Med. Sci.* **2000**, *55*, B5–B9.

[30] Elchuri, S.; Oberley, T. D.; Qi,W.; Eisenstein, R. S.; Jackson Roberts, L.; Van Remmen, H.; Epstein, C. J.; Huang, T. T. *Oncogene* **2005**, *24*, 367-380.

[31] Phillips, J. P.; Campbell, S. D.; Michaud, D.; Charbonneau, M.; Hilliker, A. J. *Proc. Natl. Acad. Sci. USA* **1989**, *86*, 2761-2765.

[32] Soh, N. *Anal. Bioanal. Chem.* **2006**, *386*, 532-543.

[33] Bonini, M.G.; Rota, C.; Tomasi, A.; Mason, R.P. *Free Rad. Biol. Med.* **2006**, *40*, 968-975.

[34] Weil, J.A.; Bolton, J.R. *Electron Paramagnetic Resonance: Elemental Theory and Practical Applications* 2nd ed., John Wiley & Sons Inc.: Hoboken, 2007.

[35] EPR spectrum adapted from http://www.bruker-biospin.com, accessed 24th July 2009.

[36] Hubbell, W.L.; Mchaourab, H.S; Altenbach, C.; Lietzow, M.A. *Structure* **1996**, *4*, 779-783.

[37] Hubbell, W.L.; Cafiso, D.S.; Altenbach, C. *Nat. Struct. Biol.* **2000**, *7*, 735-739.

[38] Blinco, J. P.; Hodgson, J. L.; Morrow, B. J.; Walker, J. R.; Will, G. D.; Coote, M. L.; Bottle, S. E. *J. Org. Chem.* **2008**, *73*, 6763-6771.

[39] Bugnon, L.; Morton, C. J. H.; Novak, P.; Vetter, J.; Nesvadba, P. *Chem. Mater.* **2007**, *19*, 2910-2914.

[40] Soule, B. P.; Hyodo, F.; Matsumoto, K.; Simone, N. L.; Cook, J. A.; Krishna, M. C.; Mitchell, J. B. *Free Radic. Biol. Med.* **2007**, *42*, 1632-1650.

[41] (a) Bordwell, F. G.; Liu, W.-Z. *J. Am. Chem. Soc.* **1996**, *118*, 10819-10823. (b) Luo, Y.-R. *Handbook of Bond Dissociation Energies in Organic Compounds*; *CRC* Press: Boca Raton, **2003**; pp 174-182.

[42] Miller,M.R.; Borthwick, S.J.; Shaw, C.A.; McLean, S.G.; McClure, D.; Mills, N.L.; Duffin, R.; Donaldson, K.; Megson, I.L.; Hadoke, P.W.F.; Newby, D.E. *Environ. Health Persp.* **2009**, *117*, 611-616.

[43] (a) Dikalov, S; Skatchkov, M.; Fink, B.; Bassenge, E. *Nitric Oxide-Biol. Ch.* **1997**, *1*, 423-431. (b) Dikalov, S.; Skatchkov, M.; Bassenge, E. *Biochem. Bioph. Res. Co.* **1997**, *230*, 54-57.

[44] Dikalov, S.; Skatchkov, M.; Bassenge, E. *Biochem. Bioph. Res. Co.* **1997**, *231*, 701-704.

[45] Janzen, E.G.; Blackburn, B.J. *J. Am. Chem. Soc.* **1968**, *90*, 5909-5910.

[46] Rosen, G.M.; Britigan, B.E.; Halpern, H.J.; Pou, S. *Free Radicals: Biology and Detection by Spin Trapping,* 1st ed. OUP, **1999**.

[47] Hay, A.; Burkitt, M.J.; Jones, C.M.; Hartley, R.C. *Arch. Biochem. Biophys.* **2005**, *435*, 336-346.

[48] Williams, H.E.; Claybourn, M.; Green, A.R. *Free Radic. Res.* **2007**, *41*, 1047-1052.

[49] Gamliel, A.; Afri, M.; Frimer, A.A. *Free Rad. Biol. Med.* **2008**, *44*, 1394-1405.

[50] Olive, G.; Mercier, A.; le Moigne, F.; Rockenbauer, A.; Tordo, P. *Free Rad. Biol. Med.* **2000**, *28,* 403-408.

[51] Hardy, M.; Chalier, F.; Ouari, O.; Finet, J.P.; Rockenbauer, A.; Kalyanaraman, B.; Tordo, P. *Chem. Commun.* **2007**, 1083-1085.

[52] Xu, Y.; Kalyanaraman, B. *Free Radic. Res.* **2007**, 41, 1–7.

[53] Roubaud, V.; Dozol, H.; Rizzi, C.; Lauricella, R.; Bouteiller, J.-C.; Tuccio, B. *J. Chem. Soc*., *Perkin Trans. 2*, **2002**, 958–964.

[54] Roubaud, V.; Lauricella, R.; Bouteiller, J.-C.; Tuccio, B. *Arch. Biochem. Biophys.* **2002**, *397*, 51–56.

[55] Janzen, E. G.; Dudley, R. L.; Shetty, R. V. *J. Am. Chem. Soc.* **1979**, *101*, 243-245.

[56] Janzen, E. D.; Kotake, Y.; Hinton, R. D. *Free Radic. Biol. Med.* **1992**, *12*, 169-173.

[57] Misik, V.; Miyoshi, N.; Riesz, P. *J. Phys. Chem.* **1995**, *99*, 3605-3611.

[58] Makino, K.; Mossoba, M.M.; Riesz, P. *J. Phys. Chem.* **1983**, *87*, 1369-1377.

[59] Hill, H. A. O.; Thornalley, P. J. *Can. J. Chem.* **1982**, *60*, 1528-1531.

[60] Sár, C. P.; Hideg, E.; Vass, I.; Hideg, K. *Bioorg. Med. Chem. Lett.* **1998**, *8*, 379-384.

[61] Floyd, R.A.; Kopke, R.D.; Choi, C.-H.; Foster, S.B.; Doblas, S.; Towner, R.A. *Free Radic. Biol. Med.* **2008**, *45*, 1361–1374.

[62] Farrell, B.; Godwin, J.; Richards, S.; Warlow, C. *J. Neurol. Neurosurg. Psychiatry* **1991**, *54*, 1044–1054.

[63] Ouari, O.; Chalier, F.; Bonaly, R.; Pucci, B.; Tordo, P. *J. Chem. Soc*., *Perkin Trans. 2* **1998**, 2299–2307.

[64] Ouari, O.; Polidori, A.; Pucci, B.; Tordo, P.; Chalier, F. *J. Org. Chem.* **1999**, *64*, 3554-3556.

[65] Durand, G.; Polidori, A.; Salles, J.-P.; Pucci, B. *Bioorg. Med. Chem. Lett.* **2003**, *13*, 859–862.

[66] Tanguy, S.; Durand, G.; Reboul, C.; Polidori, A.; Pucci, B.; Dauzat, M.; Obert, P. *Cardiovasc. Drug Ther.* **2006**, *20*, 147-149.

[67] Sklavounou, E.; Hay, A.; Ashraf, N.; Lamb, K.; Brown, E.; MacIntyre, A.; George, W.D.; Hartley, R.C.; Shiels, P.G. *Biochem. Bioph. Res. Co.* **2006**, *347*, 420-427.

[68] Frejaville, C.; Karoui, H.; Tuccio, B.; le Moigne, F.; Culcasi, M.; Pietri, S.; Lauricella, R.; Tordo, P. *Chem. Commun.* **1994**, 1793-1794.

[69] Tsai, P.; Elas, M.; Parasca, A.D.; Barth, E.D.; Mailer, C.; Halpern, H.J.; Rosen, G.M. *J. Chem. Soc*., *Perkin Trans. 2*, **2001**, 875–880.

[70] Gilbert, B.C.; Davies, M.B.; Murphy, D.M. (Eds) *Electron Paramagnetic Resonance*, Vol. 18, RSC Publishing, **2002**.

[71] Murphy, M.P.; Smith, R.A.J. *Annu. Rev. Pharmacol. Toxicol.* **2007**, *47*, 629-656.

[72] Smith, R.A.J.; Porteous, C.M.; Coulter, C.V.; Murphy, M.P. *Eur. J. Biochem.* **1999**, *263*, 709-716.

[73] Kelso, G.F.; Porteous, C.M.; Coulter, C.V.; Hughes, G.; Porteous, W.K.; Ledgerwood, E.C.; Smith, R.A.J.; Murphy, M.P. *J. Biol. Chem.* **2001**, *276*, 4588-4596.

[74] James, A.M.; Cochemé, H.M.; Smith, R.A.J.; Murphy, M.P. *J. Biol. Chem.* **2005**, *280*, 21295-21312.

[75] http://www.antipodeanpharma.com/ Accessed 16th July 2009.

[76] Skulachev, V.P. *Biochemistry – Moscow* **2007**, *72,* 1385-1396.

[77] Antonenko, Y.N.; Avetisyan, A.V.; Bakeeva, L.E.; Chernyak, B.V.; Chertkov, V.A.; Domnina, L.V.; Ivanova, O.Yu.; Izyumov, D.S.; Khailova, L.S.; Klishin, S.S.; Korshunova, G.A.; Lyamzaev, K.G.; Muntyan, M.S.; Nepryakhina, O.K.; Pashkovskaya, A.A.; Pletjushkina, O.Yu.; Pustovidko, A.V.; Roginsky, V.A.; Rokitskaya, T.I.; Ruuge, E.K.; Saprunova, V.B.; Severina, I.I.; Simonyan, R.A.; Skulachev, I.V.; Skulachev, M.V.; Sumbatyan, N.V.; Sviryaeva, I.V.; Tashlitsky, V.N.; Vassiliev, J.M.; Vyssokikh, M.Yu.; Yaguzhinsky, L.S.; Zamyatnin Jr., A.A.; Skulachev, V.P. *Biochemistry – Moscow* **2008**, *73*, 1273-1287.

[78] Bakeeva, L.E.; Barskov, I.V.; Egorov, M.V.; Isaev, N.K.; Kapelko, V.I.; Kazachenko, A.V.; Kirpatovsky, V.I.; Kozlovsky, S.V.; Lakomkin, V.L.; Levina, S.B.; Pisarenko, O.I.; Plotnikov, E.Y.; Saprunova, V.B.; Serebryakova, L.I.; Skulachev, M.V.; Stelmashook, E.V.; Studneva, I.M.; Tskitishvili, O.V.; Vasilyeva, A.K.; Victorov, I.K.; Zorov, D.B.; Skulachev, V.P. *Biochemistry – Moscow* **2008**, *73*, 1288-1299.

[79] Agapova, L.S.; Chernyak, B.V.; Domnina, L.V.; Dugina, V.B.; Efimenko, A.Yu.; Fetisova, E.K.; Ivanova, O.Yu.; Kalinina, N.I.; Khromova, N.V.; Kopnin, B.P.; Kopnin, P.B.; Korotetskaya, M.V.; Lichinitser, M.R.; Lukashev, A.L.; Pletjushkina, O.Yu.; Popova, E.N.; Skulachev, M.V.; Shagieva, G.S.; Stepanova, E.V.; Titova, E.V.; Tkachuk, V.A.; Vasiliev, J.M.; Skulachev, V.P. *Biochemistry – Moscow* **2008**, *73*, 1300-1316.

[80] Neroev, V.V.; Archipova, M.M.; Bakeeva, L.E.; Fursova, A.Zh.; Grigorian, E.N.; Grishanova, A.Yu; Iomdina, E.N.; Ivashchenko, Zh.N.; Katargina, L.A.; Khoroshilova-Maslova, I.P.; Kilina, O.V.; Kolosova, N.G.; Kopenkin, E.P.; Korshunov, S.S.; Kovaleva, N.A.; Novikova, Yu.P.; Philippov, P.P.; Pilipenko, D.I.; Robustova, O.V.; Saprunova, V.B.; Senin, I.I.; Skulachev,

M.V.; Sotnikova, L.F.; Stefanova, N.A.; Tikhomirova, N.K.; Tsapenko, I.V.; Shchipanova, A.I.; Zinovkin, R.A.; Skulachev, V.P. *Biochemistry – Moscow* **2008**, *73*, 1317-1328.

81 Anisimov, V.N.; Bakeeva, L.E.; Egormin, P.A.; Filenko, O.F.; Isakova, E.F.; Manskikh, V.N.; Mikhelson, V.M.; Panteleeva, A.A.; Pasyukova, E.G.; Pilipenko, D.I.; Piskunova, T.S.; Popovich, I.G.; Roshchina, N.V.; Rybina, O.Yu.; Saprunova, V.B.; Samoylova, T.A.; Semenchenko, A.V.; Skulachev, M.V.; Spivak, I.M.; Tsybul'ko, E.A.; Tyndyk, M.L.; Vyssokikh, M.Yu.; Yurova, M.N.; Zabezhinsky, M.A.; Skulachev, V.P. *Biochemistry – Moscow* **2008**, *73*, 1329-1342.

82 Filipovska, A.; Kelso, G.F.; Brown, S.E.; Beer, S.M.; Smith, R.A.J.; Murphy, M.P. *J. Biol. Chem.* **2005**, *280*, 24113-24126.

83 Sies, H. *Free Rad. Biol. Med.* **1993**, *14*, 313-323.

84 Salvemini D.; Wang Z.-Q.; Zweier J.L.; Samouilov A.; Macarthur H.; Misko T.P.; Currie M.G.; Cuzzocrea S.; Sikorski J.A.; Riley D.P. *Science* **1999**, *286*, 304-306.

85 Dessolin, J.; Schuler, M.; Quinart, A.; De Giorgi, F.; Ghosez, L.; Ichas, F.; *Eur. J. Pharmacol.* **2002**, *447*, 155-161.

86 Trnka, J.; Blaikie, F.H.; Smith, R.A.J.; Murphy, M.P. *Free Rad. Biol. Med.* **2008**, *44*, 1406–1419.

87 Trnka, J.; Blaikie, F.H.; Logan, A.; Smith, R.A.J.; Murphy, M.P. *Free Radical Res.* **2009**, *43*, 4-12.

88 Dhanasekaran, A.; Kotamraju, S.; Karunakaran, C.; Kalivendi, S.V.; Thomas, S.; Joseph, J.; Kalyanaraman, B. *Free Rad. Biol. Med.* **2005**, *39*, 567-583.

89 Pehar, M.; Vargas, M.R.; Robinson, K.M.; Cassina, P.; Díaz-Amarilla, P.J.; Hagen, T.M.; Radi, R.; Barbeito, L.; Beckman, J.S. *J. Neurosci.* **2007**, *27*, 7777-7785.

90 Cassina, P.; Cassina, A.; Pehar, M.; Castellanos, R.; Gandelman, M.; de León, A.; Robinson, K.M.; Mason, R.P.; Beckman, J.S.; Barbeito, L.; Radi, R. *J. Neurosci*. **2008**, *28*, 4115-4122.

91 http://www.mcw.edu/MitochondriaSpecificMRIContrastAgent.htm, Accessed 29th August 2009.

92 Murphy, M.P.; Echtay, K.S.; Blaikie, F.H.; Asin-Cayuela, J.; Cochemé, H.M.; Green, K.; Buckingham, J.A.; Taylor, E.R.; Hurrell, F.; Hughes, G.; Miwa,

S.; Cooper, C.E.; Svistunenko, D.A.; Smith, R.A.J.; Brand, M.D. *J. Biol. Chem.* **2003**, *278*, 48534-48545.

93 Hardy, M.; Chalier, F.; Ouari, O.; Finet, J.P.; Rockenbauer, A.; Kalyanaraman, B.; Tordo, P. *Chem. Commun.* **2007**, 1083-1085.

94 Xu, Y.; Kalyanaraman, B. *Free Radic. Res.* **2007**, *41*, 1–7.

95 Quin, C.; Trnka, J.; Hay, A.; Murphy, M.P.; Hartley, R.C. *Tetrahedron* **2009**, *65*, 8154-8160.

96 Hardy, M.; Rockenbauer, A.; Vásquez-Vivar, J.; Felix, C.; Lopez, M.; Srinivasan, S.; Avadhani, N.; Tordo, P.; Kalyanaraman, B. *Chem. Res. Toxicol.* **2007**, *20*, 1053-1060.

97 Robinson, K.M.; Janes, M.S.; Pehar, M.; Monette, J.S.; Ross, M.F.; Hagen, T.M.; Murphy, M.P.; Beckman, J.S. *Proc. Nat. Acad. Sci. USA* **2006**, *103*, 15038-15043.

98 Dickinson, B.C.; Chang, C.J. *J. Am. Chem. Soc.* **2008**, *130*, 9638-9639.

99 Johnson, L.V.; Walsh, M.L.; Chen, L.B. *Proc. Nat. Acad. Sci. USA* **1980**, *72*, 990-994.

100 Scaduto, Jr. R.C.; Grotyohann, L.W. *Biophys. J.* **1999,** *76*, 469-477.

101 http://www.invitrogen.com/site/us/en/home/References/Molecular-Probes-The-Handbook/Probes-for-Organelles/Probes-for-Mitochondria.html#head2. Accessed 14th September 2009.

102 Smiley, S.T.; Reers, M.; Mottola-Hartshorn, C.; Lin, M.; Chen, A.; Smith, T.W.; Steele, Jr. G.D.; Chen, L.B. *Proc. Nat. Acad. Sci. USA* **1991**, *88*, 3671-3675.

103 Pande, S.V. *Proc. Nat. Acad. Sci. USA* **1975**, *72*, 883-887.

104 Steliou, K. US Patent 6316652, **2001**.

105 El Fangour, S.; Marini, M.; Good, J.; McQuaker, S.J.; Shiels, P.G.; Hartley, R.C. *Age* **2009,** DOI: 10.1007/s11357-009-9098-z

106 Zhao, K.; Zhao, G.-M.; Wu, D.; Soong, Y.; Birk, A.V.; Schiller, P.W.; Szeto, H.H. *J. Biol. Chem.* **2004**, *279*, 34682-34690.

107 Sheu, S.-S.; Nauduri, D.; Anders, M.W. *Biochim. Biophys. Acta* **2006**, *1762*, 256-265.

108 Wipf, P.; Xiao, J.; Jiang, J.; Belikova, N.A.; Tyurin, V.A.; Fink, M.P.; Kagan, V.E. *J. Am. Chem. Soc.* **2005**, *127*, 12460-12461.

109 i) Sholle, V.D.; Krinitzkaya, L.A..; Rozantsev, E.G. *Izvest. Akad. Nauk SSSR, Ser. Khim.*, **1969**, *1*, 149-151. ii) Golubev, V.A.; Sholle, V.D.;

Rozantsev, E.G. *Izvest. Akad. Nauk SSSR, Ser. Khim.*, **1972**, *5*, 1202-1204. iii) Sholle, V.D.; Golubev, V.A.; Rozantsev, E.G. *Izvest. Akad. Nauk SSSR, Ser. Khim.*, **1972**, *5*, 1204-1206.

110 Giroud, A.M.; Rassat, A. *Bull. Soc. Chim. Fr.* **1979**, 48-55.

111 Rizzardo, E.; Solomon, D.H. *Polym. Bull.* **1979**, *1*, 529-534.

112 Griffiths, P.G.; Rizzardo, E.; Solomon, D.H. *Tetrahedron Lett.* **1982**, *23*, 1309-1312.

113 Moad, G.; Rizzardo, E.; Solomon, D.H. *J. Macromol. Sci. A* **1982**, *17*, 51-59.

114 Gillies, D.G.; Sutcliffe, L.H.; Wu, X. *J. Chem. Soc. Faraday Trans.* **1994**, *90*, 2345-2349.

115 Moad, G.; Rizzardo, E.; Solomon, D.H. *Macromolecules* **1982**, *15*, 909-914.

116 Reid, D.A.; Bottle, S.E.; Micallef, A.S. *Chem. Commun.* **1998**, 1907-1908.

117 Belton, P.S.; Sutcliffe, L.H.; Gillies, D.G.; Wu, X.; Smirnov, A.I. *Magn. Reson. Chem.* **1999**, *37*, 36-42.

118 Gueven, N.; Luff, J.; Peng, C.; Hosokawa, K.; Bottle, S.E.; Lavin, M.F. *Free Radic. Biol. Med.* **2006**, *41*, 992-1000.

119 Marx, L.; Chiarelli, R.; Guiberteau, T.; Rassat, A. *J. Chem. Soc. Perkin Trans. 1* **2000**, 1181-1182.

120 Marx, L.; Rassat A. *Angew. Chem. Int. Ed.* **2000**, *39*, 4494-4496.

121 Bottle, S.E.; Micallef, A.S. *Biomol. Chem.* **2003**, *1*, 2581–2584.

122 Griffiths, P.G.; Moad, G.; Rizzardo, E.; Solomon, D.H. *Aust. J. Chem.* **1983**, *36*, 397-401.

123 Micallef, A.S.; Bott, R.C.; Bottle, S.E.; Smith, G.; White, J.M.; Maysuda, K.; Iwamura, H. *J. Chem. Soc. Perkin Trans. 2* **1999**, 65-71.

124 Bottle, S.; Gillies, D.; Highes, D.; Micallef, A.; Smirnov, A.; Sutcliffe, L. *J. Chem. Soc. Perkin Trans. 2* **2000**, 1285-1291.

125 Miyaura, N.; Suzuki, A. *J. Chem. Soc., Chem. Commun.* **1979**, 866-867.

126 Tsuji, J. (Ed.) *Palladium in Organic Synthesis (Topics in Organometallic Chemistry)* Springer, **2005.**

127 Gupta, M.; Paul, S.; Gupta, R.; Loupy, A. *Tetrahedron Lett.* **2005**, *46*, 4957-4960.

128 Wentzel, B.B.; Donners, M.P.J.; Alsters, P.L; Feiters, M.C.; Nolte, R.J.M. *Tetrahedron*, **2000**, *56*, 7797-7803.

[129] Lucien Marx, PhD thesis "Synthèse de biradicaux et de monoradicaux nitroxydes adaptés à la détection in vivo de l'oxyde nitrique et à la polarisation dynamique nucléaire" **1999**, University Pierre et Marie Curie, Paris.

[130] Murphy, M.P.; Smith, R. A. *Annu. Rev. Pharmacol. Toxicol.* **2007**, *47*, 629–656.

[131] Shearman, G.C.; Ces, O.; Templer, R.H.; Seddon, J.M. *J. Phys.-Condens. Mat.*, **2006**, *18*, S1105-S1124.

[132] Lipinski, C.A.; Lombardo, F.; Dominy, B.W.; Feeney, P.J. *Adv. Drug Deliver. Rev.* **1997**, *23*, 3-25.

[133] Koya, K.; Li, Y.; Wang, H.; Ukai, T.; Tatsuta, N.; Kawakami, M.; Shishido, T.; Chen, L.B. *Cancer Res*. **1996**, *56*, 538-543.

[134] Fantin, V.F.; Berardi, M.J.; Scorrano, L.; Korsmeyer, S.J.; Leder, P. *Cancer Cell*, **2002**, *2*, 29-42.

[135] Weiss, M.J.; Wong, J.R.; Ha, C.S.; Bleday, R.; Salem, R.R.; Steele, Jr, G.D.; Chen, L.B. *Proc. Natl. Acad. Sci. USA* **1987**, *84*, 5444-5448.

[136] i) Rossi, M.J.; Sundararaj, K.; Koybasi, S.; Phillips, M.S.; Szulc, Z.M.; Bielawska, A.; Day, T.A.; Obeid, L.M.; Hannun, Y.A.; Ogretmen, B. *Otolaryng. Head Neck* **2005**, *132*, 55-62. ii) Szulc, Z.M.; Bielawski, J.; Gracz, H.; Gustilo, M.; Mayroo, N.; Hannun, Y.A.; Obeid, L.M.; Bielawska, A. *Bioorg. Med. Chem.* **2006**, *14*, 7083–7104. iii) Novgorodov, S.A.; Zdzislaw M. Szulc, Z.M.; Luberto, C.; Jones, J.A.; Bielawski, J.; Bielawska, A.; Hannun, Y.A.; Obeid, L.M. *J.Biol. Chem.* **2005**, *280*, 16096–16105. iv) Dindo, D.; Dahm, F.; Szulc, Z.; Bielawska, A.; Obeid, L.M.; Hannun, Y.A.; Graf, R.; Clavien, P.-A. *Mol. Cancer Ther.* **2006**, *5*, 1520–1529.

[137] Discussed in: Heterocyclic Compounds, 14, supp. 1, Pyridine and Its Derivatives, ed. Abramovitch, R.A.; Chapter 3: Quaternary Pyridinium Compounds, Rodig, O.R.

[138] N. Menschutkin, *Z. Phys. Chem.* **1890**, *5***,** 589. Reviewed in *Adv. Heterocycl. Chem.* **1978**, *22*, 71-121.

[139] Cheng, W.-C.; Kurth, M.J. *Org. Prep. Proced. Int.* **2002**, *34*, 585-608.

[140] Koelsch, C.F.; Carney, J.J. *J. Am. Chem. Soc.* **1950**, *72*, 2285-2286.

[141] Zincke, T.; *Justus Liebigs Ann. Chem.* **1903**, *330*, 361-374.

142 i) Kaiser, A.; Billot, X.; Gateau-Olesker, A.; Marazano, C.; Das, B.C. *J. Am. Chem. Soc.* **1998**, *120*, 8026-8034. ii) Michelliza, S.; Al-Mourabit, A.; Gateau-Olesker, A.;Marazano, C.J. *J. Org. Chem.* **2002**, *67*, 6474-6478.

143 i) Eda, M.; Kurth, M.J.; Nantz, M.H. *J. Org. Chem.* **2000**, *65*, 5131-5135. ii) Eda, M.; Kurth, M.J *Tetrahedron Lett.* **2001**, *42*, 2063-2068.

144 Binay, P.; Dupas, G.; Bourguignon, J.; Queguiner, G. *Can. J. Chem.* **1987**, *65*, 648.

145 Li, J.J. ed. *Name Reactions in Heterocyclic Chemistry*; Wiley-Interscience: Hoboken, **2005.**

146 Fatiadi, A. J. Synthesis **1976**, 65-104.

147 Parikh, J. R.; Doering, W. von E. *J. Am. Chem. Soc.* **1967**, *89*, 5505-5507.

148 Omura, K.; Swern, D. *Tetrahedron* **1978**, *34*, 1651-1660.

149 Gogoi, P.; Konwar, D. *Org. Biomol. Chem.* **2005**, *3*, 3473-3575.

150 Martín, S. E.; Garrone, A. *Tetrahedron Lett.* **2003**, *44*, 549-552.

151 Ozanne, A.; Pouységu, L.; Depernet, D.; François, B.; Quideau, S. *Org. Lett.* **2003**, *5*, 2903-2906.

152 Nicolaou, K.C.; Baran, P.S.; Zhong, Y.-L. *J. Am. Chem. Soc.* **2001**, *123*, 3183-3185.

153 Peterson, K.P.; Larock, R.C. *J. Org. Chem.*, **1998**, *63*, 3185-3189.

154 Kornblum, N.; Jones, W.J.; Anderson, G.J*. J.Am. Chem. Soc.* **1959**, *81*, 4113-4114.

155 Shao, P.; Li, Z.; Luo, J.; Wang, H.; Qin, J. *Synthetic Commun.* **2005**, *35*, 49-53.

156 Caldwell, S.T.; Farrugia, L.J.; Hewage, S.G.; Kryvokhyzha, N.; Rotello, V.M.; Cooke, G. *Chem. Commun.* **2009**, 1350-1352.

157 Macleod, C.; McKiernan, G.J.; Guthrie, E.J.; Farrugia, L.J.; Hamprecht, D.W.; Macritchie, J.; Hartley, R.C.; *J. Org. Chem.* **2003**, *68*, 387-401.

158 Wuts, P.G.M.; Greene, T.W. *Greene's Protecting Groups in Organic Synthesis*, 4th Edition, Wiley, **2007**.

159 Conditions for generation of hydroxyl radicals were adapted from: Rosen, G.M.; Tsai, P.; Barth, E.D.; Dorey, G.; Casara, P.; Spedding, M.; Halpern, H.J. *J. Org. Chem.* **2000**, *65*, 4460-4463.

160 Caldwell, S.T.; Quin, C.; Edge, R.; Hartley, R.C. *Org. Lett.* **2007**, *9*, 3499–3502.

[161] Veltwisch, D.; Janata, E.; Asmum, K.-D. *J. Chem. Soc. Perkin Trans. 2* **1979**, 146-153.

[162] Cannon, B.; Nedergaard, J. *Physiol. Rev.* **2004**, *84,* 277-359.

[163] Nedergaard, J.;Ricquier, D.; Kozak, L.P. *EMBO Rep.* **2005**, *6*, 917–921.

[164] Echtay, K.S.; Roussel, D.; St-Pierre, J.; Jekabsons, M.B.; Cadenas, S.; Stuart, J.A.; Harper, J.A.; Roebuck, S.J.; Morrison, A.; Pickering, S.; Clapham, J.C.; Brand, M.D. *Nature* **2002**, *415*, 96-99.

[165] Brand M.D.; Affourtit, C.; Esteves, T.C.; Green, K.; Lambert, A.J.; Miwa, S.; Pakay, J.L.; Parker, N. *Free Radic. Biol. Med.* **2004**, *37*, 755–767.

[166] Tehan, B.G.; Lloyd, E.J.; Wong, M.G.; Pitt, W.R.; Montana, J.G.; Manallack, D.T.; Gancia E. *Quant. Struct.-Act. Relat.* **2002**, *21*, 457-472.

[167] Parker, V.H. *Biochem. J.* **1965**, *97*, 658-662.

[168] Terada, H. *Environ. Health Persp.* **1990**, *87*, 213-218.

[169] Schlosser, M. (ed.) *Organometallics in Synthesis*, John Wiley & Sons Ltd., **1994**.

[170] Lo, L.-C.; Chu, C.-Y. *Chem. Commun.* **2003**, 2728-2729.

[171] Srikun, D.; Miller, E.W.; Domaille, D.W.; Chang, C.J. *J. Am. Chem. Soc.* **2008**, *130*, 4596-4597.

[172] Chang, M.C.Y.; Pralle, A.; Isacoff, E.Y.; Chang, C.J. *J. Am. Chem. Soc.* **2004**, *126*, 15392-15393.

[173] Miller, E.W.; Albers, A.E.; Pralle, A.; Isacoff, E.Y.; Chang, C.J. *J. Am. Chem. Soc.* **2005**, *127*, 16652-16659.

[174] Germain, M.E.; Knapp, M.J. *Inorg. Chem.* **2008**, *47*, 9748-9750.

[175] Jia, Y.; Bois-Choussy, M.; Zhu, J. *Org. Lett.* **2007**, *9*, 2401–2404.

[176] Colibee, S.E.; Yu, J. *Tetrahedron Lett.* **2005**, *46*, 4453-4455.

[177] Butler, R.N.; Quinn, K.F.; Welke, B. *J. Chem. Soc., Chem. Commun.* **1992**, 1481-1482.

[178] (a) H. A. Laitinen, Chemical Analysis, New York, McGraw-Hill, 1960, pp. 372-373. (b) R. F. Schneider, State University at Stony Brook, personal communication.

[179] Worlikar, S.A.; Larock, R.C. *J. Org. Chem.* **2008**, *73*, 7175.7180.

[180] Norman, M.H.; Kelley, J.L.; Hollingsworth, E.B. *J. Med. Chem*. **1993**, *36*, 3417-3423.

[181] v. Pulawski, W. *J. Prakt. Chem. (Leipzig)* **1899**, *59*, 252.

[182] Hayat, S.; Atta-ur-Rahman; Choudhary, M. I.; Khan, K.M.; Schumann, W.; Bayer, E., *Tetrahedron* **2001**, *57*, 9951-9958.

[183] Warzech, K.-D.; Lex, J.; Griesbeck, A.G. *Acta Cryst.* **2006**, *E62*, o2367-o2368.

[184] Foitzik, R.C.; Bottle, S.E.; White, J.M.; Scammells, P.J. *Aust. J. Chem.* **2008**, *61*, 168-171.

[185] Tolbert, L.M.; Haubrich, J.E. *J. Am. Chem. Soc.* **1994**, *116*, 10593-10600.

[186] Wentzel, B.B.; Donners, M.P.J; Alsters, P.L.; Feiters, M.C.; Nolte, R.J.M *Tetrahedron* **2000**, *56*, 7797-7803.

[187] Caswell, L.R.; Atkinson, P.C. *J. Heterocyclic Chem.* **1966**, *3*, 328-332.

[188] Chan, K.S.; Mak, K.W.; Tse, M.K.; Yeung, S.K.; Li, B.Z.; Chan, Y.W. *J. Organomet. Chem.***2008**, *693*, 399-407.

[189] Lee, J.M.; Park, E.U.; Cho, S.W.; Chang, S. *J. Am. Chem. Soc.* **2008**, *130*, 7824-7825.

[190] Claramunt, R. M.; Elguero, *J. Collect. Czech. Chem. Commun.* **1981**, *46*, 584–596.

[191] Sammes, M.P.; Wah, H.K.; Katritzky, A.R. *J. Chem. Soc. Perkin Trans. 1* **1977**, 327-332.

[192] Vázquez M.E.; Blanco, J.B.; Imperiali, B. *J. Am. Chem. Soc.* **2005,** *127,* 1300-1306.

[193] Bandgar, B. P.; Gaikwad, N. B. Monatsh. Chem. **1998**, *129*, 719–722.

[194] Lee, A.S.-Y.; Cheng, C.-L. *Tetrahedron* **1997**, *53*, 14255-14262.

[195] Borah, R.; Kalita, D.J.; Sarma, J.C. *Indian. J. Chem B* **2002,** *41*, 1032-1038.

[196] Yuen, A.K.L.; Jollifee, K.A.; Hutton, C.A. *Aust. J. Chem.* **2006**, *59*, 819-826.

[197] Kaegi, D.; Schlageter, M.; Widmar, E. *Eur. Patent 0280975* **1988**.

[198] Hinton, R. D.; Janzen, E. G. *J. Org. Chem*. **1992**, *57*, 2646–2651.

[199] Oszczapowicz, J.; Pines, H. *J. Org. Chem.* **1972**, *37*, 2799–2806.

[200] U.S. Patent 2930731, Upjohn Co. March 29, **1960**.

[201] Collins, R. F.; Davis, M. *J. Chem. Soc. C* **1966**, 2196–2201.

[202] *Aldrich FT-NMR* **1** (2), 1503:B.

[203] Collibee, S.E.; Yu, J. *Tetrahedron Lett.* **2005**, *46*, 4453-4455.

[204] Murata, M.; Oyama, T.; Watanabe, S.; Masuda, Y. *J. Org. Chem.* **2000**, *65*, 164-168.

[205] de Filippis, A.; Morin, C.; Thimon, C. *Synth. Commun.* **2002**, *32*, 2669-2676

[206] Haupt, G.W. *J. Res. Natl. Bur. Std.* **1952**, *48*, 414-423.

[207] O'Brien, T.A.; Nieva-Gomez, D.; Gennis, R.B. *J. Biol. Chem.* **1978**, *253*, 1749-1751.

[208] Shikita, M.; Fahey, J.W.; Golden, T.R.; Holtzclaw, D.; Talalay, P. *Biochem. J.* **1999**, *341*, 725-732.